UNIVERSITY *of the* WESTERN CAPE

MODIFICATION OF NANOSTRUCTURED CARBON BASED SUPPORTS FOR DIRECT METHANOL FUEL CELLS.

AKINDEJI JEROME SABEJEJE
Student Number: 3872155

A thesis submitted in fulfilment of the requirements for the degree of Doctor of Philosophy in Chemistry, Faculty of Natural Sciences, University of the Western Cape, South Africa.

Supervisor: Professor Lindiwe Khotseng

November, 2022.

DECLARATION

I declare that '**Modification of Nanostructured Carbon Based Supports for Direct Methanol Fuel Cells'** is my work, that it has not been submitted for any degree or examination in any other University, and that all the resources I have used or quoted have been indicated and acknowledged by means of complete references.

Akindeji Jerome Sabejeje

Student Number: 3872155

November, 2022.

UNIVERSITY *of the*

WESTERN CAPE

Signed:

i

ABSTRACT

Palladium (Pd) and Palladium-Ruthenium (Pd-Ru) nanoparticles supported by various carbon nanomaterials which include graphene oxide (GO), reduced graphene oxide (rGO) and multi-walled carbon nanotubes (MWCNTs) with their hybrids were prepared in this work. The synthesized nanoparticles were used as electrocatalysts for direct methanol fuel cell. The graphene was synthesized by modified Hummer's method and subsequently, the support materials were doped with nitrogen using melamine. The electrocatalysts were synthesized using modified polyol method. The synthesis method of the electrocatalyst was also modified by adjusting the pH of the electrocatalyst. The structural characterization of all the support materials was carried out using Fourier Transform Infrared (FT-IR) Spectroscopy and Brunauer-Emmett-Teller (BET) Technique. The FT-IR results revealed that all the support materials contain the functional groups which serve as the binding sites for the deposition of Palladium nanoparticles while the BET results revealed that the surface area ranges from 3.36 to 9.20 m^2/g for the graphene based support materials and 14.32 to 67.45 m^2/g for MWCNTs, N- MWCNTs and CNFs support materials. However, when the support materials were doped with nitrogen, the surface area improved which ranges from 6.45 to 41.92 m^2/g for graphene based and 219.50 m^2/g for N-MWCNTs support materials. Meanwhile, the surface area of the hybrid support materials was found within the range of 62.91 and 144.21 m^2/g. The structural characterisation of the mono supported Pd catalysts, hybrid supported Pd catalysts and binary (Pd-Ru) electrocatalysts was also done using X-ray diffraction (XRD) and High resolution transmission electron microscopy (HR-TEM). The XRD confirmed that all the electrocatalysts are crystalline and exhibit face-centered crystal (fcc) structure of Pd while the HR-TEM images showed spherical and agglomerated catalyst nanoparticles dispersed on the various support materials. The particle size and crystallite size of the prepared electrocatalysts were determined using HR-TEM images and XRD spectra respectively. From HR-TEM images, the particle sizes of mono supported Pd catalyst are 5, 19, 5 and 12 nm for Pd/GO, Pd/ rGO, Pd/NGO and Pd/NrGO respectively while particle sizes of Pd/MWCNTs, Pd/N-MWCNTs and Pd/CNFs were found to be 6, 6, and 2 nm respectively. The hybrid supported Pd catalysts particle sizes were also found to be 8, 9, 3, 7, 4 and 9 nm for Pd/MWCNTs-CNFs, Pd/N-MWCNTs-CNFs, Pd/NGO-MWCNTs, Pd/GO-MWCNTs, Pd/GO-N-MWCNTs and Pd/rGO-MWCNTs respectively. Meanwhile, the particle sizes of Pd-Ru binary electrocatalysts were all found to be 1 nm except for Pd-Ru/CNFs which is 11 nm. The crystallite sizes of all the synthesized electrocatalysts are similar to their respective particle sizes. The mono supported and hybrid supported Pd catalysts crystallite sizes ranges from 0.1 to 19 nm and 4 to 10 nm respectively while that of Pd-Ru binary

electrocatalysts lies within the range of 0.5 and 11.7 nm. The elemental analysis was also carried out using energy dispersive spectroscopy (EDS). The EDS results validated the presence of N-doped in NGO, NrGO and N-MWCNTs support materials while the Pd loading in monocatalysts was found to be 37.67 % but the Pd and Ru loading in binary catalysts was found to be 15.11 and 15.83 % respectively. The electrochemical characterization of all the electrocatalysts was carried out using cyclic voltammetry (CV), Electrochemical impedance spectroscopy (EIS) and chronoamperometry (CA). The CV results revealed that the electroactive surface area (ECSA) values of Pd/GO, Pd/rGO, Pd/NGO and Pd/NrGO are 1.60, 1.24, 1.84 and 1.53 m^2/g respectively while the ECSA values of Pd/MWCNTs, Pd/N-MWCNTs and Pd/CNFs were found to be 1.81, 5.53 and 0.42 m^2/g respectively. For hybrid supported electrocatalysts, Pd/MWCNTs-CNFs, Pd/N-MWCNTs-CNFs, Pd/NGO-MWCNTs, Pd/GO-MWCNTs, Pd/GO-N-MWCNTs and Pd/rGO-MWCNTs exhibited ECSA values of 2.92, 2.89, 3.99, 4.57, 2.66 and 2.03 m^2/g respectively while in binary electrocatalysts, Pd-Ru/GO, Pd-Ru/NGO, Pd-Ru/MWCNTs, Pd-Ru/N-MWCNTs and Pd-Ru/CNFs showed ECSA values of 0.05, 0.28, 0.14, 0.04 and 0.03 m^2/g respectively. Therefore, Pd/N-MWCNTs, Pd/GO-MWCNTs and Pd-Ru/NGO electrocatalysts have exhibited the highest electroactive surface area of 5.53, 4.57 and 0.28 m^2/g among mono supported, hybrid supported and binary electrocatalysts respectively. The electroactivity towards methanol oxidation of mono supported, hybrid supported and binary electrocatalysts was also examined using cyclic voltammetry. The CV results showed that Pd/N-MWCNTs, Pd/GO-MWCNTs and Pd-Ru/NGO provided better evidence towards methanol oxidation among mono supported, hybrid supported and binary electrocatalysts with current density of 22.22, 4.43 and 0.72 mA/cm^2 respectively. This enhanced performance can be ascribed to better electroactive surface area and the presence of dopant nitrogen which serves as the defect sites to amplify the nucleation of the Pd nanoparticles in Pd/N-MWCNTs and Pd-Ru/NGO and better electroactive surface area in Pd/GO-MWCNTs. Furthermore, chronoamperometry showed that electrocatalyst supported with N-MWCNTs, GO-MWCNTs and NGO among mono supported, hybrid supported and binary electrocatalysts respectively have proved to exhibit better stability with current density of 0.84, 0.19 and 2.01×10^{-2} mA/cm^2 respectively while electrochemical impedance spectroscopy (EIS) showed that Pd/N-MWCNTs, Pd/GO-MWCNTs and Pd-Ru/NGO among mono supported, hybrid supported and binary electrocatalysts with charge transfer resistance (Rct) values of 0.35, 0.54 and 3.49 KΩ respectively have proved to exhibit better chemical kinetic compared to other carbon supported catalysts examined. This can also be accorded to a better electroactive surface area in Pd/GO-MWCNTs and the presence of dopant nitrogen in Pd/N-MWCNTs and Pd-Ru NGO with the synergistic interaction between the metal nanoparticles and these support materials.

After the modification of the mono supported electrocatalysts by adjusting the pH to 13, the electrocatalysts exhibited similar particle size except for Pd/rGO and Pd/NrGO which decreased to 6 and 5 nm respectively. However, their crystallite sizes were maintained except for Pd/rGO and Pd/NrGO which reduced to 6.2 and 5.8 nm respectively. The CV results revealed the ECSA values of Pd/GO, Pd/rGO, Pd/NGO and Pd/NrGO as 1.70, 3.52, 3.87 and 3.78 m^2/g respectively while the ECSA values of Pd/MWCNTs, Pd/N-MWCNTs and Pd/CNFs were found to be 1.70, 1.78, 0.69 m^2/g. Therefore, Pd/NGO exhibited the highest electroactive surface area of 3.87 m^2/g and highest electrochemical impedance with charge transfer resistance (Rct) values of 0.71 KΩ while Pd/NrGO showed highest activity towards methanol oxidation with current density of 4.88 mA/cm^2 and highest stability with current density of 0.14 mA/cm^2. This enhanced performance in Pd/NGO and Pd/NrGO can be ascribed to a good electroactive surface area, presence of dopant nitrogen which also serves as the defect sites to amplify the nucleation of the Pd and the synergistic interaction between the metal nanoparticles and this support material. However, the electroactivity of the modified electrocatalysts did not improve when compared with their counterparts that were synthesized by modified polyol method. Hence, N-MWCNTs, GO-MWCNTs and NGO have proved in this study to be the best support materials for mono supported, hybrid supported and binary electrocatalysts respectively when the catalysts were prepared by modified polyol method. In all, N-MWCNTs has displayed the best performance among all the synthesized support materials since the Pd catalyst supported by this material showed the best electroactivity and stability in basic electrolyte compared to other synthesized supported catalysts. In conclusion, after all the results obtained from the physical and electrochemical characterisation of mono supported Pd catalysts, hybrid supported Pd catalysts and mono supported Pd-Ru binary catalysts were compared, it can be inferred that modification of electrocatalysts synthesis method by increasing the pH to 13, hybridization of the support materials and alloying of Pd nanoparticle with Ru nanoparticles in ratio 1:2 to form the catalyst mass loading, which is the same as the mass loading used for Pd monocatalysts, did not improve the activity of the support materials generally since the mono supported Pd catalysts synthesized by modified polyol method exhibited better electroactivity than others.

KEYWORDS

Graphene Oxide

Reduced Graphene Oxide

Nitrogen-doped Graphene Oxide

Nitrogen-doped educed Graphene Oxide

Carbon nanotubes

Nitrogen-doped Carbon nanotubes

Carbon nanofibers

Palladium catalyst

Hybrid support materials

Methanol oxidation reaction

Direct methanol fuel cell.

Electrochemical characterization

Physical characterization

Chemical characterization

Modified polyol method

Modified hummers method

ACKNOWLEDGEMENT

Weeping may tarry for the day but joy comes in the morning [Psalm 30:5]. I give glory and adoration to Almighty God who, in His infinite mercy, spared my life and ensured that this great feat is achieved today. May His name be blessed both now and forever more, Amen.

My sincere appreciation goes to my amiable, erudite scholar and rugged supervisor- Professor Lindiwe Eudora Khotseng for introducing me to this project, guiding me throughout my studies, providing the facilities used, and for your expertise in correcting this thesis. May God reward you abundantly. I cannot but appreciate Hydrogen South Africa (HySA System) for funding this project. Thank you so much for your financial assistance. I would also like to thank the Department of Chemistry, University of the Western Cape, South Africa for allowing me to carry out this research successfully in the Department. To all the members of the Energy and Nanomaterials Research Group and friends especially Nurudeen Adewumi Adebare, I say thank you for your support and assistance. My appreciation also goes to Dr. Omotola Babajide, Dr. Karen Koopman, Prof. Fanelwa Ajayi, Dr. Emmanuel Ameh, Dr. Frikkie George, Mrs. Lynne Johns, Sedicka Cassiem (ISSO UWC) and Mr. Musharraf Foorooskar for your supports. I would also like to appreciate my host supervisors - Prof. Daniel Miguel San Jose and Prof. Celedonio Alvarez Gonzalez; Miguel Angel Nuevo (IRO, UVa), Lidia Alba Espana (IRO, UVa) and all my colleagues in Molecular Inorganic and Organometallic with Transition Metals Research Group (MIOMeT), Department of Chemistry, University of Valladolid, Valladolid, Spain for your affectionate accommodation, kind gesture and unalloyed supports to me during my Erasmus + KA 107 (ICM) doctoral student exchange mobility programme. Gracias a todos y que Dios los bendiga abundantemente.

My appreciation also goes to my Parish Priests in Sts John & Paul Catholic Church, Belhar, South Africa-Rev. Frs. John Paul Achi, Anthony Obadina and Emmanuel Eyeowa and my home Parish Priests- Rev. Frs. Joseph Ajayi, Dominic Ayeku, Dominic Akinjo, Dominic Adeosun and Lawrence Olemija of Ondo Diocese, Nigeria for your prayers and supports.

Last but not the least, I want to sincerely express my unreserved appreciation to the entire members of Odidi Sabejeje family, especially my elder brother- Lawrence Akinpelumi Sabejeje, my darling wife- Agnes Oluwakemi Sabejeje and my loving/caring children-Aanuoluwapo Sabejeje, Temidayo Sabejeje and Toluwalase Sabejeje for your sacrifice, patience and endurance throughout the period of this study. I say thank you for your prayers, supports and assistance.

Dankie, Enkosi, Muchas Gracias. Thanks you all and God bless you abundantly.

DEDICATION

This thesis is dedicated in loving memory of my beloved parents: Mr. Julius Ilemobayo Sabejeje & Mrs. Felicia Ige Sabejeje, my grandparents: Chief Joseph Ojo Sabejeje & Mrs. Omowumi Sabejeje, my uncle and his wife: Mr. Festus Kokumo Sabejeje & Mrs. Florence Omolabake Sabejeje, my first spiritual director: Very Rev. Fr Felix Ojo Abiodun Akinseye (Ondo Diocese, Nigeria) and my first academic mentor: Prof. Victor Larewaju Ayokunle Yoloye. May their gentle souls rest in peace.

TABLE OF CONTENTS

x

LIST OF FIGURES

xiii

LIST OF TABLES

UNIVERSITY *of the*

WESTERN CAPE

LIST OF EQUATIONS

$$CH_3OH + H_2O \rightarrow CO_2 + 6H^+ + 6e^-$$ Equation 1.1

$$3O_2 + 12H^+ + 6e^- \rightarrow 6H_2O$$ Equation 1.2

$$CH_3OH + {}^3/_2\, O_2 \rightarrow CO_2 + 2H_2O$$ Equation 1.3

$$n\lambda = d\sin\theta$$ Equation 3.1

$$d = {}^{0.9\lambda}/_{\beta\cos\theta}$$ Equation 3.2

$$H^+_{(aq)} + e^- + site \rightarrow H_{(ad)}$$ Equation 4.1

$$2H_{(ad)} \rightarrow H_{2(ad)}$$ Equation 4.2

$$nH_{2(ad)} \rightarrow nH_{2(g)} + 2n - sites$$ Equation 4.3

$$ECSA_{Pd,cat}(cm^2/mg) = {}^{Q(C/cm^2)}/_{420\,\mu C/cm^2\, L_{Pd}(mg/cm^2)}$$ Equation 4.4

LIST OF ABBREVIATIONS

AFCs	Alkaline fuel cells
ACL	Anode catalyst layer
AGDL	Anode gas diffusion layer
BET	Brunauer-Emmett-Teller
CB	Carbon black
CCL	Cathode catalyst layer
CGDL	Cathode gas diffusion layer
CNFs	Carbon nanofibers
CA	Chronoamperometry
CV	Cyclic voltammetry
CVD	Chemical vapour deposition
DMFCs	Direct methanol fuel cells
DEFCs	Direct ethanol fuel cells
DFAFCs	Direct formic acid fuel cells
ECSA	Electroactive surface area
EDS	Energy dispersive spectroscopy
EIS	Electrochemical impedance spectroscopy
FT-IR	Fourier Transform Infrared Spectroscopy
GNS	Graphene nanosheets
GO	Graphene oxide
HR-TEM	High resolution transmission electron microscopy
IUPAC	International union of pure and applied chemistry
MC	Mesoporous carbon
MEA	Membrane electrode assembly
MeOH	Methanol
MOR	Methanol oxidation reaction
MWCNTs	Multi-walled carbon nanotubes
NGO	Nitrogen doped graphene oxide
N-MWCNTs	Nitrogen doped multi-walled carbon nanotubes
NPs	Nanoparticles
NrGO	Nitrogen doped reduced graphene oxide
OMC	Ordered mesoporous carbon
ORR	Oxygen reduction reaction

PANI	Polyaniline
PAFCs	Phosphoric acid fuel cells
PBIs	Polybenzimidazole
PECVD	Plasma enhanced chemical vapour deposition
PEMFCs	Proton exchange membrane fuel cells
rGO	Reduced graphene oxide
SEM	Scanning electron microscopy
SOFCs	Solid oxide fuel cells
THF	Tetrahydrofuran
TPB	Triple phase boundary
XRD	X-ray diffraction

REASEARCH OUTPUTS

Manuscript submitted for publication

❖ (Sabejeje *et al*., 2022): Development of carbonaceous supports for direct methanol fuel cells.

Drafted manuscript

❖ (Sabejeje *et al*., 2022): Electrochemical evaluation of Pd-based binary catalyst on various nanostructured support materials for direct methanol fuel cells.

Presentations

❖ (Sabejeje *et al*., 2022): The physico-chemical study of supports materials on binary catalysts for direct methanol fuel cells. The 73rd Annual Meeting (Conference) of the International Society of Electrochemistry (online), 12th – 16th September 2022.

❖ (Sabejeje & Khotseng 2021): Modification of carbon support for direct methanol fuel cells. Joint International Workshop on South Africa and China, (NRF/MOST Project 2020-2021), 29th September, 2021.

❖ (Sabejeje *et al*., 2021): Effects of hybrid support materials on electrocatalyst for direct methanol fuel cells. The 72nd Annual Meeting (Conference) of the International Society of Electrochemistry, 29th August– 3rd September 2021, Jeju Island, Korea.

❖ (Sabejeje *et al*., 2021): Development of carbonaceous supports for direct methanol fuel cells. Young Chemists Symposium, 8th - 9th July 2021, Cape Town, South Africa.

❖ (Sabejeje *et al*., 2020): Development of graphene-based support materials for direct methanol fuel cells. The 71st Annual Meeting (Conference) of the International Society of Electrochemistry, 30th August – 4th September 2020.

❖ (Sabejeje *et al*., 2019): Development of carbon support materials for direct methanol fuel cells. The 70th Annual Meeting (Conference) of the International Society of Electrochemistry, 4th – 9th August, 2019, Durban, South Africa.

CHAPTER ONE

1   INTRODUCTION

1.1   Background of the study

As a result of exponential increase in fossil fuel consumption leading to increase in environmental pollution caused by emission of carbon monoxide, the need to generate alternative source of energy has become a major concern (Gavidia *et al*., 2017; Wang *et al*., 2016). These have drawn the attention of government and researchers on how to develop, improve and commercialize greener alternative, renewable and sustainable sources of energy (Wang *et al*., 2016). Fuel cell technology has been recommended to be one of most active areas associated with this green energy (Abaza *et al*., 2021; Priya *et al*., 2014; Ramli & Kamarudin, 2018; You & Kamarudin, 2017). It offers a lot of benefits more than fossil fuel combustion engine which include production of non-hazardous by-products which are mainly water and heat unlike carbon monoxide produced during the burning of fossil fuel which is hazardous to human health and ecological environment. It is therefore imperative for the development of fuel cells which has become a prospective candidate for replacing the conventional combustion engine in powering devices and transportation applications (Antolini, 2009; Kamarudin *et al*., 2007, 2009; Wongyao *et al*., 2011).

A fuel cell is an electrochemical device that converts the chemical energy of a fuel (such as hydrogen, methanol, and ethanol etc.) and an oxidant (such as air and pure oxygen) in the presence of a catalyst into electricity, heat and water (Abaza *et al*., 2021; Chalgin *et al*., 2020; Karim *et al*., 2015; Sharma & Pollet, 2012). Fuel cells generally consist of three main components which are refers to as membrane electrode assembly (MEA). The first part is the anode, the positive electrode of the fuel cell which conducts the electrons that are released from the hydrogen molecules such that they can be used in the external circuit. It contains channels etched which release the hydrogen gas equally on the surface of the catalyst used. The second part is the cathode, the negative electrode of the fuel cell. It also has channels etched in it which distribute the oxygen to the surface of the catalyst used. The electrolyte, which is the proton exchange membrane (PEM), is the third part of the MEA. It conducts the positively charged ions but prevents electron flow. The membrane must always be hydrated for it to function effectively and remain stable in proton exchange membrane fuel cells (PEMFCs) (Abaza *et al*., 2021). The catalyst, which is a part of the fuel cell, is a unique material that increases the reaction rate of oxygen and hydrogen. In most cases, Platinum nanoparticles which are finely coated on carbon blacks are used. The catalysts are usually rough and highly porous such that their maximum surface area is exposed to the hydrogen and

1

oxygen. When hydrogen collides with the catalyst, it splits into protons and electrons. The protons move straight to the cathode while the electrons move through an external circuit. Consequently, the electrons power a motor or device before combining with the protons again and oxygen on the cathode side to eventually produce water as illustrated in Figure 1.1. In as much as fuel and oxygen are supplied steadily, fuel cells can produce electrons to power a motor or device for a long time consistently (Bahrami & Faghri, 2013).
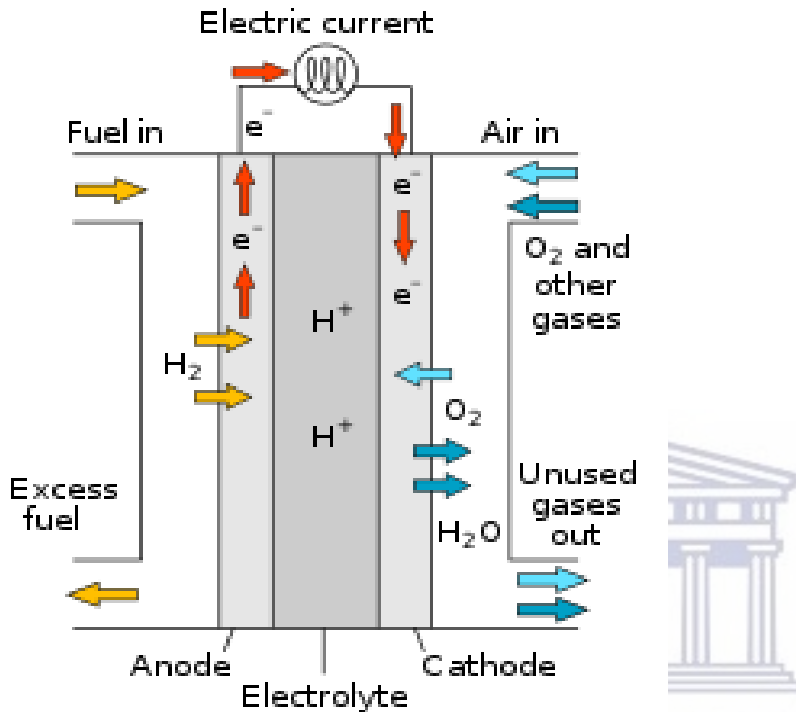
Figure 1.1: Schematic diagram of Proton Exchange Membrane Fuel Cells.
Source: https://en.wikipedia.org/wiki/Fuel_cell.

1.2   Types of fuel cells

There are different types of fuel cells which include:

- Alkaline fuel cells (AFCs)
- Proton exchange membrane fuel cells (PEMFCs)
- Phosphoric acid fuel cells (PAFCs)
- Solid oxide fuel cells (SOFCs)
- Direct methanol fuel cells (DMFCs).
- Direct ethanol fuel cells (DEFCs)
- Direct formic acid fuel cells (DFAFCs)

The difference in these various fuel cells is based on the type of the electrolyte used as illustrated in Table 1.1 (Seselj *et al*., 2015). The DMFCs produce high energy density and is easy to transport. Also, it uses methanol as fuel that could be produced from biomass which is non-hazardous to the environment (Hasegawa *et al*., 2010; Seselj *et al*., 2015) Therefore, for the purpose of this study, our discussion shall be limited to DMFCs.

Table 1.1: Overview of electrochemical reactions, electrolyte and electrode catalysts in different types of fuel cells.

Types of fuel cells and reaction	Electrolyte	Catalyst	Ref.
AFCs A: $2H_2 + 4OH^- \rightarrow 4H_2O + 4e^-$ C: $O_2 + 2H_2O + 4e^- \rightarrow 4OH^-$	Aqueous alkaline solution (KOH)	A: Pt, Ru, Pd, Rh, Pt-noble metal alloys, Raney nickel. C: Perovskites and spinels, Silica, Ag, C.	(Spendelow & Wieckowski, 2007)
PEMFCs A: $H_2 \rightarrow 2H^+ + 2e^-$ C: $^1/_2 O_2 + 2H^+ + 2e^- \rightarrow H_2O$	Polymer electrolyte exchange membrane (proton exchange membrane).	A and C: Pt, Pt-M alloy (M = Pd, Cu, Fe, Ru, Ni)	(Gasteiger et al., 2005; Mehta & Cooper, 2003)
PAFCs A: $H_2 \rightarrow 2H^+ + 2e^-$ C: $O_2 + 4H^+ + 2e^- \rightarrow H_2O$	Phosphoric acid	A and C: Pt, Pt-M alloy (M = Co, Ce, Al, Si, Ti, Sr,W, P, V)	(Watanabe et al., 1994)
SOFCs A: $H_2 + O_2^- \rightarrow H_2O + 2e^-$ C: $^1/_2 O_2 + 2e^- \rightarrow O_2^-$	Solid oxide (Ca, Zr) or ceramic	A and C: Rh, Ni, Ru, Ru/CeO$_2$	(Minh, 1993)
DMFCs A: $CH_3OH + H_2O \rightarrow 6H^+ + 6e^- + CO_2$ C: $^3/_2 O_2 + 6H^+ + 6e^- \rightarrow 3H_2O$	Proton exchange membrane	A and C: Pt, Pt-M alloy (M = Pd, Au, Ru)	(Seselj *et al*., 2015)

3

DEFCs	Proton	A: Pt, Pt M alloy (M =	(Ermete Antolini,
	exchange	Mo, Ru, Co, Fe, Sn, Ni)	2007)
A:$C_2H_5OH + 3H_2O \rightarrow 12H^+ + 12e^- +$	membrane		
CO_2		C: Pt, Pt-Co, Pt-Ni	
C: $3O_2 + 12H^+ + 12e^- \rightarrow 2H_2O$			
DFAFC	Proton	A: Pt-Ru, Pt-Pd	(Yu & Pickup, 2008)
	exchange		
A: $HCOOH \rightarrow CO_2 + 2H^+ + 2e^-$	membrane	C: Pt, Pt-M (M = Au,	
		Ru, Pd)	
C: $^1/_2 O_2 + 2H^+ + 2e^- \rightarrow H_2O$			

Source: (Seselj *et al*., 2015)

1.3 Direct Methanol Fuel Cells (DMFCs)

A DMFCs is a low temperature PEMFCs that make use of liquid methanol as fuel. This methanol, which serves as the fuel, can be produced from biomass which is non-hazardous to the environment (Hasegawa *et al*., 2010). The operating principle of a DMFCs comprises five major porous layers which include anode gas diffusion layer (AGDL), anode catalyst layer (ACL), polymer electrolyte membrane (PEM), cathode catalyst layer (CCL) and cathode gas diffusion layer (CGDL) as shown in Fig. 1.2. The methanol fed into the anode diffuses through the AGDL to ACL where it is oxidized as shown in equation 1.1. During the cell operation, equation 1.1 proceeds forwards to form carbon dioxide, protons and electrons (Bahrami & Faghri, 2013).

$$CH_3OH + H_2O \rightarrow CO_2 + 6H^+ + 6e^-$$
Equation 1.1

The reaction in the ACL occurs in three-phase boundary which include catalyst particles, carbon support and electrolyte (membrane). The electron produced at ACL are transferred through the carbon support to the AGDL where they move through the external circuit and converted to electric current while the remaining unconverted electrons move to the cathode side of the fuel cell. However, the proton generated are transferred through the ACL ionomer phase to the membrane. The membrane is impermeable to the electron and gaseous species. At the cathode, oxygen gas is being forced in as it diffuses through the CGDL to CCL where it is reduced to heat and water in the presence of electrons and protons as shown in equation 1.2 (Bahrami & Faghri, 2013). These prominent features enable DMFCs to be considered as a promising device to supply power in portable devices (Gálvez *et al*., 2013; Gavidia *et al*., 2017; Tang *et al*., 2010).
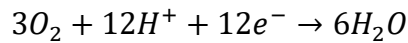
$$3O_2 + 12H^+ + 12e^- \rightarrow 6H_2O \qquad\qquad\text{Equation 1.2}$$
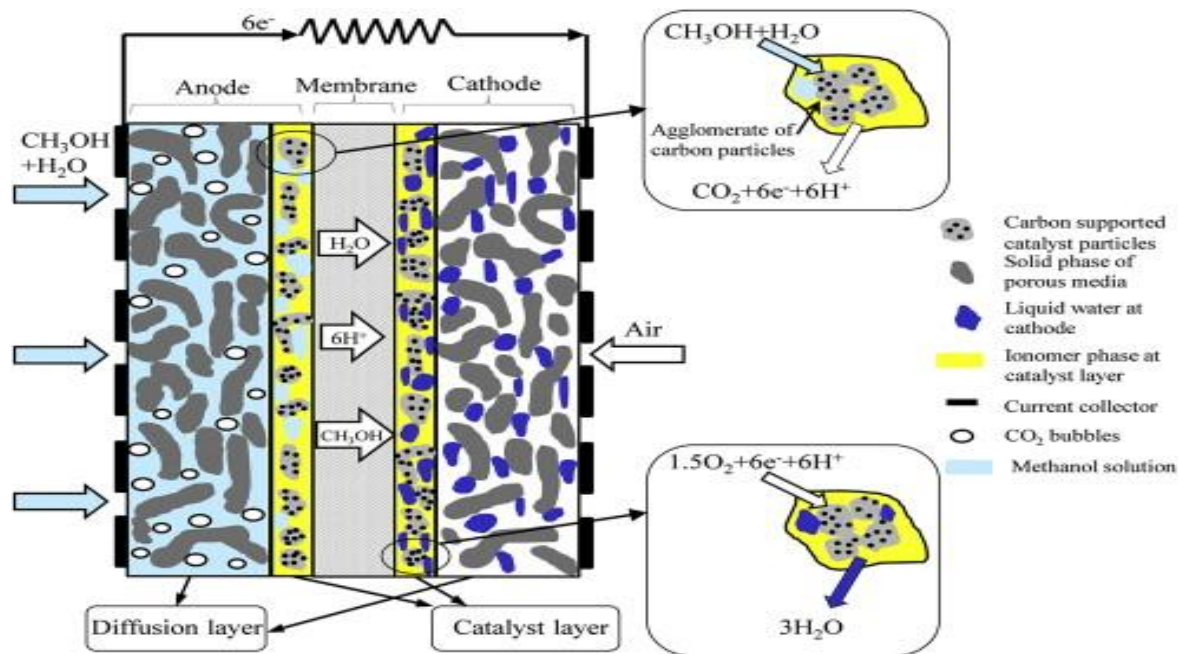
Figure 1.2: Schematic of a DMFCs during normal operation.
Source: (Bahrami & Faghri, 2013).

The net equation for DMFCs reaction can be summarized as:
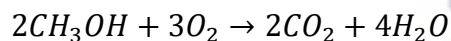
$$2CH_3OH + 3O_2 \rightarrow 2CO_2 + 4H_2O \qquad\qquad\text{Equation 1.3}$$

The aim of DMFCs research is to develop low cost, high performance and durable cells that can power portable devices (Ramli & Kamarudin, 2018). A lot of research has been carried out with the intension of reducing the cost and increasing the performance of the fuel cells using different strategies. Some of these strategies include reducing the electrocatalyst loading in fuel cell electrodes, developing novel nanostructured thin-film Platinum such as 3M's nanostructured thin film (NSTF) electrode, decreasing the electrocatalyst nanoparticles size, reducing Platinum dependence by developing metallic alloy either as binary or as ternary and Platinum-free electrocatalysts, improving electrocatalyst dispersion using novel fabrication methods, developing membrane electrode assembly (MEA) fabrication methods to enable better catalyst dispersion and utilization, using new techniques to increase mass-transport at the fuel cells electrode surface, improving the performance of carbonaceous electrocatalyst supports and exploring novel non-carbonaceous electrocatalyst support materials (Ramli & Kamarudin, 2018; Sharma & Pollet, 2012).

5

1.4   Support Materials

At this juncture, it is imperative to mention that high performance of DMFCs also depend majorly on the properties of the support materials used (Munjewar *et al*., 2017). Electrocatalyst support materials play a crucial role in enhancing electrocatalyst activity during DMFCs operation. Through their electronic and atomic structure, they provide a good surface area for homogenous dispersion, better particle size and also promote the stability of the catalyst nanoparticles (Basri *et al*., 2010; Ju *et al*., 2008; Priya *et al*., 2014; Rodríguez-reinoso, 1998; Sharma & Pollet, 2012; Wang *et al*., 2016; Wang *et al*., 2013). Since the instability of the catalyst support materials results to detachment of catalyst nanoparticles from the support materials causing the loss of activity of the electrocatalysts, the support materials can therefore significantly influence the activity of the catalysts and prolong their stability (Khotseng *et al*., 2016; Li *et al*., 2015). Therefore, the activity and stability of electrocatalysts are function of the type of support materials used (Zhao *et al*., 2016). Supported metal catalysts have been discovered to show higher stability and activity compared to the unsupported ones (Li *et al*., 2015).

Furthermore, ideal support materials are expected to possess the following features namely: good catalyst support interaction; large surface area, ability to maximize the triple-phase boundary (TPB) (i.e. the mesoporous structure should enable the ionomer and polymer electrolyte to bring the catalyst nanoparticles close to the reactant), enhance high electroactive areas caused by better dispersion of nanoparticles, improve electroactive species diffusion through the porous structure of carbon supports, promote electronic transfer either for the presence of surface functional groups or decrease in Fermi level of the catalyst, good electrical conductivity, give the reactant gas easy access to reach the electrocatalyst, possess good water-handling capability where water is generated at the anode to avoid flooding, exhibit a very high resistance to corrosion, must be chemically and electrochemically stable and easy recovery of the catalyst (Li *et al*., 2003; Munjewar *et al*., 2017; Shaari & Kamarudin, 2017; Tang *et al*., 2010; Wang *et al*., 2016).

A lot of research has been carried out on large number of carbon support materials. Due to their high availability and low cost, carbon black materials have been widely explored as support materials for Pt and Pt alloyed electrocatalysts in low temperature fuel cells such as DMFCs (Antolini, 2009; Chen *et al*., 2008; Li *et al*., 2003; Priya *et al*., 2014; Sahoo *et al*., 2015; Song *et al*., 2015; Tang *et al*., 2010; Wang *et al*., 2016; You & Kamarudin, 2017). Among the carbon black support materials developed include Vulcan XC-72, Black Pearls 2000, Acetylene Black, Ketjen

Black and Mascorb and they all exhibit high surface area (>100 m^2g^{-1}) and good electrical conductivity (>1Scm^{-1}). Among these carbon black support materials, Vulcan XC-72 with BET surface area of 250 m^2g^{-1}, mesoporous and macroporous percentage of 54% and electric conductivity of 2.77 Scm^{-1} has been reported to show a significant performance in fuel cell environment (Alexeyeva *et al*., 2011; Priya *et al*., 2014; Tang *et al*., 2010; Wang *et al*., 2016). Furthermore, carbon materials with high nanoarchitectural graphitic structures such as multi-walled carbon nanotubes (MWCNTs) and carbon nanofibers (CNFs) have also been critically examined. This is as a result of their unique features as they offer better crystalline structure, high electrical conductivity, excellent corrosion resistance with high level of purity. MWCNTs in particular, is of great interest because of the specific structural, mechanical and electrical properties they exhibit (Antolini, 2009; Khotseng *et al*., 2016). Mesoporous carbons (MCs) which include ordered mesoporous carbons (OMCs) have also been extensively studied as support materials for Pt and Pt alloyed electrocatalysts (Antolini, 2009; Wang *et al*., 2016). Compared to carbon blacks, mesoporous carbon materials possess higher surface area with little or no micropores which facilitate the high dispersion of the catalyst nanoparticles on their surface and their pores. This results in large effective surface area of the electrocatalyst with high catalytic activity. Mesoporous structure with mesoporous size of 2-50 nm enhance easy mass transport, producing high limiting current value (Maiyalagan & Scott, 2010; Park & Baker, 1998, 1999; Park *et al*., 2007; Steigerwalt *et al*., 2001; Stein, 2003; Wang *et al*., 2016).

Recently, research interest has also been diverted, towards prominent 2D graphene and its N-doped derivatives (Farooqui *et al*., 2018). This attraction is due to their unique graphitic forms, high charger-carrier mobility (up to 105 $cm^2V^{-1}S^{-1}$), super conductivity, ambipolar electric field effect, quantum Hall effect at room temperature, high mechanical strength (130 GPa) and high surface area (2600 m^2g^{-1}) (Seselj *et al*., 2015). Graphene surface area contains enough oxygen functional groups which give it a better advantage over other support materials. This enables graphene to disperse any metal nanoparticles easily and efficiently. It also possesses the ability to remove a lot of accumulated carbon monoxide which act as a poison during the adsorption of the catalyst nanoparticles thereby increasing the electrocatalytic activity of the catalyst (Antolini, 2003; Choi *et al*., 2011; Muneendra Prasad *et al*., 2012; Nirmala Grace & Pandian, 2006; Selvaraj *et al*., 2009). Moreover, N-doped graphene has also been discovered to be a good catalyst support material due to its ability to introduce chemically active sites for reaction and anchoring sites for metal nanoparticles deposition, modify electronic properties and give carbon materials a metallic character (Dector *et al*., 2013). Doping of graphene with nitrogen, which serves as a strong metal-

7

support link, facilitate reduction in CO_{ads} accumulation on the surface of the electrocatalyst, thereby increasing the catalyst poison tolerance, high electrocatalytic activity and long durability (Seselj *et al*., 2015). Other carbon supports that have been investigated as support materials for electrocatalysts include carbon gels (CGs), carbon nanohorns (CNHs), carbon nanocoils (CNCs), activated carbon fibers (ACFs) and boron-doped diamonds (BDDs) (Bulushev *et al*., 2004; Kasuya *et al*., 2002).

1.5   Problem Statement

Despite a lot of research has been carried out on catalyst support materials for DMFCs, DMFCs still suffer from slow electrode kinetics, support corrosion and short term stability which are technical barriers restricting their commercialization (Jha *et al*., 2011; Khotseng *et al*., 2016; Priya *et al*., 2014; Ramli & Kamarudin, 2018; Gavidia *et al*., 2017). This is because none of the developed carbon support materials has been able to meet all the prescribed requirements for ideal support materials as stated earlier. Also, since electrocatalyst support materials can enhance the electrocatalyst performance, the choice of support material is very vital in determining the performance, stability and cost effect of the electrocatalyst and the fuel cell as a whole (Sharma & Pollet, 2012). It is therefore imperative to develop robust nanostructured carbon support materials and modify the existing ones to be extremely resistant to corrosion with high degree of CO tolerance under critical and aggressive fuel cell condition (Tang *et al*., 2010). Hence, this research work is focusing on the modification of nanostructured carbon supports materials that can withstand the challenges of corrosion, instability and low durability in order to improve the activity of the catalysts and take DMFCs to a commercial level at low cost.

1.6   Research Rationale and Motivation of the study

Increase in global population and technological advancement has led to high rate of fossil fuel consumption over the years. Therefore, there is need to source for alternative ways of generating energy (Rivera Gavidia et al., 2017b). DMFCs have been discovered as a prospective substitute for high power source especially for low-to-medium portable power applications (Gálvez *et al*., 2013). However, DMFCs is still limited by cost, low performance of electrocatalysts due to methanol crossover, CO poisoning, slow anode kinetics and corrosion which has jeopardized its commercialization. Mostly, electrocatalysts of DMFCs suffer degradation which include dissolution, agglomeration and detachment of catalyst nanoparticles. Acute corrosion of supports does facilitate this electrocatalyst degradation thereby destroying the loading sites and debilitate

8

the synergistic interaction between the support materials and the catalyst nanoparticles (Du *et al*., 2016). Also, carbon support materials, if properly developed with features of ideal support materials can help to reduce the amount of catalyst used thereby reducing the cost and also improve the catalyst activity so that DMFCs can be taken to commercial level. As a result of this, the development of novel nanostructure carbon support materials is imperative to minimize these challenges. This study therefore investigated the performance of different nanostructured carbonaceous support materials using Pd and Ru catalysts with the aim of improving the activity and stability of the electrocatalyst. Pt catalyst, which is the best suited catalyst for direct methanol fuel cells (DMFCs) (Priya *et al*., 2014) is easily poisoned at low temperatures with CO species (Li *et al*., 2009; Priya *et al*., 2014). This poisoning usually results to instability as well as reduction in DMFCs performance which has posed a great challenge and reduce its commercialization. Hence, Palladium (Pd) is used in this study as alternative to Pt due to its lower poisoning effect, similar electronic configuration and lattice constant. Pd is also more abundant in nature than Pt and exhibits the capacity to enhance the oxidation of several alcohols in alkaline media with significant electrochemical stability (Bianchini & Shen, 2009). This study is focused on modifying the existing carbon support materials for direct methanol fuel cells.

1.7   Thesis statement

Novel catalyst supports can be obtained by modifying the existing carbon support materials which could enhance the catalyst performance during direct methanol fuel cells operating conditions.

1.8   Research questions

The following research questions were generated to be addressed in this study:

- Can the functionalization of MWCNTs in the presence of oxygen improve its activity towards methanol oxidation reaction?
- Will the use of melamine as nitrogen precursor amplify the performance of the support materials?
- Can the modified support materials boost the electron kinetics of the catalysts?
- Will the modified support materials enhance methanol oxidation reaction than the conventional support materials?
- Will the modified support materials increase the catalysts stability under real DMFCs operating conditions?

1.9   Research Aims and Objectives

The aims of this study is to develop novel carbon support materials for catalysts in DMFCs in order to reduce the cost, improve the activity and durability of the catalysts. To actualize this, the following objectives were set up:

- Synthesize various support materials which include MWCNTs, CNFs, Graphene oxide with their reduced, nitrogen-doped and hybrids counterparts.
- Examine the surface area of the synthesized support materials using BET technique.
- Elucidate the crystallinity of the structure of the synthesized electrocatalysts using XRD.
- Determine the electroactive surface area (ECSA) of the synthesized electrocatalysts using Cyclic Voltammetry
- Determine the activity of synthesized electrocatalysts towards methanol electrooxidation in alkaline medium (KOH) using Cyclic Voltammetry
- Evaluate the kinetics of the electrocatalysts in the presence of methanol in alkaline medium (KOH) using electrochemical Impedance Spectroscopy
- Determine the electrochemical stability of the supported catalysts in the presence of methanol in alkaline medium (KOH) using Chronoamperometry.

1.10   Thesis Delimitation

Conventionally, MWCNTs have been functionalized in saturated nitrogen in acidic medium. However, in this study MWCNTs were functionalized in the presence of air to ensure that more oxygen can be introduced into the surface of the support materials thereby increasing the binding sites for the Pd nanoparticles.

1.11   Thesis Overview

This thesis is divided into eight (8) chapters including this current chapter 1. The thesis structure is as follows:

Chapter 1 contains introduction which provide background information to the study, outlines the problem statement, aims and objectives of the study, thesis delimitation and thesis overview.

Chapter 2 presents an overview of all the related literature on various carbon and non-carbon support materials with their hybrids. A comparative study of different synthetic methods and support materials is made with more attention on carbon support materials.

Chapter 3 focuses on all the materials, methods used and the chemical characterization. It gives the experimental details of the synthesis procedure of the various mono and hybrid support

materials produced with their respective catalysts. The catalyst film, chemical characterization and the electrochemical evaluation procedures were also stated.

Chapter 4 showcase the results obtained from the characterization of graphene based support materials and their catalysts. A comparison of the surface area of the support materials was made. This chapter further shows and compares the electrochemical evaluation results of all the synthesized graphene supported Palladium electrocatalysts. A conclusion was drawn on the best among them.

Chapter 5 features the results obtained from the characterization of non-graphene based support materials and their catalysts. A comparison of the surface area of the support materials and the performance of their catalyst was made. This chapter also compares the results of Pd/NGO with Pd/N-MWCNTs as they exhibited the best electrocatalytic activity among their respective counterparts and conclusion was drawn on the best between the two.

Chapter 6 This chapter presents and compares the results obtained from the characterization of hybrid support materials and their catalysts. The electrochemical evaluation results of all the synthesized hybrid supported Palladium electrocatalysts are also presented and compared. A conclusion was drawn on the best among them.

Chapter 7 features the results obtained from the characterization of binary catalysts. Their electrochemical evaluation results are also presented and compared. A conclusion was drawn on the best among them.

Chapter 8 provides the final conclusion of this research work based on the results obtained and recommendations for future study.

CHAPTER TWO

2 REVIEW OF RELATED LITERATURE

2.1 Introduction

Low-temperature fuel cells using hydrogen, methanol, ethanol and other fuel is a technology which has drawn the attention of many researchers because they serve as means of generating power by direct conversion of the fuel and oxygen into water, electrochemically (Antolini, 2009; Gómez *et al*., 2016). The aim of DMFCs technology is to develop high performance, low cost and durable fuel cell device (Ramli & Kamarudin, 2018; Sharma & Pollet, 2012). In contrary, the present DMFCs system is very expensive (mainly due to catalyst used) with low performance and less durability. One of the major factors to be considered in designing high performance and more durable DMFCs is the catalyst support materials (Bianchini & Shen, 2009; Chalgin *et al*., 2020) since they have been discovered to reduce the cost, improve the catalytic activity and durability of DMFCs if properly developed (Du *et al*., 2016).

2.1.1 Carbon Supports

Several carbon support materials have been investigated. Previously, carbon blacks such as Vulcan XC-72, Black Pearls 2000, Acetylene Black, Ketjen Black and Mascorb were used extensively as catalyst support materials for Pt and Pt alloy electrocatalysts in low temperature fuel cells such as DFMCs due to their high availability and low cost (Antolini, 2009; Chen *et al*., 2008; Li *et al*., 2003; Priya *et al*., 2014; Sahoo *et al*., 2015; Song *et al*., 2015; Tang *et al*., 2010; Wang *et al*., 2016; You & Kamarudin, 2017). In the recent years, nanostructured carbon materials have been investigated and tested as support materials in order to improve the electrochemical activity and stability of the fuel cell catalysts. Some of these support materials include, multi-walled carbon nanotubes (MWCNTs) (Akalework *et al*., 2012; Daoush & Imae, 2012; Lee *et al*., 2006; Sahoo *et al*., 2015; Zhang *et al*., 2018; Zhu *et al*., 2008) carbon nanofibers (CNFs) (Antolini, 2009; Boskovic *et al*., 2005; Knupp *et al*., 2008; Yuan & Ryu, 2004), graphene or reduced graphene oxide (rGO) (Anwar *et al*., 2019; Avouris & Dimitrakopoulos, 2012; Bharti & Cheruvally, 2017; Emiru & Ayele, 2017; Park *et al*., 2018; Seselj *et al*., 2015; Shaari & Kamarudin, 2017), graphene oxide (GO) (Bojarska *et al*., 2019; Chen *et al*., 2012; Farooqui *et al*., 2018; Gupta *et al*., 2017; Pandey *et al*., 2017; Sohail *et al*., 2017; Zakil *et al*., 2016) among others with their nitrogen-doped counterparts such as N-MWCNTs, NGO and NrGO (Chen *et al*., 2011; Du *et al*., 2008; Higgins *et al*., 2010; Long *et al*., 2010; Maiyalagan *et al*., 2005; Narreddula *et al*., 2019; Vinayan *et al*., 2012; Wang *et al*., 2012; Wei *et al*., 2012; Xiong *et al*., 2013; Xu *et al*., 2013) and hybrids (Anwar

et al., 2019; Jafri *et al*., 2010; Jha *et al*., 2011; Aravind *et al*., 2011; Lee *et al*., 2006; Li *et al*., 2015; Pham *et al*., 2016; Ramesh *et al*., 2008; Wang *et al*., 2014; Zhao *et al*., 2016).

Support materials has been discovered to play a vital role in the performance of catalysts as they provide high dispersion surface area and stability for the catalysts nanoparticles (Khotseng *et al*., 2016). They are also important in enhancing mass transfer management in a fuel cell, improve electroactive species diffusion through the porous structure of the carbon supports, promotion of the electronic transfer either for the presence of surface functional group or the decrease in Fermi level of the catalyst and enhancement of high electroactive area caused by a better dispersion of catalyst nanoparticles (Calderón *et al*., 2012; Du *et al*., 2016). Therefore, catalysts are usually supported on electronic conductive and porous materials due to the fact that supported catalysts have been discovered to exhibit higher activity and better stability than unsupported catalysts (Sharma & Pollet, 2012). Hence, one of the means of increasing the activity of the catalyst is to modify and upgrade the support materials (Wang *et al*., 2016).

Since activity and stability of direct methanol fuel cells (DMFCs) are anchored on the strong chemical synergistic interaction between the catalysts and the supporting materials which determines the proper dispersion of the catalyst nanoparticles at low metal loading (Wang *et al*., 2016), ideal catalyst support materials should therefore contain the following features among others: sufficient electrical conductivity, large surface area, high resistance to electrochemical corrosion, suitable porosity and porous structure, strong stability in acidic or alkaline medium, good proton conductivity and crystallinity, good compatibility with electrodes, good water handling to avoid flooding and easy recovery of catalysts which all result into strong chemical synergistic interaction between the support and the catalyst nanoparticles as shown in Fig 2.1 (Antolini, 2009; Anwar *et al*., 2019; Li *et al*., 2003; Wang *et al*., 2016). Carbon support materials have been reported to be the best choice as catalyst support due to their large specific surface area, strong and better corrosion resistance and relatively low price (Tang *et al*., 2010).
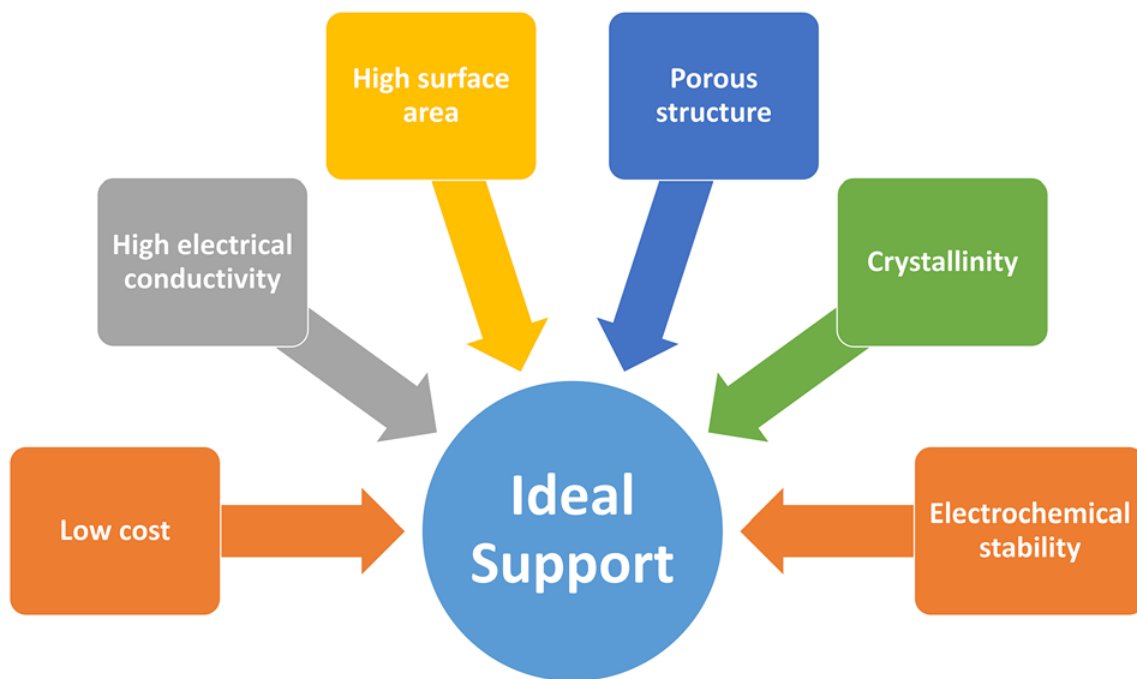
Figure 2.1: Properties of an ideal catalyst support

Source: (Anwar *et al*; 2018)

2.1.2   Carbon Supported Catalysts used in Direct Methanol Fuel Cells.

Electrocatalysts has been noted to play a significant role in DMFCs architecture and have been extensively explored to enhance the rate of electrochemical reactions in order to get desirable results (Samad *et al*., 2018). These catalysts are either used as anode catalyst where oxidation reaction occurs or as cathode catalyst where reduction reaction takes place. They could be developed as electrode itself or coated on the surface of the electrode. Platinum and Palladium are mostly used in DMFCs as pure metal doped on carbon support materials or as alloyed with other metals (Antolini *et al*., 2008; Ermete Antolini, 2018; Bianchini & Shen, 2009).

Platinum has been extensively used in DMFCs being the known most active metal for methanol oxidation reaction and oxygen reduction reaction among other pure metals when supported on a conductive carbon material (Antolini *et al*., 2008; Samad *et al*., 2018). However, the activity for the methanol oxidation reaction of Pt metal alone is very low (Ermete Antolini, 2018) as it suffers kinetic limitation and also readily poisoned by CO specie, a product of methanol oxidation at low temperature (Gottesfeld & Zawodzinski, 2008; Pollet *et al*., 2012). This poisoning effect usually result to instability as well as reduction in DMFCs performance. Hence, the use of additional metal with Pt such as Ru, Ni, Co, and Mo as alloy has been developed (Shukla *et al*., 2004; L. Xiong & Manthiram, 2004). The bifunctional mechanism explains that the second metal supplies oxygen to oxidised the Pt-adsorbed methanol oxidation intermediate specie, while the electronic effect states

14

that the second metal modifies the Pt electronic configuration, thereby weakening the adsorption of the methanol oxidation intermediate specie on Pt (Ermete Antolini, 2018). It is also known that the corrosion of carbon black increases in the presence of Pt nanoparticles. This results to detachment of the Pt from the support and the agglomeration of the Pt nanoparticles (Samad *et al*., 2018).

Significant efforts have been made to develop new catalyst for DMFCs anode with little or no Pt metal and are able to tolerate poisoning by CO specie with fast kinetics (Bianchini & Shen, 2009). Pd has aroused notable interest in electrocatalysts since it is more abundant in nature than Pt and exhibits the capacity to enhance the oxidation of several alcohols in alkaline media with significant electrochemical stability (Bianchini & Shen, 2009). The attraction of Pd-based electrocatalyst emanated from the fact that, unlike Pt-based electrocatalyst, they can be highly active for oxidation of large variety of substrate in alkaline medium. The alloying of Pd with non- noble metal in catalytic architecture capable of rapidly and stably oxidizing alcohols in anode electrodes is expected to decrease the cost of the membrane electrode assembly (MEA) so as to boost the commercialization of DMFCs (Bianchini & Shen, 2009) but their performance was still found to be lower than expected (Antolini *et al*., 2008).

Therefore, performance of different modified carbonaceous support materials using Pd catalyst with the aim of improving the activity and stability of the electrocatalyst has been investigated in this research. Pt catalyst, which is the best suited catalyst for direct methanol fuel cells (DMFCs) (Priya *et al*., 2014), has been known to suffers kinetic limitation and easily poisoned at low temperatures with CO species (Li *et al*., 2009; Priya *et al*., 2014). This poisoning usually results to instability as well as reduction in DMFCs performance. This has posed a great challenge and reduce its commercialization. Hence, Palladium (Pd) is used in this study as alternative to Pt due to its lower poisoning effect, similar electronic configuration and lattice constant. Pd is also more abundant in nature than Pt and exhibits the capacity to enhance the oxidation of several alcohols in alkaline media with significant electrochemical stability (Bianchini & Shen, 2009).

2.2   Types of Carbon Support

2.2.1   Carbon Black

For the past decades, conductive carbon black have been used as catalyst support materials for DMFCs (Ermete Antolini, 2009) and polymer electrolyte membrane fuel cells (PEMFCs) (Wang *et al*., 2016) because of their low cost and are readily available (L. Li et al., 2015b). Several types

15

of carbon black have been extensively studied and reported which include Acetylene black, Ketjen black, Oil-furnace black and Vulcan XC-72 (Antolini, 2009; Munjewar *et al*., 2017; Wang *et al*., 2016). The structure of carbon black is shown in Figure 2.2.
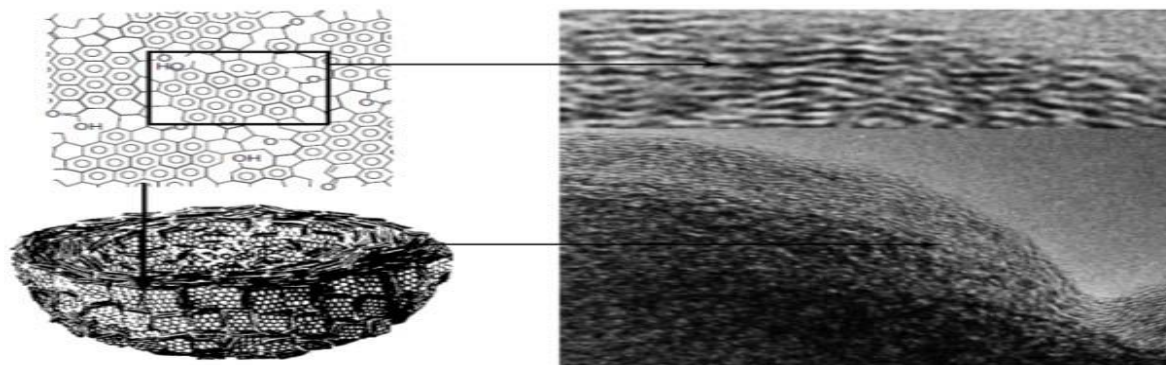
Figure 2.2: Structure of Carbon black

Source: (Tessonnier, 2017)

Among the various carbon black materials that have been investigated, Vulcan XC-72 has been reported as the most widely used support material for DMFCs catalyst which may be due to its more abundant defect sites and organic-surface groups which lead to a more homogenous metal dispersion and high electronic conductivity (Li *et al*., 2015; Munjewar *et al*., 2017; Tang *et al*., 2010). It has also been known to possesses high mesoporous and macroporous distribution, good graphite character with a high surface area of 250 m^2g^{-1} which can meet the requisites of a good support for catalyst (Munjewar *et al*., 2017; Tang *et al*., 2010).

A lot of research has been carried out on the effect of the characteristic of carbon black on dispersion and electrocatalytic activity of supported catalyst (Antolini *et al*., 2002; Antolini, 2010; Fraga *et al*., 2002; Gharibi *et al*., 2005; Rao *et al*., 2005; Wang *et al*., 2016). (Uchida *et al*., 1995) has reported the effect of specific surface area of various carbon supports on Platinum particle size of Pt/C catalyst. It was revealed that the Platinum particle size reduces with an increase in specific surface area of the carbon black support (Antolini, 2009). However, the Platinum particles in these pores are not contributing to the reaction taking place in the PEMFC as the ionomer particles are bigger than the diameters of the pore and the Platinum particles will have no contact with the ionomer. Meanwhile, pores with size lesser than 3 nm always reduce the methanol oxidation. Since the pore size is too small, there will be no efficient supply of fuel which will reduce the activity of the catalyst. Hence, pores with size 3-8nm are very useful for the diffusion of methanol fuel

16

(Antolini, 2009; Wang *et al*., 2016). (McBreen *et al*., 1981) also reported the dispersion of Platinum deposited by colloidal method on Vulcan XC-72, Regal 600R, Monarch 1300, CSX98 and Mogul L. It was revealed that Vulcan XC-72 and Regal 600R show better Platinum dispersion than others. The high Platinum dispersion on VulcanXC-72 was assigned to its high internal porosity while that of Regal 600R was assigned to surface properties of the carbon support which led to a very strong Platinum-Carbon synergistic interaction. The comparison between Vulcan XC-72R and high surface area graphite (HSAG) 300 Lonza materials has also been reported. Results showed that catalyst supported on Vulcan XC-72R has higher active surface area than the one supported on HSAG (Antolini, 2009).

2.2.1.1   *Activation of Carbon Black*

In general, it is expected that inert catalyst support materials are activated before their use in order to increase their catalytic activity and metal dispersion. This can be done in two ways namely: physical activation or thermal treatment and chemical activation or oxidative treatment (Antolini, 2009).

2.2.1.1.1 **Physical Activation**

The physical activation involves thermal treatment or heating of carbon support which is done under inert atmosphere (800-1100 ºC) or in air/steam (400-500 ºC) with the intension of removing any impurity present at the surface of the support. It was reported by (Oliveira-Netoa *et al*., 2003) during their research on the preparation of carbon-supported Platinum using Vulcan XC-72 powder, Shawinigan black and fullerene soot that thermal treatment was carried out on these supports under two conditions: argon atmosphere at 850 ºC for 5 hours followed by steam at 500 ºC for 2 ½ hours. Cyclic voltammetry (CV) measurement revealed, after the two treatments, that all the carbon supports exhibit an increase in capacity current because of removal of surface impurities. Due to this treatment, the Platinum catalyst showed an increase of about 50% active surface area for both Vulcan and Shawinigan carbon supports. It was noted that the active surface area for Platinum supported on Shawinigan carbon was smaller compared to that of Platinum supported on Vulcan carbon. However, Platinum supported on Shawinigan and fullerene supports exhibit similar active surface area which is smaller than that of Platinum supported on Vulcan support. Tafel plots for oxygen reduction showed that the catalyst supported on Vulcan and Shawinigan show similar activities and both are superior to catalyst supported on fullerene support (Antolini, 2009).

2.2.1.1.2 Chemical Activation

Chemical activation is an oxidative pre-treatment of catalyst supports which has become indispensable in determining the catalytic activity of carbon-supported catalysts. It has been reported that the surface chemistry of carbon i.e. surface functional groups, is of paramount importance in determining the catalytic activity of carbon support materials. This chemical activation increases their catalytic activity and metal dispersion (Derbyshire *et al*., 1986). The oxygen-containing functional groups introduced into the surface of the carbon supports as surface oxides during oxidative treatment such as carboxylic, lactonic, phenolic and etheric groups among others, provide binding sites or anchor for the catalyst particles and they are also responsible for both the redox and acid/base properties of the supports (Li *et al*., 2015; Poh *et al*., 2008; Rajalakshmi *et al*., 2005; Sepúlveda-Escribano *et al*., 1998; Wang *et al*., 2006). However, they do not increase the quantity of the metal particles binding to the supports (Coloma *et al*., 1994; Ehrburger *et al*., 1976). Meanwhile, the effect of oxidative pre-treatment of carbon support materials on Pt group metal dispersion has resulted into contrasting and antithetical results in literature reports. According to some researchers, (Antolini, 2009; Torres *et al*., 1997), the dispersion of the metal nanoparticles increases as the number of the oxygen surface groups in the support materials increases. It has been reported that the treatment of the carbon supports with oxidizing agents such as HNO_3/H_2SO_4, H_2O_2, O_3 and O_2 result into the formation of surface acidic sites but destroying surface basic sites. (Torres *et al*., 1997) revealed that the effect of these oxidizing agents can be attributed to the nature of the functional groups present on the surface of the carbon supports. Carbon supports treated with HNO_3/H_2SO_4 have shown a high density of both the strong and weak acid sites whereas those treated with H_2O_2 and O_3 showed a high concentration of weak acid sites. The isotherm of H_2PtCl_6 catalyst in the liquid phase at 25 ^oC revealed a stronger binding interaction of the precursor of the metal with a carbon of low acidic properties such as those treated with H_2O_2 or O_3 than with high acidic carbon treated with HNO_3. The carbon supports treated with a weak oxidizing agent, which form moderate acidic sites and exhibit strong interaction with H_2PtCl_6 during impregnation would facilitate Platinum dispersion on the surface of the carbon supports (Torres *et al*., 1997). It has also been argued that the size and the loading efficiency of metal clusters depend on the surface characteristics of the carbon supports and their method of preparation (Kim & Park, 2006). Carbon supported Platinum, treated with a base, has also been reported to show the smallest particle size and highest loading among the carbon-supported Platinum catalyst that were chemically treated. It was noted that the electroactivity of the catalyst was improved when the carbon supports were treated with basic or neutral agents. The reverse was the case for acid-treated carbon support Platinum which experience decay in their

18

electroactivity (Antolini, 2009). (Suh *et al*., 1993; Fraga *et al*., 2002; Torres *et al*., 1997) have reported that the dispersion of metal particles increases with increasing number of oxygen surface group in the carbon supports but (Coloma *et al*., 1994; Ehrburger *et al*., 1976; Román-Martínez *et al*., 1995) reported that the presence of surface oxygen-containing functional group on supports reduces the metal particle dispersion. This was buttressed by (Guerrero-Ruiz *et al*., 1998) that micro-calorimetric measurement of CO adsorption showed that the presence of oxygen surface groups reduces the metal-support interaction. The reduction in the Platinum particles dispersion with an increase in the total surface oxygen is as a result of the decrease in the number of surface basic sites which happens to be the centers for strong adsorption of the metal particles. The dependence of Platinum dispersion on oxygen and the total surface oxygen content of the support has also been reported. The quantity of Platinum particles deposited and retained on the support depends on the oxidative treatment of the carbon support materials (Fraga *et al*., 2002).The surface of carbon supports can also be functionalized by citric acid treatment. This results in the formation of functional groups like carboxyl which produces acidic sites and hydroxide which produces basic sites (Poh *et al*., 2008). They also found that Platinum nanoparticles which were deposited on Vulcan XC-72 carbon by microwave-assisted polyol process after being functionalized by citric acid treatment showed smaller particle size than those deposited on unfunctionalized carbon.

The activity of methanol electro-oxidation of Pt-Ru catalysts supported by ozone-treated Vulcan XC-72 and untreated carbon has been examined. The cyclic voltammetry of CH_3OH/H_2SO_4 solution revealed that the catalytic activity of Pt-Ru catalysts supported on O_3-treated carbon for methanol oxidation is higher than that supported on unfunctionalized carbon (Wang *et al*., 2006). Some researchers have also reported that carbon black functionalized using C_2F_2 radio frequency plasmas is very useful as electrocatalyst support for PEMFC catalyst. They reported that the hydrophobic state of the support and the distorted electronic state of the supported Platinum particle are responsible for the improvement of the catalytic activity (Shioyama *et al*., 2006). (Fuente *et al*., 2006) submitted that CO oxidation depends on the nature of the support instead of the nature of the Platinum particle when investigated the effect of chemical modification of Vulcan XC-72R on the activity for H_2/CO oxidation of Platinum nanoparticles. Above all, the oxidative pre-treatment of support materials using HNO_3/H_2SO_4 has been discovered to be the best among others as this has been widely used and reported with better positive results (Gui *et al*., 2013; Khotseng *et al*., 2016; Malek Abbaslou *et al*., 2009; Moraes *et al*., 2011; Ramli & Kamarudin, 2018; Wang *et al*., 2005).

2.2.1.2 Disadvantages of Carbon Black

The synergy between the features of carbon black supports and its effect on the stability of both the supports and the supported metals has been reported. Sintering of Platinum particles and Platinum release from the carbon black support materials is usually caused by the instability of carbon black support materials which affects the loss of Platinum surface areas. (Stonehart, 1984; Uchida *et al*., 1995; Wang *et al*., 2007; Watanabe *et al*., 1988). (Uchida *et al*., 1995) carried out a durability test on carbon black support materials in sulphuric acid solution at 60 ⁰C and observed that there was a change in the colour of the sulphuric acid solution which indicated the dissolution of carbon black support materials. The colour from carbon blacks with the larger surface area were darker than those from carbon black with small surface area and those from the furnace blacks were darker than those from acetylene blacks. Therefore, the furnace black with a larger surface area is likely to be more soluble and unstable. X-ray fluorescence measurement showed that some impurities were present in the acetylene blacks. However, Ca, S, Fe, and Cl were discovered as impurities in the furnace black which could affect the solubility of the carbon blacks (Uchida *et al*., 1995).

(Wang *et al*., 2007) have also argued that Vulcan XC-72 has a higher corrosion resistance than black pearl 2000 (BP-2000) when investigated the effect of carbon black support corrosion on the stability of Pt/C catalyst. It was noted that Pt/Vulcan performed better than Pt/BP-2000. The result of XPS analysis revealed that fewer Platinum particles were retained on the Pt/BP-2000 compared to Pt/Vulcan catalyst after durability test. XRD result also revealed that Pt/BP-2000 catalyst exhibits higher Platinum size growth. The decrease in the performance of Pt/BP-2000 was due to its low corrosion resistance.

The effect of pH value during impregnation of Platinum precursor on carbon black support materials with thermal treatment at high temperature has been reported. It was noted that the lower the pH, the lower the activation energy of the particle growth. The mechanism of Platinum particle growth and the stability of metal particle depend on the acid-base surface properties of the carbon black support materials. The oxygen-containing functional groups present at the surface of the carbon black support materials act as a binding site for metal particles thereby promoting their dispersion (Antolini, 2009).

Despite the advantages offer by carbon blacks, they still suffer some limitations. Acetylene black could not exhibit highly dispersed surface area; although, Ketjen black exhibit better surface area

20

for highly dispersed nanoparticle catalysts, it still suffers setback in mass transportation and high ohmic resistance during fuel cell operation (Raghuveer & Manthiram, 2004) while Vulcan XC-72 still suffers from high carbon corrosion and degradation of the catalyst due to its large number of defect sites and long term DMFCs working condition (Li *et al*., 2015; Ranganathan *et al*., 1999; Shaari & Kamarudin, 2017; Wang *et al*., 2016) and its nanoparticles are not monodispersed (Antolini, 2009). Other setbacks of carbon black support materials include deep crack surface (Raghuveer & Manthiram, 2004) side reactions which produces H_2O_2, low surface area, low resistance to corrosion caused by electrochemical oxidation of the carbon surface (Antolini, 2010) and poorly connected micropores in the amorphous particles of carbon black which prevent the smooth supply of the methanol fuel. This usually result into limited mass transfer and low catalytic performance (Wang *et al*., 2016).

2.2.2 Recent/Modern Carbon Materials

Various recent and modified carbon materials, which are nanostructured carbon materials, have been investigated and reported as catalyst support materials in DMFCs because of their different nanoarchitectural structures. These nanostructured carbon materials include multi-walled carbon nanotubes (Akalework *et al*., 2012; Daoush & Imae, 2012; Lee *et al*., 2006; Sahoo *et al*., 2015; Zhang *et al*., 2018; Zhu *et al*., 2008) carbon nanofibers (Antolini, 2009; Boskovic *et al*., 2005; Knupp *et al*., 2008; Yuan & Ryu, 2004), graphene (Anwar *et al*., 2019; Avouris & Dimitrakopoulos, 2012; Bharti & Cheruvally, 2017; Emiru & Ayele, 2017; Park *et al*., 2018; Seselj *et al*., 2015; Shaari & Kamarudin, 2017), graphene oxide (Bojarska *et al*., 2019; Chen *et al*., 2012; Farooqui *et al*., 2018; Gupta *et al*., 2017; Pandey *et al*., 2017; Sohail *et al*., 2017; Zakil *et al*., 2016) among others with their N-doped counterparts (Chen *et al*., 2011; Du *et al*., 2008; Higgins *et al*., 2010; Long *et al*., 2010; Maiyalagan *et al*., 2005; Narreddula *et al*., 2019; Vinayan *et al*., 2012; Wang *et al*., 2012; Wei *et al*., 2012; Xiong *et al*., 2013; Xu *et al*., 2013) and hybrids (Anwar *et al*., 2019; Jafri *et al*., 2010; Jha *et al*., 2011; Aravind *et al*., 2011; Lee *et al*., 2006; Li *et al*., 2015; Pham *et al*., 2016; Ramesh *et al*., 2008; Wang *et al*., 2014; Zhao *et al*., 2016) . Their special physicochemical structures have led to better stability and catalytic activity through their physical and /or chemical modifications. Under despotic or severe chemical and electrochemical oxidation conditions, these new carbon materials appear to prevent some durability matters like carbon corrosion, Platinum dissolution and aggregation and Ostwald ripening owing to their unique structures and synergistic relationship with metal nanoparticles during fuel cell operations (Li *et al*., 2015; Wang *et al*., 2016). It is very important to note that the porosity and texture of carbon materials play a vital role in the efficacy of electrocatalyst. Hence, the International Union of Pure

21

and Applied Chemistry (IUPAC) has categorized pores to their width as micropores (< 2 nm), mesopores (2-50 nm) and macropores (>50 nm). Though, carbon black exhibit large specific surface area but comprises majorly micropores less than 1nm which makes the easy supply of fuel a bit difficult thereby limit the electrocatalytic activity. When the average diameter of the pore is less than 2 nm, smooth supply of fuel becomes a big challenge (Antolini, 2009).

It has also been reported that carbon support with high surface area and good crystallinity enhance electron transfer despite providing high dispersion of metal nanoparticles resulting in better fuel cell performance (Park *et al*., 2004). This has now led to more research focused on carbon-based nanostructured materials with good porosity and graphitized structure such as carbon nanotubes, carbon nanofibers, mesoporous carbon and graphene which have also been considered recently as new catalyst support materials for DMFC catalysts. This is as a result of their specific characteristics which include better crystalline structure with high electrical conductivity, high surface area, good corrosion resistance, low CO poisoning, better purity, good pore length and connectivity, better pore size distribution and relatively good stability in acidic and alkaline media compared to the conventional carbon back during extended use and repeated cycling under fuel cell operation (Antolini, 2010; Wang *et al*., 2016). They exhibit different morphology at nanoscopic level with respect to their pore texture (such as mesoporous carbon) and at macroscopic level with respect to their form (such as microsphere) compare to carbon black (Wang *et al*., 2016). They can be synthesized in form of microsphere as in ordered mesoporous carbons (OMCs), using spherical template (Ryoo *et al*., 2001) and carbon gels (Kim *et al*., 2006), or grow directly on the surface of carbon (Su *et al*., 2006), polymeric (X.-J. Huang et al., 2006) or metal (Han *et al*., 2006) microsphere as in carbon nanotubes. Carbon microspheres (CMSs) can be synthesized by ultrasonic spray pyrolysis (USP) (Bang *et al*., 2007; Skrabalak & Suslick, 2006), template method (Ryoo *et al*., 2001), hydrothermal method (Xu *et al*., 2007) and sol-gel method (Kim *et al*., 2006). Carbon microspheres have a diameter of about 1-2µm which is significantly higher than that of carbon black (Antolini, 2009).

However, based on higher surface area, higher electrical conductivity, greater mechanical and electrical properties, better crystallinity and stability, higher charge transport mobility, presence of large oxygen containing functional group which can easily disperse catalyst nanoparticles and oxidize accumulated CO thereby enhancing the electrocatalytic activity, better resistance against carbon corrosion during fuel cell operation, higher tendency to introduce chemically active sites for reaction and anchoring sites for metal deposition among others than other recent carbon support

materials (Antolini, 2009; Farooqui *et al*., 2018; Guo & Sun, 2012; Munjewar *et al*., 2017; Priya *et al*., 2014; Samad *et al*., 2018; Sharma & Pollet, 2012; Wang *et al*., 2016; Zhou *et al*., 2014), carbon nanofibers, multi-walled carbon nanotubes and graphene with their nitrogen-doped counterparts and hybrids were used as catalyst support materials in this study which are discussed below.

2.2.2.1 *Multi-walled Carbon nanotubes (MWCNTs)*

2.2.2.1.1 *Structural features*

The MWCNTs are hollow tubular structures with a highly graphite multilayer wall. As a result of their unique structural and electrical properties, they have been discovered to be the best nanostructured carbons with good result as catalyst support for DMFCs. They are more stable and highly conductive because of their high crystalline status (Wang *et al*., 2016). MWCNTs are more stable and can outlast the lifetime of Vulcan XC-72 (Prabhuram *et al*., 2006). Special features of MWCNTs which also make them useful as catalyst supports are their moderate outer diameter, inner diameter and length. Research reports have also revealed that MWCNTs are better than carbon black as catalyst support for DMFCs (Li *et al*., 2015). MWCNTs are two-dimensional cylindrical nanostructure tubes which are formed by rolled-up single sheet of hexagonally arranged carbon atoms. They can exist as single-walled carbon nanotubes (SWCNTs) or multi-walled carbon nanotube (MWCNTs), depending on the structure. A SWCNTs is a graphene sheet rolled into a cylindrical shape and a MWCNTs is a coaxially arranged graphene rolled into a cylinder as shown in Figure 4a and 4b respectively. The MWCNTs are stacked onto each other, accompanied by many carbon nanoparticles and carbonaceous impurities (Antolini, 2010).

(a)   (b)
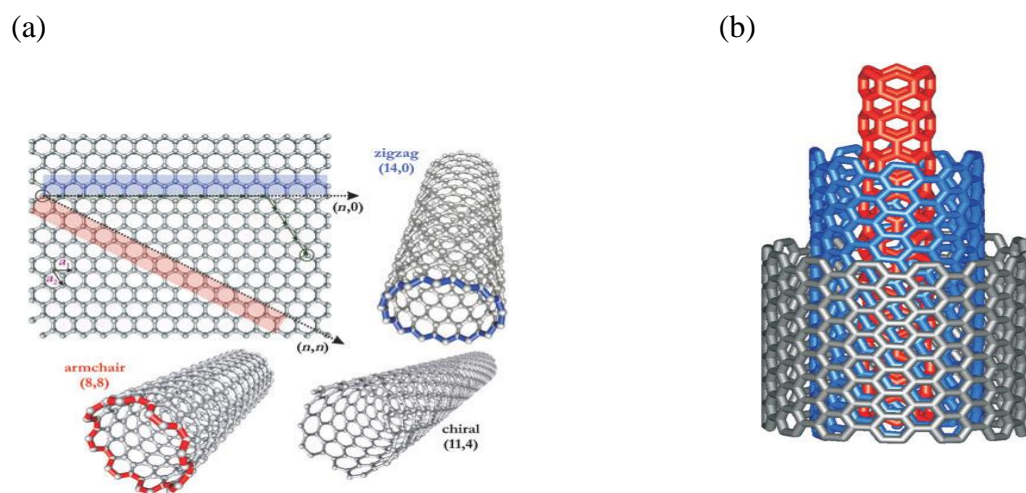
Figure 2.3: The structures of SWCNTs (a) and MWCNTs (b).

Source: (Balasubramanian & Burghard, 2005)

Studies have revealed that SWCNTs provide larger surface area while MWCNTs are more conductive when compare the two (Sharma & Pollet, 2012). According to (Serp, 2003), pores in MWCNTs are divided into inner hollow cavities of diameter between 3-6nm (narrowly distributed) and aggregated pores of diameter 20-40 nm (widely distributed) formed by interaction of isolated MWCNTs. MWCNTs with small tube diameter and high surface area can be obtained using small catalyst particles for synthesis (Wang *et al*., 2004). Theoretically, SWCNTs can either be metallic or semiconducting depending on the tube diameter and helicity (Saito *et al*., 1992). However, scanning tunneling spectroscopy (STS) measurement revealed that MWCNTs conductivity is due to the outer shell which is usually larger than SWCNTs. Hence, MWCNTs should exhibit relatively high electrical conductivity (Kasumov *et al*., 1998). It has also been reported that MWCNTs are more active than the conventional carbon black (Vulcan XC-72) because of their unique structural features (Antolini, 2009; Guo *et al*., 2008; Li *et al*., 2003; Maiyalagan *et al*., 2005; Prabhuram *et al*., 2006; Wei *et al*., 2008) Furthermore, the nitrogen-doped multi-walled carbon nanotubes (N-MWCNTs) have also been reported to improve the catalytic activity of catalysts. N-MWCNTs was reported to enhanced the catalytic activity of Platinum catalyst by ten folds compared to the conventional Vulcan XC-72 supported catalysts (Maiyalagan *et al*., 2005). This was ascribed to the higher dispersion and good interaction between the support and the Platinum nanoparticles. According to the authors, the nitrogen functional group on the surface of MWCNTs intensifies the electron withdrawing effect against the Platinum and the decrease in electron density of Platinum facilitate the oxidation of methanol fuel (Maiyalagan *et al*., 2005). This optimum amount is about 10 % which implies that the isolated nitrogen sites favours the better crystallite size (Antolini, 2009). The N-dopants in MWCNTs also serve as the defect sites to enhance the nucleation of Platinum catalyst nanoparticles (Du *et al*., 2008).

In terms of stability, N-doped supported catalysts have been investigated and reported to be more stable than the conventional supported catalysts. The N-doped MWCNTs electrodes were discovered to be the most stable for direct methanol electrooxidation. This was attributed to the tubular morphology and the nitrogen functionality of the support which influenced the better dispersion and enhanced stability of the electrode (Maiyalagan *et al*., 2005). The higher the nitrogen functional group on the MWCNTs support materials which prevent the catalyst agglomeration, the better the catalyst activity. A strong metal-support link which is induced by the presence of nitrogen on the surface of the support materials resulted into decrease in accumulation of carbon monoxide ($CO_{(ads)}$) on the Platinum catalyst thereby increasing the catalyst poison tolerance (B. Xiong et al., 2013)

2.2.2.1.2 Synthesis methods

MWCNTs can be synthesized using carbon-arc, discharge, laser ablation of carbon, chemical vapour deposition (CVD) and plasma enhanced chemical vapour deposition (PECVD) (Chhowalla *et al*., 2001; Hofmann *et al*., 2003; Li *et al*., 2003; Ren *et al*., 1998). Li *et al* prepared MWCNTs using high-purity graphite in a classical arc-discharge evaporated technique. However, due to high curvature and inertness of MWCNTs surface, it is difficult to bind metal nanoparticles to the support surface (Li *et al*., 2015; Li *et al*., 2003). Pre-treatment of MWCNTs has therefore become imperative before metal deposition to obtain optimal and strong synergistic interaction between the metal precursor and the support (Priya *et al*., 2014). Some oxygen-containing functional groups like carbonyl, carboxyl, hydroxyl, phenolic, lactonic, etheric etc. and defect sites are introduced onto the support surface by harsh acid oxidation such as refluxing in nitric and sulphuric acids at varying temperature 90-140 °C (Alexeyeva *et al*., 2011; Prabhuram *et al*., 2006; Wei *et al*., 2008; Xing, 2004). These serve as a nucleation center and binding sites for subsequent anchoring and reductive conversion of precursor metal ions to metal nanoparticles so that the metal nanoparticles can attach to the MWCNTs surface easily (Rajalakshmi *et al*., 2005). Meanwhile, this activation of MWCNTs surface can take place not only before but also after the metal deposition on the carbon supports (Antolini, 2009).

MWCNTs has been previously prepared using sodium nitrite to produce intermediate diazonium salts from substituted anilines, forming benzene sulfonic group on the surface of the MWCNTs which increases the solubility in water (Hudson *et al*., 2004; Stephenson *et al*., 2006). (Yang *et al*., 2008) dispersed Palladium particles on the MWCNTs which were functionalized in a mixture of sulfuric acid and 4-aminobenzenesulfonic acid. TEM image revealed that Palladium dispersion on unsulfonated MWCNTs is low and large Palladium cluster can be seen. However, higher Palladium dispersion was observed on sulfonated-multiwall carbon nanotubes (S-MWCNTs) despite little agglomeration of Palladium nanoparticles on the support. This is as a result of chemically active and hydrophilic surface of MWCNTs after benzene sulfonic treatment. Although, this functionalization process introduces nucleation sites for the catalyst nanoparticles, however, the introduction of defect sites and oxygen containing functional groups denature the graphitized MWCNTs surface. This reduces the conductivity of the MWCNTs and accelerates its corrosion (Bojarska *et al*., 2019; Priya *et al*., 2014). These setbacks result to low efficiency in catalytic performance (Li *et al*., 2015). Doping with heteroatoms such as nitrogen (Higgins *et al*., 2010) to modify the support surface has also been found to improve the morphology of MWCNTs. Nitrogen-doped multi-walled carbon nanotubes (N-MWCNTs) has been investigated and found to

25

exhibit a bamboo-like structure with diameter over 100 nm, BET surface area of about 870 m^2/g in which 450 m^2/g was discovered to be electrochemically accessible. The presence of nitrogen atom enhances the mass transfer and catalyst loading sites and stability (Hung et al., 2016; B. Xiong et al., 2013).

(C. Kim et al., 2004; K. Lee et al., 2006; Matsumoto et al., 2004) reported the synthesis of MWCNTs and nanofibers-supported Platinum catalysts for PEMFC. It was noted that without functionalization, most MWCNTs are deficient of enough binding sites for anchoring precursor metal ions which resulted to poor dispersion and agglomeration of metal ions especially at high loading conditions. Only less than 30 wt% Pt/MWCNTs catalyst was obtained due to high Platinum loading on untreated MWCNTs which tend to agglomerate. It can be seen that most of the support, after pre-treatment by purification and slow oxidation in a mixture of HNO_3 and H_2SO_4, are isolated and virtually no carbon nanoparticle agglomeration is observed. Deposition, distribution and crystalline size of metal nanoparticles supported on MWCNTs are mainly affected by synthesis method, metal precursors and oxidative treatment. (Moraes *et al*., 2011) investigated the electrochemical effect of acid functionalization of MWCNTs to be used in sensors development. It was revealed that acid (HNO_3/H_2SO_4) functionalization significantly improves the electrotalytic properties of the multi-walled carbon nanotubes. This was also corroborated by (Malek Abbaslou *et al*., 2009) when they investigated the effect of pre-treatment on physico-chemical properties and stability of MWCNTs supported Iron Fischer-Tropsch catalyst. It was noted that the acid treatment increased the number of defects which were considered as anchoring site for metal particles. (Gui *et al*., 2013) also reported in their study on multi-walled carbon nanotubes modified with (3-aminopropyl)triethoxysilane for effective carbon dioxide adsorption that more amine groups were well attached covalently on the MWCNTs surface due to the presence of high binding sites as a result of the acid pre-treatment. Hence, the mixture of HNO_3/H_2SO_4 acids was used for pre-treatment of the carbon support materials in this study.

Despite MWCNTs is one of the preferred supports for catalysts, its synthesis, metal loading and electrode preparation still have challenges in DMFCs development. Another challenge of MWCNTs as catalyst support is how to use them to fabricate high-performance working electrode. Using MWCNTs' properties like electrical, mechanical and structural could be of good help in developing new electrode structure (Anwar *et al*., 2019). This aspect was part of the focus of this study.

2.2.2.2 Carbon nanofibers or Graphite nanofibers

2.2.2.2.1 Structural features

Carbon nanofibers (CNFs) or Graphite nanofibers (GNFs) have also been discovered as new nanostructure support materials for electrocatalyst. They show high surface area to volume ratio when used in different applications (Munjewar *et al.*, 2017). Due to their unique structure, their application as catalyst support in fuel cells has drawn a lot of attention (Bessel *et al.*, 2001; Park & Baker, 1998, 1999; Park *et al.*, 2007; Steigerwalt *et al.*, 2001). CNFs have also been reported to show better electrical conductivity and higher surface area than carbon black. There are various types of CNFs which include platelet, ribbon, tubular, fishbone, herringbone or cup-stacked, spiral etc. depending on the atomic structure as shown in Figure 2.4. Platelets and herringbone structures show surface oxygen groups for metal anchoring (Antolini, 2009; Anwar *et al.*, 2019).

(a)   **(b)**

(c)
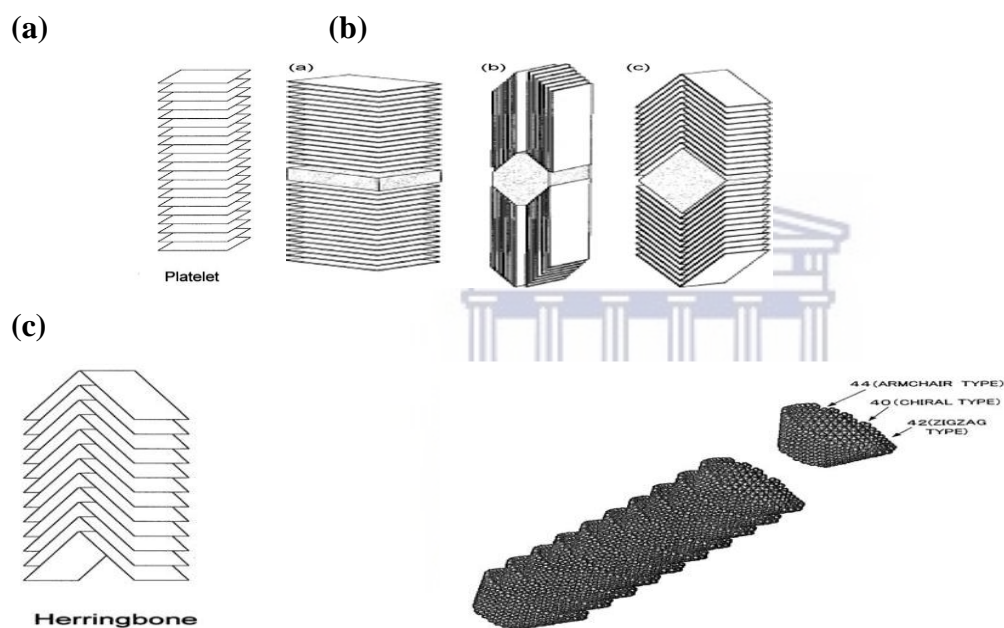
Figure 2.4: The schematic representations of (a) the platelet, (b) ribbon and (c) herringbone or cup-stacked structures of CNFs

Source: (Ermete Antolini, 2009; Tessonnier, 2017)

In CNFs, only the edge regions are exposed unlike in graphite and nanotubes materials where the basal plane is also exposed. CNFs also lack hollow cavity and are used as supports without any chemical pre-treatment (unlike graphite and nanotubes) due to the presence of highly active edge planes on which the electrocatalyst nanoparticles are bonded (Antolini, 2009).

2.2.2.2.2 Synthesis methods

Synthesized CNFs are new support materials obtained from decomposition of carbon-containing gases over some metals surface. A lot of investigations have been carried out on CNFs by researchers using thermal CVD at temperature between 600-660 °C. CNFs was synthesized on the surface of carbon fibers in an ethylene-hydrogen environment using copper-nickel catalyst in ration 3:7 at 600 °C. The introduction of carbon nanofilaments on the surface of the fibers strengthens the surface by forming interlocking networks and by increasing the surface area (Down & Baker, 1995). (Boskovic *et al*., 2005) synthesized CNFs on a carbon fiber cloth using plasma enhanced chemical vapour density (PECVD) from a gas mixture of acetylene and ammonia. Cobalt colloid is used as catalyst to enhance better coverage of nanofibers on the surface of the carbon fibers in the cloth. The CNFs formed exhibit bamboo-like structure, showing higher degree of crystallinity and graphene layers with characteristic interlayer spacing of 0.34 nm. Three types of CNFs have been prepared by CVD method namely ribbon, spiral and platelet-like CNFs. Their surface area was 85, 45 and 120 m^2g^{-1} respectively while the diameter and length varied from 100-50 nm and 5-50 µm respectively (Park & Baker, 1998, 1999) . (Gangeri *et al*., 2005) also obtained CNFs by CVD on two different types of micro-shaped carbon fibers support. Low magnification TEM image revealed the absence of hollow cavity in some parts, showing no metallic particle because they were covered by carbon. High magnification TEM image however, showed that CNFs were herring-bone. Some authors have also reported the synthesis of CNFs-supported catalysts in fuel cells; their metal dispersion and electrocatalytic activity were compared with that of commercial carbon (Gangeri *et al*., 2005; Yuan & Ryu, 2004)

2.2.2.3 Graphene

2.2.2.3.1 Structural features

Graphene has recently been discovered as a highly prospective support in PEMFCs applications due to its unique conductivity, high charge-transport mobility, better transparency, high mechanical flexibility, good elastic properties, large surface area and thermal properties (Farooqui *et al*., 2018; Guo & Sun, 2012; Priya *et al*., 2014; Samad *et al*., 2018; Zhou *et al*., 2014) . It is a two dimensional one-atom thick planer sheet of hexagonally arrayed, 2-D sp^2 carbon atom which can provide resistance against carbon corrosion during PEMFC operation (Priya *et al*., 2014; Samad *et al*., 2018). Graphene surface contains oxygen functional groups which can easily disperse catalyst nanoparticles and oxidized accumulated CO thereby enhancing the electrocatalytic activity (Priya *et al*., 2014). However, the relatively inert and hydrophobic nature of their surface does not enhance the deposition of Platinum nanoparticles (Li *et al*., 2015).

28

2.2.2.3.2 Synthesis methods

Graphene can be synthesized by several techniques which include chemical reduction (Stankovich *et al*., 2007), electrochemical method (Tripathi *et al*., 2013), solvothermal synthesis with pyrolysis (Choucair *et al*., 2009) and chemical vapour deposition (Avouris & Dimitrakopoulos, 2012). Graphene oxide (GO) can also be synthesized by different methods but the most widely used, common and low-cost technique is the oxidation of graphite to GO using a strong oxidizing agent and strong mineral acid followed by exfoliation in water as shown in Fig. 2.5 (Farooqui *et al*., 2018). This facilitates good dispersion of catalyst nanoparticles and reduces the challenge of stability. To synthesize graphene nanosheets (GNS) however, the exfoliation stage is followed by reduction of GO to GNS using strong reducing agent. The most important step in GNS synthesis is the reduction stage as it removes the oxygen functional group from GO and reinstate the electrical features of the synthesized graphene (Stankovich *et al*., 2007). During this process of reduction, the brown dispersed GO particles turned black, agglomerated and eventually formed precipitates. This implies that the reduced graphene oxide (rGO) had become less hydrophilic as a result of the removal of oxygen functional groups (Stankovich *et al*., 2006, 2007).
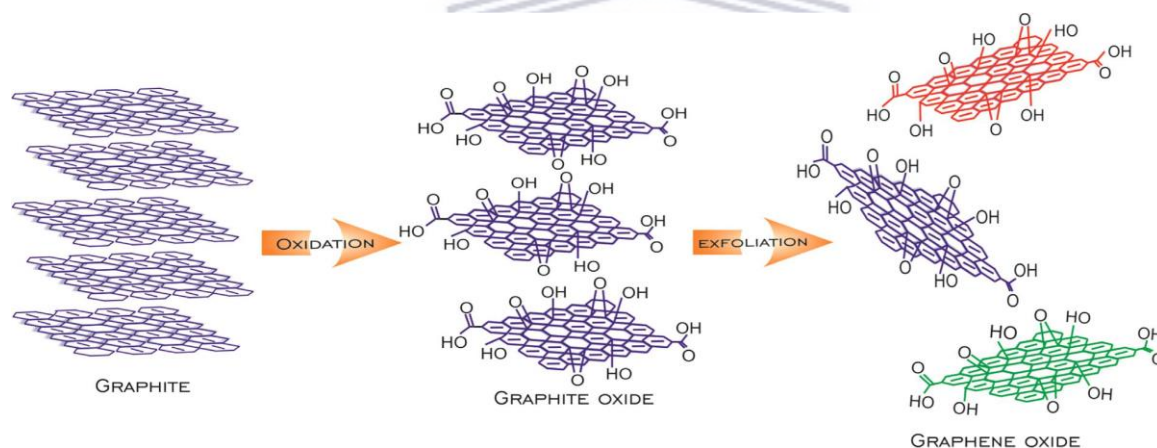
Figure 2.5: Synthesis of graphite oxide and graphene oxide (GO) from natural graphite
Source: (Farooqui *et al*., 2018).

(Stankovich *et al*., 2007) synthesized GO as an intermediate product to produce reduced graphene oxide (rGO). They discovered hydrazine hydrate ($H_2NNH_2.H_2O$) as the best reducing agent to produce a very thin graphene. The rGO showed a notable increase in carbon to oxygen atomic ratio of 10.3 as against GO with 2.7. (Cheng et al., 2014; EunJoo Yoo et al., 2009) reported the features of graphene as catalyst support in a nanosheets form. It was noted that graphene nanosheets (GNS) exhibit better catalytic activity compared to commercial carbon because of the higher carbon spaces and defects in GNS, causing good synergistic interaction between the metal

nanoparticles and the support materials (EunJoo Yoo et al., 2009). GNS with pores was further examined and discovered that it significantly enhanced the electrochemical activity due to increase in the mass diffusion rate and reaction rate caused by the pores (Cheng *et al*., 2014). However, since the inert and hydrophobic nature of graphene surface does not enhance the deposition of catalyst nanoparticles, graphene can be functionalized with heteroatoms like B, N, P, S and Se. Among these heteroatoms, nitrogen has the larger electronegativity (Groves *et al*., 2012).

Nitrogen-doped graphene (NG) has been discovered as a prospective carbon support material in fuel cells. This is due to its good mechanical properties, ability to introduce chemically active sites for reaction and anchoring sites for metal nanoparticles deposition, modify electronic properties and give carbon materials a metallic character (Qu *et al*., 2010; Wang *et al*., 2012). In addition, the extent of dispersion of the catalyst nanoparticles increases with increasing nitrogen content (He *et al*., 2013; Muhich *et al*., 2013; Wu *et al*., 2008).. When compared with commercial supported catalyst, the performance of nitrogen-doped (N-doped) supported catalyst was twice that of commercial supported catalyst (Li *et al*., 2015). N-doped graphene oxide has also been noted to exhibit good stability and oxidation current overtime (Xiong et al., 2013). It's 2D-structure has been reported to enhance electron transfer (Wu *et al*., 2007). The incorporation of dopant nitrogen atoms which exhibit electronegativity with carbon atoms in the graphitic lattice could result into polarization in the SP^2 hybridized network and regroup of the electronic state (Zhao *et al*., 2020). This dopant nitrogen present on the surface of the graphene significantly influenced the growth mechanism of the catalyst NPs which is not limited to controlling the size and shape of the catalyst nanoparticles (NPs) but also enhance the uniform dispersion of the catalyst NPs (Kuniyil *et al*., 2019). This in turn enhances the chemical activity, electrical conductivity and adsorption potential of the graphene materials thereby increasing the catalytic activity (Zhao *et al*., 2020). Hence, nitrogen from melamine was used as the doping element in this research work.

The stability of NG supported catalyst has also been examined and reported. Pt/NG stability was tested by running a membrane electrode assembly (MEA) which was assembled a Pt/C anode catalyst for 100 hours at a voltage of 0.5 V at 60 °C without ant back pressure. The MEA with Pt/NG as the cathode catalyst showed no degradation performance throughout the period of the testing. This showed that doping of graphene with nitrogen atoms result in strong binding between the metal nanoparticles and the graphene surface which prevent the detachment of the metal nanoparticles from the graphene support materials and their agglomeration during the fuel cell operation thereby enhancing the long term stability of the electrode. Therefore, the synthesis of

30

nitrogen-doped materials with larger amount of nitrogen atoms on graphene surfaces is highly important for enhancing the activity and stability of the Pt/NG catalyst (Li *et al*., 2015).

In summary, the main features of carbon materials and carbon supported catalyst are reported in Table 2.1

Table 2.1: Specific surface area, porosity and electronic conductivity of the different carbon materials and properties of supported catalysts.

Carbon Materials	Specific Surface Area (m^2g^{-1})	Porosity	Electronic Conductivity (Scm^{-1})	Supported Catalyst Properties	Refs.
Vulcan XC-72R	254	Mesoporous	4.0	Good metal dispersion, low gas flow	(Spendelow & Wieckowski, 2007)
OMC	400-1800	Mesoporous	$0.3x10^{-2}$-1.4	High metal dispersion, high gas flow, low metal accessibility	(Calvillo et al., 2007)
Carbon gel	400-900	Mesoporous	>1	High metal dispersion, high gas flow, high metal accessibility	(Job et al., 2006)
CNTs	400-900 (SWCNTs)	Microporous (SWCNTs)	$10-10^4$ depending on the nanotube alignment	Good metal dispersion, high gas flow.	(Prabhuram et al., 2006; Wang et al., 2006)
	200-400 (MWCNTs)	Mesoporous (MWCNTs)	0.3-3 (functionalized MWCNTs)	Low metal accessibility, high metal stability	
CNH, CNC	150	Micro/mesoporous	3-200	High metal dispersion, high gas flow,	(Sano & Ukita, 2006; Sevilla et al., 2007)
ACF	>1000	Microporous	13	Good metal dispersion, low gas flow, high metal stability	(De Miguel et al., 2002; H. X. Huang et al., 2008; Jang & Ryu, 2006; Eunjoo Yoo et al., 2008)

CNFs	10-300	Mesoporous	10^2-10^4	High metal dispersion, high gas flow, high metal stability	(Bessel et al., 2001; Kim & Park, 2006; Serp, 2003; Yuan & Ryu, 2004)
Graphene	>2000	Mesoporous	10^3-10^4	Good metal dispersion, high gas flow.	(Lee et al., 2012; Li et al., 2015)
BDD	2	_	1.5	Low metal dispersion, low metal stability, high metal stability on BDD	(Fischer & Swain, 2005)

Source: (Antolini, 2009; Wang *et al*., 2016).

2.2.3   Hybrid Supports Materials

Several carbonaceous support materials such as carbon blacks (CBs), multi-walled carbon nanotubes (MWCNTs), graphene, graphene oxides, carbon nanofibers (CNFs) and mesoporous carbon among others have been explored as electrocatalyst support materials in DMFCs. Unfortunately, DMFCs applications still suffer some setback such as high cost, low electronic conductivity, insufficient electrochemical activity, thermal instability, catalyst degradation, corrosion and short term durability. In order to alleviate some of these challenges, attention has now been drawn to the development of hybrid supports (Yin *et al*., 2013) with different carbon supports such as graphene-CB, graphene-MWCNTs, SWCNTs-MWCNTs (Li *et al*., 2012; Ramesh *et al*., 2008) or combined non-carbon and carbon supports like SnO_2-MWCNTs (Du *et al*., 2009), TiO_2-MWCNTs (Xia *et al*., 2012), IrO_2-MWCNTs (Wang *et al*., 2013), $TaNbTiO_2$-C (Li *et al*., 2015) and ITO-graphene (Kou *et al*., 2011) which are now considered as prospective catalyst supports for fuel cell electrocatalyst applications (Li *et al*., 2015).

2.2.3.1   Carbon Black-Based as Hybrid Support Materials

 (Li *et al*., 2012) impregnated carbon black (CB) particles with reduced graphene oxide (rGO) sheet which was obtained via Hummer's method with the intention of avoiding stacking rGO sheet and improve the frequency of electron transfer in the graphene sheet and across the Platinum

32

nanoparticles-rGO interface. They discovered that the well mixed rGO/CB composite structure did not only aid the catalytic activity but also improve the durability of the catalyst. The accelerated degrading testing (ADT) revealed that the final ECSA of the Platinum nanoparticles on the hybrid rGO/CB support with rGO-CB ratio 1:1 showed almost 100% of the original value after 20,000 ADT cycles which is much higher than the commercial catalyst. This excellent performance was attributed to the flexible 2-dimentional structure of rGO may act as mesh which prevents leaching of soluble Platinum nanoparticles into the electrolyte and the ability of CBs to regain and renucleate Platinum clusters (Li *et al*., 2012; Zhao *et al*., 2016). Carbon black has also been combined with metal oxide in order to obtain higher corrosion resistance, better metal support interaction and enhanced hydrophilicity with higher electrical conductivity. (Han *et al*., 2009) as reported by (Anwar *et al*., 2019) examined hybrid support comprises carbon and ruthenium oxide (C-RuO_2). It was noted that C-RuO_2 enhanced catalytic activity better than commercial carbon when RuO_2 was kept below 8%. RuO_2 was discovered to act as voltage buffer during current fluctuation. (Wang *et al*., 2014) as reported by (Li *et al*., 2015) synthesized C-$TaNbTiO_2$ support for Pt-Pd alloy catalyst for ORR. It was found to have higher specific surface area, favouring the homogenous distribution of Pt-Pd alloy nanoparticles and sufficient electronic conductivity for electron transfer between the Pt-Pd alloy nanoparticles and the support of the ORR compared to $TaNbTiO_2$ or pure carbon.

Hybrid polymer CBs supports have also been investigated. The electrochemical activity of the catalysts supported on hybrid polymer-CBs especially Vulcan XC-72, was noted to be higher than the same catalyst supported on single CBs or single polymer (Antolini, 2010). (Ermete Antolini, 2010) also reported that (Xu and co-workers, 2008) proposed PANI-C as hybrid support material. It was noted that the anti-poisoning ability of the hybrid support was three times higher than the Vulcan XC-72. The presence of PANI enhanced the water absorption on the catalyst and formation of active oxy-compound Pt-$OH_{(ads)}$ which facilitate CO oxidation to CO_2. To buttress this, (Kakaei, 2012) also examined PANI-C to enhance the interface properties for ORR. It was noted that PANI-C hybrid support showed higher ECSA and higher conductivity which enhance catalytic activity better than the commercial carbon. (Gharibi *et al*., 2010) synthesized hybrid PANI-C support by adding Vulcan XC-72 and pre-synthesized PANI doped with trifluoromethane sulfonic acid. The results revealed that PANI facilitate electron and proton conductivities at the electrode, doubled methanol diffusion coefficient and reduced the onset potential of methanol oxidation and catalyst vulnerability to poisoning (Antolini, 2010). (Aghabarari *et al*., 2013) examined chitosan derivative-CB as electrocatalyst support through Michael method with amidation process. The CB

33

was coated with chitosan derivative which served as protective layer in severe acidic condition and also provide amine groups. The amine groups showed attraction towards the metallic ions and cations formation. The BET surface area of the carbon reduced with increased chitosan materials which resulted into lower ECSA compared with commercial carbon. Despite the lower ECSA, chitosan derivative-CB still exhibited similar catalytic enhancement as commercial due to the better interaction between the support and the catalyst nanoparticles, ease of proton transfer as a result of formation of amine group and increase in electron transfer due to the presence of nitrogen atoms. Despite all these efforts, CB-based hybrid support materials still suffer from corrosion and short term stability (Anwar *et al*., 2019).

2.2.3.2 Multi-Walled Carbon Nanotubes-Based as Hybrid Support Materials

A lot of efforts have been made to combine multi-walled carbon nanotubes (MWCNTs) with other materials like single walled-carbon nanotubes (SWCNTs), conducting polymers such as polyaniline (PANI) and nitrides (such as WN & TiN). For instance, (Ramesh *et al*., 2008) investigated SWCNTs-MWCNTs hybrid as catalyst support. The SWCNTs-MWCNTs hybrid exhibited higher mass activity than SWCNTs because the addition of MWCNTs enhanced the mass transport in the catalyst layer. (Wang *et al*., 2007; Wu *et al*., 2006) synthesized PANI-SWCNTs by electrochemical polymerization of aniline with SWCNTs. (Wu *et al*., 2006) noted that PANI-SWCNTs nanocomposite film exhibited higher polymeric degree, lower defect density, increase accessible surface area, higher electronic conductivity and better charge transfer at polymer electrolyte interface compared with pure SWCNTs. (Wang *et al*., 2007) also discovered that PANI-SWCNTs showed more porous structure, higher surface area, better dispersion and stability of catalyst nanoparticles for methanol oxidation. Furthermore, (Shi *et al*., 2007) synthesized PANI-MWCNTs nanocomposite via electro-polymerization of aniline with MWCNTs. It was noted that the electrical conductivity and porosity of the PANI-MWCNTs nanocomposite was significantly higher than the pristine PANI due to the addition of the MWCNTs. This higher porosity in composite enhanced the dispersion of the catalyst nanoparticles on the composite film. The solubility and poor compatibility of MWCNTs with polymer however restricts the synthesis of polymer-MWCNTs composites. To resolve this, (Zhu *et al*., 2008) synthesized homogenous PANI-MWCNTs nanocomposite by electrochemical polymerization of aniline with pre-functionalized MWCNTs via diazotization reaction. The nanocomposite was found to exhibit higher mass activity and long term stability than only MWCNTS. (Santhosh *et al*., 2006) in their own case grafted PANI into amine-functionalized MWCNTS by electro-polymerization to produce PANI-MWCNTS nanocomposite. The grafting of MWCNTS surface

with PANI create uniform surface with positively charged protonated amine/imine sites. This stabilizes the catalyst nanoparticles and prevents their aggregation. (Kuo *et al*., 2012) synthesized hybrid support material made of N-doped carbon and surface coated MWCNTs by polymerization and oxidation of PANI over MWCNTs surface. It was reported that the mass activity and electrochemical conductivity of NC-MWCNTSPANI was higher than the commercial carbon due to the surface coating which invariably influence better dispersion of Pt Nanoparticles over the surface of the hybrid support material. Other polymers such as polypyrrole (Ppy) and Poly (N-acetyl aniline) (PAANI) polysiloxane and pyridine-polybenzimidazole (PyPBI) have also been coated on MWCNTs. Their electrostatic interaction with MWCNTs has facilitated higher degree of electron delocalization thereby enhanced the conductivity of the nanocomposite (Antolini, 2010).

Another modification strategy employed for MWCNTs-based hybrid support materials is surface coating with metallic oxide (such as TiO_2, WO_3, IrO_3, MnO_2, SnO_2) and use them as catalyst supports in order to enhance the homogenous dispersion of catalyst nanoparticles over the MWCNTs surface, improve electrical conductivity and durability (Chen *et al*., 2011; Jiang & Gao, 2003; Xia & Mokaya, 2005). To buttress this, (Xia *et al*., 2012) synthesized hybrid support by grafting TiO_2 nanosheets on MWCNTs through solvothermal process and trailed by calcination. The result showed that TiO_2-MWCNTs exhibited higher ECSA retention than MWCNTs which suggest enhanced durability. (Akalework *et al*., 2012) however, combined ultrathin Titania with MWCNTs in order to improve the surface area. It was reported that the addition of Titania on MWCNTs surface improved the ECSA as a result of good dispersion of catalyst nanoparticles in the hybrid support materials. (Meza *et al*., 2011) also examined the tungsten oxide-MWCNTs hybrid support materials for ORR in PEMFCs. WO_3-MWCNTs hybrid support material was reported to show better electrochemical stability compared with MWCNTs only (Meza *et al*., 2011). Iridium has also been tested with MWCNTs to reduce dissolution of catalyst in severe environment. (Wang *et al*., 2013) investigated IrO_2-MWCNTs hybrid support. The result showed that IrO_2 particles were evenly dispersed on MWCNTS which aided the homogenous distribution of catalyst nanoparticles on the hybrid support. In order to reduce the overall cost of PEMFCs which is a big concern for commercialization due to the high cost of catalyst, (S. Yu et al., 2014) examined MnO_2-MWCNTs. It was noted that the presence of MnO_2 enhanced oxygen reduction. O^{2-} from MnO_2 coordinate with H^+ to form MnOOH as intermediate which further converted to O_2 thereby accelerating ORR.

35

Coating of MWCNTs with tin-based materials is another means of improving corrosion resistance in MWCNTs. Meanwhile, tin-based coating may result to bi-functional mechanism which facilitates the activity of the supported catalyst while the mesoporous structure would accelerate oxygen transport towards the active site (Anwar *et al*., 2019). (Du *et al*., 2009) investigated the mesoporous SnO_2-coated MWCNTs synthesized through hydrothermal method using cetyltrimethylammonium bromide (CTAB) as catalyst support. The result revealed that the support exhibited enhanced corrosion resistance and long-term stability compared to MWCNTs. This better stability was ascribed to the mesoporous form of SnO_2 and high corrosion resistance of the support. (Sun *et al*., 2010) also synthesized SN-MWCNTs by thermal evaporation method. It was noted that SN-MWCNTs showed bi-functional effect which improve mass transport, gas permeability and metal support interaction. Despite SnO_2 serves as good support materials, it suffers from inadequate electrical conductivity coupled with poor distribution of catalyst nanoparticles at the surface. In quest to solve conductivity problem, (Guo & Jing, 2011) examined fluorine tin oxide (FTO)-MWCNTs hybrid support prepared via sol-gel process coupled with hydrothermal treatment as anode catalyst support. When compared with SnO_2-MWCNTs, FTO-MWCNTs showed better electrical conductivity and lower resistance to electron transfer. This enhanced performance was ascribed to better catalyst nanoparticles dispersion, bi-functional mechanism and electronic effect of FTO-MWCNTs (Guo & Jing, 2011). In spite of the uniqueness of MWCNTs-based hybrid supports, the coating of MWCNTs reduces the active site compared with functionalized MWCNTs and the synthetic method for MWCNTs is also difficult and costly. Moreover, stability still pose a great challenge to their usage as effective catalyst support which limits the electroactivity of the catalysts and commercialization of fuel cells (Anwar *et al*., 2019).

2.2.3.3 Graphene-Based as Hybrid Support Materials

The application of graphene as catalyst support has been limited by their agglomeration due to restacking of graphene sheets. This has led to the combination of MWCNTs with graphene to form another hybrid support material. It has been reported that when MWCNTs is squeeze between graphene layers, it facilitates mass transport in fuel cell reactions thereby overcoming the prominent restacking issue in graphene (Liu *et al*., 2019). (Jafri *et al*., 2010; Jha *et al*., 2011) tried to improve the durability of catalyst support by mixing functionalized MWCNTs (*f*-MWCNTs) with functionalized graphene (*f*-G) to form a hybrid support material. It was reported that the hybrid support with *f*-MWCNTs and *f*-G in ratio 1:1 showed better performance. This was credited to increase in the d spacing of graphene sheets by addition of *f*-MWCNTs which reduced or prevented the restacking of exfoliated graphene sheets thereby provide better surface for catalyst

loading. In addition, (Aravind *et al.*, 2011) proposed the addition of solar exfoliated graphene and functionalized MWCNTs as hybrid support. It was also reported that the hybrid support showed better performance towards ORR when compared with functionalized solar graphene only. This was credited to the synergistic interaction between the graphene and the MWCNTs. The MWCNTs provided good pathway for electron transfer with increasing the space between the basal planes of graphene thereby preventing restacking of the graphene sheet while the graphene provides good surface area for homogenous dispersion of the catalyst nanoparticles. In the case of (Sahoo *et al.*, 2015), they synthesized hybrid support material by adding partially exfoliated MWCNTs (obtained by chemical vapour deposition method followed by partial oxidation and reduction) with graphene as catalyst support for PEMFCs. The results revealed that Pt nanoparticles were evenly dispersed over the surface of the hybrid materials. The distinctive combination of 1-D MWCNTs and 2-D graphene structures facilitate the homogenous dispersion of the Pt nanoparticles which promote Pt utilization. In order to utilize the sharp graphene edges and sustaining the MWCNTs porous structure, (Pham *et al.*, 2016) developed a novel hybrid support comprises MWCNTs and graphene in which graphene was produced directly onto MWCNTs which can function as efficacious and stable hybrid support material for Pt catalyst. It was noted that this MWCNTs-graphene hybrid support material enhanced electrochemical stability better compared with commercial carbon. (Karthikeyan *et al.*, 2015) reported from their own investigation that the electrochemical performance of MWCNTs-graphene hybrid support material can also be improved by functionalization. They examined hybrid material made of few layer graphene (FLG) and MWCNTs with nitrogen and oxygen functionalities. Enhanced I_D/I_G ratio was observed for this hybrid support which obviously indicates the formation of abundant defects created mainly by pyrrolic nitrogen after nitrogen doping. This resulted into higher mass activity, better electrochemical surface area retention and durability in the hybrid support compared with commercial carbon (Karthikeyan *et al.*, 2015).

The combination of metal oxide with graphene has recently been reported to aid the performance of graphene support. For instance, (Xu *et al.*, 2013) combined niobium oxide (NbO_2) with graphene as hybrid catalyst support for ORR. The presence of NbO_2 was found to enhance the electrical conductivity and durability of the graphene support. (Kepenienè *et al.*, 2015) also synthesized Nb_2O_5-graphene as hybrid support material for Pt and Pt-Co catalysts. It was noted that Nb_2O_5-graphene performed better when compared with graphene support only. (Kou *et al.*, 2011) further grown indium tin oxide on graphene (ITO-G) as hybrid support material for Pt

37

catalyst. Pt nanoparticles were evenly dispersed on ITO-G but formed agglomeration on graphene due to restacking of the graphene sheets.

In quest to further solve this restacking problem, (Li *et al*., 2015) combined polybenzimidazole (PBI) grafted graphene and functionalized carbon black (FCB) to form hybrid support material. The results revealed that this hybrid (PBI-graphene + FCB) showed better performance when compared with CBs, PBI-CBs, graphene and PBI-graphene. This better performance was ascribed to the synergistic interaction between the graphitic nature of graphene, PBI and FCBs. PBI, being a stable and good proton conductor, enhanced the nucleation of the catalyst nanoparticles while the graphene and FCB provide a better surface area and increase the mass activity. Nevertheless, graphene-based hybrid supports exhibit numerous benefits; their large scale production for commercial purpose is not economically viable (Anwar *et al*., 2019).

Based on the review of related literature, it is highly evident that support materials are important as they contribute immensely to the activity, stability and durability of catalyst and consequently enhance the performance of the fuel cells. Despite the new carbon support materials that have been explored, the DMFCs electrocatalysts still suffer from dissolution, agglomeration, detachment from support materials and corrosion of support materials as shown in Figure 2.6. These challenges between the properties of these novel support materials and their real application under fuel cell operating system still create gaps which need to be rectified. Therefore, there is a need to modify these support materials by optimizing their properties in respect to fuel cell practical working condition by considering selection of appropriate support materials, their combination ratio (for the hybrid supports), synthesis procedure, MEA preparation and their integration into fuel cell system.
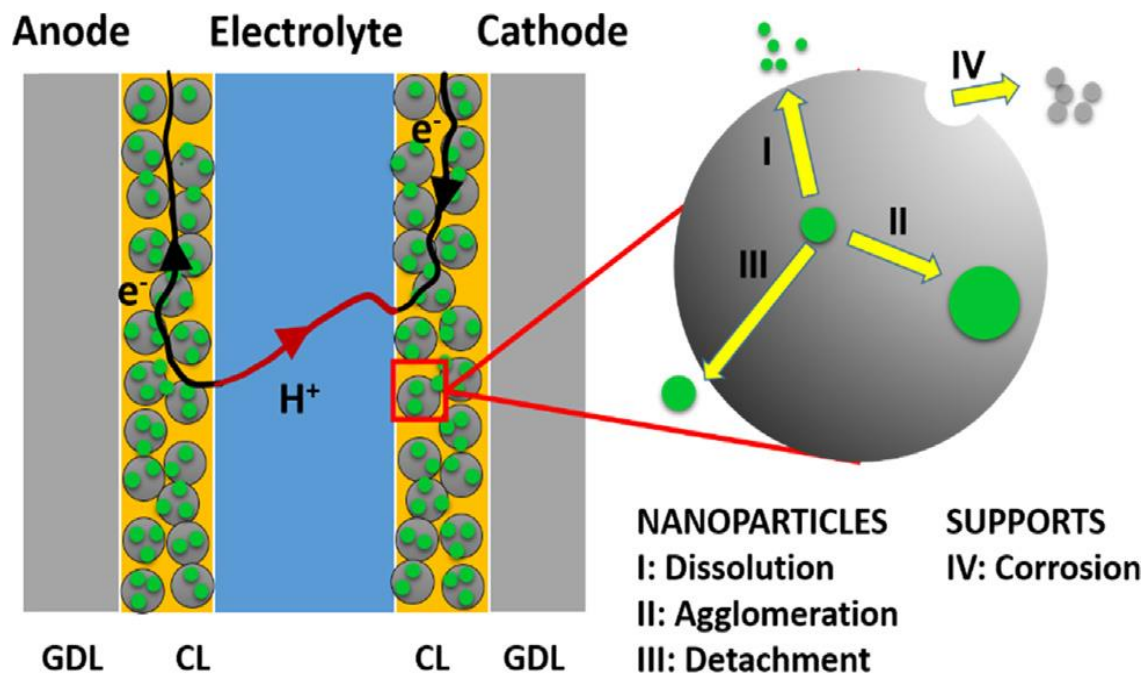
Figure 2.6: Schematic illustration of electrocatalysts degradation.

Source: (Du *et al*., 2016)

CHAPTER THREE

3 Experimental Section

3.1 Chemicals

All the chemicals used in this research are analytical purity grade and were used as received without any further purification. The chemicals used for the synthesis include Ethanol (99 %), Ethylene Glycol (99.9 %), Methanol (99.9 %), Nitric Acid (60 %), Potassium Hydroxide (85 %), Sodium Hydroxide (98.87 %) and Potassium Permanganate which were purchased from Kimix Chemical and Laboratory Suppliers, Cape Town, South Africa. Sodium nitrate (99 %), Melamine (99 %), Graphite powder, Carbon nanofibers, 2-Propanol (99.5 %) were purchased from Sigma-Aldrich while Hydrochloric Acid (32 %) and Hydrogen Peroxide (50 %) were purchased from B&M Scientific. Palladium Chloride was purchased from SA Precious Metal PTY Ltd while Nafion solution was purchased from Ion Power Inc. The MWCNTs were bought from Carbon Nano-materials Technology Co. Ltd, Gargdong, Gyongju, Gyeonggi, South Korea with a width of ∼20 nm and a length of ∼10 μm. All synthesis was done using deionized water from the Milli-Q water purification system (Millipore, Bedford, MA, USA).

3.2 Synthesis of different support materials for Palladium catalyst

3.2.1 *Functionalization of Multi-walled carbon nanotubes and Carbon nanofibers*

The as received multi-walled carbon nanotubes (MWCNTs) and carbon nanofibers (CNFs) were first oxidized in a hot solution of HNO_3/H_2SO_4 (3:1 v/v) at 65 °C under refluxing conditions for 4 hours to remove impurities and generate surface functional groups. The ratio used is the best ratio for the functionalization after other ratios have been tested. The functionalized MWCNTs and CNFs were filtered using vacuum filtration process. After filtration, the sample was washed with ultra-pure water until the pH reached 7. The samples were dried at about 60 °C for 3-4 days. (Khotseng *et al*., 2016).

3.2.2 *Synthesis of graphene oxide, reduced graphene oxide and the N-doped counterparts*

Graphene oxide and reduced graphene oxide were synthesized using the modified Hummer's method (Eigler *et al*., 2013; Priya *et al*., 2014). As shown in Figure 3.1, 1 g of natural flake graphite powder, 0.5 g of sodium nitrate and 50 mL of sulphuric acid were mixed at 0 °C ice-water bath. 3 g of potassium permanganate, being a strong oxidizing agent, was added slowly into the solution every half an hour to oxidize the graphite powder, three times in total. After that 46 mL of hot de-

40

ionized water was added into the suspension drop-wise. In this step the temperature was kept at 90 °C and maintained for 1 hour. Subsequently to that, 20 mL of H_2O_2 was added into the suspension drop-wise to neutralize any unreacted potassium permanganate that remains (Zarrin *et al*., 2011). The solution was taken to an ultrasonicator for 30 minutes with the power of 200 W. The suspension was centrifuged for 30 minutes at a rotation speed 3000 rpm to remove exfoliated GO particles (Zhao *et al*., 2013) and a mud-like material was obtained. The material was washed with de-ionized water and ethanol five times, respectively. Lastly, the product was dried at 80 °C in an oven for two days. Subsequently, the GO was reduced by dispersing 1g of graphene oxide in 1 liter of water by means of 1hour ultrasonic treatment as shown in Figure 3.2. As a result, a homogeneous brown graphene oxide aqueous suspension was obtained. The pH of the suspension was adjusted to 10 by addition of ammonium hydroxide while 700 μL of hydrazine solution in THF was added into the suspension in drops as a reducing agent (Nassr *et al*., 2013). The suspension was then refluxed at 80 °C for a period of 24 hours. A black flocculent substance gradually precipitated out of the solution. The product was obtained by vacuum filtration process. Finally, the resulting black product was washed with methanol and ultrapure water, dried at 80 °C for 24 hours in an oven and stored in vial. Thereafter, the GO, rGO and CNT were doped with nitrogen using melamine as precursor.

1 g of natural flake graphite powder.

1 g of Graphite powder+ 0.5 g of $NaNO_3$+50 ml of H_2SO_4 in ice-bath at 0ºC.

3 g of $KMnO_4$ was added + 46 ml of de-ionized H_2O at 90 ºC followed by stirring for 1hr.

20 ml of H_2O_2

Stirring continues as H_2O_2 is added. (For NGO, 1g of melamine was added and stirred for 12 h at 30ºC before adding H_2O_2

Sonicated for 30 minutes.

The sample was centrifuged for 30 minutes.

Filtration of mud-like sample and washing with de-ionized water and ethanol.

Oven dried at 60 °C for 48 hours
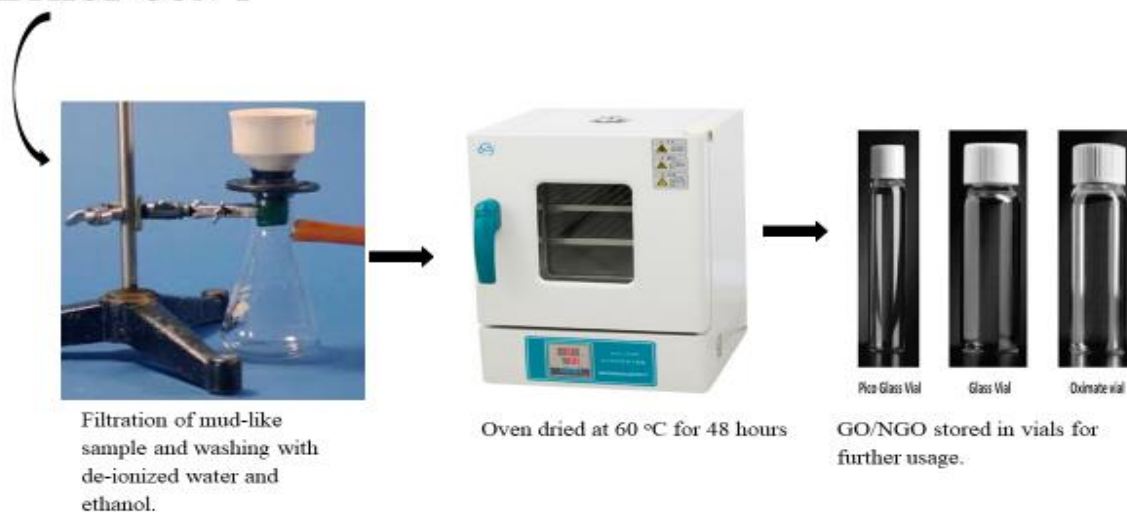
GO/NGO stored in vials for further usage.

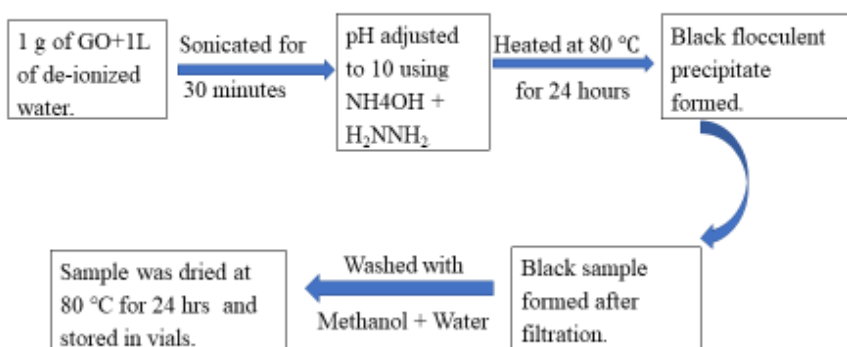Figure 3.1: Synthesis procedure of Graphene oxide (GO) and Nitrogen-doped graphene oxide (NGO).

Figure 3.2: Synthesis procedure of reduced graphene oxide (rGO).

3.2.3 *Synthesis of hybrid support materials*

0.4 g of the mixture of functionalized MWCNTs and CNFs in ratio 1:1 was dispersed in 15-20 mL of ethylene glycol, ultra-sonicated for 40 minutes and magnetically stirred for 24 hours. Since graphene sheet has the natural tendency to agglomerate due to Van der Waals interaction, this treatment was done to enhance reduction of restacking (Jha *et al*., 2011). Subsequent to this, the hybrid material was obtained by the vacuum filtration process. Finally, the resulting black product was washed up to seven times with ultrapure water, dried at 80 °C for two days in an oven and stored in vial. The same procedure was used for the synthesis of N-MWCNTs-CNFs, GO-MWCNTs, rGO-MWCNTs, GO-N-MWCNTs and NGO-MWCNTs (Jha *et al*., 2011).

42

3.3 Synthesis of Palladium catalyst using modified polyol method

0.4 g of the support materials were dispersed in a 15 mL of ethylene glycol under stirring conditions followed by a sonication in an ultrasonic bath for 15 minutes. To this dispersion, a solution of $PdCl_2$ in 15 mL of ethylene glycol was added and left under stirring for 15 minutes. The pH of the solution was adjusted with freshly prepared 2 M NaOH in ethylene glycol solution to pH $\sim$ 12 in the modified polyol method used for synthesizing monosupported, hybrid supported and binary catalysts. This was later modified by changing the pH from 12 to 13 for monosupported Pd catalyst only. The mixture was sonicated for 15 minutes to aid homogeneous adsorption of the metal precursor onto the surface of the support. For the reduction of Pd ions and Pd-Ru ions for the binary electrocatalysts, the mixture was transferred into an oil bath and heated at 165 °C for 6 hours consecutively under stirring and reflux conditions. After completing the reduction, the mixture was left under stirring overnight to cool down to room temperature and then filtered and washed with water. Finally, the catalyst was dried in an oven at 80 °C for 24 hours in order to remove all water content and stored in vial (Daoush & Imae, 2012; Farsadrooh *et al*., 2020; Nassr *et al*., 2013).

3.4 Preparation of catalyst ink

A stock solution of 20 % isopropanol and 0.02 % Nafion ionomer was prepared by mixing 79.6 mL of water, 20 mL of isopropanol and 0.4 mL of 5 wt. % Nafion solution in 100 mL volumetric flask. The Nafion ionomer was added to improve the adhesion of the catalyst film to the electrode surface. 10 mg of the catalyst was measured and dispersed in 10 mL borosilicate vial containing 5 mL of the stock solution and mixed by sonication in an ultrasonic bath for 1 hour to form catalyst ink. (Garsany *et al*., 2010).

3.5 Preparation of catalyst film on working electrode

The glassy carbon electrode with 5 mm diameter and a geometric surface area of 0.196 cm^2 embedded in a Teflon cylinder (Metrohm instrument) was polished with a 0.3 and 0.05 μm Aluminum oxide (Al_2O_3) particle suspension on a moistened polishing cloth (Buehler micro-cloth) in a 'figure eight' pattern for four minutes to a mirror finish. The polished electrode was rinsed very well with ultrapure water and dried at room temperature in air for 20 minutes before use. Subsequent to this, a 10 μL volume of the freshly prepared catalysts ink was transferred through a micropipette onto the freshly polished (mirror finish) glassy carbon electrode to give the desired Pd loading of 0.02 mg.cm^{-2}. This Pd loading gave a good thin film on the glassy carbon electrode

as thicker films may result in increased mass transport resistance through the catalyst layer, giving incomplete access to the electrochemical area of the catalyst and therefore producing incorrect data (Garsany *et al.*, 2010; Zhao *et al.*, 2016).

3.6   Characterisation Techniques

3.6.1   Physical characterisation

The physical characterisation of the prepared support materials and electrocatalysts was carried out using different analytical techniques required to determine and elucidate the various properties of the prepared samples. The prepared support materials were characterized using Fourier Transform Infrared (FT-IR) Spectroscopy and Brunauer-Emmett-Teller (BET) technique while X-ray diffraction microscopy (XRD) and high-resolution transmission electron spectroscopy (HR-TEM) were used for electrocatalysts. The following subsections explain the above respective techniques used for the physical characterisation.

3.6.1.1   The Fourier Transform Infrared Spectroscopy

The Fourier Transform Infrared (FT-IR) Spectroscopy was used for the identification of the functional groups present in the support materials (Subramanian & Rodriguez-Saona, 2009). The FT-IR instrument, as shown in Figure 3.3, works by sending infrared radiation of approximately 10,000 - 100 cm^{-1} through the test sample with selective absorption of some radiation while others passed through the sample. The absorbed radiation is converted into rotational and /or vibrational energy by the sample molecules. The absorbed radiation causes the change of dipole moment of the sample molecules. Hence, the vibrational energy level of the sample molecules shifts from ground state to excited state. The frequency of the absorption peak is determined by the vibrational energy gap. The various absorption peaks are affiliated to different vibrational freedom of the molecules. The intensity of the absorption peaks is associated to the change of the dipole moment and the feasibility of the transition of the energy level. The resulting signal at the detector end is presented as a spectrum between 4000 - 400 cm^{-1} which represent a molecular fingerprint of the test sample. Each sample molecule exhibits a unique spectra fingerprint which makes FT-IR technique an ideal tool for sample identification (Perkins, 1986).

Figure 3.3: Working station of FT-IR spectroscopy

Source:http://faculty.sdmiramar.edu/fgarces/labmatters/instruments/FT-IR/FT-IR_Operations/index.html

Hence in this work, the presence of carboxyl groups in the functionalized carbon nanotubes, nitrogen in the N-doped supports and other functional groups in all the synthesized mono and hybrid support materials were confirmed using Fourier Transform Infrared spectroscopy (FT-IR). About 10 mg of each support material was placed on the attenuated Total Reflectance (ATR) metal disc sample holder of Perkin Elmer spectrum 100 FT-IR spectrometer. Force was gently applied to the sample and IR spectra were obtained within a range of 4000 - 400 cm^{-1} to identify the functional groups present. Baseline correction was done for background noise which was subtracted from the spectra before data collection.

3.6.1.2 *Brunauer-Emmett-Teller*

The Brunauer-Emmett and Teller (BET) technique was used to determine the surface area, pore volume and pore size of all synthesized nano-support materials. The analysis is usually carried out by the BET instrument as shown in Figure 3.4. The prepared samples are immersed in a liquid nitrogen bath as the BET instrument carry out the nitrogen adsorption tests. Nitrogen gas is usually used as a probe molecule and is exposed to a solid under study at liquid nitrogen temperature of -196 °C (Zielinski *et al.*, 2013). The adsorption process is kinetically limited and the low temperature of the liquid nitrogen aids rapid kinetic equilibrium. The surface area of the solid is evaluated from the measured monolayer capacity and knowledge of the cross-sectional area of the molecule being used as a probe. For nitrogen, the cross-sectional area is 16.2 Å per molecule. As the testing proceeds, the instrument introduces certain amount of absolute nitrogen gas into the

45

tube while recording the pressure (P/Po) which enable the plotting and determination of the parameters present (Brame & Griggs, 2016).
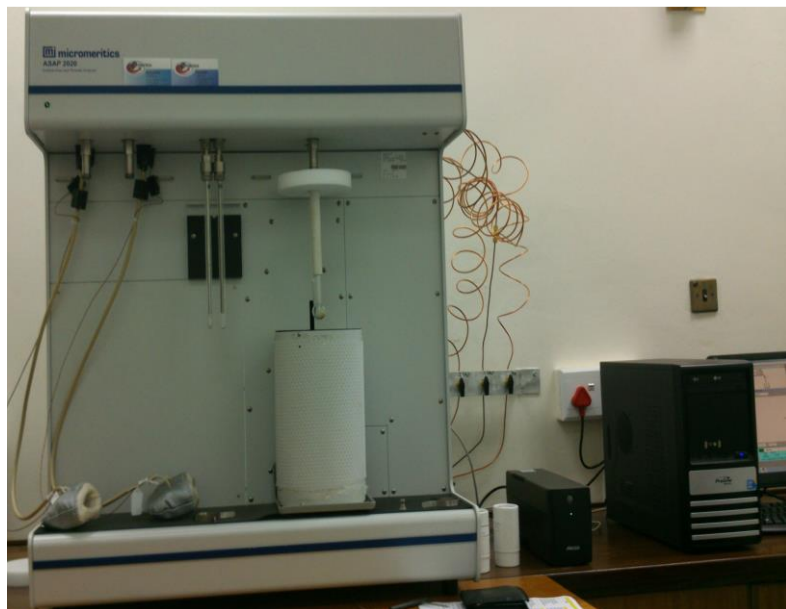

Figure 3.4: Working station of BET

Source:(Matshitse, 2010)

In this work, the surface area and porosity of the synthesized support materials was carried out using BET. The samples were degassed for 12 hours at a temperature of 120 °C under a vacuum pressure in order to remove moisture and other volatile impurity. Physisorption was conducted using a TriStar II 3020 (Micromeritics) with liquid N_2 as analysis adsorptive. The surface area and pore size of the samples were evaluated by the BET model and the t-plot measurements was used to differentiate between the external surface area and microporous area. Density functional theory (DFT) model was used to determine the pore size distributions while the total pore volume was determined using the Horvath-Kawazoe (HK) model at P/Po ∼ 0.99

3.6.1.3 *X-ray Diffraction Microscopy*

X-ray diffraction spectroscopy (XRD) was used to determine the crystallinity of all the synthesized electrocatalysts. It gives information on structure, phases, crystallinity, crystalline size, crystal defect and crystal orientation among others. Therefore, XRD is an indispensable technique for materials characterisation (Bunaciu *et al*., 2015). In XRD analysis, X-rays are generated in a cathode ray tube by heating the filament to generate electrons as shown in Figure 3.5. These electrons are then accelerated towards the target material by applying voltage and bombarding the target material with electrons. When the electrons acquire enough energy, to displace the inner

46

shell electrons of the target materials, a characteristic X-ray spectra are produced. Copper is usually used as the target material for single-crystal diffraction with a Cu Kα radiation of 1.5418 Å. These X-rays are paralleled and directed onto the sample. As the sample and the detector are rotated, the intensity of the reflected X-ray is recorded. The interaction of the incident rays with the samples produces constructive interference and a peak intensity appears when the conditions obey Bragg's law (Equation 3.1). The detector records, processes the X-ray signal and converts it to a count rate which comes out as an output from the device used such as computer or printer.

$$n\lambda = dsin\,\theta$$ <div align="right">Equation 3.1</div>

By varying angle Θ, the Bragg's law conditions are met by different d-spacing in the materials. Plotting the angular positions against the intensities of the resultant diffracted peaks of radiation produce a graphical pattern which represent the sample where a mixture of different phase is present. The addition of individual pattern results into a diffractograms. Based on the principle of X-ray diffraction; physical, structural and chemical information about the materials under investigation can be obtained (Uvarov & Popov, 2007).

To determine the average particle size, Scherrer equation is used which is given as

$$d = {k\lambda}/{\beta Cos\theta}$$ <div align="right">Equation 3.2</div>

where d is the crystallite size, K is the Scherrer constant which also depends on the crystal shape and the diffraction line indexes, λ is the X-ray wavelength which is equal to 0.154 nm, β (2Θ) in radian is the width of the peak (full width at half maximum, (FWHM) or integral breadth) after correcting for instrumental peak broadening and Θ is the Bragg angle (Uvarov & Popov, 2007).

The crystallite size is determined by measuring the broadening of a particular peak in a different pattern associated with a particular planar reflection from within the crystal unit of the sample. The particle size is inversely related to the half-width at half maximum of an individual peak. The narrower and more intense the peak, the more crystalline the sample. A broad peak is usually associated with small particle size and amorphous materials (Uvarov & Popov, 2007).
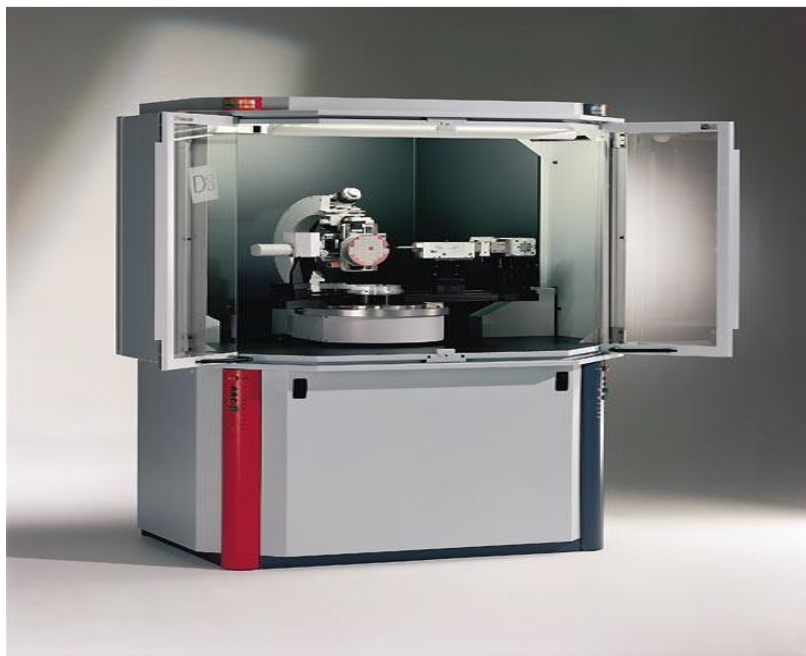
Figure 3.5: X-ray Power Diffraction (XRD).

Source: https://serc.carleton.edu/research_education/geochemsheets/techniques/XRD.htmI

In this study, the phase purity and crystal structure of the synthesized electrocatalysts were determined by X-ray diffraction (XRD) patterns using Bruker AXSD8 Advance instrument (Cramerview South Africa) with Cu-Kα radiation operated at 40 kV and 40 mA with λ of 1.5406 Å to analyse and collect spectra data. A standard α-Al_2O_3 sample was employed for the assurance of the instrumental commitment onto top profile parameters. The catalysts samples were prepared by grinding the samples into a fine powder which was pressed onto a rectangular polypropylene sample holder. It was then clipped into the XRD instrument. The samples were scanned over a range of 10º to 90º 2-theta (Bragg's angle array) with a scanning step of 0.035 º/s. The crystalline phases were identified by carrying out a match search and comparing the diffraction spectra with the database of standard peak patterns provided by International Centre for Diffraction Data (ICDD) assisted with High score Expert software. The XRD results were also used to determine the average particle sizes.

3.6.1.4 The High-Resolution Transmission Electron Spectroscopy

High-resolution transmission electron spectroscopy (HR-TEM) was used to determine the dispersion of catalyst nanoparticles on the support materials and particle size of all the prepared electrocatalysts. It is a technique whereby a beam of electrons generates a micrograph when transmitted through a sample. The sample is usually prepared as ultrathin area below 100 nm thick or a suspension on a grid. The micrograph is produced from the association of electrons with the

sample as the beam of electrons is transmitted through the sample. The image is therefore amplified and centered onto the imaging device, a fluorescent screen, a layer of photographic film or a sensor like a charge-coupled device.

An ideal HR-TEM comprises the light source, condenser lens, specimen stage, objective lens and projector lens as shown in Figure 3.6 (Reimer & Kohl, 2008). It is effective for imaging at higher resolution because of the little de-Broglie wavelength of the electrons. This enhances the instrument to detect fine detail even as little as a single section of atoms. At lower amplifications, HR-TEM micrograph contrast because of differential absorption of electrons by the materials due to contrast in the arrangement/thickness of the materials. At higher amplification, complex wave synergy tweaks the intensity of the picture, requiring experienced examination of the micrographs. Other interchangeable mode enables the instrument to detect tweaks in crystal arrangement, electronic structure, chemical properties and sample induced electron stage shift apart from the standard absorption-based imaging (Bonnamy & Oberlin, 2016).
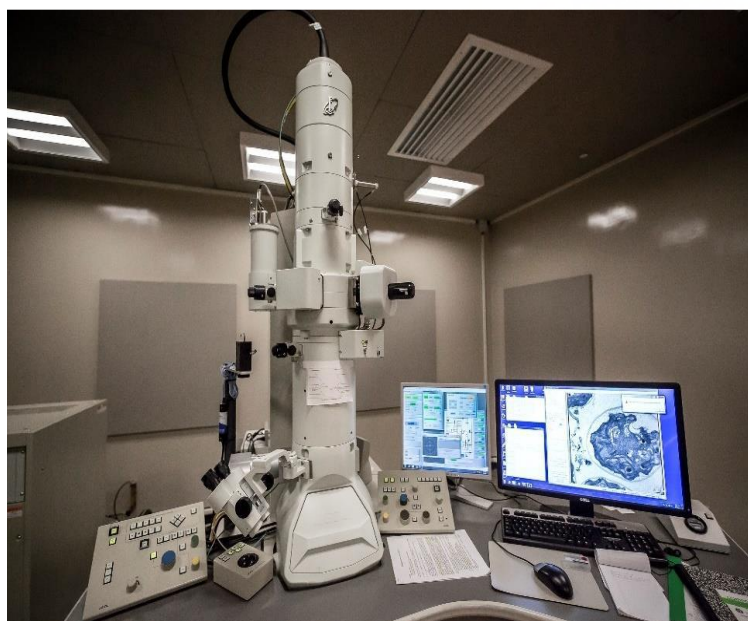

Figure 3.6: The High-resolution transmission electron spectroscopy (HR-TEM)
Source: (Bozzola & Dee Russell, 2022).

In this study, the high-resolution transmission electron spectroscopy (HR-TEM) micrograph of the electrocatalysts were obtained using JEOL 2010 TEM system (Carl Zeiss, Jena, Germany), operating at 200 kV. The HR-TEM samples were prepared by dispersing the supported electrocatalysts in ethanol. A drop of the sample suspension was then cast onto the carbon film covered Cu grid for the analysis. This HR-TEM analysis was carried out to examine the micro

49

structure, formation and distribution of Pd particles on the various support surfaces while the particle size determined using HR-TEM was obtained by Image J software (Image Processing and Analysis in Java developed at the National institute of Health and the Laboratory for Optical and Computational Instrumentation LOCI, University of Wisconsin, Madison, WI, USA) over different selected areas of each electrocatalyst.

3.6.2 Elemental Analysis

The elemental analysis was carried out using energy dispersive spectroscopy.

Energy Dispersive Spectroscopy (EDS)

Energy dispersive spectroscopy was used to determine the elemental composition of the support materials and catalysts metal loading. EDS is a micro-analysis technique used for quantitative elemental analysis related to electron microscopy based on the production of unique X-rays which shows the various elements present in a sample (Scimeca *et al*., 2018). When the beam of the electrons bombards the sample surface, various emissions including X-rays are generated. The EDS detector is used to separate the unique X-rays of various elements into an energy spectrum. The EDS system software is then used to analyze the energy spectrum in order to ascertain the abundance of each element present in the sample as shown in Figure 3.7 (Reed, 1995). EDS is used to determine the chemical compositions of materials sample down to a small unit micro size and to develop elemental composition maps over a large raster area. The system consists of a sensitive X-ray detector, a liquid nitrogen Dewar for cooling and the software to analyze the energy spectra. The detector is located in the sample chamber of the main instrument which is being cooled by liquid nitrogen. The most widely used detectors are made of Si (Li) crystals which operate at low voltages to enhance its sensitivity. The detector contains a crystal that absorbs the energy of incoming X-rays by ionization thereby producing free electrons in the crystal which become conductive and produce electric charge. The electrical pulses correspond to the characteristic X-rays of each element. An EDX spectrum is then shown as a plot of X-ray count against energy (in K eV). The energy peaks produced correspond to different elements in the sample. They are generally narrow and easily resolved but some elements produce multiple peaks. Elements in low abundance will produce X-ray peaks which may not be resolved from the background radiation (Reed, 1995). The EDS set-up is shown in Figure 3.7.

50

Figure 3.7: Energy Dispersive X-ray spectroscopy (EDS) work station.

Source: https://www.iitk.ac.in/dord/energy-dispersive-spectroscopy

Thus, in this study, the elemental compositions of the prepared carbon support materials, Pd and Ru catalyst metal loading were determined using energy dispersive X-ray spectroscopy (EDS). The analysis was carried out using TECNAI G2 F20 X-TWIN MAT 200 kV field emission where nickel grid was used to coat the material for better conductivity with an average imaging resolution of 1.5 nm. The magnification, resolution and working distance was captured on each sample micrograph. At each focus spot, the elemental compositions of the sample were determined.

3.6.3   Electrochemical Characterisation

In this section, different electrochemistry techniques that were employed for the electrochemical characterization of the prepared samples are briefly discussed. These techniques include: cyclic voltammetry (CV), chronoamperometry (CA) and electrochemical impedance spectroscopy (EIS).

3.6.3.1   Cyclic voltammetry

Cyclic voltammetry (CV) is a multifaceted and potent electrochemical technique usually used to investigate the electroactive cum the reduction and oxidation processes of molecular species (Elgrishi *et al*., 2018). Hence, CV was used in this research to determine the electroactive surface area and activity of all the electrocatalysts towards methanol oxidation reaction. It provides experimental information and insights into the kinetics and thermodynamic details of several chemical systems (Marken *et al*., 2005). CV is also indispensable in studying electron transfer-

initiated chemical reactions including catalysis (Elgrishi *et al.*, 2018). Its efficacy came from its ability to swiftly discover the redox behaviour over a wide potential range (Kissinger & Heineman, 1983). CV comprises cycling of potential of a working electrode which is usually immersed in an unstirred electrolyte and measuring the output current. The potential of this working electrode is controlled against a reference electrode such as silver/silver chloride (Ag/AgCl). The controlling potential applied across the two electrodes is known as excitation signal (Elgrishi *et al.*, 2018). A cyclic voltammogram resulted from measuring the current at working electrode during potential scan. This voltammogram is considered as the response signal to the potential excitation signal. The CV shows the response, which is the current, in vertical axis and the parameter imposed on the system, which is the potential, in the horizontal axis. Since the potential varies linearly with time, the horizontal axis can as well be considered as a time axis (Kissinger & Heineman, 1983). The scan rate controls how fast the applied potential is scanned. The faster the scan rate, the decrease the size of the diffusion layer and consequently, higher current is observed (Elgrishi *et al.*, 2018).

The instrument employed in this study is an Autolab M204 (Metrohm SA) with a potential range of $\pm$ 10 V, compliance voltage of $\pm$ 20 V, maximum current of $\pm$ 400 mA, current range of $\pm$ 100 mA – 10 nA, potentials accuracy of $\pm$ 0.2 %, current resolution of 0.0003 % (of current range), input impedance > 100 GOhm and potentiostat bandwidth of 1 MHz. The experimental setup further includes three standard electrodes electrochemical cell as shown in Figure 3.8. A glassy carbon electrode with a geometric area of 0.196 cm^2 which serves as a substrate for the catalyst film was used as the working electrode, Platinum wire as a counter electrode and Ag/AgCl as a reference electrode. All potentials were quoted against the Ag/AgCl reference electrode as the electrochemical measurements were carried out in a 1 M KOH supporting electrolyte. The CV measurements in the presence and absence of methanol were performed with potential ranging from -1.0 V to 0.4 V vs Ag/AgCl in nitrogen saturated electrolyte at scan rate of 20 mVs^{-1} for monosupported and hybrid supported Pd catalysts while the binary electrocatalysts were scanned at rate of 5 mVs^{-1} after scanning at 20 mVs^{-1} initially and no peak was observed. All the electrochemical characterizations were performed at ambient temperature.

Figure 3.8: An electrochemical working station

Source: https://www.metrohm.com/en-gb/support-and-service/autolab-video-tutorials/

3.6.3.2 Chronoamperometry

Chronoamperometry (CA) was used in this research to determine the stability of all the synthesized electrocatalysts. CA is when the potential of a working electrode is stepped from a rate at which no Faradaic reactions happen to a potential at which the surface concentration is effectively zero. When CA is carried out, current is measured as a function of time after application of a potential step perturbation (Rieger, 1993). CA is usually used to determine the diffusion coefficient of the surface area of the working electrode or the electroactive species. During the experimental testing, the current-time curve generated reflect the change in the concentration gradient. This include the sluggish expansion of the diffusion layer which relate to the depletion of the reactant as the testing time progresses. Consequently, the current decays with time (Rieger, 1993). In this study, the instrument used is the same as that of CV shown in Figure 3.6 which has been described above. The CA testing was carried out for the duration of 1800 seconds at potential of – 0.3 V with scan rate of 0.02 Vs^{-1} at interval of 5 seconds.

3.6.3.3 Electrochemical impedance spectroscopy

The electrochemical impedance spectroscopy (EIS) was used in this research to determine the electron kinetics of all the electrocatalysts. It is an effective tool which gives room for a deep in situ kinetic analysis of catalytic phenomena and the separation of different processes contributing to overpotential based on frequency domain (Ciureanu & Roberge, 2001). Impedance is a measure

53

of the capacity of a circuit to resist the flow of electric current. It refers to the frequency dependent resistance to current flow of a circuit element (such as resistor, inductor and capacitor among others). Impedance assumes an alternating current of a specific frequency in Hertz. From EIS measurement, overall ohmic resistance (or high-frequency resistance, HFR) of the entire fuel cell device, charge transfer resistance related to activation polarization which occurs on catalytic surface and mass transfer resistance as a result of diffusive limitations arising at high current density can be obtained (Latorrata *et al*., 2018). This technique utilises little sinusoidal perturbation potential at various frequencies. EIS is used in evaluating both rapid and gradual delivery phenomenon as it examines every single and variety of frequencies. This check helps to signify resistance to electron transfer at some stages in electrochemical reactions, mass transfer resistance and ionic resistance through the membrane. The information obtained can therefore be used to determine various impedances. EIS estimates an extensive variety of frequencies and track the resulting variation value and segment of the cell voltage and current with a frequency response analyser to ascertain the complex impedance (Z' and Z'') of the fuel cell (Latorrata *et al*., 2018). The same instrument shown in Figure 3.6 was used for the EIS in this study as discussed earlier. The measurement was carried out at potential of – 0.3 V with scan rate of 0.02 Vs^{-1}.
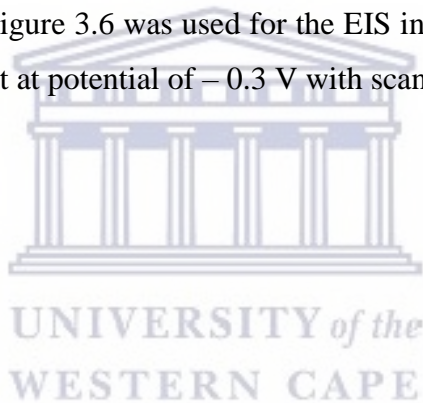
4 Results and Discussions of Graphene Supported Palladium Catalysts

This section presents the results obtained from the various characterization carried out on all the prepared graphene support materials and their electrocatalysts using different appropriate techniques as discussed in chapter three. In this study, the pH was adjusted to 13 and the results were compared to pH 12 which is the normal pH used in the modified polyol method in order to know if pH 13 electrocatalysts will perform better than pH 12 electrocatalysts. First, the energy dispersive X-ray spectroscopy (EDS) coupled with the scanning electron microscopy (JOEL JSM-7500F Scanning Electron Microscope, Mundelein, II, USA, was used to evaluate the Pd metal loading in graphene supported Pd catalysts and was found to be 37.67 % which was the same for all the synthesized graphene supported Pd catalysts.

4.1 Surface Characterization

Fourier-Transform Infrared (FT-IR) and Brunauer-Emmett-Teller (BET) were used for the surface characterization of the synthesized carbon support materials while X-ray diffraction microscopy (XRD) and high-resolution transmission electron spectroscopy (HR-TEM) were used for the electrocatalysts.

4.1.1 Fourier-Transform Infrared Spectroscopy of Graphene Support Materials

In this section, the presence of carbonyl group, hydroxyl group, nitrogen for the N-doped support materials and other functional groups in all the synthesized graphene support materials were confirmed using Fourier-Transform Infrared (FT-IR) Spectroscopy. The obtained spectra are shown in Figure 4.1. For FT-IR analysis of GO, the band around 1708 and 1049 cm^{-1} were assigned to C=O and C-O of carboxylic acid respectively while the band around 1228, 1582, 2988 and 1394 cm^{-1} were assigned to C-O alcohol, C=C aromatic, C-H alkane and C-H alkane (bend) respectively. The appearance of C=O and C-O peaks of carboxylic acid in GO is an indication of the formation of GO from graphite powder by chemical oxidation (J. Li *et al*., 2014). In rGO spectra, the band around 1712, 3436 and 1196 cm^{-1} were assigned to C=O carboxylic acid, strong peak of O-H and C-O of alcohol respectively while the band around 1564 cm^{-1} was assigned to the C=C aromatic. The significant reduction in C=O peak of carboxylic acid, disappearance of prominent C-O peak of carboxylic acid and appearance of O-H peak of alcohol in addition to the C-O peak of alcohol in rGO show the reduction of GO to rGO (Al-Marri *et al*., 2016; Yao *et al*., 2016). Furthermore, the FT-IR spectra of NGO shows the C=O and C-O bands of carboxylic acid with C-N band of

amine which were observed around 1716, 1050 and 1223 cm^{-1} respectively while the band around 2988, 1580, 1394 and 780 cm^{-1} were assigned to C-H alkane, C=C aromatic, C-H alkane (bend) and C-H aromatic. The appearance of C-N peak of amine which displaced the C-O of alcohol in NGO spectra is an indication of the formation of NGO from GO. In addition, the spectra of NrGO shows a medium peak of O-H band around 3414 cm^{-1} which correspond to that of hydrogen bonded alcohol; 1728, 1564 and 1188 cm^{-1} which correspond to C=O carboxylic acid, NO$_2$ nitro compound and C-O alcohol respectively. The significant reduction in C=O peak of carboxylic acid, disappearance of prominent C-O peak of carboxylic acid and appearance O-H peak of alcohol in addition to the C-O peak of alcohol in NrGO show the reduction of NGO to NrGO (Kuniyil *et al*., 2019) while the appearance of NO$_2$ peak still indicate the doping with nitrogen. All these observed bands are summarized in Table 4.1. The presence of N-doped in NGO and NrGO was validated using EDS as shown in Figure 4.2.
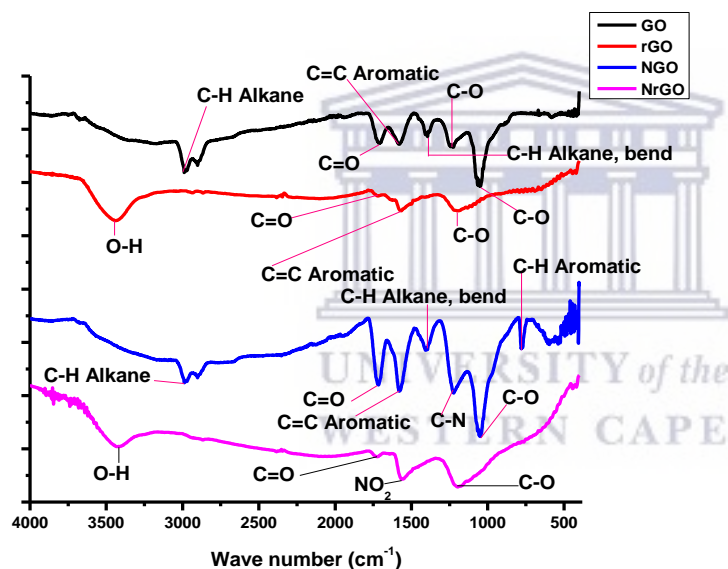
Figure 4.1: The FT-IR Spectra of synthesized GO, rGO, NGO and NrGO support materials.

Table 4.1: Observed FT-IR Spectra for Synthesized Graphene Support Materials.

Support Materials	Functional Groups	Observed bands (cm^{-1})
GO	C=O Carboxylic acid	1708
	C-O Carboxylic acid	1049
	C-O Alcohol	1228
	C=C Aromatic	1580
	C-H Alkane	2988
	C-H Alkane (bend)	1394
rGO	C=O Carboxylic acid	1712
	C-O Alcohol	1196
	O-H Alcohol	3436
	C=C Aromatic	1564
NGO	C=O Carboxylic acid	1716
	C-O Carboxylic acid	1050
	C-N Amine	1223
	C=C Aromatic	1580
	C-H Alkane	2988
	C-H Aromatic	780
NrGO	C=O Carboxylic acid	1728
	C-O Alcohol	1188
	NO$_2$ Nitro compound	1564
	O-H Hydrogen bonded alcohol	3414
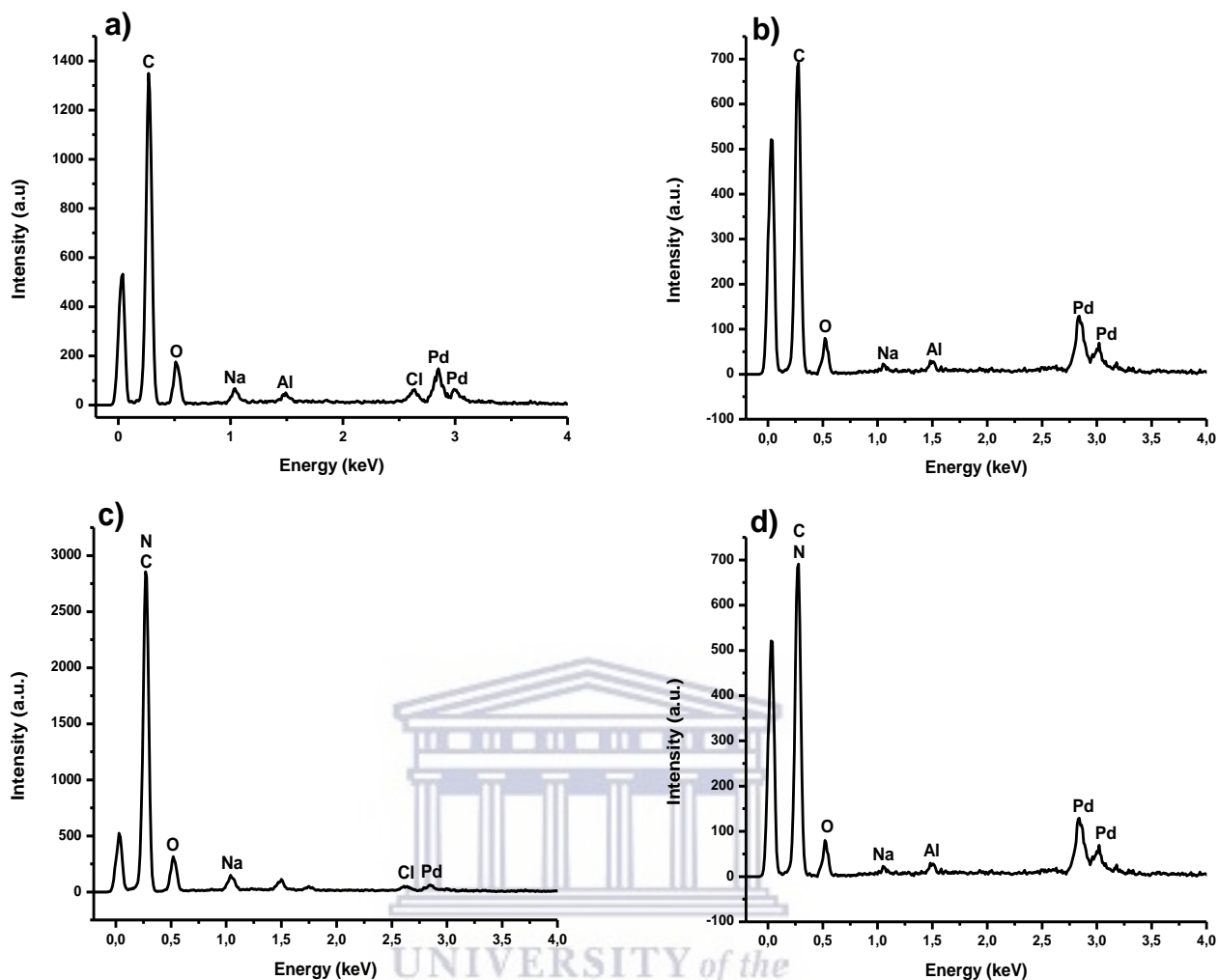
Figure 4.2: The EDS Spectra of synthesized (a) Pd/GO (b) Pd/rGO, (c) Pd/NGO, (d) Pd/NrGO.

4.1.2 Brunauer-Emmett-Teller of Graphene Support Materials

The specific surface area, pore volume and pore size of the prepared graphene support materials were also investigated using Brunauer-Emmett-Teller (BET) as presented in Table 4.1. Surface area measurements were taken from the support materials to first evaluate the surface area of the carbon support materials used. Among the prepared graphene support materials, NGO showed the highest surface area, pore volume and pore size of 41.92 m^2 g^{-1}, 0.05 cm^3/g and 308.50 Å respectively. Since the performance of catalysts increases with increase in the support surface area and pore volume, the catalyst must therefore be supported with a high surface area and pore volume support materials for proper dispersion of the catalyst nanoparticles which aids the catalyst activity and make low catalyst loading feasible for fuel cell operations (Antolini, 2009). Figure 4.3 and

58

Figure 4.4 show the adsorption–desorption and pore distribution graphs of synthesized graphene support materials respectively.

Table 4.2: The BET surface area, pore volume and pore size of synthesized graphene-based support materials

Support Materials	Surface Area (m²/g)	Pore Volume (cm³/g)	Pore size (Å)
GO	9.20	0.03	67.50
rGO	3.36	0.02	277.23
NGO	41.92	0.05	308.50
NrGO	6.46	0.03	173.76
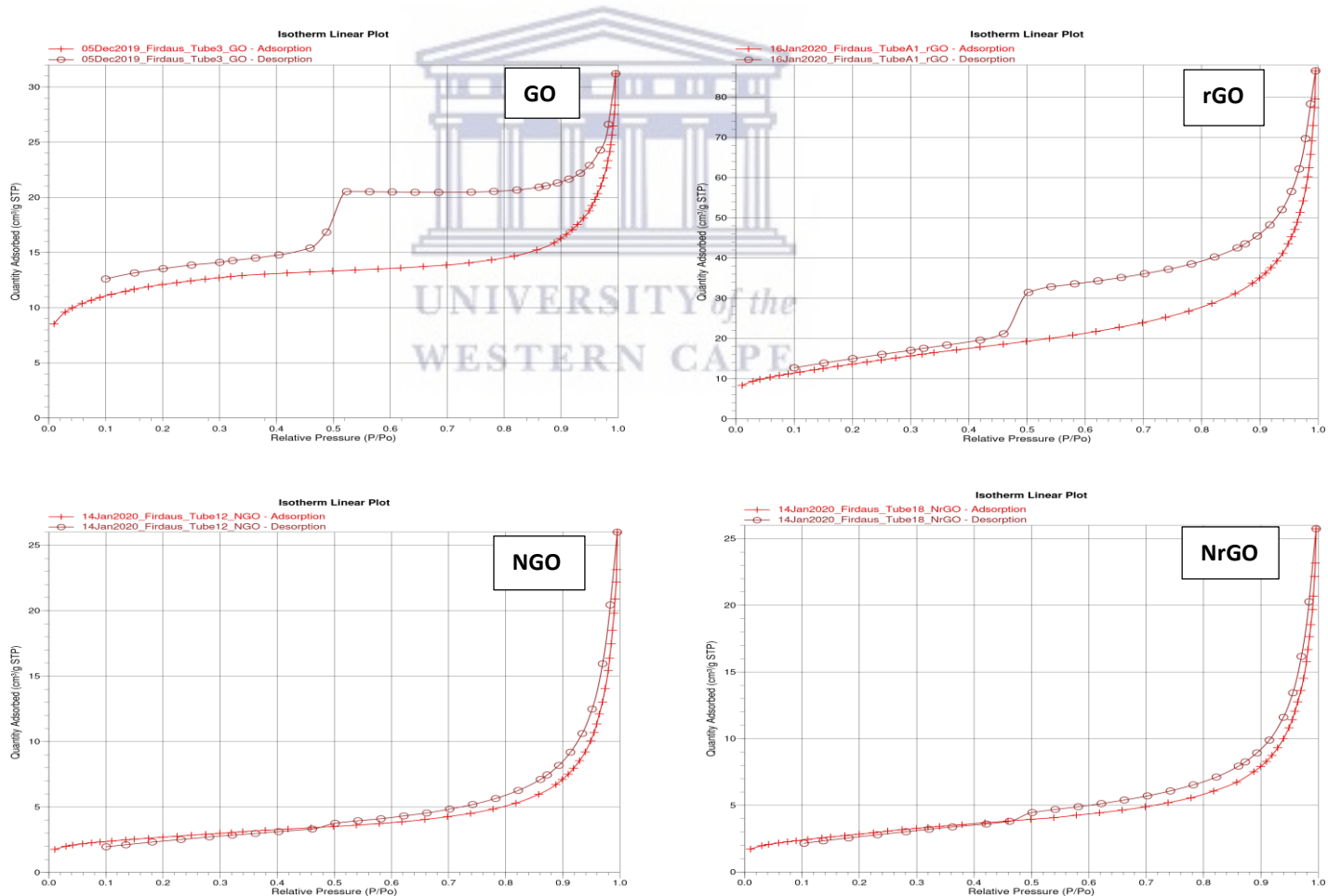
Figure 4.3: Adsorption-desorption graphs of synthesized GO, rGO, NGO and NrGO.
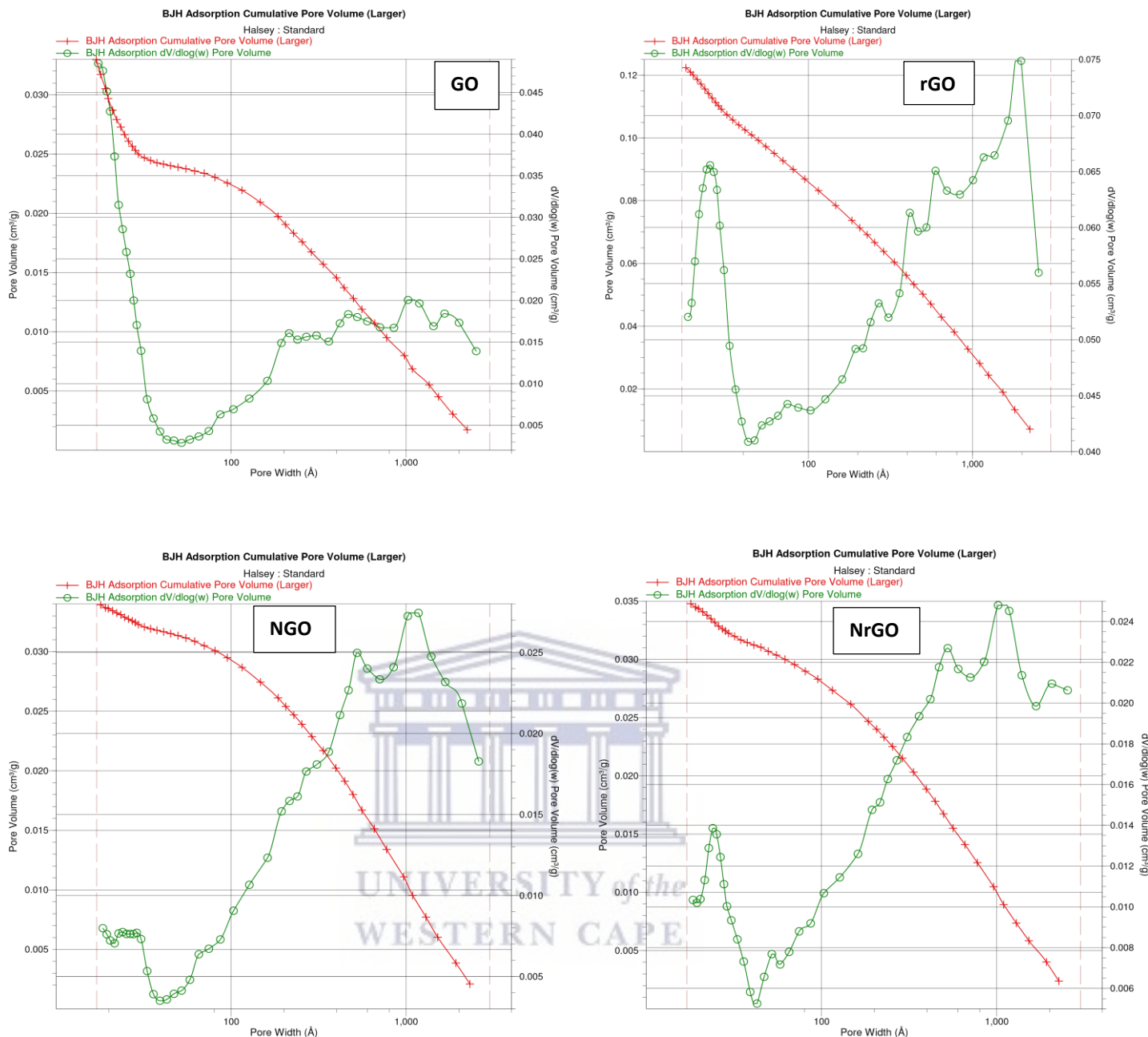
Figure 4.4: Pore distribution graphs of synthesized GO, rGO, NGO and NrGO.

4.1.3   X-ray Diffraction of Graphene Supported Palladium Catalysts

The crystallinity and crystallite size of graphene supported Pd catalysts were determined using XRD spectra and classical Debye-Scherrer equation respectively as stated in equation 3.2. The sharpest and the most intense peak of all the prepared Pd catalysts appeared around 40º 2-theta scale which is indexed as (111). This peak was used to determine the crystallite size of all the electrocatalysts. The XRD graphitic pattern of prepared graphene supported Pd catalysts synthesized by modified polyol method and the modified counterparts at pH 13 show five

60

diffraction peaks at 2-theta value around 40.0276º, 46.5107º, 68.0866º, 81.9789º and 86.8841º and are indexed to the (111), (200), (220), (311) and (222) crystal plane of Pd face-centered cubic (fcc) crystallographic structure as shown in Figure 4.3 and Figure 4.5 respectively (Carrera-Cerritos *et al*., 2014; Dector *et al*., 2013; Klaas *et al*., 2020). The broad peak located at approximately 25º 2-theta scale on the other hand corresponds to the plane (002) of carbon (Dector *et al*., 2013; Groves *et al*., 2012; Yi *et al*., 2015). The XRD spectra confirmed that all the graphene supported Pd catalysts are crystalline as illustrated in Figure 4.3. This is also corroborated with selected area electron diffraction (SAED) as shown in Figure 4.4. The better the crystallinity, the lower the ohmic resistance and the better the electron flow (Rao *et al*., 2005).
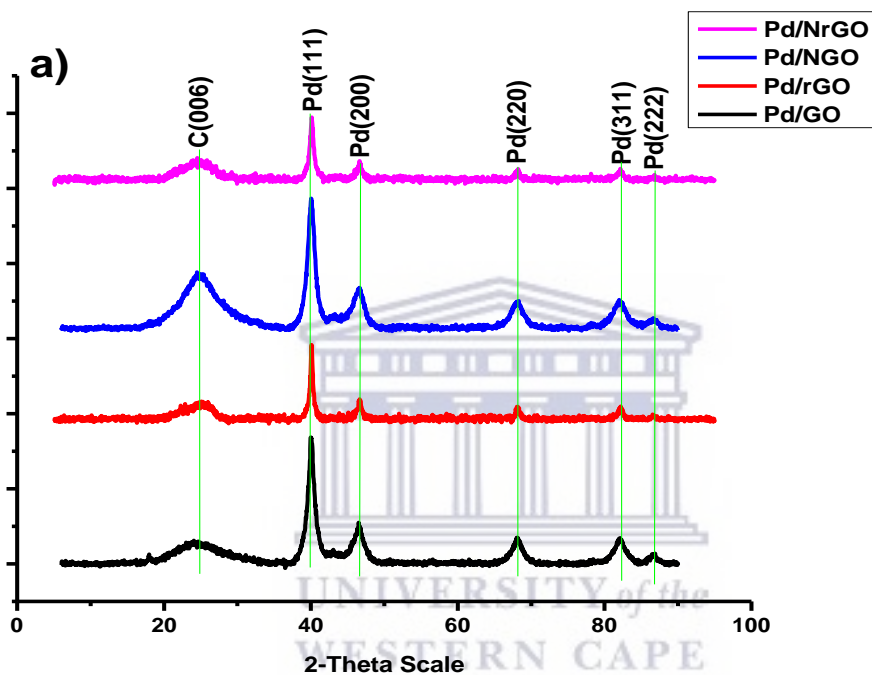
Figure 4.5: XRD spectra of graphene supported Pd catalysts synthesized by modified polyol method.
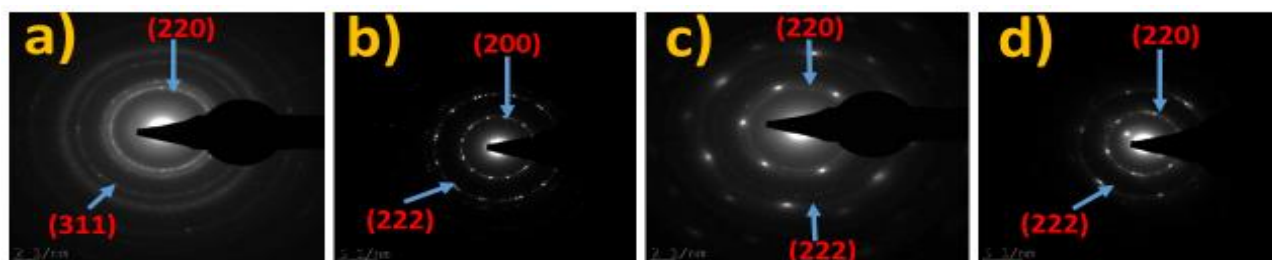
Figure 4.6: Selected area electron diffraction (SAED) of graphene supported Pd catalysts synthesized by modified polyol method: (a) Pd/GO (b) Pd/rGO (c) Pd/NGO (d) Pd/NRGO.

61

Table 4.3: The particle size and crystallite size of the graphene support Pd catalysts synthesized by modified polyol method.

Electrocatalyst	Particle size (nm) HR-TEM	Crystallite size (nm) XRD
Pd/GO	5 ± 1.6	5.5
Pd/rGO	19 ± 1.0	19.0
Pd/NGO	5 ± 1.2	5.8
Pd/NrGO	12 ± 1.0	12.8

In case of the modified counterparts of graphene supported Pd catalysts at pH 13, the XRD spectra also revealed their crystalline structures too with the sharpest and most intense peak indexes as (111) at 40º 2-theta scale as shown in Figure 4.5. The selected area electron diffraction (SAED) indicated in Figure 4.6 also corroborate the crystallinity of all the modified electrocatalysts.
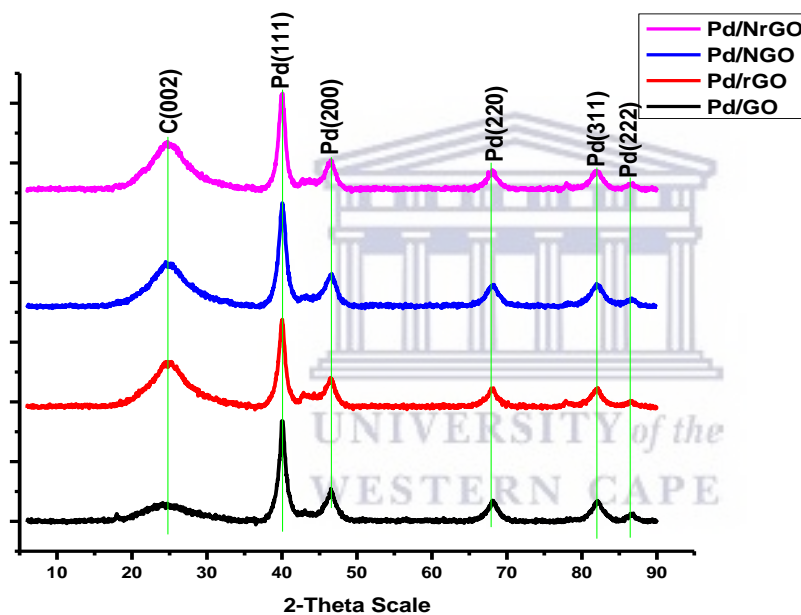
Figure 4.7: XRD spectra of modified counterparts of graphene supported Pd catalyst.
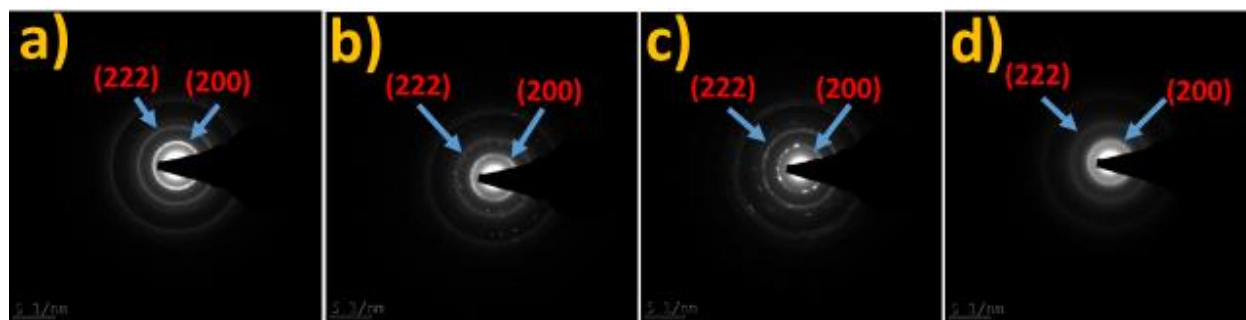
Figure 4.8: Selected area electron diffraction (SAED) of modified counterparts of graphene supported Pd catalysts: (a) Pd/GO, (b) Pd/rGO, (c) Pd/NGO, (d) Pd/NRGO.

Table 4.4: The particle size and crystallite size of the modified counterparts of graphene supported Pd catalysts.

Electrocatalyst	Particle size (nm) HR-TEM	Crystallite size (nm) XRD
Pd/GO	5 ± 1.0	6.0
Pd/rGO	6 ± 1.2	6.2
Pd/NGO	5 ± 0.7	5.9
Pd/NrGO	5 ± 0.6	5.8

4.1.4 *The High-Resolution Transmission Electron Spectroscopy of Graphene Supported Palladium Catalysts synthesized by modified polyol method*

Figure 4.7 and Figure 4.8 show the nanomorphological structures of all the synthesized graphene supported Pd catalysts examined using HR-TEM with their frequency distribution from 50 randomly selected nanoparticles. For graphene (GO, rGO, NGO and NrGO) supported Pd catalysts synthesized by modified polyol method, the images revealed a homogenous with relatively small particle size (since nanoparticles usually show a nanodimensional size of 1-100 nm (Cookson, 2012)) distribution which ranges between 5 to 19 nm as shown in their respective histograms in Figure 4.7.
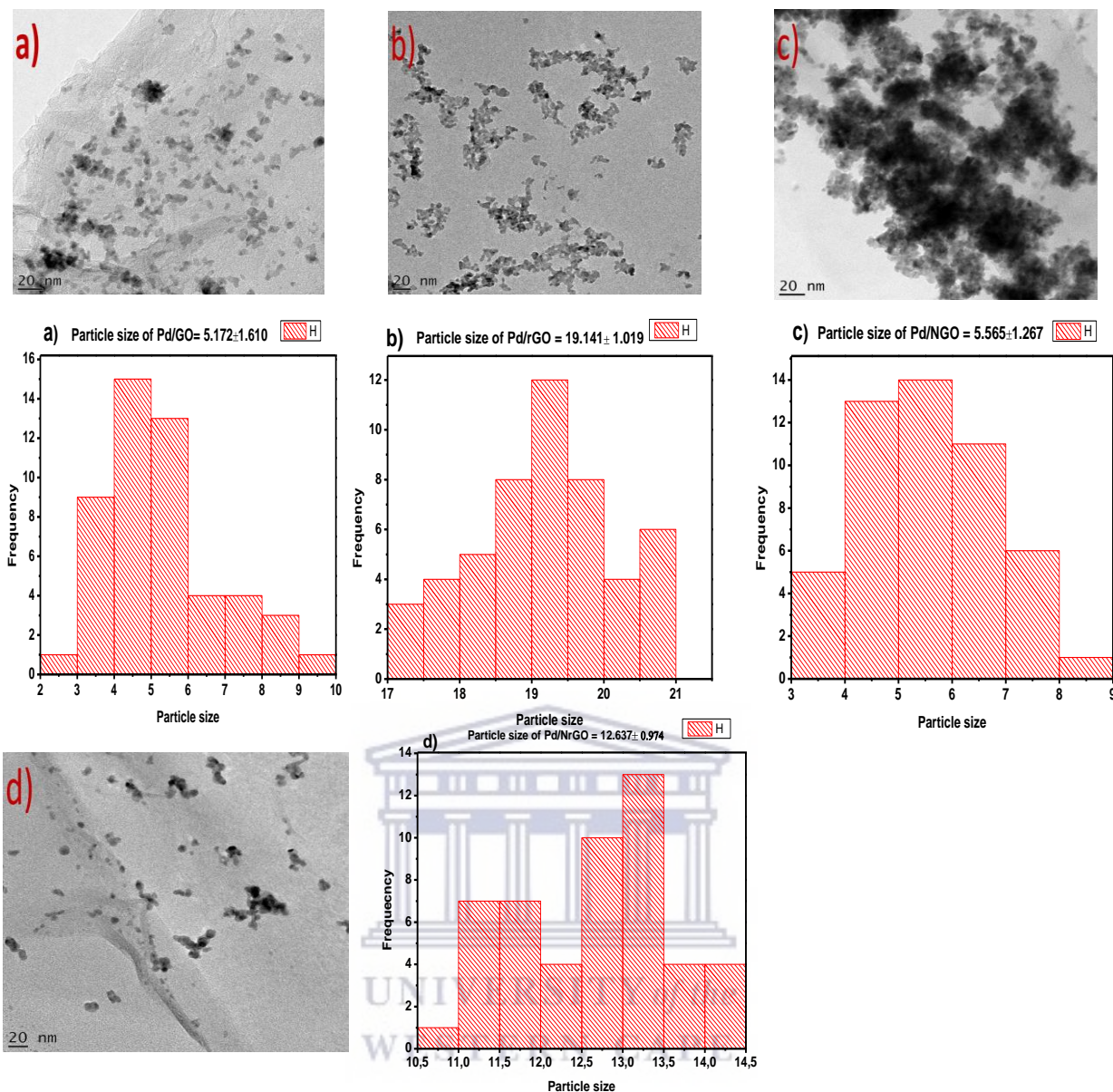
Figure 4.9: HR-TEM images with their respective histograms for graphene supported Pd catalysts synthesized by modified polyol method: (a) Pd/GO (b) Pd/rGO (c) Pd/NGO and (d) Pd/NrGO.

In case of modified counterparts of graphene (GO, rGO, NGO and NrGO) supported Pd catalyst, the images also revealed a homogenous distribution with relatively small particle size distribution which ranges between 5 and 6 nm as shown in their respective histograms in Figure 4.8.
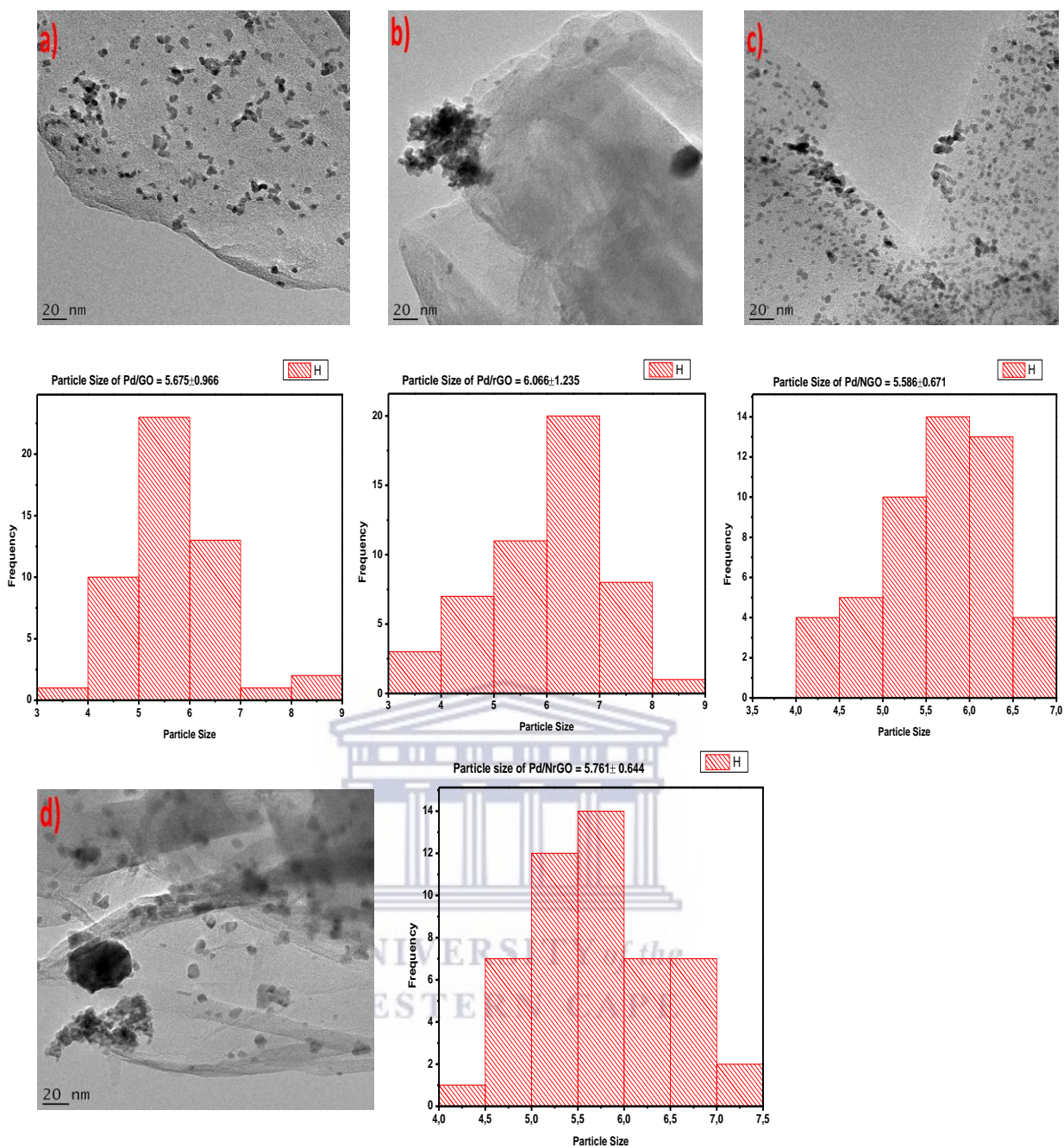
Figure 4.10: HR-TEM images with their respective histograms for modified counterparts of graphene supported Pd catalysts: (a) Pd/GO (b) Pd/rGO, (c) Pd/NGO and (d) Pd/NrGO.

4.2 Electrochemical Evaluation of Graphene Supported Palladium Electrocatalysts

4.2.1 Cyclic Voltammetry

The electrochemical properties of graphene supported Palladium electrocatalysts synthesized by modified polyol method and their modified counterparts in alkaline (1M KOH) solution were first examined by cyclic voltammetry (CV) with Pd loading of 0.02 mgcm^{-2}. The CV curves of each

65

catalyst were obtained from the stabilized curve after scanning 20 cycles (Zhao & Zhao, 2013). The cyclic voltammetry shows the adsorption/desorption peaks in the hydrogen region at negative potentials. As more negative potentials were applied, the reduction of H$^+$ and the adsorption of H atoms become stronger:

$$H^+_{(aq)} + e^- + site \rightarrow H_{(ad)}$$
<div align="right">Equation 4.1</div>

This process continued as electrode potentials became more negative until the formation of a H (ad) monolayer was achieved. Immediately the Pd surface was fully covered by hydrogen atoms, the adsorption of H$_2$ molecules occurred:

$$2H_{(ad)} \rightarrow H_{2(ad)}$$
<div align="right">Equation 4.2</div>

These adsorbed hydrogen molecules came together to form hydrogen bubbles which left the Pd electrode surface when they have grown large enough:

$$nH_{2(ad)} \rightarrow nH_{2(g)} + 2n - sites$$
<div align="right">Equation 4.3</div>

At this period, a high cathodic potential was applied on the electrode and many free sites were exposed to the solution. Immediately the above reaction occurred at a high rate, the sharp cathodic current, known as the hydrogen evolution, increased. The formation of the H(ad) monolayer can be easily detected at the potential where the cathodic current increases rapidly. When the potential is reversed, the opposite process (anodic currents in the hydrogen region) occurs (Doña Rodríguez *et al*., 2000).

 The oxidation peak of all the prepared electrocatalysts was not well pronounced (Yi *et al*., 2015) while a significant cathodic reduction peak which is attributed to the reduction of PdO produced on the forward potential scan was observed between -0.2 V and -0.4 V (Klaas *et al*., 2020) for all the prepared electrocatalysts. Among electrocatalysts synthesized by modified polyol method, Pd/NGO exhibited the most intense cathodic reduction peak with highest current density which implies that it provided better evidence for the widest electroactive surface area (ECSA) among the graphene supported Pd catalysts synthesized by modified polyol method as shown in Figure 4.9a (Maiyalagan *et al*., 2005; Narreddula *et al*., 2019). However, for the modified electrocatalysts, Pd/NGO exhibited the most intense cathodic reduction peak as shown in Figure 4.9b which implies that it provided better evidence for the widest electroactive surface area among the modified graphene supported Pd catalysts (Bock *et al*., 2004; Maiyalagan *et al*., 2005).

The ECSA values of all the graphene supported Pd catalysts synthesized by modified polyol method and their modified counterparts were determined by peak area of the cathodic reduction peak of PdO using the equation (Garsany *et al*., 2010; Klaas *et al*., 2020):

$$ECSA_{Pd,cat}(cm^2/mg) = \frac{Q(C/cm^2)}{420 \, \mu C/cm^2 \, L_{Pd}(mg/cm^2)}$$

<div align="right">Equation 4.4</div>

where Q (C/cm^2) is the charge associated with the reduction peak of the catalysts in Coulomb, L_{Pd} (mg/cm^2) is the working electrode Pd loading (0.02 mg/cm^2) while 420 $\mu C/cm^2$ is the value for oxygen monolayer of Pd in equation (4.1) (Klaas *et al*., 2020). From the CV results of graphene (GO, rGO, NGO and NrGO) supported electrocatalysts synthesized by modified polyol method, it is clear that Pd/NGO have the highest ECSA value of 1.84 m^2/g compared to other graphene supported Pd catalysts as indicated in Table 4.4. For the modified counterparts too, it is also evident from the CV results that Pd/NGO exhibited the highest ECSA value of 3.87 m^2/g among graphene supported Pd catalysts as illustrated in Table 4.5.
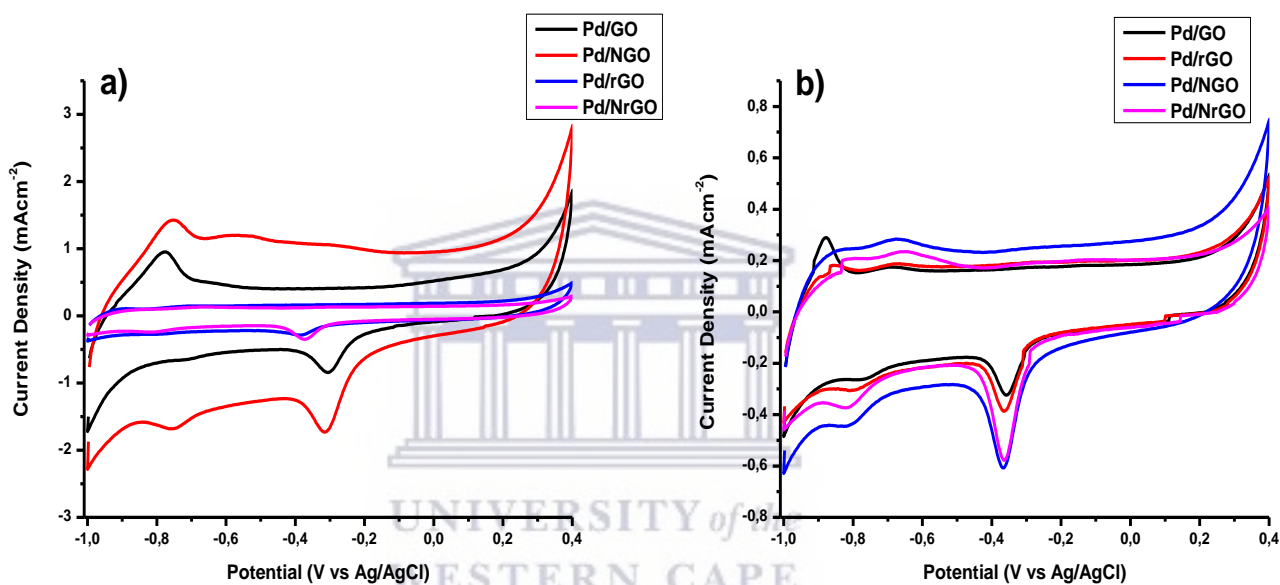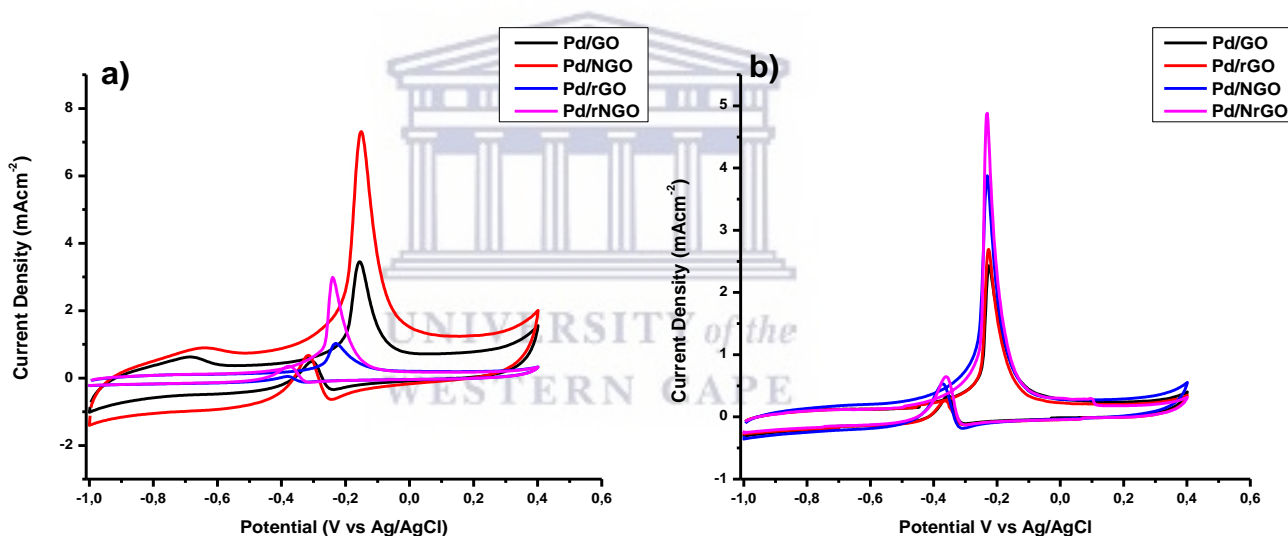

Figure 4.11: The cyclic voltammetry of (a) graphene supported Pd catalysts synthesized by modified polyol method (b) modified counterparts of graphene supported Pd catalysts in N_2 saturated 1 M KOH at scan rate of 0.02 Vs^{-1}.

Table 4.5: Comparison of ECSA with current densities (MOR and Chrono) of graphene supported Pd catalysts synthesized by modified polyol method as determined from the anodic sweep (-0.1 to 0.4 V) at scan rate of 0.02 Vs^{-1}.

Catalysts	Electroactive Surface Area (m^2/g)	Current Density (mA/cm^2) for MOR	Current Density (mA/cm^2) for Chronoamperometry
Pd/GO	1.60	3.45	0.07
Pd/rGO	1.24	1.02	0.03
Pd/NGO	1.84	7.38	0.14
Pd/NrGO	1.53	2.99	0.11

Table 4.6: Comparison of ECSA with current densities (MOR and Chrono) of modified graphene supported Pd catalyst as determined from the anodic sweep (-0.1 to 0.4V) at scan rate of 0.02 Vs^{-1}.

Catalysts	Electroactive Surface Area (m^2/g)	Current Density (mA/cm^2) for MOR	Current Density (mA/cm^2) for Chronoamperometry
Pd/GO	1.70	2.43	0.05
Pd/rGO	3.52	2.70	0.06
Pd/NGO	3.87	3.88	0.14
Pd/NrGO	3.78	4.88	0.14

4.2.2   Methanol Oxidation Reaction

The electrocatalytic activity of the as-synthesized graphene supported Pd catalysts synthesized by modified polyol method and their modified counterparts towards methanol oxidation reaction (MOR) in alkaline (1M KOH) solution in the presence of methanol was examined by cyclic voltammetry (CV) as illustrated in Figure 4.10. In the forward scan, the oxidation peaks correspond to the oxidation of freshly chemosorbed species coming from methanol adsorption. The reverse scan peaks are basically associated with the removal of carbonaceous species which were not completely oxidized in the forward scan than the oxidation of freshly chemosorbed species (Liu *et al*., 2007). The onset potential of graphene supported Pd catalysts synthesized by modified polyol method and their modified counterparts varies from one to another as summarized in Table 4.6 and Table 4.7 respectively. After the anodic scan, the anodic current density declined sharply as a result of the formation of PdO on the electrocatalysts surface at high anodic potential. As the backward scan commenced, the PdO began to reduce and the catalysts surface is reactivated and methanol oxidation occurred again (Yi *et al*., 2011). Among the graphene (GO, rGO, NGO and NrGO) supported Pd catalysts synthesized by modified polyol method, NGO supported Pd catalyst

display the highest anodic peak current density while NrGO supported Pd catalyst display the highest anodic peak current density among the modified graphene supported Pd catalysts, which implies better electroactivity towards methanol electrooxidation on forward scan of negative sweep as illustrated in Figures 4.10a and 4.10b and shown in Table 4.4 and 4.5 respectively. This enhanced performance of Pd/NGO as well as Pd/NrGO which also concur to their stability test, can be ascribed to their better electroactive surface area and incorporation of dopant nitrogen (Bianchini & Shen, 2009; Bock *et al*., 2004; Gómez *et al*., 2016; Du *et al*., 2008; Kiyani *et al*., 2017; Narreddula *et al*., 2019; Zhang *et al*., 2016). The nitrogen functional group on the surface of these support materials intensifies the electron withdrawing effect against the Pd and the decrease in electron density of Pd facilitate the oxidation of methanol fuel (Maiyalagan *et al*., 2005). The N-dopant also serve as defect sites to enhance the nucleation of catalyst nanoparticles (Du *et al*., 2008).

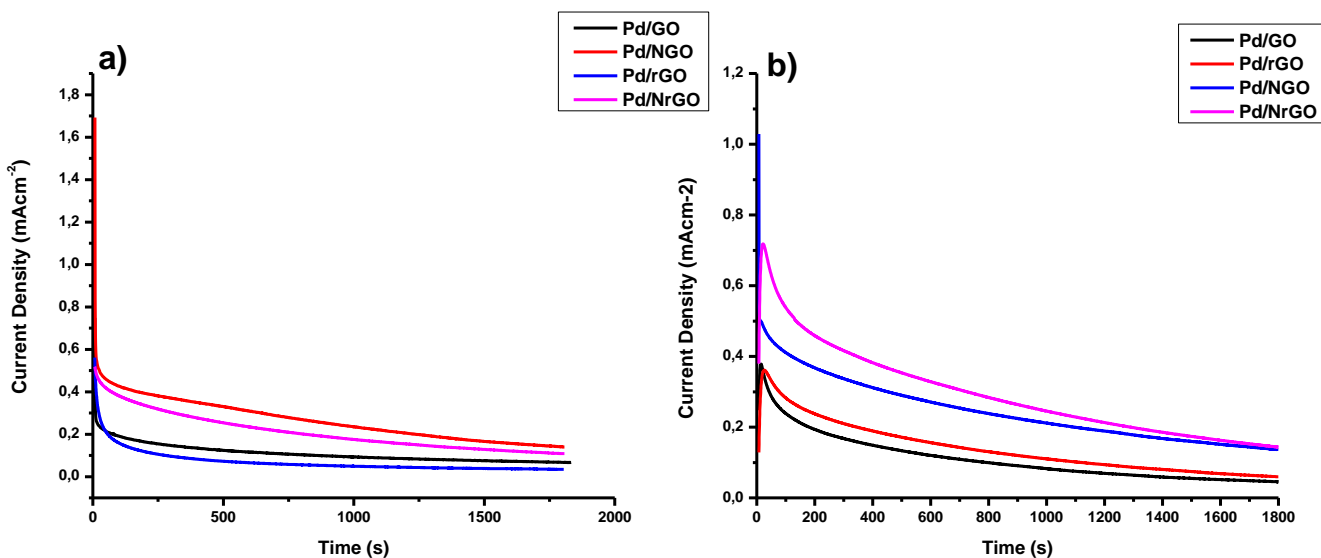Figure 4.12: The cyclic voltammetry curves of methanol oxidation on (a) graphene supported Pd catalysts synthesized by modified polyol method (b) modified graphene supported Pd catalysts in N$_2$ saturated 1 M MeOH + 1 M KOH at scan rate of 0.02 Vs^{-1}.

69

Table 4.7: Results of the study of CVs of graphene supported Pd catalysts synthesized by modified polyol method in 1 M KOH + 1 M Methanol (MeOH).

Electrocatalyst	Onset Potential (V vs Ag/AgCl)	Anodic peak for forward scan I_f (mAcm^{-2})	Anodic peak for reverse scan I_r (mAcm^{-2})	I_f/I_r ratio
Pd/GO	-0.38	3.45	0.49	7.06
Pd/rGO	-0.42	1.02	0.05	21.79
Pd/NGO	-0.36	7.31	0.68	10.83
Pd/NrGO	-0.49	2.99	0.35	8.54

Table 4.8: Results of the study of CVs of modified graphene supported Pd catalysts in 1 M KOH + 1 M MeOH

Electrocatalyst	Onset Potential (V vs Ag/AgCl)	Anodic peak for forward scan I_f (mAcm^{-2})	Anodic peak for reverse scan I_r (mAcm^{-2})	I_f/I_r ratio
Pd/GO	-0.44	2.43	0.35	6.94
Pd/rGO	-0.45	2.70	0.25	10.76
Pd/NGO	-0.46	3.88	0.53	7.28
Pd/NrGO	-0.47	4.88	0.65	7.57

The ratio of forward anodic peak current (I_f) to reverse anodic peak current (I_r) indicate the tolerance ability of electrocatalyst to accumulation of carbonaceous products and less poisoned. This ratio is the supplementary method used to determine the CO tolerance of the catalysts. All the prepared graphene supported Pd catalysts display higher ratio values in excess of 1 which are larger than those reported in literature (Yi *et al*., 2011). Large value of I_f/I_r shows higher oxidation of methanol and better CO tolerance (Garsany *et al*., 2010; Jha *et al*., 2011; Yi *et al*., 2011). From the results shown in Table 4.6 and Table 4.7, it is observed among graphene (GO, rGO, NGO and NrGO) supported Pd catalysts synthesized by modified polyol method and their modified counterparts that Pd/rGO exhibited the highest I_f/I_r ratio of 21.79 and 10.76 respectively. Therefore, Pd/rGO show the best activity towards complete methanol oxidation in both cases. This implies that those with lower activity towards complete methanol oxidation experienced CO poisoning which practically reduces their expected performance (Yi *et al*., 2015).

70

4.2.3 Electrochemical Stability

The electrochemical stability of the synthesized graphene supported Pd catalysts was also tested by chronoamperometry at -0.3 V for 30 minutes. In all the current density-time curves of the graphene supported catalysts, the oxidation current density rapidly reduced in the first 64 seconds while in their modified counterparts, it rapidly reduced in the first 20 seconds which was followed by a slower decay until it attained a steady state. The high current displayed at the beginning of stability testing could be ascribed to the double layer charging between the interface of electrode/electrolyte (Yi *et al*., 2015). The gradual decrease in current density with time which was significantly observed may be attributed to poisoning of the electrocatalysts and decrease in electroactive surface area as the stability test progresses (Yi *et al*., 2015). After 30 minutes' stability study in 1 M KOH + 1 M methanol solution, it was observed among graphene (GO, rGO, NGO and NrGO) supported Pd catalysts synthesized by modified polyol method that the chronoamperometric responses show a different electroactivity order to that experienced in methanol oxidation. The NrGO supported Pd catalyst show more stability than GO supported Pd catalyst while NGO and rGO supported Pd catalysts still exhibit highest and lowest stability respectively in the following order: Pd/NGO > Pd/NrGO > Pd/GO > Pd/rGO as shown in Figure 4.11a. This implies that Pd/NGO, among graphene supported Pd catalysts, still shown better stability than other synthesized electrocatalyst with current density 0.1398 mAcm^{-2}. This better stability in Pd/NGO, which also concur to the MOR result, can also be attributed to the better electroactive surface area and incorporation of nitrogen into the support materials. This influenced the good dispersion of Pd nanoparticles and the stability of the electrodes (Maiyalagan *et al*., 2005). Also, Pd/NrGO display better stability among the modified graphene (GO, rGO, NGO and NrGO) supported Pd catalysts as shown in Figures 4.11b which also show similar MOR results (Anwar *et al*., 2019; Bock *et al*., 2004; Du *et al*., 2008; Aravind *et al*., 2011; Narreddula *et al*., 2019; Pham *et al*., 2016; Sahoo *et al*., 2015; Zhang *et al*., 2016). The current density for the stability test of graphene supported Pd catalysts synthesized by modified polyol method and their modified counterparts is illustrated in Table 4.4 and Table 4.5 respectively.

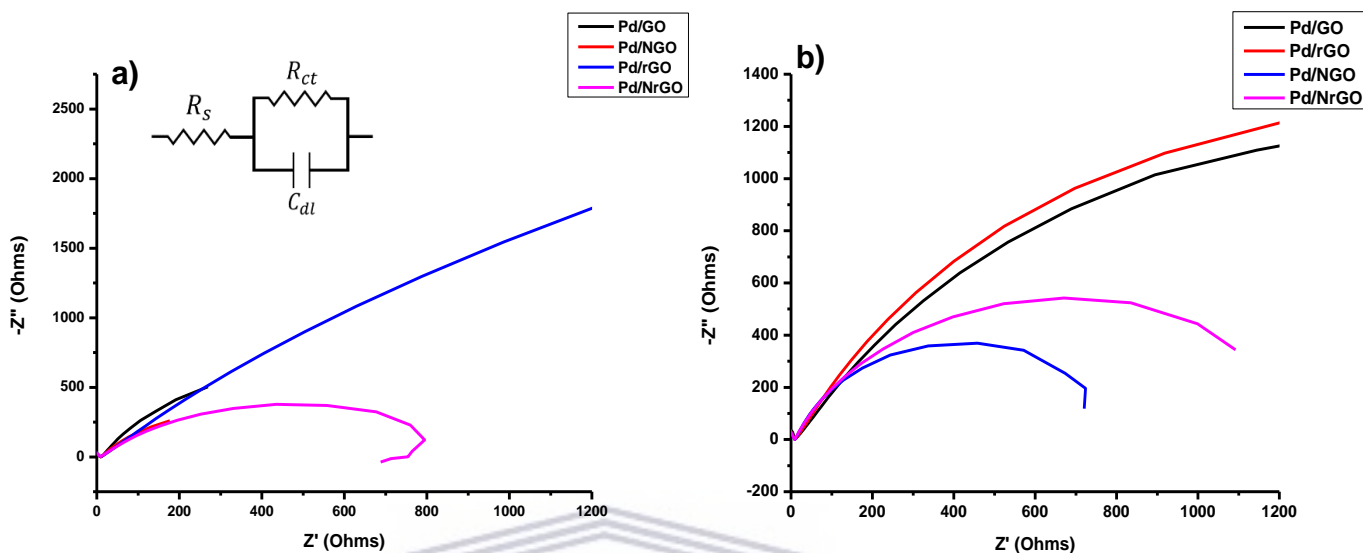Figure 4.13: The chronoamperometry of (a) graphene supported Pd catalysts synthesized by modified polyol method (b) modified graphene supported Pd catalysts in N$_2$ saturated 1 M MeOH + 1 M KOH at potential of -0.3 V.

4.2.4 *Electrochemical Impedance Spectroscopy*

The electrochemical impedance spectroscopy (EIS) revealed the thermodynamic properties of the as-synthesized electrocatalysts. It was used to explore the electrocatalytic kinetics regarding the methanol electrochemical oxidation. EIS is among the most effective techniques used to explore the electrochemical parameters of the electron/electrolyte interface (Ajeel *et al*., 2016; Klaas *et al*., 2020). Figure 4.12 show the interfacial behavior of the prepared electrocatalysts in KOH electrolyte containing methanol at potential of -0.3 V vs Ag/AgCl. An equivalent circuit was employed for fitting the Nyquist plots (inset) which include solution resistance (Rs), charge transfer resistance (Rct) and double layer capacitance (Qdl). Basically, each plot shows a semicircle in the high frequency related to charge transfer. Among the graphene (GO, rGO, NGO and NrGO) supported Pd catalysts synthesized by modified polyol method, NrGO supported Pd catalyst exhibited the least electrochemical impedance. This implies that Pd catalysts supported by this support material show better chemical kinetics than other synthesized Pd catalysts as indicated by Nyquist plot in Figure 4.12a as the charge transfer kinetic of Pd catalyst on this support material significantly improved which encourage mass transfer. This was also confirmed by its resistance charge transfer (Rct) value of 0.723 kΩcm^2 which was determined using Randels-Sevcik cell fitting under open circuit as illustrated in Table 4.8 which was also used for all other prepared electrocatalysts (Du *et al*., 2008; Narreddula *et al*., 2019; Zhang *et al*., 2016). Furthermore, among

72

modified graphene (GO, rGO, NGO and NrGO) supported Pd catalysts, NGO supported Pd catalysts showed the least electrochemical impedance. This also implies that Pd catalysts supported by this material show better chemical kinetics among their counterparts as indicated by Nyquist plot in Figure 4.12b and confirmed by its resistance charge transfer (Rct) value of 0.708 kΩcm^2 as reported in Table 4.9 (Bianchini & Shen, 2009; Bock *et al*., 2004; Kiyani *et al*., 2017).

Figure 4.14: The electrochemical impedance spectroscopy of (a) graphene supported Pd catalysts synthesized by modified polyol method (b) modified graphene supported Pd catalysts in N$_2$ saturated 1 M MeOH +1 M KOH at potential of -0.3 V.

Table 4.9: Summary of electrochemical impedance spectroscopy of graphene supported Pd catalysts synthesized by modified polyol method.

Electrocatalyst	Rct (kΩcm^2)	Rs (kΩcm^2)	CPE [Yo] (mF)	N (CPE Exponent)
Pd/GO	2.40	0.02	0.74	1.00
Pd/rGO	13.60	0.01	0.12	1.00
Pd/NGO	0.88	0.01	1.82	1.00
Pd/NrGO	0.72	0.06	0.22	1.00

http://etd.uwc.ac.za/

Table 4.10: Summary of electrochemical impedance spectroscopy of modified graphene supported Pd catalysts.

Electrocatalyst	Rct (kΩcm^2)	Rs (kΩcm^2)	CPE [Yo] (mF)	N (CPE Exponent)
Pd/GO	3.37	0.03	0.47	1.00
Pd/rGO	3.43	0.03	0.46	1.00
Pd/NGO	0.71	0.03	0.61	1.00
Pd/NrGO	1.17	0.04	0.30	1.00

In conclusion, when graphene supported Palladium catalysts synthesized by modified polyol method were compared with their modified counterparts, it was noted that the modified counterparts did not improve. The graphene supported Palladium catalysts synthesized by modified polyol method showed better activity towards methanol oxidation and more stability than modified graphene supported Palladium catalysts in which Pd/NGO synthesized by modified polyol method was identified as the best. This better performance in graphene supported Palladium catalysts synthesized by modified polyol method than their modified counterparts may be attributed to better dispersion of catalyst nanoparticles on their support materials and lower pH since the higher the pH, the more the OH group present at the surface of the catalyst which reduces the interaction of the Palladium catalyst with the methanol fuel for effective oxidation reaction to take place by blocking the active surface of the Palladium catalyst (Spendelow & Wieckowski, 2007).

UNIVERSITY of the
WESTERN CAPE

5 Results and Discussion of Multi-Walled Carbon Nanotubes, Nitrogen-doped Multi-Walled Carbon Nanotubes and Carbon Nanofibers Supported Palladium Catalysts

This section presents the results obtained from the various characterization carried out on prepared multi-walled carbon nanotubes (MWCNTs), nitrogen-doped multi-walled carbon nanotubes (N-MWCNTs) and carbon nanofibers (CNFs) support materials with their electrocatalysts synthesized by modified polyol method and their modified counterparts using different appropriate techniques as discussed in chapter three in order to know which of the two categories of the electrocatalysts will perform better. First, the energy dispersive X-ray spectroscopy (EDS) coupled with the scanning electron microscopy (JOEL JSM-7500F Scanning Electron Microscope, Mundelein, II, USA, was used to evaluate the Pd metal loading in Pd electrocatalysts and was found to be 37.67 % which was the same for all the synthesized supported Pd catalysts.

5.1 Surface Characterization

The surface characterization carried out include Fourier-Transform Infrared (FT-IR) and Brunauer-Emmett-Teller (BET) for the support materials and X-ray diffraction (XRD) microscopy with High-Resolution Transmission Electron Spectroscopy (HR-TEM) for the supported Pd catalysts.

5.1.1 Fourier-Transform Infrared (FT-IR) of MWCNTs, N-MWCNTs and CNFs Support Materials

In this section, the presence of carbonyl group from the functionalized carbon nanotubes and carbon nanofibers, nitrogen in the N-doped carbon nanotubes and other functional groups in these support materials were confirmed using Fourier-transform infrared (FT-IR) analysis. Figures 5.1 show the FT-IR spectra of the MWCNTs, N-MWCNTs and CNFs support materials. The FT-IR analysis of MWCNTs shows C-O, C=O, O-H bands of carboxylic acid around 1023, 1670 and 2645 cm^{-1} respectively. The appearance of noticeable C-O and C=O peaks of carboxylic acid in functionalized MWCNTs shows that it was activated compared with the unfunctionalized one which does not show significant bands of C-O and C=O carboxylic acid. More so, the FT-IR spectra of N-MWCNTs also show C-O, C=O, O-H bands of carboxylic acid around 1135, 1691, and 2700 cm^{-1} respectively while NO$_2$ band of nitro compound and $C \equiv N$ of nitrile bands were observed around 1556 and 2313 cm^{-1} respectively. The appearance of nitro and nitrile bands in

N-MWCNTs spectra indicate the successful doping of MWCNTs with nitrogen. The presence of N-doped in N-MWCNTs was also validated using EDS as shown in Figure 5.2. The FT-IR analysis of CNFs shows distinctive bands around 1065 and 3668 cm^{-1} which were assigned to C-O and O-H of carboxylic acid respectively while the band around 2962 cm^{-1} was assigned to C-H alkane. The appearance of C-O and O-H peaks of carboxylic acid in activated CNFs shows its functionalization compared with the unactivated one which has none of these bands (Banerjee *et al.*, 2015; Mironenko *et al.*, 2015; Vanyorek *et al.*, 2016). The summary of the observed bands is illustrated in Table 5.1.
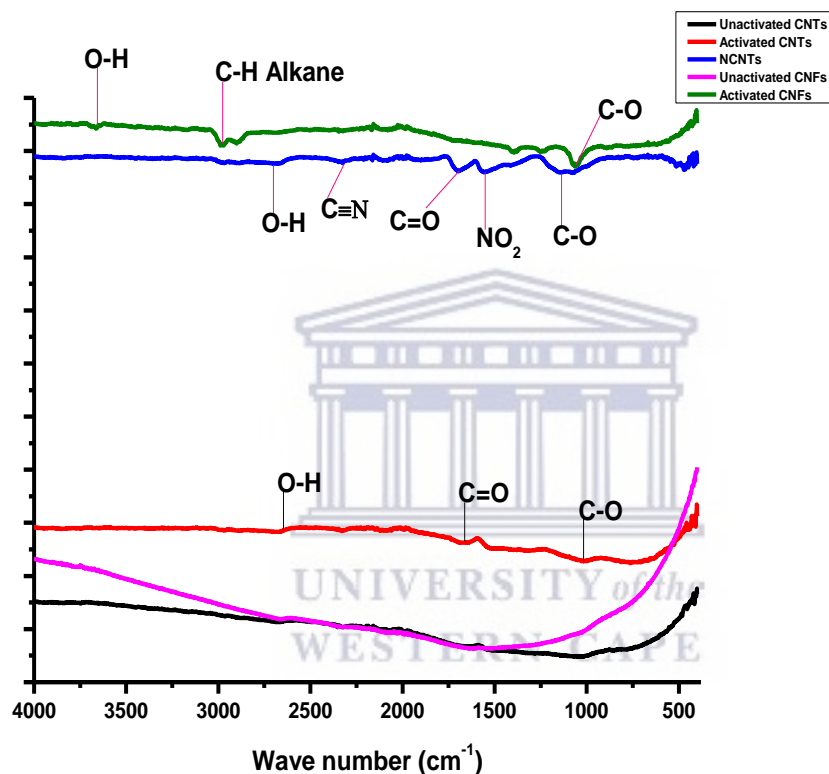
Figure 5.1: The FT-IR Spectra of synthesized MWCNTs, N-MWCNTs and CNFs support materials.

Table 5.1: Observed FT-IR Spectra for Synthesized MWCNTs, N-MWCNTs and CNFs Support Materials.

Support Materials	Functional Groups	Observed bands (cm^{-1})
Activated MWCNTs	C=O Carboxylic acid	1670
	C-O Carboxylic acid	1023
	O-H Carboxylic acid	2645
N-MWCNTs	C=O Carboxylic acid	1691
	C-O Carboxylic acid	1135
	O-H Carboxylic acid	2700
	NO$_2$ Nitro compound	1556
	$C \equiv N$ Nitrile	2313
Activated CNFs	C-O Carboxylic acid	1065
	O-H Carboxylic acid	3668
	C-H Alkane	2962
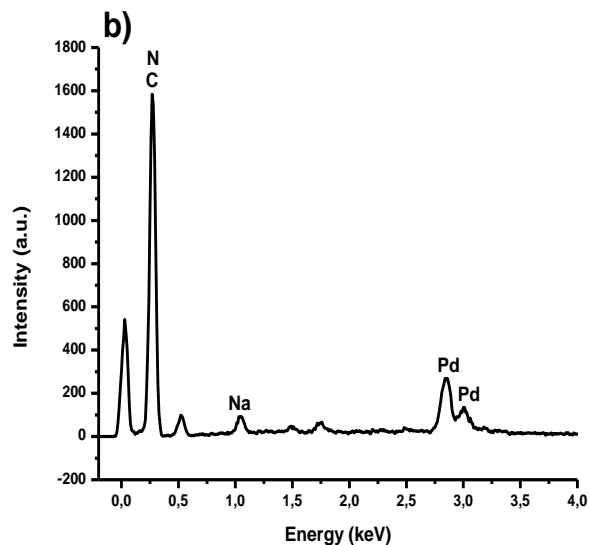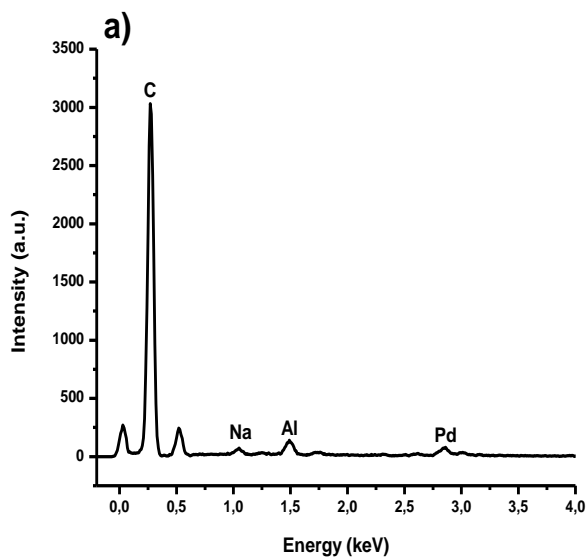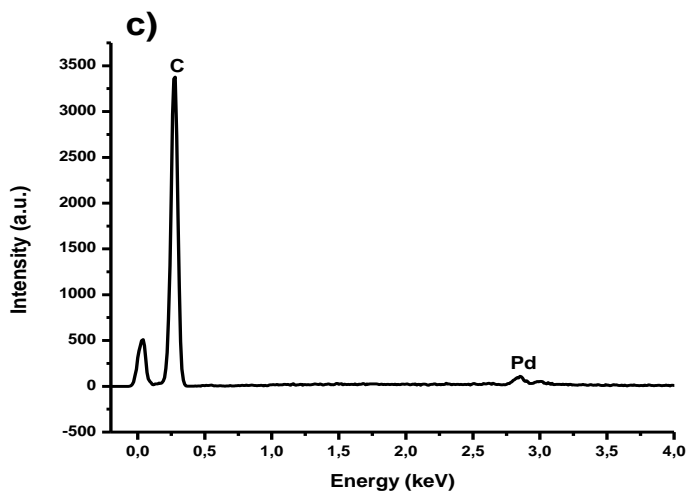
Figure 5.2: The EDS Spectra of synthesized (a) Pd/MWCNTs (b) Pd/N-MWCNTs, (c) Pd/CNFs.

5.1.2 Brunauer-Emmett-Teller of MWCNTs, N-MWCNTs and CNFs Support Materials

The specific surface area, pore volume and pore size of the prepared MWCNTs, N-MWCNTs and CNFs support materials were also investigated using Brunauer-Emmett-Teller (BET) as presented in Table 5.1. Surface area measurements were taken from the support materials to first evaluate the surface area of the carbon support materials used. Among these prepared support materials, N-MWCNTs showed the highest surface area and pore volume of 219.50 m^2 g^{-1} and 0.77 cm^3/g respectively but with pore size of 132.21 Å which is a little bit lower than that of MWCNTs which is 169.95 Å. This better surface area in N-MWCNTs can be ascribed to the presence of dopant nitrogen which also serves as the defect sites to amplify the nucleation of the Pd metal nanoparticles while the decrease in the pore size can be attributed to its higher agglomeration compared to MWCNTs as shown in HR-TEM image in Figure 5.6.

Since the performance of electrocatalysts increases with increase in the support surface area and pore volume, the catalyst must therefore be supported with a high surface area and pore volume support materials for proper dispersal of the catalyst nanoparticles which aids the catalyst activity and make low catalyst loading feasible for fuel cell operations (Antolini, 2009). Figure 5.3 and Figure 5.4 show the adsorption-desorption and pore distribution graphs of synthesized MWCNTs, N-MWCNTs and CNFs respectively.

Table 5.2: The BET surface area, pore volume and pore size of the prepared MWCNTs, N-MWCNTs and CNFs support materials.

Support Materials	Surface Area (m²/g)	Pore Volume (cm³/g)	Pore size (Å)
MWCNTs	67.45	0.29	169.95
N-MWCNTs	219.50	0.77	132.21
CNFs	14.32	0.04	105.30
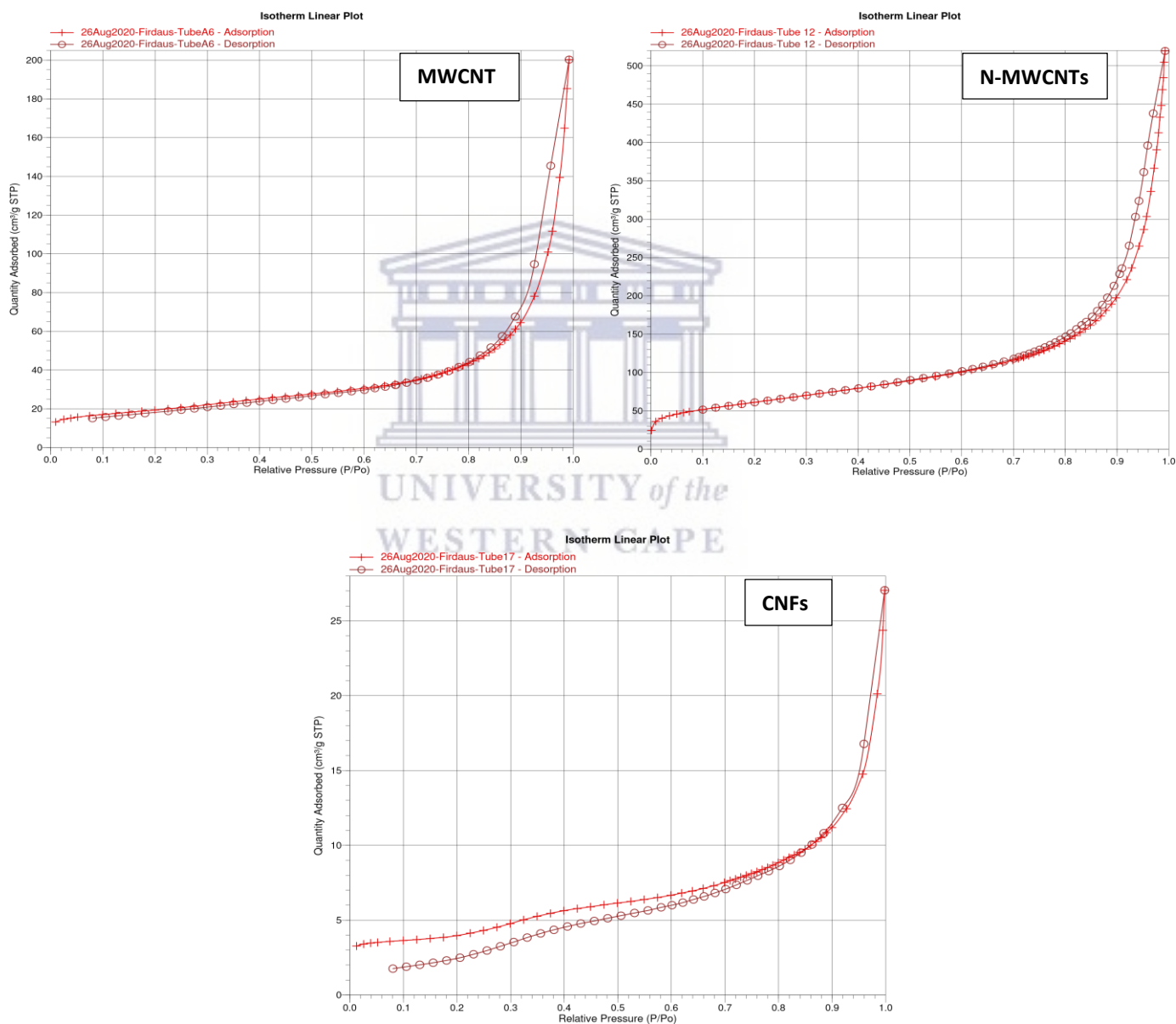
Figure 5.3: Adsorption-desorption graphs of synthesized MWCNTs, N-MWCNTs and CNFs.

79
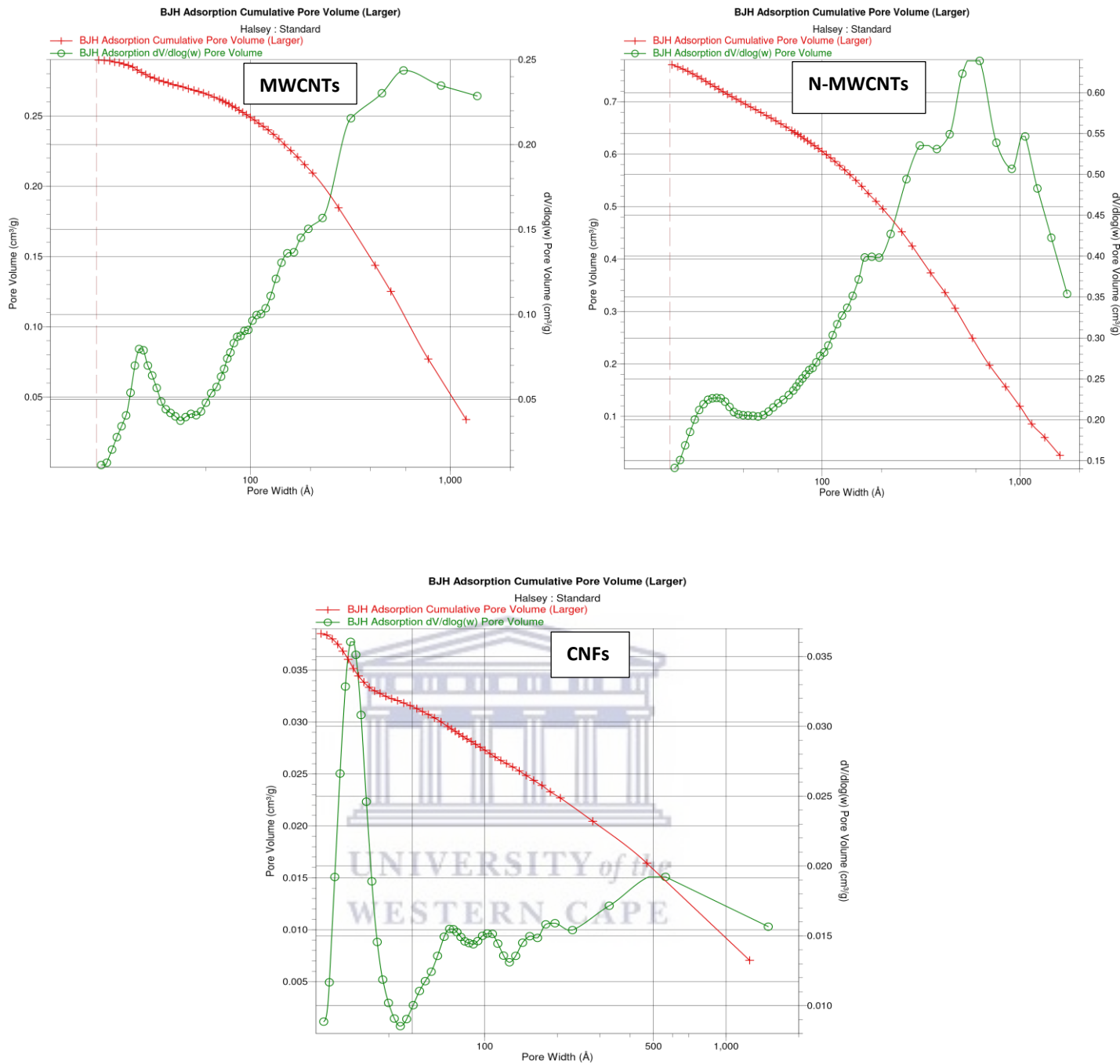
Figure 5.4: Pore size distribution graphs of synthesized MWCNTs, N-MWCNTs and CNFs.

However, when the BET surface area of MWCNTs, N-MWCNTs and CNFs was compared with the graphene based support materials, the BET results of MWCNTs and N-MWCNTs with surface area of 67.45 and 219.50 m^2/g respectively showed that they exhibit higher surface area than graphene based support materials- GO, rGO, NGO and NrGO with surface area of 9.20, 3.36, 41.92 and 6.46 m^2/g respectively while CNFs showed lower BET surface area of 14.32 m^2/g than NGO with surface area of 41.92 m^2/g.

5.1.3 X-ray Diffraction of MWCNTs, N-MWCNTs and CNFs Supported Palladium Catalysts

The crystallinity and crystallite size of MWCNTs, N-MWCNTs and CNFs supported Palladium catalysts synthesized by modified polyol method and their modified counterparts were also determined using XRD spectra and classical Debye-Scherrer equation respectively as stated in equation 3.2. The sharpest and the most intense peak of all the prepared electrocatalysts appeared around 40º 2-theta scale which is indexed as (111). This peak was used to determine the crystallite size of all the electrocatalysts. The XRD graphitic pattern of electrocatalysts synthesized by modified polyol method and their modified counterparts show five diffraction peaks at 2-theta value around 40.0276º, 46.5107º, 68.0866º, 81.9789º and 86.8841º and are indexed to the (111), (200), (220), (311) and (222) crystal plane of Pd face-centered cubic (fcc) crystallographic structure as shown in Figure 5.3a and Figure 5.3b respectively (Carrera-Cerritos *et al.*, 2014; Dector *et al.*, 2013; Klaas *et al.*, 2020). The broad peak located at approximately 25º 2-theta scale on the other hand corresponds to the plane (002) of carbon (Dector *et al.*, 2013; Groves *et al.*, 2012; Yi *et al.*, 2015). The XRD results showed that all the electrocatalysts are crystalline in nature as shown in Figure 5.3a and Figure 5.3b which is also corroborated with selected area electron diffraction (SAED) as shown in Figures 5.4 and 5.5.
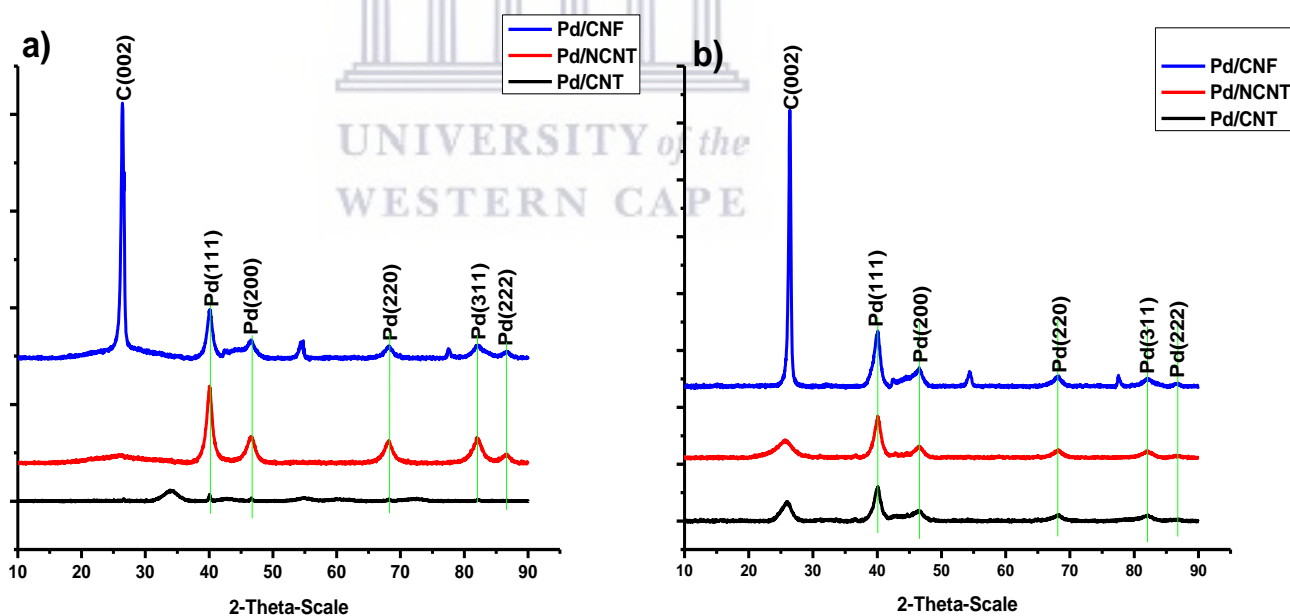
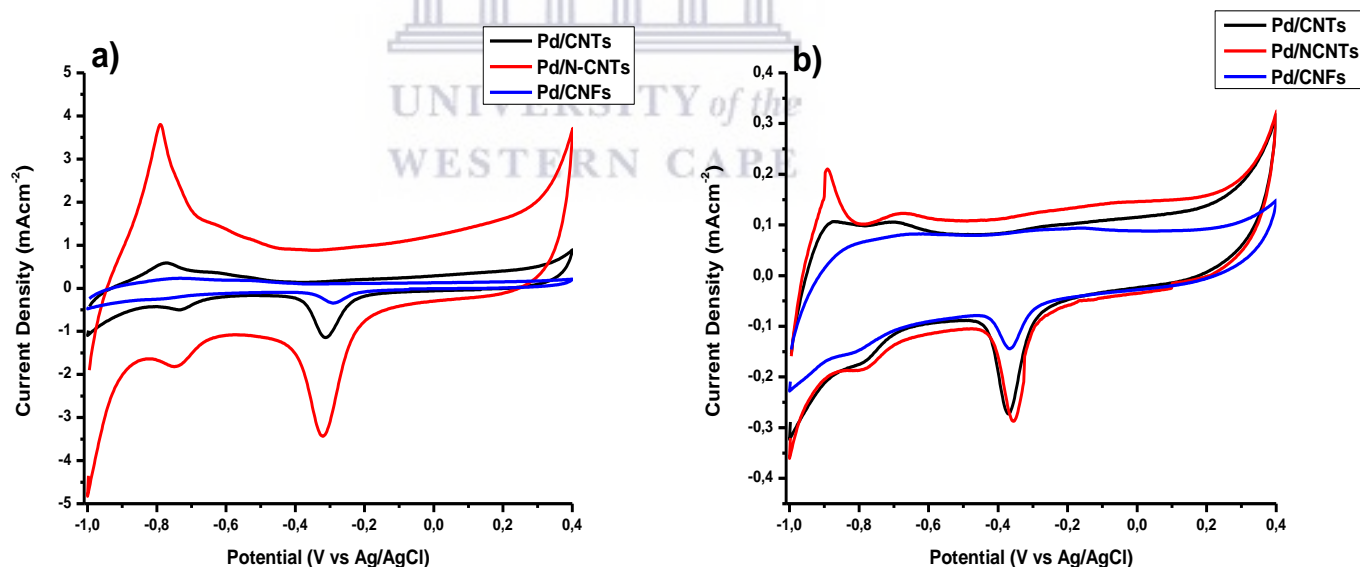

Figure 5.5: XRD spectra of (a) MWCNTs, N-MWCNTs and CNFs supported Pd catalysts synthesized by modified polyol method (b) modified MWCNTs, N-MWCNTs and CNFs supported Pd catalysts.

81
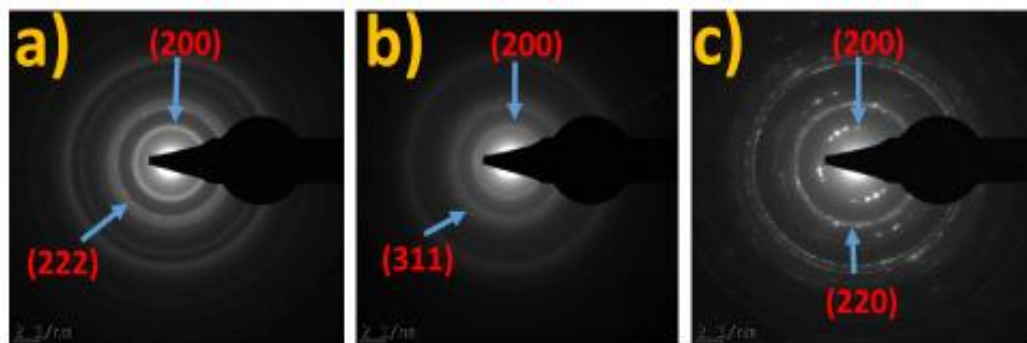
Figure 5.6: Selected area electron diffraction (SAED) of supported Pd catalysts synthesized by modified polyol method: (a) Pd/MWCNTs (b) Pd/N-MWCNTs and (c) Pd/CNFs.

Table 5.3: The particle size and crystallite size of MWCNTs, N-MWCNTs and CNFs supported electrocatalysts synthesized by modified polyol method.

Electrocatalyst	Particle size (nm) HR-TEM	Crystallite size (nm) XRD
Pd/MWCNTs	6 ± 2.2	6.2
Pd/N-MWCNTs	6 ± 2.0	5.8
Pd/CNFs	2 ± 2.1	0.1
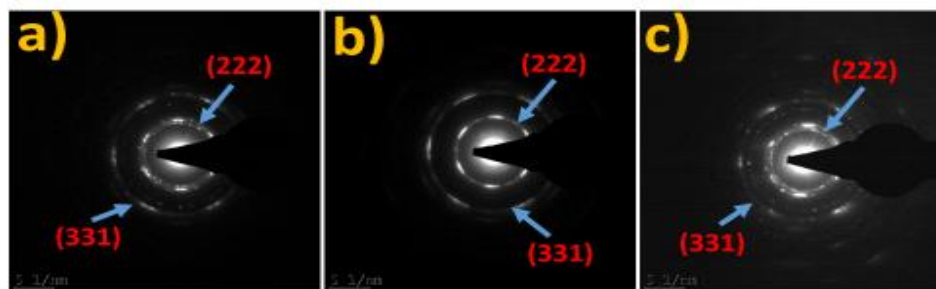
Figure 5.7: Selected area electron diffraction (SAED) of modified supported Pd catalysts: (a) Pd/MWCNTs (b) Pd/N-MWCNTs and (c) Pd/CNFs.

Table 5.4: The particle size and crystallite size of modified MWCNTs, N-MWCNTs and CNFs supported electrocatalysts.

Electrocatalyst	Particle size (nm) HR-TEM	Crystallite size (nm) XRD
Pd/MWCNTs	6 ± 0.9	6.1
Pd/N-MWCNTs	6 ± 0.8	6.0
Pd/CNFs	3 ± 0.8	0.1

82

5.1.4 *The High-Resolution Transmission Electron Spectroscopy of MWCNTs, N-MWCNTs and CNFs Support Palladium Catalysts*

Figure 5.6 and Figure 5.7 show the nanomorphological structures of the synthesized MWCNTs, N-MWCNTs and CNFs supported electrocatalysts examined using High-Resolution Transmission Electron Spectroscopy (HR-TEM) with their frequency distribution from 50 randomly selected nanoparticles. For the MWCNTs, N-MWCNTs and CNFs supported Pd catalysts synthesized by modified polyol method, the images revealed a homogenous with relatively small particle size (since nanoparticles usually show a nanodimensional size of 1-100 nm (Cookson, 2012)) which ranges between 2 and 6 nm as illustrated in Table5.2. However, agglomeration was observed in all the synthesized supported electrocatalysts.
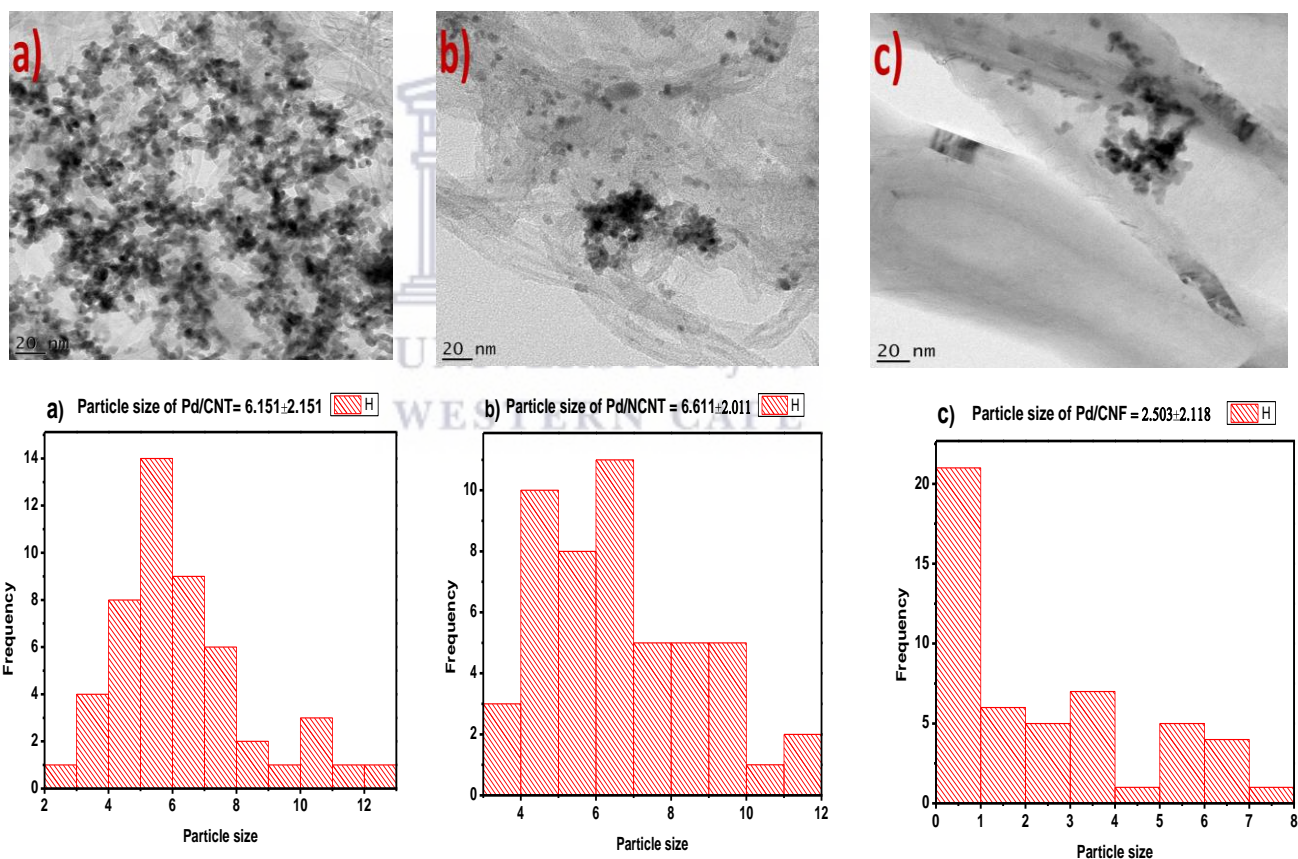
Figure 5.8: HR-TEM images with their respective histograms for supported Pd catalysts synthesized by modified polyol method: (a) Pd/MWCNTs (b) Pd/N-MWCNTs and (c) Pd/CNFs.

In case of modified MWCNTs, N-MWCNTs and CNFs supported Pd catalysts, the images also revealed a homogenous distribution as shown in Figure 5.7 with relatively small particle size which ranges between 3 and 6 nm as illustrated in Table 5.3.
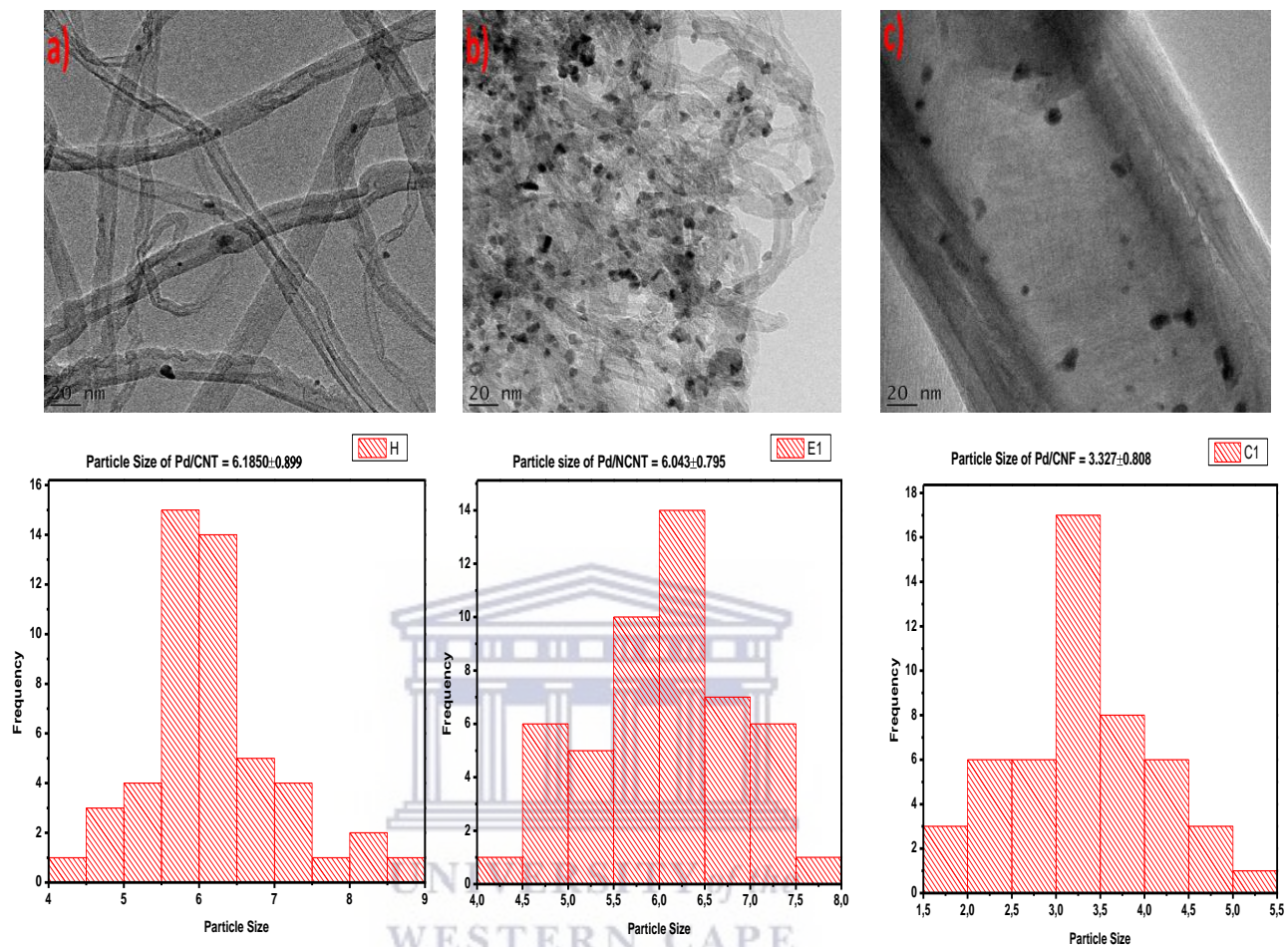
Figure 5.9: HR-TEM images with their respective histograms for modified supported Pd catalysts: (a) Pd/MWCNTs (b) Pd/N-MWCNTs and (c) Pd/CNFs.

5.2 Electrochemical Evaluation of MWCNTs, N-MWCNTs and CNFs Supported Palladium Catalysts

5.2.1 Cyclic Voltammetry

The electrochemical properties of MWCNTs, N-MWCNTs and CNFs supported Pd catalysts synthesized by modified polyol method and their modified counterparts in alkaline (1M KOH) solution were first examined by cyclic voltammetry (CV) with Pd loading of 0.02 mgcm^{-2}. The CV curves of each Pd electrocatalyst were also obtained from the stabilized curve after scanning 20 cycles (Zhao & Zhao, 2013). The CV curves shows the adsorption/desorption peaks in the

hydrogen region at negative potentials. As more negative potentials were applied, the reduction of H^+ and the adsorption of H atoms become stronger. Details of this reaction steps have been discussed earlier in chapter 4. From the cyclic voltammetry of the prepared Pd electrocatalysts, the oxidation peak of all the prepared Pd electrocatalysts was not well pronounced (Yi *et al*., 2015) while a significant cathodic reduction peak which is attributed to the reduction of PdO produced on the forward potential scan is observed between -0.2 V and -0.4 V (Klaas *et al*., 2020) for all the prepared Pd electrocatalysts. Among MWCNTs, N-MWCNTs and CNFs supported Pd catalysts synthesized by modified polyol method and their modified counterparts, Pd/N-MWCNTs exhibited the most intense cathodic reduction peak with highest current density which implies that it provided better evidence for the widest electroactive surface area (ECSA) among MWCNTs, N-MWCNTs and CNFs supported Pd catalysts as shown in Figure 5.8a and b (Maiyalagan *et al*., 2005; Narreddula *et al*., 2019). The ECSA values of MWCNTs, N-MWCNTs and CNFs supported Pd catalysts were also determined by peak area of the cathodic reduction peak of PdO using the equation 4.1 (Garsany *et al*., 2010; Klaas *et al*., 2020).

From the CV results of MWCNTs, N-MWCNTs and CNFs supported Pd catalysts synthesized by modified polyol method and their modified counterparts, it is clear in both cases that Pd/N-MWCNTs have the highest ECSA value of 5.53 and 1.78 m^2/g respectively compared to MWCNTs and CNFs supported Pd catalysts as indicated in Table 5.4 and Table 5.5 respectively.
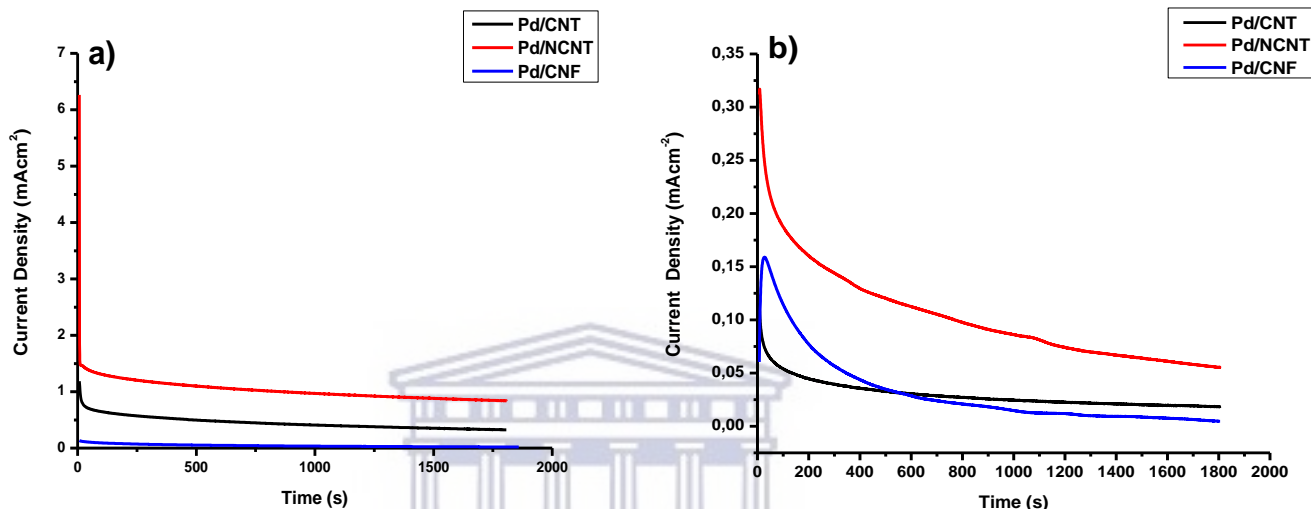

Figure 5.10: The cyclic voltammetry of (a) MWCNTs, N-MWCNTs and CNFs supported electrocatalysts synthesized by modified polyol method (b) modified MWCNTs, N-MWCNTs and CNFs supported electrocatalysts in N_2 saturated 1 M KOH at scan rate of 0.02 Vs^{-1}.

85

Table 5.5: Comparison of ECSA with current densities (MOR and Chrono) of MWCNTs, N-MWCNTs and CNFs supported Pd catalysts synthesized by modified polyol method as determined from the anodic sweep (-0.1 to 0.4 V) at scan rate of 0.02 Vs^{-1}.

Catalysts	Electroactive Surface Area (m^2/g)	Current Density (mA/cm^2) for MOR	Current Density (mA/cm^2) for Chronoamperometry
Pd/MWCNTs	1.81	9.09	0.32
Pd/N-MWCNTs	5.53	22.22	0.84
Pd/CNFs	0.42	1.90	0.02

Table 5.6: Comparison of ECSA with current densities (MOR and Chrono) of modified MWCNTs, N-MWCNTs and CNFs supported Pd catalyst films determined from the anodic sweep (-0.1 to 0.4V) at scan rate of 0.02 Vs^{-1}.

Catalysts	Electroactive Surface Area (m^2/g)	Current Density (mA/cm^2) for MOR	Current Density (mA/cm^2) for Chronoamperometry
Pd/MWCNTs	1.70	1.46	0.02
Pd/N-MWCNTs	1.78	1.98	0.06
Pd/CNFs	0.69	1.49	0.01

5.2.2 Methanol Oxidation Reaction

The electrocatalytic activity of MWCNTs, N-MWCNTs and CNFs supported Pd catalysts synthesized by modified polyol method and their modified counterparts towards methanol oxidation reaction (MOR) in alkaline (1M KOH) solution in the presence of methanol was also examined by cyclic voltammetry (CV) as illustrated in Figure 5.9a and b. In the forward scan, the oxidation peaks correspond to the oxidation of freshly chemosorbed species coming from methanol adsorption. The reverse scan peaks are basically associated with the removal of carbonaceous species which were not completely oxidized in the forward scan than the oxidation of freshly chemosorbed species (Liu *et al*., 2007). The onset potential of MWCNTs, N-MWCNTs and CNFs supported Pd catalysts synthesized by modified polyol method and their modified counterparts varies from one to another as summarized in Table 5.6 and Table 5.7 respectively. After the anodic scan, the anodic current density also declined sharply as a result of the formation of PdO on the electrocatalysts surface at high anodic potential. As the backward scan commenced, the PdO began to reduce and the catalysts surface is reactivated and methanol oxidation occurred again (Yi *et al*., 2011). Among MWCNTs, N-MWCNTs and CNFs supported Pd catalysts

86

synthesized by modified polyol method and their modified counterparts, N-MWCNTs supported Pd catalysts display the highest anodic peak current density which implies better electroactivity towards methanol electrooxidation on forward scan of negative sweep as illustrated in Figures 5.9a and b and summarized in Table 5.4 and 5.5 respectively. This enhanced performance in Pd/N-MWCNTs which also concur to the stability test, can be ascribed to better electroactive surface area and incorporation of dopant nitrogen (Bianchini & Shen, 2009; Bock *et al.*, 2004; Gómez *et al.*, 2016; Du *et al.*, 2008; Kiyani *et al.*, 2017; Narreddula *et al.*, 2019; Zhang *et al.*, 2016). The N-dopant in the support materials serve as defect sites to enhance the nucleation of catalyst nanoparticles (Du *et al.*, 2008).
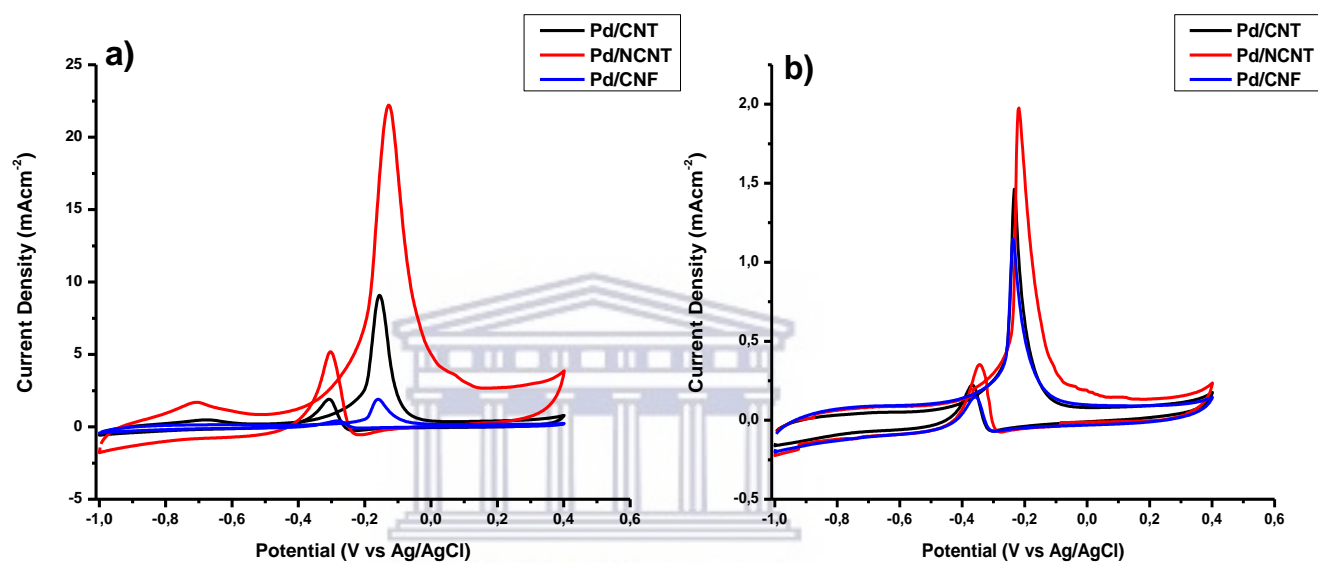
Figure 5.11: The cyclic voltammetry curves of methanol oxidation on (a) MWCNTs, N-MWCNTs and CNFs supported Pd catalysts synthesized by modified polyol method (b) modified MWCNTs, N-MWCNTs and CNFs supported Pd catalysts in N_2 saturated 1 M MeOH + 1 M KOH at scan rate of 0.02 Vs^{-1}.

Table 5.7: Results of the study of CVs of MWCNTs, N-MWCNTs and CNFs supported Pd catalysts synthesized by modified polyol method in 1 M KOH + 1 M MeOH.

Electrocatalyst	Onset Potential (V vs Ag/AgCl)	Anodic peak for forward scan I_f ($mAcm^{-2}$)	Anodic peak for reverse scan I_r ($mAcm^{-2}$)	I_f/I_r ratio
Pd/MWCNTs	-0.41	9.74	1.86	5.23
Pd/N-MWCNTs	-0.43	22.21	5.18	4.29
Pd/CNFs	-0.34	1.90	0.41	4.68

87

Table 5.8: Results of the study of CVs of modified MWCNTs, N-MWCNTs and CNFs supported Pd catalysts in 1 M KOH + 1 M MeOH.

Electrocatalyst	Onset Potential (V vs Ag/AgCl)	Anodic peak for forward scan I_f (mAcm^{-2})	Anodic peak for reverse scan I_r (mAcm^{-2})	I_f/I_r ratio
Pd/MWCNTs	-0.48	1.46	0.22	6.56
Pd/N-MWCNTs	-0.42	1.98	0.35	5.62
Pd/CNFs	-0.43	1.15	0.15	7.84

From the results shown in Table 5.6 and Table 5.7, it is observed that Pd/MWCNTs, among N-MWCNTs and CNFs supported Palladium electrocatalysts synthesized by modified polyol method, with I_f/I_r ratio of 5.23 as well as Pd/CNFs, among the modified MWCNTs and N-MWCNTs supported Palladium electrocatalysts, with I_f/I_r ratio of 7.84 show the best activity towards complete methanol oxidation. This implies that those with lower activity towards complete methanol oxidation experienced CO poisoning which invariably reduces their expected performance (Yi *et al*., 2015).

5.2.3 Electrochemical Stability

The electrochemical stability of the synthesized MWCNTs, N-MWCNTs and CNFs supported Pd catalysts was also tested by chronoamperometry at -0.3 V for 30 minutes. In all the current density-time curves of these supported catalysts, the oxidation current density rapidly reduced in the first 20 seconds while in their modified counterparts, it rapidly reduced in the first 165 seconds which was followed by a slower decay until it attained a steady state. The high current displayed at the beginning of stability testing could also be ascribed to the double layer charging between the interface of electrode/electrolyte (Yi *et al*., 2015). The gradual decrease in current density with time which was significantly observed may be attributed to poisoning of the Pd electrocatalysts and decrease in electroactive surface area as the durability test progresses (Yi *et al*., 2015). After 30 minutes' stability study in 1 M KOH + 1 M methanol solution, it was also observed among MWCNTs, N-MWCNTs and CNFs supported Pd catalysts synthesized by modified polyol method and their modified counterparts that the results still concur with the methanol electrooxidation in the following order: Pd/N-MWCNTs > Pd/MWCNTs > Pd/CNFs as shown in Figure 5.10a and b (Anwar *et al*., 2019; Bock *et al*., 2004; Du *et al*., 2008; Aravind *et al*., 2011; Narreddula *et al*., 2019; Pham *et al*., 2016; Sahoo *et al*., 2015; Zhang *et al*., 2016).This implies that Pd/N-MWCNTs,

among MWCNTs and CNFs supported Pd catalysts synthesized by modified polyol method and their modified counterparts, shown better stability in both cases than other synthesized Pd catalysts with current density of 0.84 and 0.06 mAcm^{-2} respectively. This better stability in Pd/N-MWCNTs, which is also concur to the MOR result, can also be attributed to its better electroactive surface area and incorporation of nitrogen into the support materials as the nitrogen functionality in tubular N-MWCNTs influence the dispersion of Pd nanoparticles and the stability of the electrodes (Maiyalagan *et al*., 2005). The current density for the stability test of all these electrocatalysts is illustrated in Table 5.4 and Table 5.5.

Figure 5.12: The chronoamperometry of (a) MWCNTs, N-MWCNTs and CNFs supported Pd catalysts synthesized by modified polyol method (b) modified MWCNTs, N-MWCNTs and CNFs supported Pd catalysts in N$_2$ saturated 1 M MeOH + 1 M KOH at potential of -0.3 V.

5.2.4   *Electrochemical Impedance Spectroscopy*

The electrochemical impedance spectroscopy (EIS) of MWCNTs, N-MWCNTs and CNFs supported Pd catalysts synthesized by modified polyol method and their modified counterparts was also carried out. Among the MWCNTs, N-MWCNTs and CNFs supported Pd catalysts synthesized by modified polyol method, N-MWCNTs supported Pd catalysts also exhibited the least electrochemical impedance. This implies that catalysts supported by this support material show better chemical kinetics than other counterparts as indicated by Nyquist plot in Figure 5.11a as the charge transfer kinetic of Pd catalyst on this support material significantly improve which encourage mass transfer. This was also confirmed by resistance charge transfer (Rct) value of 0.35 kΩcm^2 respectively which was determined using Randels-Sevcik cell fitting under open circuit as illustrated in Table 5.8 which was also used for all other prepared Pd catalysts (Du *et al*., 2008;

Narreddula *et al*., 2019; Zhang *et al*., 2016). However, among the modified MWCNTs, N-MWCNTs and CNFs supported Pd catalysts, MWCNTs supported Pd catalysts showed the least electrochemical impedance. This implies that Pd catalysts supported by MWCNTs show better chemical kinetics than its counterparts as indicated by Nyquist plot in Figure 5.11b and confirmed by resistance charge transfer (Rct) value of 2.05 kΩcm^2 as illustrated in Table 5.9 (Bianchini & Shen, 2009; Bock *et al*., 2004; Kiyani *et al*., 2017).
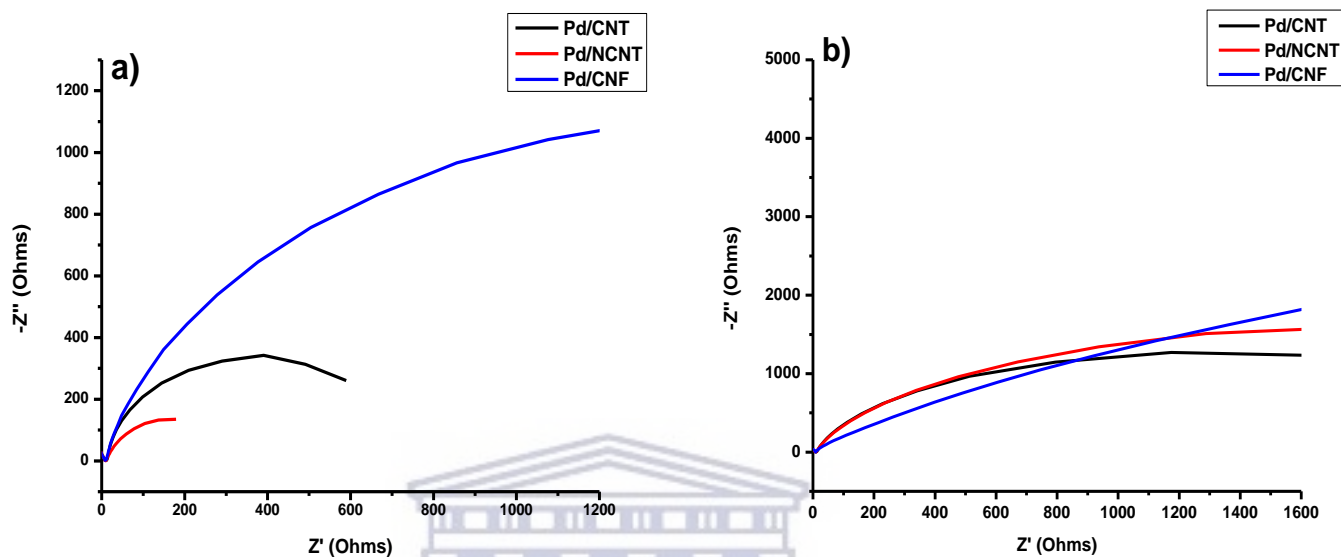
Figure 5.13: The electrochemical impedance spectroscopy of (a) MWCNTs, N-MWCNTs and CNFs supported Pd catalysts synthesized by modified polyol method (b) modified MWCNTs, N-MWCNTs and CNFs supported Pd catalysts in N_2 saturated 1 M MeOH +1 M KOH at potential of -0.3 V.

Table 5.9: Summary of electrochemical impedance spectroscopy of MWCNTs, N-MWCNTs and CNFs supported Pd catalysts synthesized by modified polyol method.

Electrocatalyst	Rct (kΩcm^2)	Rs (kΩcm^2)	CPE [Yo] (mF)	N (CPE Exponent)
Pd/MWCNTs	0.71	0.01	1.19	1.00
Pd/N-MWCNTs	0.35	0.01	4.49	1.00
Pd/CNFs	3.01	-0.01	0.09	1.00

Table 5.10: Summary of electrochemical impedance spectroscopy of modified MWCNTs, N-MWCNTs and CNFs supported Pd catalysts.

Electrocatalyst	Rct (kΩcm²)	Rs (kΩcm²)	CPE [Yo] (mF)	N (CPE Exponent)
Pd/MWCNTs	2.05	0.12	0.19	1.00
Pd/N-MWCNTs	3.61	0.02	0.27	1.00
Pd/CNFs	38.00	-0.19	0.04	0.99

In conclusion, when MWCNTs, N-MWCNTs and CNFs supported Palladium catalysts synthesized by modified polyol method at pH 12 were compared with their modified counterparts at pH 13, it was noted that MWCNTs, N-MWCNTs and CNFs supported Palladium catalysts synthesized by modified polyol method showed better activity towards methanol oxidation and more stability than the modified MWCNTs, N-MWCNTs and CNFs supported Palladium electrocatalysts in which Pd/N-MWCNTs synthesized by modified polyol method was identified as the best. This better performance in MWCNTs, N-MWCNTs and CNFs supported Palladium catalysts synthesized by modified polyol method than their modified counterparts may be attributed to better dispersion of catalyst nanoparticles on their support materials and lower pH. The higher the pH, the more the OH group present at the surface of the electrocatalyst which reduces the interaction of the Palladium catalyst with the methanol fuel for effective oxidation reaction to take place by blocking the active surface of the Pd catalyst (Spendelow & Wieckowski, 2007).

5.3 Comparison of Electrochemical Evaluations of Pd/NGO and Pd/N-MWCNTs Synthesized by Modified Polyol Method

From the results obtained in the analysis of all the graphene, MWCNTs, N-MWCNTs and CNFs supported Pd catalysts, it was observed that carbon supported Pd catalysts synthesized by modified polyol method performed better than their modified counterparts. This section therefore presents the comparison of NGO and N-MWCNTs supported Pd catalysts which are the Pd electrocatalysts that exhibited the best electroactivity among all the Pd electrocatalysts synthesized by the modified polyol method.

5.3.1 Cyclic Voltammetry

The electrochemical properties of Pd/NGO and Pd/N-MWCNTs synthesized by modified polyol method in alkaline (1 M KOH) solution were further examined by cyclic voltammetry (CV) with Pd loading of 0.02 mgcm^{-2}. The CV curves of each Pd electrocatalyst were also obtained from the stabilized curve after scanning 20 cycles (Zhao & Zhao, 2013). The CV curve shows the adsorption/desorption peaks in the hydrogen region at negative potentials. As more negative potentials were applied, the reduction of H$^+$ and the adsorption of H atoms become stronger. Details of this reaction steps have been discussed earlier in chapter 4. From the CV curves of these Pd electrocatalysts, their oxidation peaks were not well pronounced (Yi *et al*., 2015) while a significant cathodic reduction peak which is attributed to the reduction of PdO produced on the forward potential scan is observed between -0.2 V and -0.4 V (Klaas *et al*., 2020) for both prepared Pd electrocatalysts. The CV results show that Pd/N-MWCNTs exhibits the most intense cathodic reduction peak with highest current density than Pd/NGO which implies that it provided better evidence for the widest electroactive surface area (ECSA) as shown in Figure 5.12 (Maiyalagan *et al*., 2005; Narreddula *et al*., 2019). The ECSA values of Pd/NGO and Pd/N-MWCNTs were also determined using the peak area of the cathodic reduction peak of PdO as stated in equation 4.1 earlier in chapter 4. From the CV results of Pd/NGO and Pd/N-MWCNTs, it was observed that Pd/N-MWCNTs shows the highest ECSA value of 5.53 m^2/g compared to Pd/NGO with ECSA value of 1.84 m^2/g as indicated in Table 5.10.
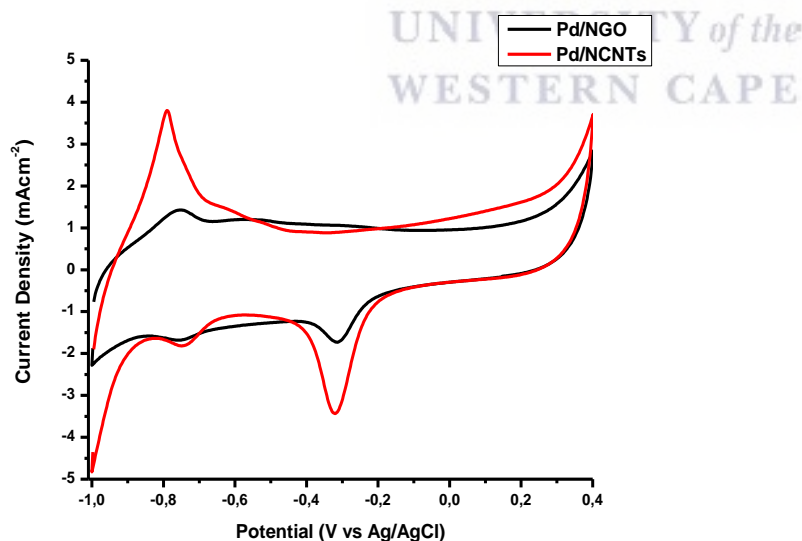
Figure 5.14: The cyclic voltammetry of Pd/NGO and Pd/N-MWCNTs electrocatalysts in N$_2$ saturated 1 M KOH at scan rate of 0.02 Vs^{-1}.

Table 5.11: Comparison of ECSA with current densities (MOR and Chrono) of prepared Pd/NGO and Pd/N-MWCNTs films determined from the anodic sweep (-0.1 to 0.4 V) at scan rate of 0.02 Vs-[1].

Catalysts	Electroactive Surface Area (m^2/g)	Current Density (mA/cm^2) for MOR	Current Density (mA/cm^2) for Chronoamperometry
Pd/NGO	1.84	7.38	0.14
Pd/N-MWCNTs	5.53	22.22	0.84

5.3.2   Methanol Oxidation Reaction

The electrocatalytic activity of Pd/NGO and Pd/N-MWCNTs towards methanol oxidation reaction (MOR) in alkaline (1M KOH) solution in the presence of methanol was also examined by cyclic voltammetry (CV). In the forward scan, the oxidation peaks correspond to the oxidation of freshly chemosorbed species coming from methanol adsorption. The reverse scan peaks are also associated with the removal of carbonaceous species which were not completely oxidized in the forward scan than the oxidation of freshly chemosorbed species (Liu *et al*., 2007). The onset potential of both electrocatalyst also varies from one to another as summarized in Table 5.11. After the anodic scan, the anodic current density declined sharply as a result of the formation of PdO on the Pd electrocatalysts surface at high anodic potential. As the backward scan commenced, the PdO began to reduce and the Pd electrocatalysts surface is reactivated and methanol oxidation occurred again (Yi *et al*., 2011). From the results obtained, Pd/N-MWCNTs display the highest anodic peak current density of 22.22 mA/cm^2 compared to Pd/NGO with current density of 7.38 mA/cm^2 which implies that Pd/N-MWCNTs show better electroactivity towards methanol electrooxidation on forward scan of negative sweep as illustrated in Figure 5.13. This enhanced performance of Pd/N-MWCNTs which also agree to the stability test, can be ascribed to its better electroactive surface area and kinetic with lesser impedance than Pd/NGO (Bianchini & Shen, 2009; Bock *et al*., 2004; Gómez *et al*., 2016; Du *et al*., 2008; Kiyani *et al*., 2017; Narreddula *et al*., 2019; Zhang *et al*., 2016)
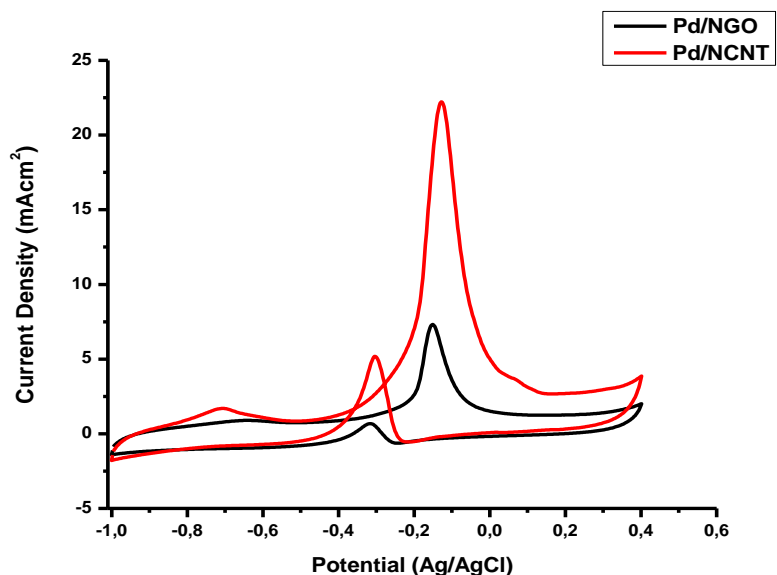
Figure 5.15: The cyclic voltammetry curves of methanol oxidation on Pd/NGO and Pd/N-MWCNTs electrocatalysts in N_2 saturated 1 M MeOH + 1 M KOH at scan rate of 0.02 Vs^{-1}.

Table 5.12: Results of the study of CVs of the prepared Pd/NGO and Pd/N-MWCNTs in 1 M KOH + 1 M Methanol (MeOH).

Electrocatalyst	Onset Potential (V vs Ag/AgCl)	Anodic peak for forward scan I_f (mAcm^{-2})	Anodic peak for reverse scan I_r (mAcm^{-2})	I_f/I_r ratio
Pd/NGO	-0.36	7.31	0.68	10.83
Pd/N-MWCNTs	-0.43	22.21	5.18	4.29

The ratio of forward anodic peak current (I_f) to reverse anodic peak current (I_r) of Pd/NGO and Pd/N-MWCNTs was also evaluated and shows higher ratio values in excess of 1 which are larger than those reported in literature as large value of I_f/I_r shows higher oxidation of methanol and better CO tolerance (Garsany et al., 2010; Jha et al., 2011; Yi et al., 2011). From the results shown in Table 5.11, it is observed that Pd/NGO shows the best activity towards complete methanol oxidation. This implies that Pd/N-MWCNTs experienced more CO poisoning which practically reduces its expected performance (Yi et al., 2015) otherwise, the catalytic performance would have been better than what was observed.

94

5.3.3 Electrochemical Stability

The electrochemical stability of both Pd/NGO and Pd/N-MWCNTs were also tested by chronoamperometry at -0.3 V for 30 minutes. After 30 minutes' stability study in 1 M KOH + 1 M methanol solution, the result revealed that Pd/N-MWCNTs show better stability with current density of 0.84 mA/cm^2 than Pd/NGO with current density 0.14 mA/cm^2 as shown in Figure 5.14. This results, which concur to the MOR result, can also be attributed to the better electroactive surface area, kinetics and tubular morphology of N-MWCNTs in Pd/N-MWCNTs than Pd/NGO (Maiyalagan *et al*., 2005). The high current displayed at the beginning of stability testing could be ascribed to the double layer charging between the interface of electrode/electrolyte (Yi *et al*., 2015). The gradual decrease in current density with time was significantly observed which may be attributed to poisoning of the electrocatalysts and decrease in electroactive surface area as the stability test progresses (Yi *et al*., 2015). The current density for the stability test of these electrocatalysts is illustrated in Table 5.10
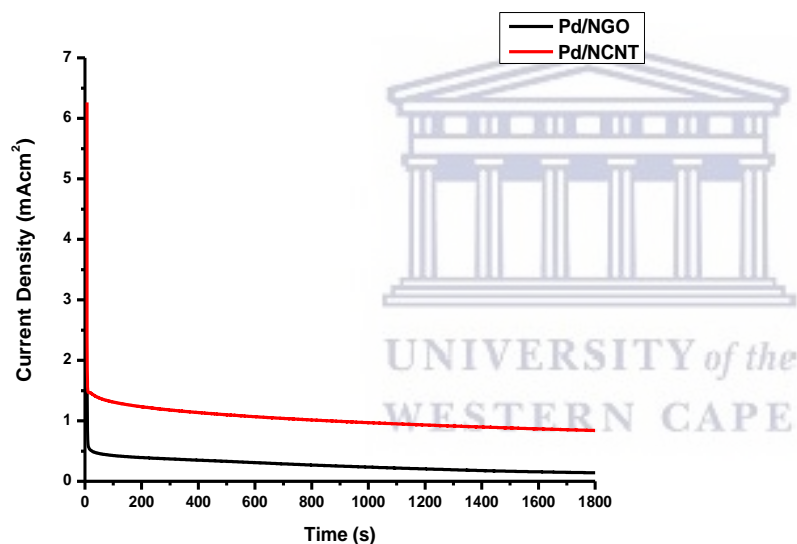
Figure 5.16: The chronoamperometry of Pd/NGO and Pd/N-MWCNTs in N$_2$ saturated 1 M MeOH + 1 M KOH at potential of -0.3 V.

5.3.4 Electrochemical Impedance Spectroscopy

The electrochemical impedance spectroscopy (EIS) of Pd/NGO and Pd/N-MWCNTs was carried out in KOH electrolyte containing methanol at potential of -0.3 V vs Ag/AgCl. An equivalent circuit was also employed for fitting the Nyquist plots which include solution resistance (Rs), charge transfer resistance (Rct) and double layer capacitance (Qdl). Each plot shows a semicircle in the high frequency related to charge transfer. From the result obtained, N-MWCNTs supported

electrocatalysts exhibited the least electrochemical impedance compared with Pd/NGO. This implies that catalysts supported by N-MWCNTs materials show better chemical kinetics than the one supported by NGO as indicated by Nyquist plot in Figure 5.15. This was also confirmed by their resistance charge transfer (Rct) value of 0.35 kΩcm^2 and 0.88 kΩcm^2 respectively which were determined using Randels-Sevcik cell fitting under open circuit as illustrated in Table 5.12 (Du *et al*., 2008; Narreddula *et al*., 2019; Zhang *et al*., 2016).
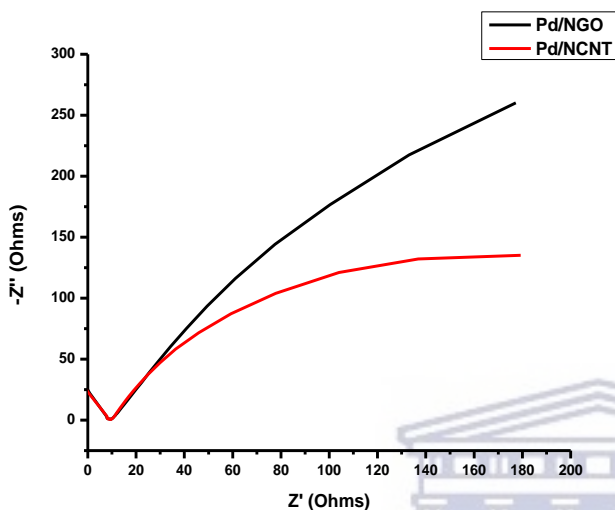
Figure 5.17: The electrochemical impedance spectroscopy of Pd/NGO and Pd/N-MWCNTs in N$_2$ saturated 1 M MeOH +1 M KOH at potential of -0.3 V.

Table 5.13: Summary of electrochemical impedance spectroscopy of prepared Pd/NGO and Pd/N-MWCNTs

Electrocatalyst	Rct (kΩcm^2)	Rs (kΩcm^2)	CPE [Yo] (mF)	N (CPE Exponent)
Pd/NGO	0.88	0.01	1.82	1.00
Pd/N-MWCNTs	0.35	0.01	4.49	1.00

In conclusion, from all the results obtained, it is obvious that N-MWCNTs provided better evidence for supportive activity than NGO as the catalyst supported by N-MWCNTs shows better electrocatalytic activity than the catalyst supported by NGO. These better performances of Pd/N-MWCNTs can be ascribed to the higher ECSA value, better dispersion of catalyst nanoparticles on N-MWCNTs support material and more synergistic interaction between the catalyst nanoparticles and the support material.

6   Results and Discussion of Hybrid Supported Palladium Catalysts

This chapter presents, compares and discusses the results of hybrid support materials and their Pd electrocatalysts in order to know the best hybrid support material among others. The rationale of synthesizing the hybrid support materials is to increase the surface area of the support materials and to reduce agglomeration especially in graphene support materials due to restacking of the graphene sheets (Liu *et al*., 2019). Since graphene with other carbon supported catalysts synthesized by modified polyol method gave the best results after comparing with their modified counterparts, the hybrid supported Pd catalysts were therefore synthesized by modified polyol method only. First, the energy dispersive X-ray spectroscopy (EDS) coupled with the scanning electron microscopy (JOEL JSM-7500F Scanning Electron Microscope, Mundelein, II, USA, was used to evaluate the Pd metal loading in Pd electrocatalysts and was also found to be 37.67 % which was the same for all the synthesized hybrid supported Pd catalysts.

6.1   Surface Characterization

The surface characterization carried out include Fourier-Transform Infrared (FT-IR) and Brunauer-Emmett-Teller (BET) for the hybrid support materials and X-ray diffraction (XRD) with high-resolution transmission electron spectroscopy (HR-TEM) for the hybrid supported Pd catalysts.

6.1.1   Fourier-Transform Infrared of Hybrid Support Materials

The FT-IR results of all hybrid support materials are shown in Figure 6.1. For FT-IR analysis of MWCNTs-CNFs, the bands around 1224 and 1736 cm^{-1} were assigned to C-O and C=O of carboxylic acid respectively which is an indication of the functionalization of the hybrid support materials by chemical oxidation while the band around 3688 cm^{-1} was assigned to strong peak of O-H carboxylic acid. Also, the FT-IR spectra of N-MWCNTs-CNFs shows NO_2 band of nitro compound around 1542 and 1368 cm^{-1} which is an indication of the presence of dopant nitrogen from melamine while the band around 1228, 1736 and 3688 cm^{-1} were assigned to C-O, C=O and O-H of carboxylic acid respectively. In addition, the FT-IR spectra of NGO-MWCNTs shows a medium peak of C-N band of amide around 1208 cm^{-1}. The band around 1546 and 1382 cm^{-1} were assigned to NO_2 compound while the band around 1736 and 3688 cm^{-1} correspond to C=O and O-H of carboxylic acid. The appearance of NO_2 peak in NGO-MWCNTs is also an indication of the presence of dopant nitrogen from melamine. For GO-MWCNTs, the FT-IR spectra also show

C-O, C=O, O-H bands of carboxylic acid around 1060, 1716 and 3450 cm^{-1} respectively while the band around 1562 cm^{-1} was assigned to C=C aromatic. FT-IR analysis of GO-N-MWCNTs also show C-O, C=O, O-H bands of carboxylic acid around 1060, 1716 and 3688 cm^{-1} respectively while NO$_2$ band of nitro compound and C-N bands of amide were observed around 1570 and 1374 cm^{-1} respectively. The appearance of NO$_2$ and C-N peaks in GO-N-MWCNTs indicate of the presence of dopant nitrogen from melamine. The FT-IR spectra of rGO-MWCNTs show distinctive bands around 1066 and 3430 cm^{-1} which were assigned to C-O and O-H of alcohol respectively while the band around 1582 cm^{-1} was assigned to C=C aromatic. The presence of C-O and O-H of alcohol in rGO-MWCNTs indicate that rGO has not been oxidized to GO (Al-Marri *et al*., 2016; Banerjee *et al*., 2015; Kuniyil *et al*., 2019; J. Li *et al*., 2014; Mironenko *et al*., 2015; Vanyorek *et al*., 2016; Yao *et al*., 2016). Meanwhile, the presence of N-doped in N-MWCNTs-CNFs, NGO-MWCNTs, GO-N-MWCNTs was also validated using EDS as shown in Figure 6.2. The summary of the observed bands in all the hybrid support materials is illustrated in Table 6.1.
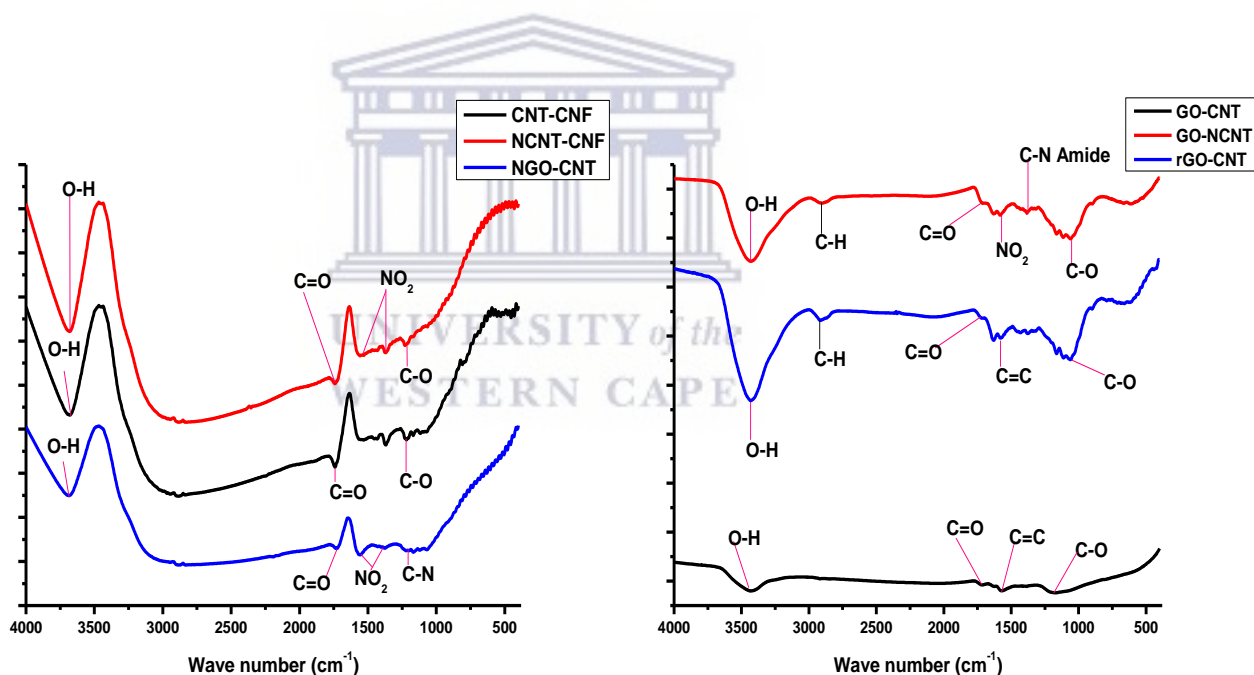
Figure 6.1: The FT-IR Spectra of synthesized MWCNTs-CNFs, N-MWCNTs-CNFs, NGO-MWCNTs, GO-MWCNTs, GO-N-MWCNTs and rGO-MWCNTs hybrid support materials.

Table 6.6.1: Observed bands of FT-IR Spectra for Synthesized Hybrid Support Materials.

Support Materials	Functional Groups	Observed bands (cm^{-1})
MWCNTs-CNFs	C=O Carboxylic acid	1736
	C-O Carboxylic acid	1224
	O-H Carboxylic Acid	3688
N-MWCNTs-CNFs	C=O Carboxylic acid	1736
	C-O Carboxylic acid	1228
	O-H Carboxylic acid	3688
	NO$_2$ Nitro compound	1542 & 1368
NGO-MWCNTs	C=O Carboxylic acid	1736
	O-H Carboxylic acid	3688
	C-N Amide	1208
	NO$_2$ Nitro compound	1382 & 1546
GO-MWCNTs	C=O Carboxylic acid	1716
	C-O Carboxylic acid	1060
	O-H Carboxylic acid	3450
	C=C Aromatic	1562
GO-MWCNTs	C=O Carboxylic acid	1716
	C-O Carboxylic acid	1060
	O-H Carboxylic acid	3688
	C-N Amide	1374

	NO$_2$ Nitro compound	1570
	C-H Alkane	2920
rGO-MWCNTs	C=O Carboxylic acid	1716
	C-O Alcohol	1066
	O-H Alcohol	3430
	C=C Alkene	1582
	C-H Alkane	2920
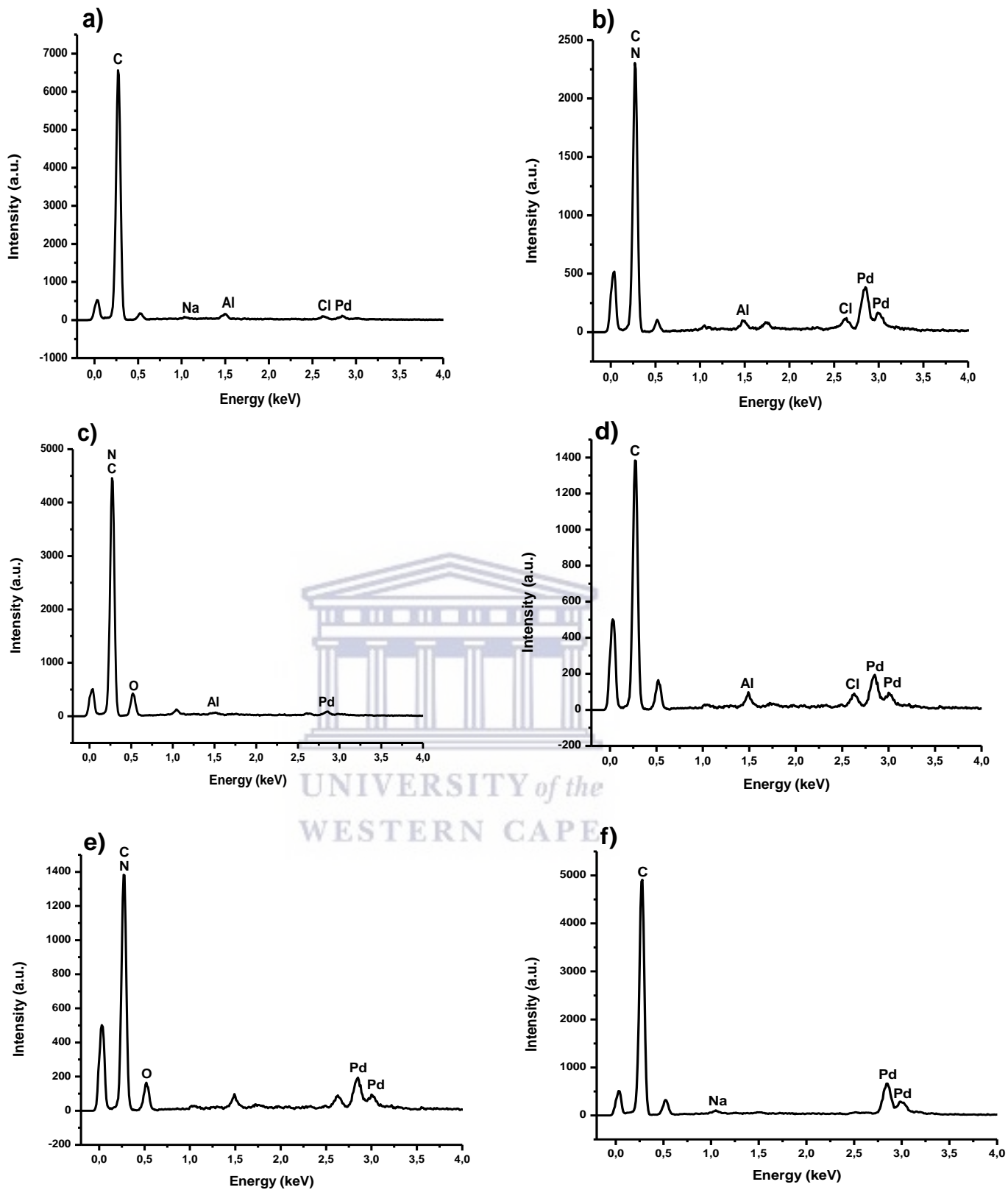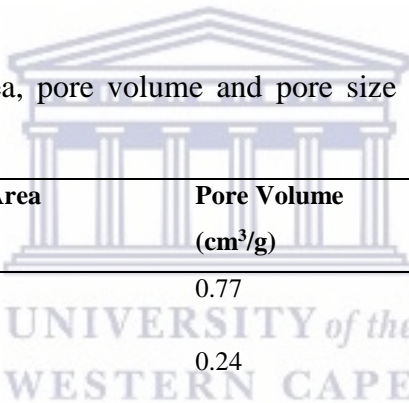
Figure 6.2: The EDS Spectra of synthesized (a) Pd/MWCNTs-CNFs (b) Pd/N-MWCNTs-CNFs (c) Pd/NGO-MWCNTs (d) Pd/GO-MWCNTs (e) Pd/GO-N-MWCNTs (f) Pd/rGO-MWCNTs.

101

6.1.2 Brunauer-Emmett-Teller of Hybrid Support Materials

The Specific surface area, pore volume and pore size of all the prepared hybrid support materials were also investigated using Brunauer-Emmett-Teller (BET). Surface area measurements were taken from the support materials to first evaluate the surface area of the carbon support materials used. Among the prepared hybrid support materials, NGO-MWCNTs showed the highest surface area and pore volume of 144.81 m^2 g^{-1} and 1.02 cm^3/g respectively while GO-MWCNTs exhibit the highest pore size of 236.74 Å as presented in Table 6.1. This better surface area and pore volume in NGO-MWCNTs can be ascribed to proper mixture and better synergy between the combined support materials. Since the performance of catalysts increases with increase in the support surface area and pore volume, the catalyst must therefore be supported with a high surface area and pore volume support materials for proper dispersal of the catalyst nanoparticles which aids the catalyst activity and make low catalyst loading feasible for fuel cell operations (Antolini, 2009). Figure 6.3 and Figure 6.4 show the adsorption-desorption and pore distribution graphs of the synthesized hybrid support materials.

Table 6.2: The BET surface area, pore volume and pore size of the prepared hybrid support materials.

Support Materials	Surface Area (m²/g)	Pore Volume (cm³/g)	Pore size (Å)
MWCNTs-CNFs	112.21	0.77	172.06
N-MWCNTs-CNFs	70.24	0.24	135.81
NGO-MWCNTs	144.81	1.02	188.44
GO-MWCNTs	134.11	0.87	236.74
GO-N-MWCNTs	62.91	0.21	130.11
rGO-MWCNTs	107.59	0.53	192.63
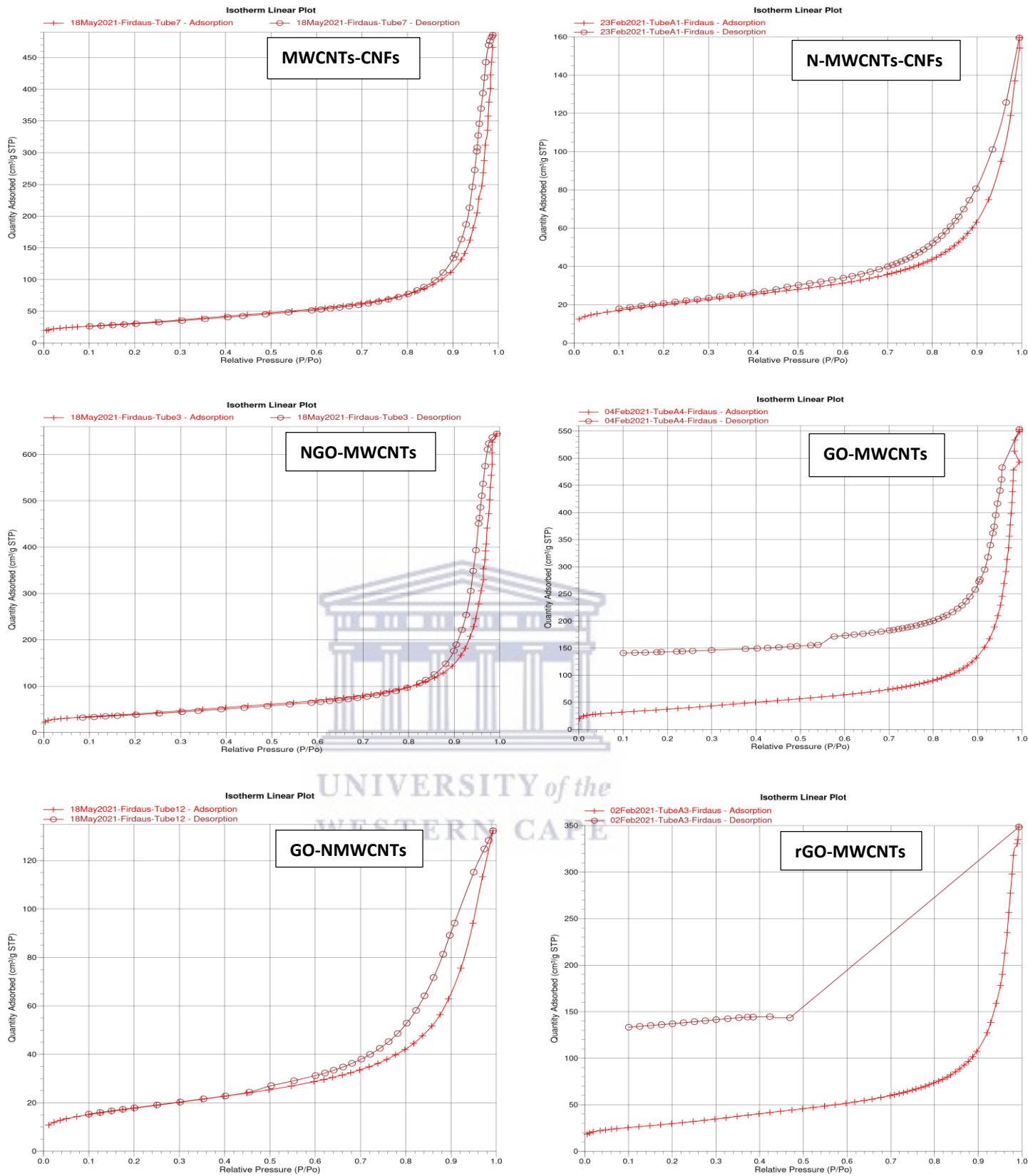
Figure 6.3: Adsorption-desorption graphs of synthesized hybrid support materials.
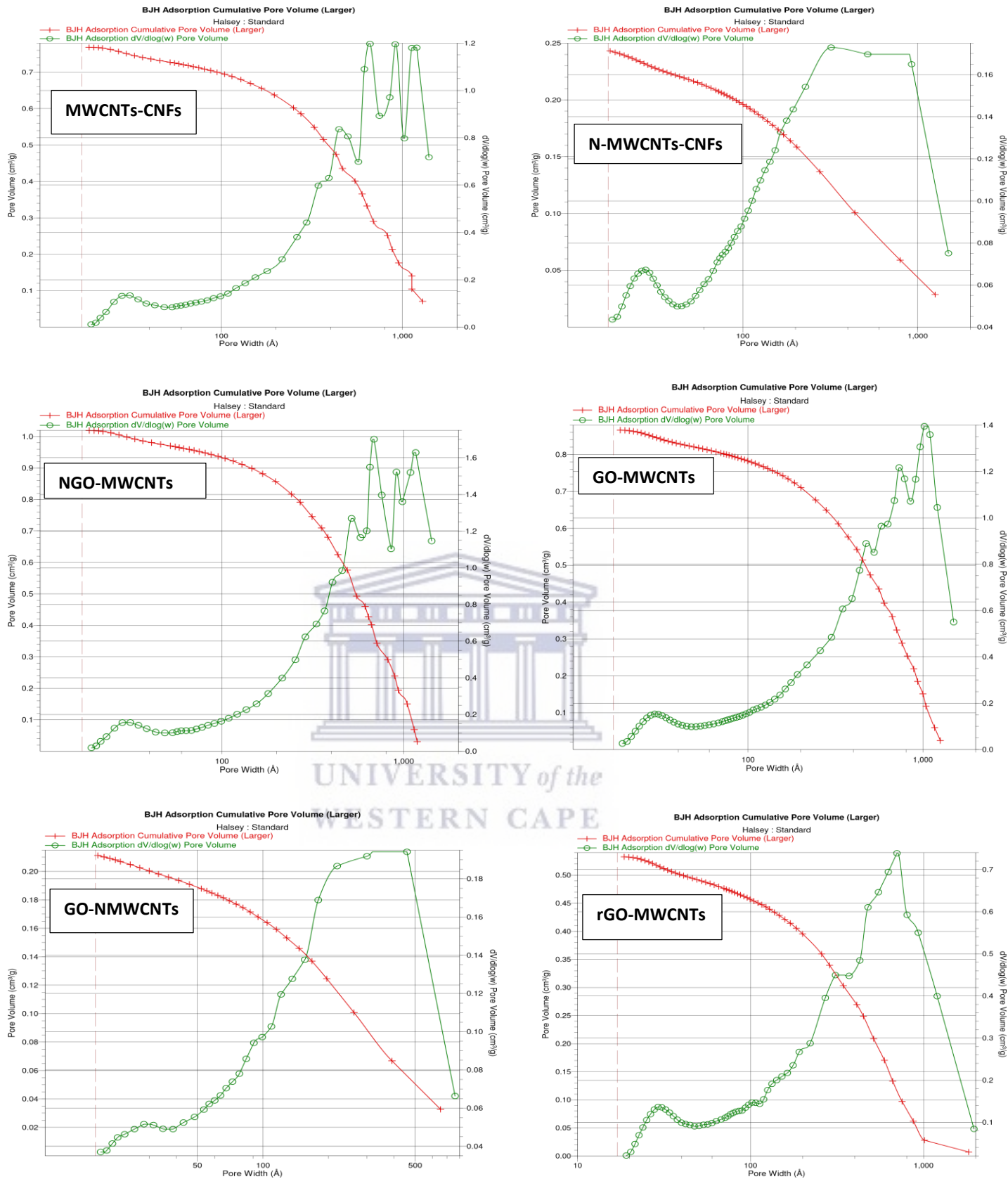
Figure 6.4: Pore distribution graphs of synthesized hybrid support materials.

6.1.3 X-ray Diffraction of Hybrid Supported Palladium Catalysts

The crystallinity and crystallite size of hybrid supported Palladium catalysts were also determined using XRD spectra and classical Debye-Scherrer equation respectively as stated in equation 3.2. The sharpest and the most intense peak of all the prepared Pd electrocatalysts appeared around 40º 2-theta scale which is indexed as (111). This peak was used to determine the crystallite size of all the Pd electrocatalysts. The XRD spectra revealed that all hybrid supported Pd catalysts are crystalline in nature as illustrated in Figure 6.3. This is also corroborated with selected area electron diffraction (SAED) as shown in Figure 6.4.
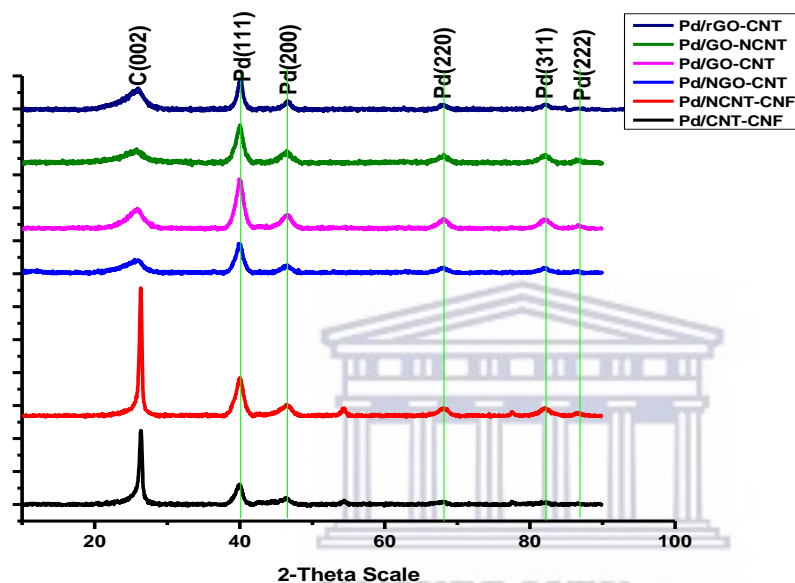
Figure 6.5: XRD spectra of synthesized hybrid supported Pd catalysts.
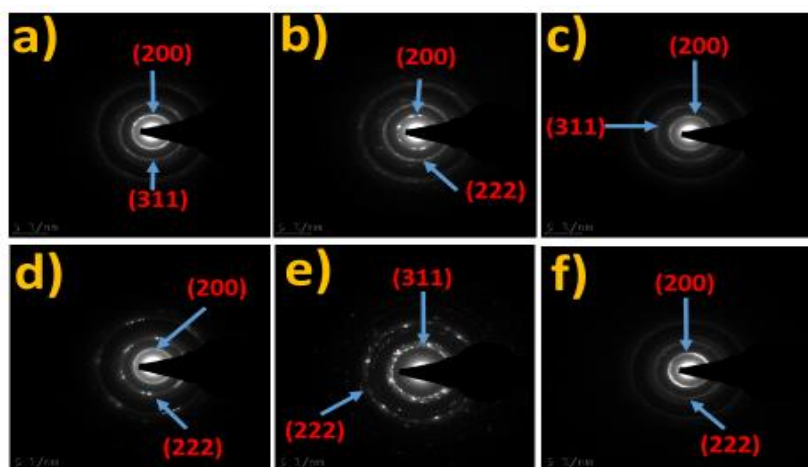
Figure 6.6: Selected area electron diffraction (SAED) of synthesized hybrid supported Pd catalysts: (a) Pd/MWCNTs-CNFs (b) Pd/N-MWCNTs-CNFs (c) Pd/NGO-MWCNTs (d) Pd/GO-MWCNTs (e) Pd/GO-N-MWCNTs and (f) Pd/rGO-MWCNTs.

105

Table 6.3: The particle size and crystallite size of the prepared hybrid supported Pd catalysts.

Electrocatalyst	Particle size (nm) HR-TEM	Crystallite size (nm) XRD
Pd/MWCNTs-CNFs	8 ± 1.3	8.1
Pd/N-MWCNTs-CNFs	9 ± 1.8	10.9
Pd/NGO-MWCNTs	3 ± 0.6	3.7
Pd/GO-N-MWCNTs	4 ± 0.5	4.4
Pd/GO-MWCNTs	7 ± 0.7	7.0
Pd/rGO-MWCNTs	9 ± 0.6	9.6

6.1.4   The High-Resolution Transmission Electron Spectroscopy of Hybrid Supported Palladium Catalysts

Figure 6.5 shows the nanomorphological structures of all the synthesized hybrid supported Pd catalysts examined using high-resolution transmission electron spectroscopy (HR-TEM) with their frequency distribution from 50 randomly selected nanoparticles. For the hybrid supported Pd catalysts, the images also revealed a homogenous with relatively small particle size distribution which ranges between 3 and 9 nm as display in their respective histograms in Figure 6.5 and presented in Table 6.2.
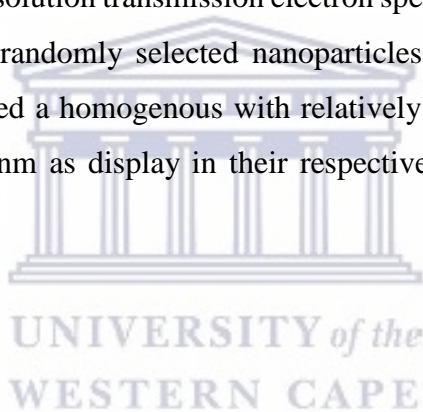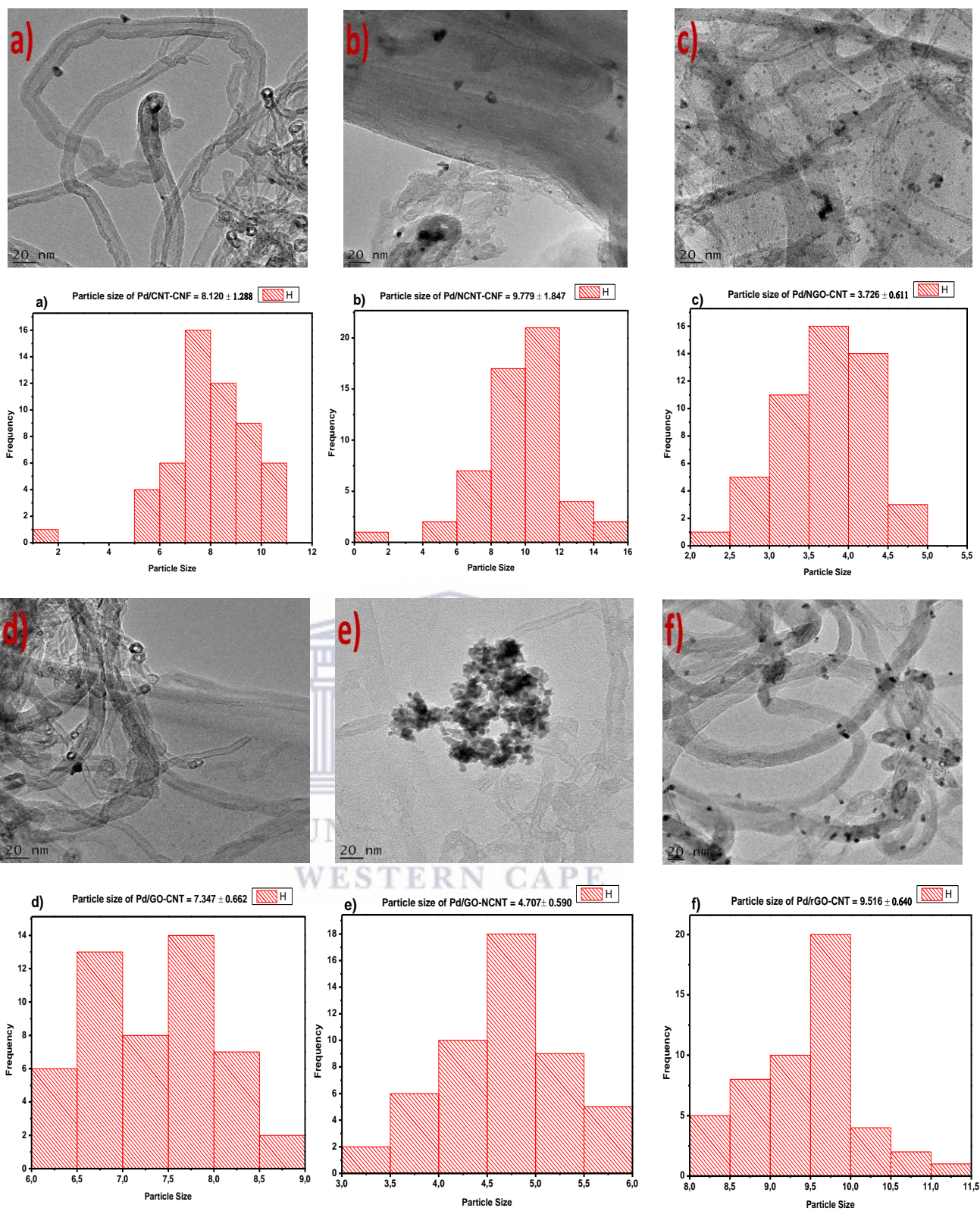
Figure 6.7: HR-TEM images with their respective histograms for hybrid supported electrocatalysts: (a) Pd/MWCNTs-CNFs (b) Pd/N-MWCNTs-CNFs (c) Pd/NGO-MWCNTs (d) Pd/GO-MWCNTs (e) Pd/GO-N-MWCNTs (f) Pd/rGO-MWCNTs.

107

6.2 Electrochemical Evaluation of Hybrid Supported Palladium Electrocatalysts

6.2.1 *Cyclic Voltammetry*

The electrochemical properties of hybrid supported Pd catalysts in alkaline (1M KOH) solution were first examined by cyclic voltammetry (CV) with Pd loading of 0.02 mgcm^{-2}. The CV curves of each Pd electrocatalyst were also obtained from the stabilized curve after scanning 20 cycles (Zhao & Zhao, 2013). The CV curves shows little adsorption/desorption peaks in the hydrogen region at negative potentials. As more negative potentials were applied, the reduction of H$^+$ and the adsorption of H atoms become stronger. Details of this reaction steps have been discussed earlier in chapter 4. From the CV curves of these hybrid supported Pd electrocatalysts, their oxidation peaks were also not well pronounced (Yi *et al*., 2015) while a significant cathodic reduction peak which is attributed to the reduction of PdO produced on the forward potential scan is observed between -0.2 V and -0.4 V (Klaas *et al*., 2020) for all the hybrid supported Pd electrocatalysts. The CV results show that Pd/GO-MWCNTs exhibits the most intense cathodic reduction peak with highest current density than other hybrid supported Pd electrocatalysts which implies that it provided better evidence for the widest electroactive surface area (ECSA) as shown in Figure 6.6 (Maiyalagan *et al*., 2005; Narreddula *et al*., 2019). The same formula used in chapters 4 as stated in equation 4.4 was also used to determine the ESCA values of all the hybrid supported Pd electrocatalysts. The CV results revealed that, Pd/GO-MWCNTs displayed the most intense cathodic reduction peak with highest ECSA value of 4.57 m^2/g among all the hybrid supported Pd electrocatalysts as shown in Figure 6.6 and presented in Table 6.3 (Anwar *et al*., 2019; Aravind *et al*., 2011).
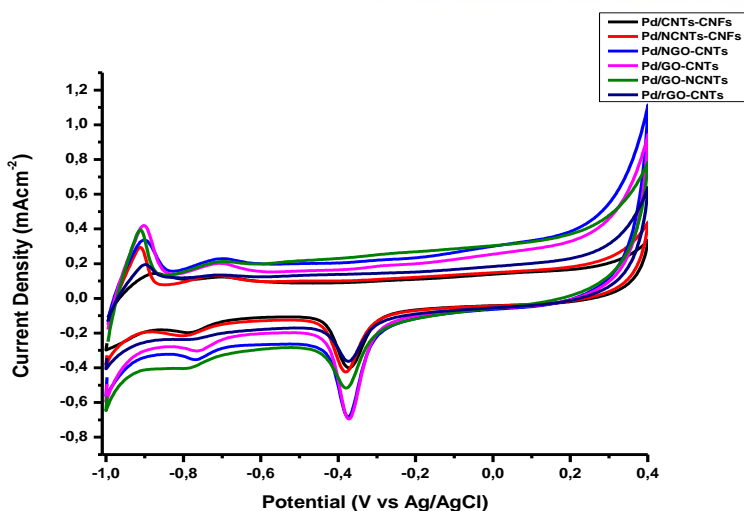
Figure 6.8: The cyclic voltammetry of hybrid supported Pd catalysts in N$_2$ saturated 1 M KOH at scan rate of 0.02 Vs^{-1}.

Table 6.4: Comparison of ECSA with current densities (MOR and Chrono) of prepared hybrid supported Pd catalyst films determined from the anodic sweep (-0.1 to 0.4 V) at scan rate of 0.02 Vs-[1].

Catalysts	Electroactive Surface Area (m^2/g)	Current Density (mA/cm^2) for MOR	Current Density (mA/cm^2) for Chronoamperometry
Pd/MWCNTs-CNFs	2.92	3.03	0.07
Pd/N-MWCNTs-CNFs	2.89	2.93	0.04
Pd/NGO-MWCNTs	3.99	4.12	0.15
Pd/GO-MWCNTs	4.57	4.43	0.19
Pd/GO-N-MWCNTs	2.66	2.76	0.09
Pd/rGO-MWCNTs	2.03	1.89	0.01

6.2.2 Methanol Oxidation Reaction

The electrocatalytic activity of hybrid supported Pd catalysts towards methanol oxidation reaction (MOR) in alkaline (1M KOH) solution in the presence of methanol was also examined by cyclic voltammetry (CV). In the forward scan, the oxidation peaks also correspond to the oxidation of freshly chemosorbed species coming from methanol adsorption. The reverse scan peaks are also associated with the removal of carbonaceous species which were not completely oxidized in the forward scan than the oxidation of freshly chemosorbed species (Liu *et al*., 2007). The onset potential of each hybrid supported Pd electrocatalyst also varies from one to another as summarized in Table 6.4. After the anodic scan, the anodic current density also declined sharply as a result of the formation of PdO on the Pd electrocatalysts surface at high anodic potential. As the backward scan commenced, the PdO began to reduce and the Pd electrocatalysts surface is reactivated and methanol oxidation occurred again (Yi *et al*., 2011). The results obtained indicate that, GO-MWCNTs supported electrocatalysts display the highest anodic peak current density among other hybrid supported Pd catalysts which implies better electroactivity towards methanol electrooxidation on forward scan of negative sweep as shown in Figures 6.7 and reported in Table 6.3. This enhanced performance, which also concur to the stability test can also be ascribed to the better electroactive surface area and electrochemical impedance (Anwar *et al*., 2019; Aravind *et al*., 2011; Narreddula *et al*., 2019; Pham *et al*., 2016; Sahoo *et al*., 2015; Zhang *et al*., 2016).
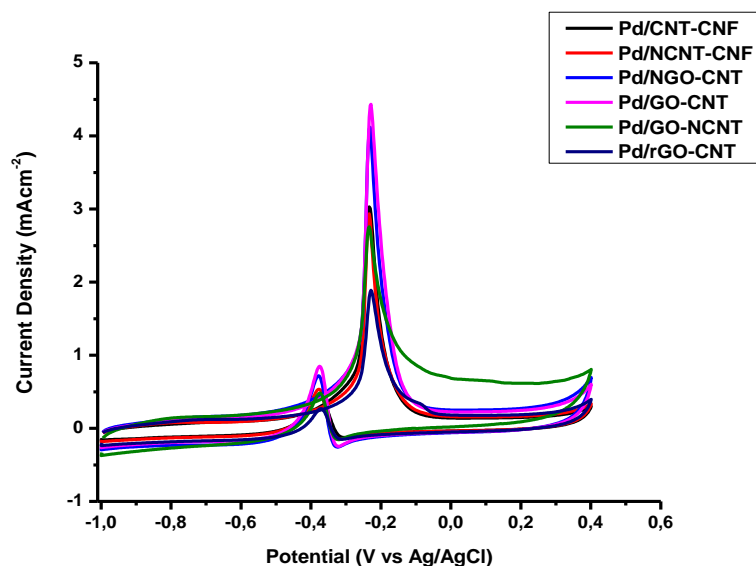
Figure 6.9: The cyclic voltammetry curves of methanol oxidation of hybrid supported Pd catalysts in N_2 saturated 1 M MeOH + 1 M KOH at scan rate of 0.02 Vs^{-1}.

Table 6.5: Results of the study of CVs of the prepared hybrid supported Pd catalysts in 1 M KOH + 1 M MeOH.

Electrocatalyst	Onset Potential (V vs Ag/AgCl)	Anodic peak for forward scan I_f ($mAcm^{-2}$)	Anodic peak for reverse scan I_r ($mAcm^{-2}$)	I_f/I_r ratio
Pd/MWCNTs-CNFs	-0.46	3.03	0.44	6.89
Pd/N-MWCNTs-CNFs	-0.50	2.93	0.54	5.49
Pd/NGO-MWCNTs	-0.46	4.12	0.72	5.74
Pd/GO-N-MWCNTs	-0.47	2.76	0.48	5.71
Pd/GO-MWCNTs	-0.48	4.43	0.85	5.22
Pd/rGO-MWCNTs	-0.47	1.89	0.27	7.02

The activity towards complete methanol oxidation was also examined among the hybrid supported Pd catalysts. From the results shown in Table 6.4, it is observed that Pd/rGO-MWCNTs shows the best activity towards complete methanol oxidation with I_f/I_r ratio of 7.02. This also implies that those with lower activity towards complete methanol oxidation experienced CO poisoning which practically reduces their expected performance (Yi *et al*., 2015) .

110

6.2.3 Electrochemical Stability

The electrochemical stability of hybrid supported Pd catalysts was also carried out at potential of -0.3 V for 30 minutes. In all the current density-time curves of these supported catalysts, the oxidation current density rapidly reduced in the first 193 seconds which was followed by a slower decay until it attained a steady state. The high current displayed at the beginning of stability testing could also be ascribed to the double layer charging between the interface of electrode/electrolyte (Yi *et al*., 2015). The gradual decrease in current density with time which was significantly observed may be attributed to poisoning of the hybrid supported Pd catalysts and decrease in electroactive surface area as the stability test progresses (Yi *et al*., 2015). After 30 minutes' stability study in 1 M KOH + 1 M methanol solution, it was observed that Pd/GO-MWCNTs also display a better stability among all the hybrid supported Pd catalysts as shown in Figure 6.8 which also concur to MOR results (Anwar *et al*., 2019; Bock *et al*., 2004; Du *et al*., 2008; Aravind *et al*., 2011; Narreddula *et al*., 2019; Pham *et al*., 2016; Sahoo *et al*., 2015; Zhang *et al*., 2016). The current density for the stability test of all these hybrids supported Pd catalysts is illustrated in Table 6.3.
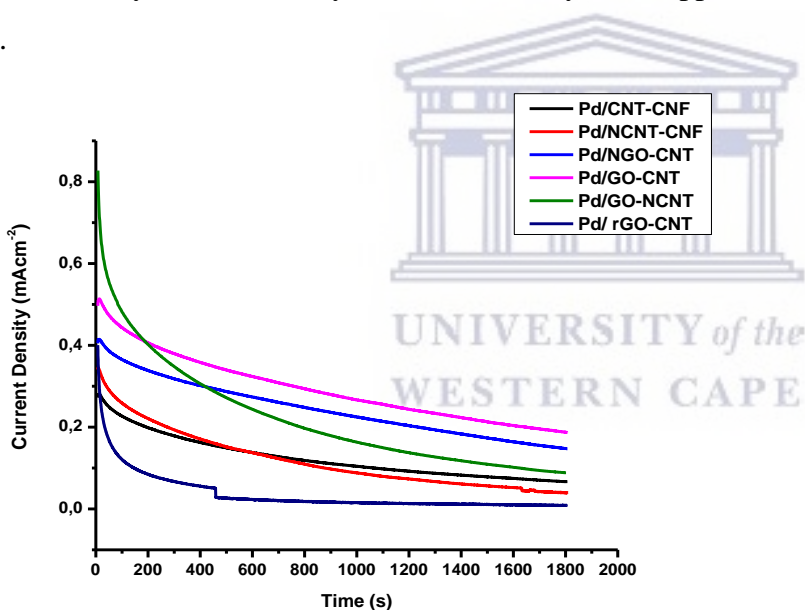
Figure 6.10: The chronoamperometry of hybrid supported Pd catalysts in N_2 saturated 1 M MeOH + 1 M KOH at potential of -0.3 V.

6.2.4 Electrochemical Impedance Spectroscopy

The electrochemical impedance spectroscopy (EIS) of hybrid supported Pd catalysts was also carried out. An equivalent circuit was also employed for fitting the Nyquist plots which include solution resistance (Rs), charge transfer resistance (Rct) and double layer capacitance (Qdl). Each plot shows a semicircle in the high frequency related to charge transfer. The EIS results showed

111

that, among all the synthesized hybrid supported Pd catalysts, GO-MWCNTs supported Pd catalysts provided better chemical kinetics evidence as shown in Figure 6.9 with Rct value of 0.54 $k\Omega cm^2$ as the charge transfer kinetic of Pd catalyst on this hybrid support material significantly improve which encourage mass transfer. The Rct values were determined using Randels-Sevcik cell fitting under open circuit (Anwar *et al*., 2019; Aravind *et al*., 2011; Pham *et al*., 2016; Sahoo *et al*., 2015). The summary of electrochemical impedance spectroscopy results for all the prepared hybrid supported Pd catalysts is illustrated in Table 6.5.
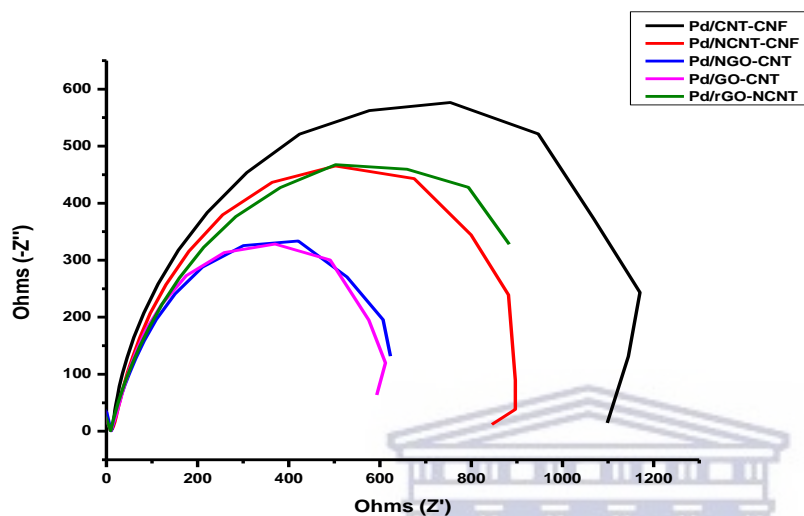
Figure 6.11: The electrochemical impedance spectroscopy of hybrid supported Pd catalysts in N_2 saturated 1 M MeOH +1 M KOH at potential of -0.3 V.

Table 6.6: Summary of electrochemical impedance spectroscopy of prepared hybrid supported Pd catalysts.

Electrocatalyst	Rct (KΩ)	Rs (KΩ)	CPE [Yo] (mF)	N (CPE Exponent)
Pd/MWCNTs-CNFs	1.05	0.05	0.28	1.00
Pd/N-MWCNTs-CNFs	0.86	0.04	0.32	1.00
Pd/NGO-MWCNTs	0.60	0.04	0.94	1.00
Pd/GO-N-MWCNTs	0.82	0.04	0.30	1.00
Pd/GO-MWCNTs	0.54	0.05	0.83	1.00
Pd/rGO-MWCNTs	13.10	0.02	0.12	1.00

In conclusion, all the results obtained from the analyses of hybrid supported Palladium catalysts show that GO-MWCNTs provided better evidence for supportive activity than all other hybrid support materials since the catalyst supported by GO-MWCNTs shows better electrocatalytic activity than other hybrid supported Pd catalysts. This better electroactivity in Pd/GO-MWCNTs can be attributed to higher ECSA value, better chemical kinetics and better dispersion of catalyst nanoparticles on the GO-MWCNTs hybrid support materials.

7 Results and Discussions of Carbon Supported Pd-Ru Binary Catalysts

The Pd electrocatalyst still suffer little CO poisoning during methanol oxidation reaction. This poisoning effect usually result to instability as well as reduction in DMFCs performance. Hence, the use of additional metal with Pd which is Ru was employed (Shukla *et al*., 2004; L. Xiong & Manthiram, 2004) in ratio 1:2 of Pd to Ru to form the catalysts mass loading of 0.02 mgcm^{-2}. The bifunctional mechanism explains that the second metal supplies oxygen to oxidise the Pd-adsorbed methanol oxidation intermediate specie, while the electronic effect states that the second metal modifies the Pd electronic configuration, thereby weakening the adsorption of the methanol oxidation intermediate specie on Pd. In this chapter, the experimental findings of all the results of synthesized carbon supported Pd-Ru binary catalysts are presented, compared and discussed in order to determine the best performing Pd-Ru electrocatalyst among them. The support materials used include graphene oxide (GO), N-doped graphene oxide (NGO), multi-walled carbon nanotubes (MWCNTs), N-doped multi-walled carbon nanotubes (N-MWCNTs) and carbon nanofibers (CNFs). All these support materials were characterized using Fourier-Transform Infrared (FT-IR) and Brunauer-Emmett-Teller (BET) as earlier discussed in chapters 3 and 4. First, the energy dispersive X-ray spectroscopy (EDS) coupled with the scanning electron microscopy (JOEL JSM-7500F Scanning Electron Microscope, Mundelein, II, USA, was used to evaluate the metal loading of Pd and Ru in the carbon supported Pd-Ru binary catalysts and were found to be 15.11 and 15.83 % respectively which were the same for all the synthesized Pd-Ru binary electrocatalysts.

7.1 Surface Characterization

Fourier-Transform Infrared (FT-IR) and Brunauer-Emmett-Teller (BET) techniques were used for the surface characterization of the synthesized carbon support materials as discussed earlier in chapter four while X-ray diffraction microscopy (XRD) and High-Resolution Transmission Electron Spectroscopy (HR-TEM) were used for the surface characterization of the binary catalysts.

7.1.1 X-ray Diffraction of Pd-Ru Binary Catalysts

The crystallinity and crystallite size of carbon supported binary electrocatalysts were also determined using XRD spectra and classical Debye-Scherrer equation respectively as stated in equation 3.2. The sharpest and the most intense peak of all the prepared Pd-Ru binary

electrocatalysts appeared around 40º 2-theta scale which is indexed as (111). This peak was used to determine the crystallite size of all the Pd-Ru binary electrocatalysts. The XRD graphitic pattern of the prepared carbon supported Pd-Ru binary catalysts show four diffraction peaks at 2-theta value around 39.9970 º, 54.4420 º, 68.2690 º and 77.6720 º except that the 2-theta value of the Pd diffraction peaks gradually shifted to higher values as illustrated in Figure 7.1 which is an indication of alloying in Pd-Ru binary catalysts. There is no distinguishable diffraction peak for Ru or RuO_2 crystal peaks which suggest a good significant alloy formation between the Pd and Ru by incorporation of the Ru atoms into the face centred cubic crystal lattice of Pd (Kim *et al*., 2017). The XRD results revealed that all the carbon supported Pd-Ru binary catalyst are crystalline in nature which is also corroborated with selected area electron diffraction (SAED) as indicated in Figure 7.2. The summary of the particle size and crystallites size is indicated in Table 7.1.
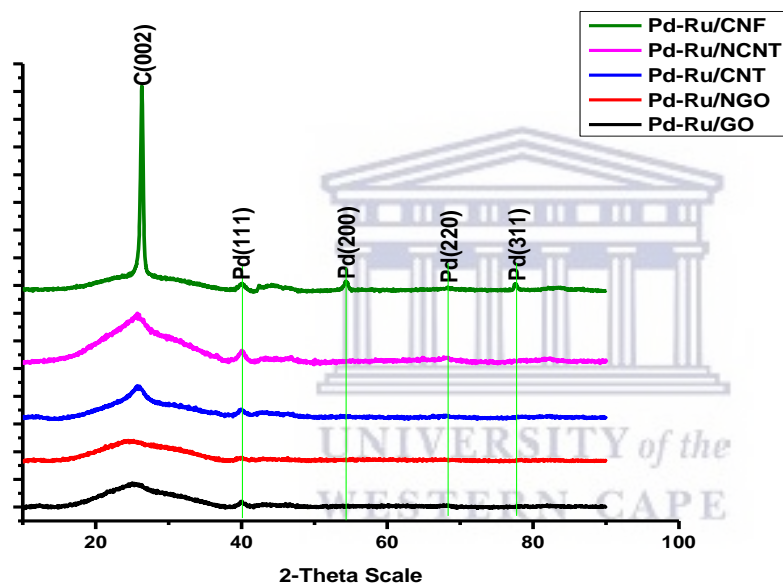
Figure 7.1: XRD spectra of synthesized Pd-Ru binary electrocatalysts.
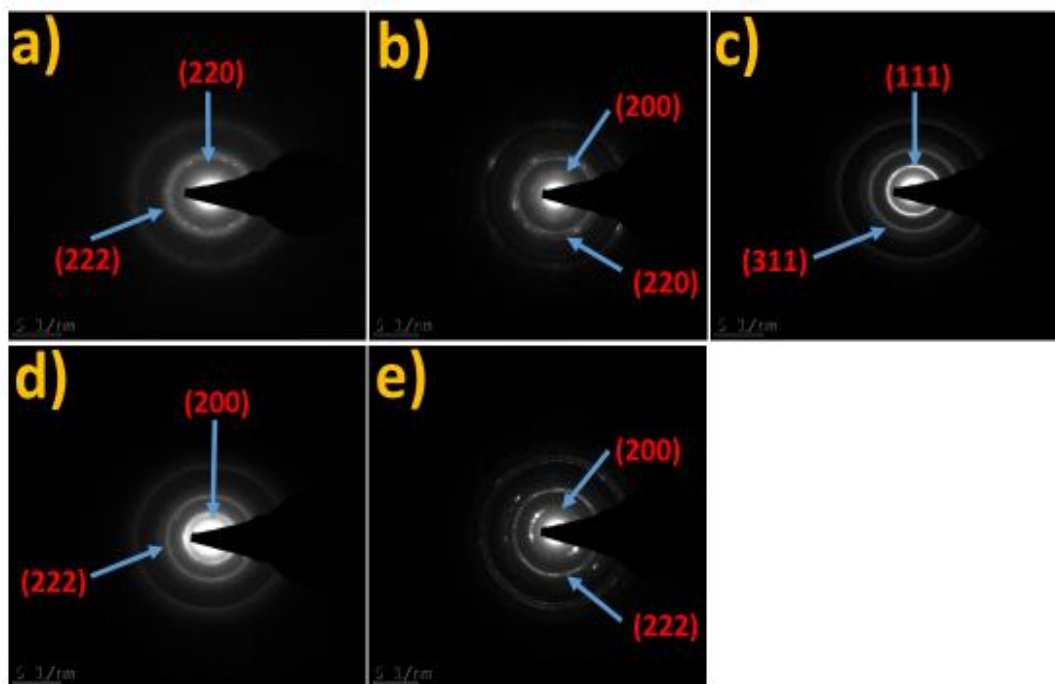
Figure 7.2: Selected area electron diffraction (SAED) of Pd-Ru binary electrocatalysts: (a) Pd-Ru/GO (b) Pd-Ru/NGO (c) Pd-Ru/MWCNTs (d) Pd-Ru/N-MWCNTs and (e) Pd-Ru/CNFs.

Table 7.1: The particle size and crystallite size of the prepared Pd-Ru binary electrocatalysts

Electrocatalyst	Particle size (nm) HR-TEM	Crystallite size (nm) XRD
Pd-Ru/GO	1 ± 0.7	0.5
Pd-Ru/NGO	1 ± 0.6	0.5
Pd-Ru/MWCNTs	1 ± 0.6	0.8
Pd-Ru/N-MWCNTs	1 ± 0.3	0.6
Pd-Ru/CNFs	11 ± 0.4	11.7

7.1.2   *The High-Resolution Transmission Electron Spectroscopy of Pd-Ru Binary Catalysts*

The nanomorphological structures of all the synthesized carbon supported Pd-Ru binary catalysts were examined using HR-TEM with their frequency distribution from 50 randomly selected nanoparticles. The HR-TEM images of the Pd-Ru binary electrocatalysts revealed a homogenous with relatively small particle size distribution as shown in Figure 7.3 which ranges between 1.0 and 11.0 nm. Details of these results are presented in Table 7.1.

116
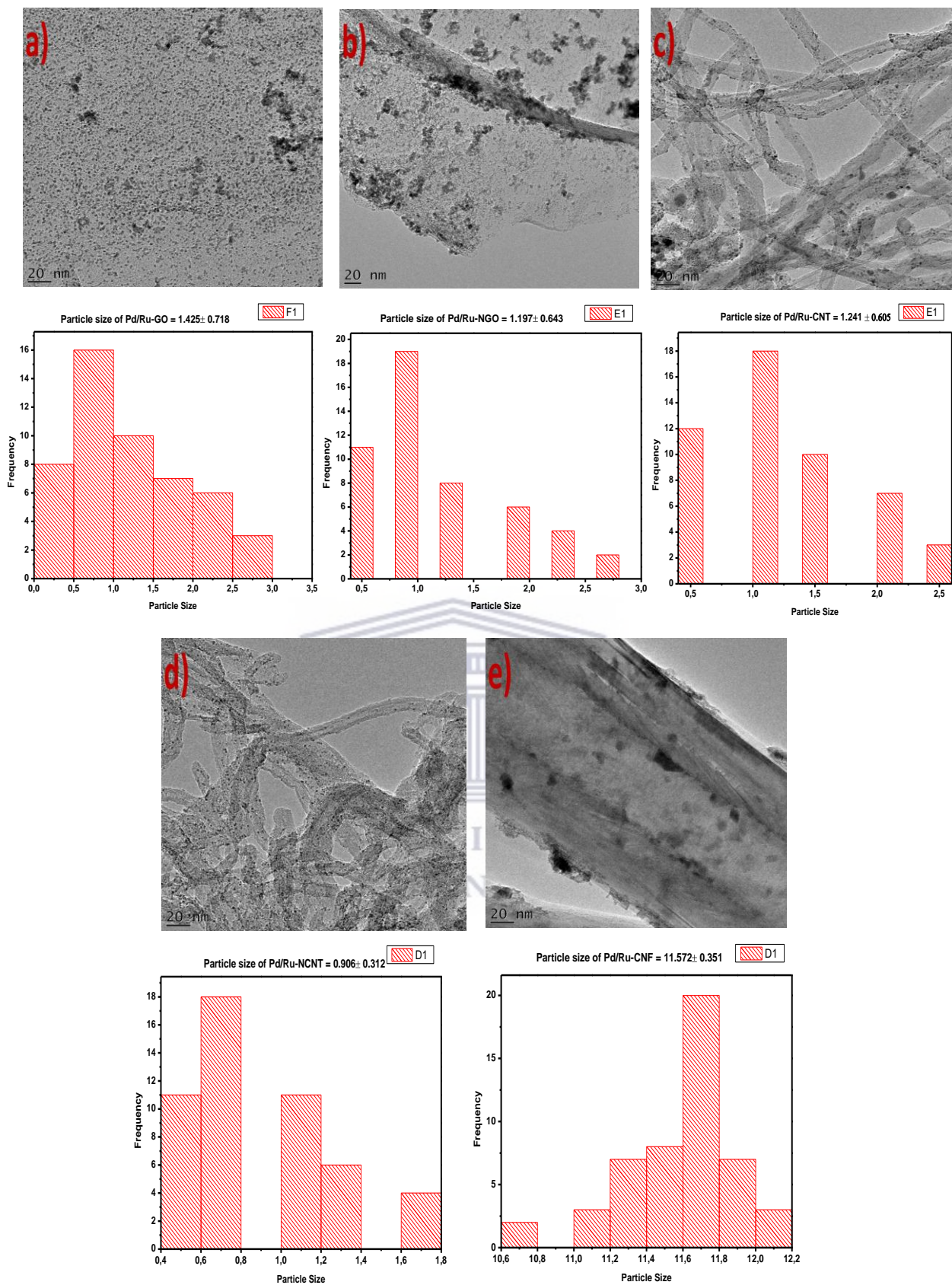
Figure 7.3: HR-TEM images with the respective histograms for Pd-Ru binary electrocatalysts: (a) Pd-Ru/GO (b) Pd-Ru/NGO (c) Pd-Ru/MWCNTs (d) Pd-Ru/N-MWCNTs and (e) Pd-Ru/CNFs.

117

7.2   Electrochemical Evaluations of Pd-Ru Binary Catalysts

The electrochemical evaluations of the Pd-Ru binary electrocatalysts were carried out using cyclic voltammetry (CV), chronoamperometry (CA) and electrochemical impedance spectroscopy (EIS).

7.2.1   *Cyclic Voltammetry*

The electrochemical properties of all the prepared carbon supported Pd-Ru binary catalysts in alkaline (1M KOH) solution were first examined by cyclic voltammetry (CV) with Pd-Ru loading of 0.02 mgcm^{-2}. The CV curves of each Pd-Ru binary electrocatalyst were also obtained from the stabilized curve after scanning 20 cycles (Zhao & Zhao, 2013). CV curves shows very little adsorption/desorption peaks in the hydrogen region at negative potentials. As more negative potentials were applied, the reduction of H$^+$ and the adsorption of H atoms become stronger. Details of this reaction steps have been discussed earlier in chapter 4. From the CV curves, the oxidation peak of all the prepared Pd-Ru binary electrocatalysts was not well pronounced too (Yi *et al*., 2015) while a significant cathodic reduction peak which is attributed to the reduction of PdO produced on the forward potential scan is observed between -0.2 V and -0.4 V at scan rate of 0.005 V (Klaas *et al*., 2020) for all the carbon supported Pd-Ru binary electrocatalysts. The same procedure and formula as stated in equation 4.4 in chapter 4 was also use to determine the ESCA values of all the electrocatalysts. Among all the carbon supported Pd-Ru binary catalysts, Pd-Ru/NGO exhibited the most intense cathodic reduction peak as shown in Figure 7.4 with highest current density which implies that it provided better evidence for the widest electroactive surface area (ECSA) of 0.28 m^2/g among other carbon supported Pd-Ru binary catalysts as reported in Table 7.2 (Zhang *et al*., 2016).
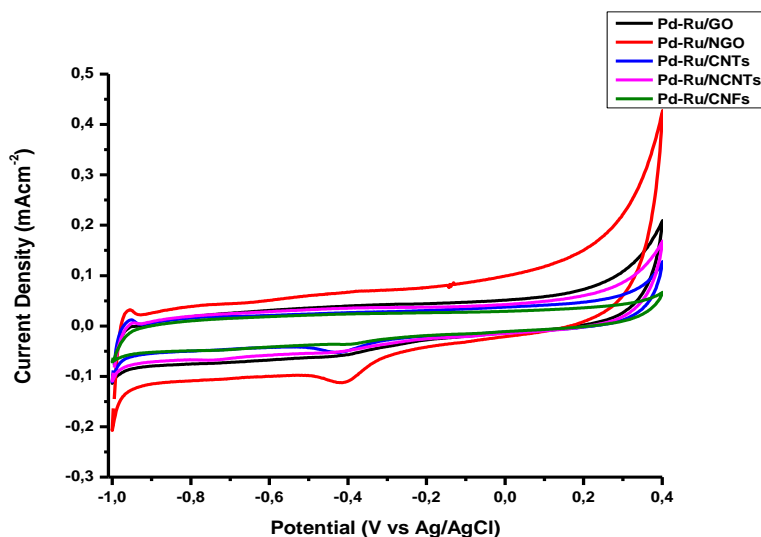
Figure 7.4: The cyclic voltammetry of synthesized Pd-Ru binary electrocatalysts in N_2 saturated 1 M KOH at scan rate of 0.005 Vs^{-1}.

Table 7.2: Comparison of ECSA with current densities (MOR and Chrono) of prepared Pd-Ru binary electrocatalyst films determined from the anodic sweep (-0.2 to 0.4 V) at scan rate of 0.005 Vs^{-1}.

Catalysts	Electroactive Surface Area (m^2/g)	Current Density (mA/cm^2) for MOR	Current Density (mA/cm^2) for Chronoamperometry
Pd-Ru/GO	0.05	0.11	2.90E-3
Pd-Ru/NGO	0.28	0.72	2.01E-2
Pd-Ru/MWCNTs	0.14	0.43	1.63E-4
Pd-Ru/N-MWCNTs	0.04	0.12	6.38E-4
Pd-Ru/CNFs	0.03	0.08	-2.91E-4

7.2.2 Methanol Oxidation Reaction

The electrocatalytic activity of the as-synthesized Pd-Ru binary electrocatalysts towards methanol oxidation reaction (MOR) in alkaline (1M KOH) solution in the presence of methanol was also examined by cyclic voltammetry (CV) between -0.2 V and -0.4 V at scan rate of 0.005 V as shown in Figure 7.5. In the forward scan, the oxidation peaks also correspond to the oxidation of freshly chemosorbed species coming from methanol adsorption. The reverse scan peaks are basically associated with the removal of carbonaceous species which were not completely oxidized in the forward scan than the oxidation of freshly chemosorbed species (Liu *et al*., 2007). The onset potential of each Pd-Ru binary electrocatalyst also varies from one to another as summarized in

119

Table 7.3 After the anodic scan, the anodic current density also declined sharply as a result of the formation of PdO on the electrocatalysts surface at high anodic potential. As the backward scan commenced, the PdO began to reduce and the Pd-Ru electrocatalysts surface is reactivated and methanol oxidation occurred again (Yi *et al*., 2011). From the results obtained among all the synthesized carbon supported Pd-Ru binary catalysts, Pd-Ru/NGO displayed the highest anodic peak current density of 0.72 mA/cm^2 as illustrated in Table 7.2 which implies better electroactivity towards methanol electrooxidation on forward scan of negative sweep. This enhanced performance of Pd-Ru/NGO, which also concur to the stability test, can be ascribed to better electroactive surface area and incorporation of dopant nitrogen (Bianchini & Shen, 2009; Bock *et al*., 2004; Gómez *et al*., 2016; Du *et al*., 2008; Kiyani *et al*., 2017; Narreddula *et al*., 2019; Zhang *et al*., 2016). The N-dopant in the support materials serve as defect sites to enhance the nucleation of catalyst nanoparticles (Du *et al*., 2008).
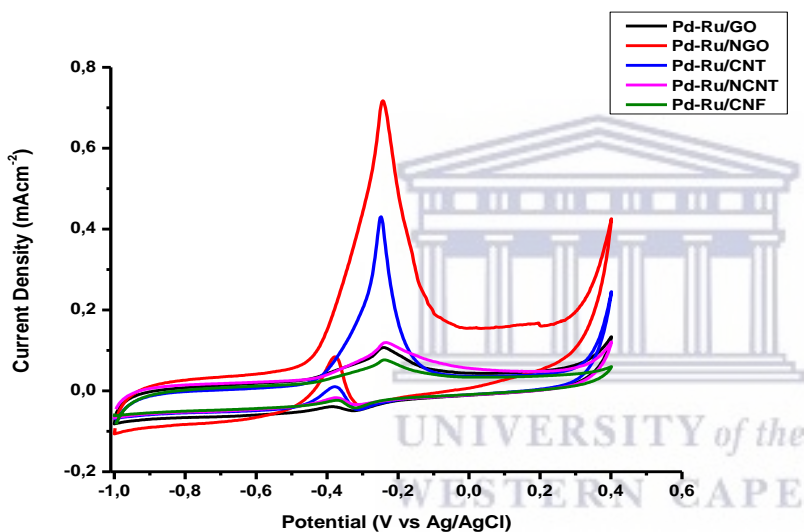
Figure 7.5: The cyclic voltammetry curves of methanol oxidation of Pd-Ru binary electrocatalysts in N$_2$ saturated 1 M MeOH +1 M KOH at scan rate of 0.005 Vs^{-1}.

Table 7.3: Results of the study of CVs of the prepared Pd-Ru binary electrocatalysts in 1 M KOH + 1 M MeOH

Electrocatalyst	Onset Potential (V vs Ag/AgCl)	Anodic peak for forward scan I_f (mAcm^{-2})	Anodic peak for reverse scan I_r (mAcm^{-2})	I_f/I_r ratio
Pd-Ru/GO	-0.47	0.11	-0.04	-2.74
Pd-Ru/NGO	-0.47	0.72	0.08	8.51
Pd-Ru/MWCNTs	-0.46	0.43	0.01	41.41
Pd-Ru/N-MWCNTs	-0.47	0.12	-0.02	-7.02
Pd-Ru/CNFs	-0.46	0.08	-0.02	-3.26

The ratio of forward anodic peak current (I_f) to reverse anodic peak current (I_r) which indicate the tolerance ability of electrocatalyst to accumulation of carbonaceous products and less poisoned was also determined among the synthesized carbon supported Pd-Ru binary electrocatalysts. This ratio is the supplementary method used to determine the CO tolerance of the catalysts. Large value of I_f/I_r shows higher oxidation of methanol and better CO tolerance (Garsany *et al*., 2010; Jha *et al*., 2011; Yi *et al*., 2011). From the results shown in Table 7.3, it is observed that Pd-Ru/MWCNTs shows the best activity towards complete methanol oxidation among all the synthesized carbon supported Pd-Ru binary electrocatalysts. This also implies that those with lower activity towards complete methanol oxidation experienced CO poisoning which practically reduces their expected performance (Yi *et al*., 2015) .

7.2.3 *The Electrochemical Stability*

The electrochemical stability of the synthesized carbon supported Pd-Ru binary catalysts was also tested by chronoamperometry at -0.3 V for 30 minutes. In all the current density-time curves of these supported catalysts, the oxidation current density rapidly reduced in the first 112 seconds which was followed by a slower decay until it attained a steady state. The high current displayed at the beginning of stability testing could also be ascribed to the double layer charging between the interface of electrode/electrolyte (Yi *et al*., 2015). The gradual decrease in current density with time which was significantly observed may be attributed to poisoning of the Pd-Ru electrocatalysts and decrease in electroactive surface area as the stability test progresses (Yi *et al*., 2015). After 30 minutes' stability study in 1 M KOH + 1 M methanol solution, it was observed that Pd-Ru/NGO provided better evidence as the best stable support materials as shown in Figure 7.6 with current density of 2.01E-2 compared with other synthesized carbon supported Pd-Ru binary catalysts as illustrated in Table 7.2.

121
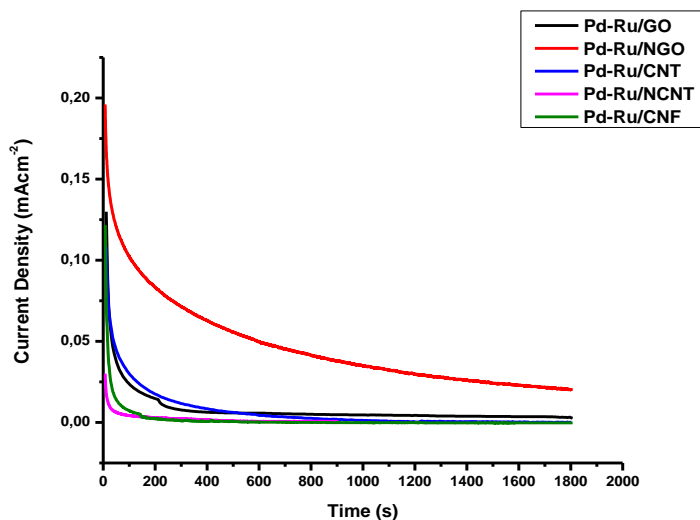
Figure 7.6: The chronoamperometry of Pd-Ru binary electrocatalysts in N_2 saturated 1 M MeOH + 1M KOH at potential of -0.3 V.

7.2.4 Electrochemical Impedance Spectroscopy

The electrochemical impedance spectroscopy (EIS) of all the synthesized carbon supported Pd-Ru binary electrocatalysts was also investigated. Figure 7.7 shows the interfacial behavior of the prepared carbon supported Pd-Ru binary catalysts in KOH electrolyte containing methanol at potential of -0.3 V vs Ag/AgCl. An equivalent circuit was also employed for fitting the Nyquist plots which include solution resistance (Rs), charge transfer resistance (Rct) and double layer capacitance (Qdl). Basically, each plot shows a curve in the high frequency related to charge transfer. From the EIS results, Pd-Ru/NGO among all the synthesized carbon supported Pd-Ru binary electrocatalysts exhibited the least electrochemical impedance. This implies that Pd-Ru binary catalyst supported by NGO show better chemical kinetics than other synthesized carbon supported Pd-Ru binary electrocatalysts as indicated by Nyquist plot in Figure 7.7. This was also confirmed by resistance charge transfer (Rct) value of 3.49 kΩcm^2 for Pd-Ru/NGO which is the least Rct value among all other synthesized carbon supported Pd-Ru binary catalysts as presented in Table 7.4. The Rct values were determined using Randels-Sevcik cell fitting under open circuit (Anwar *et al*., 2019; Jyothirmayee Aravind *et al*., 2011; Pham *et al*., 2016; Sahoo *et al*., 2015)

122
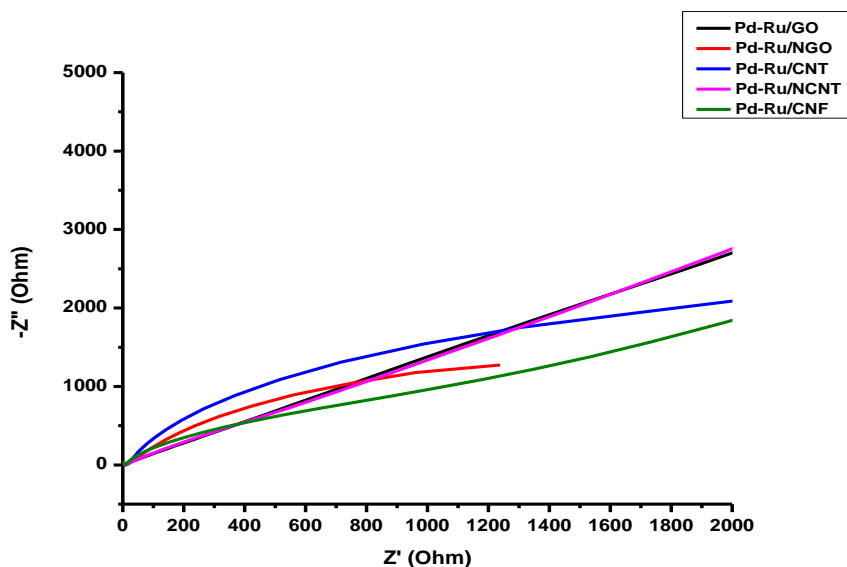
Figure 7.7: The electrochemical impedance spectroscopy of Pd-Ru binary electrocatalysts in N_2 saturated 1 M MeOH +1 M KOH at potential of -0.3 V.

Table 7.4: Summary of electrochemical impedance spectroscopy of prepared Pd-Ru binary electrocatalysts.

Electrocatalyst	Rct (kΩ)	Rs (kΩ)	CPE [Yo] (mF)	N (CPE Exponent)
Pd-Ru/GO	54.20	-54.40	2.94E-8	1.01
Pd-Ru/NGO	3.49	0.02	0.52	1.00
Pd-Ru/MWCNTs	6.05	-0.01	0.26	1.00
Pd-Ru/N-MWCNTs	49.20	-0.05	3.23E-8	1.01
Pd-Ru/CNFs	33.80	-34.20	4.70E-8	1.01

From all the results obtained from the analyses of carbon supported Pd-Ru binary catalysts, it can be concluded that NGO provided better evidence for supportive activity than other support materials since the Pd-Ru binary catalyst supported by NGO shows better electrocatalytic activity than other supported Pd-Ru binary catalysts. This better electroactivity in Pd-Ru/NGO can be attributed to its higher ECSA value, better chemical kinetics and better dispersion of catalyst nanoparticles on the NGO support materials than other support materials. When all the results obtained from the Pd monocatalysts were compared with that of Pd-Ru binary electrocatalysts, it was discovered that Pd monocatalysts showed better electroactivity than the Pd-Ru binary electrocatalysts. Hence, the presence of Ru metal did not improve the activity of the carbon support materials.

123

8 Conclusion and Recommendations for Future Study

8.1 Conclusion

The physical characterization, electroactive surface area, electrocatalytic activity and stability of Pd and Pd-Ru on different synthesized carbon support materials towards methanol oxidation were investigated in basic (KOH) medium. Different carbon support materials with their N-doped and hybrids were synthesized which include GO, rGO, NGO, NrGO, MWCNTs, N-MWCNTs, CNFs, MWCNTs-CNFs, N-MWCNTs-CNFs, NGO-MWCNTs, GO-MWCNTs GO-N-MWCNTs and rGO-MWCNTs. However, the synthesis method of the hybrid support materials was modified using different prepared carbon support materials in ratio 1:1. Palladium nanoparticles were alloyed with these synthesized support materials as monocatalysts and Palladium with Ruthenium for the binary electrocatalyst by modified polyol method. The synthesis method of the mono supported Pd electrocatalysts was also modified by adjusting the pH of the electrocatalyst from pH 12 to pH 13.

The structural characterization of all the support materials was carried out using Fourier Transform Infrared (FT-IR) Spectroscopy and Brunauer-Emmett-Teller (BET) Technique. The FT-IR results revealed that all the support materials contain the functional groups which serve as the binding sites for the deposition of Pd and Pd-Ru nanoparticles in monocatalysts and binary catalysts respectively while the BET results revealed that the surface area ranges from 3.36 to 9.20 m^2/g for the graphene based support materials and 14.32 to 67.45 m^2/g for MWCNTs, N- MWCNTs and CNFs support materials. When the support materials were doped with nitrogen, the surface area improved which ranges from 6.45 to 41. 92 m^2/g for graphene based and 219.50 m^2/g for N-MWCNTs support materials. Meanwhile, the surface area of the hybrid support materials was found within the range of 62.91 and 144.21 m^2/g. The structural characterisation of the mono supported Pd catalysts, hybrid supported Pd catalysts and Pd-Ru binary catalysts was also done using X-ray diffraction (XRD) and high resolution transmission electron microscopy (HR-TEM). The XRD confirmed that all the electrocatalysts are crystalline and exhibit face-centered crystal (fcc) structure of Pd while the HR-TEM images showed spherical and agglomerated catalyst nanoparticles dispersed on the various support materials. The particle size and crystallite size of the prepared electrocatalysts were determined using HR-TEM images and XRD spectra respectively. From HR-TEM images, the particle size of the mono supported and hybrid supported Pd catalysts ranges from 2 to 19 nm and 3 to 9 nm respectively while the particle size of Pd-Ru

binary catalysts lies within the range of 1 and 11 nm. Meanwhile, the crystallite size of mono supported and hybrid supported Pd catalysts ranges from 0.1 to 19 nm and 4 nm to 10 nm respectively while that of Pd-Ru binary catalysts ranges from 0.5 to 11.7 nm. The elemental analysis was also carried out using energy dispersive spectroscopy (EDS). The EDS results validated the presence of N-doped in NGO, NrGO and N-MWCNTs support materials while the Pd metal loading in monocatalysts was found to be 37.67 % but the Pd and Ru metal loading in binary catalysts was found to be 15.11 and 15.83 % respectively.

The electrochemical characterization of all the electrocatalysts was carried out using cyclic voltammetry (CV), electrochemical impedance spectroscopy (EIS) and chronoamperometry (CA). The results of each electrocatalysts were compared with their respective counterparts and conclusions were drawn. The CV results revealed that the electroactive surface area (ECSA) value of Pd/GO, Pd/rGO, Pd/NGO and Pd/NrGO are 1.60, 1.24, 1.84 and 1.53 m^2/g respectively while the ECSA values of Pd/MWCNTs, Pd/N-MWCNTs and Pd/CNFs were found to be 1.81, 5.53 and 0.42 m^2/g respectively. For hybrid supported Pd catalysts, Pd/MWCNTs-CNFs, Pd/N-MWCNTs-CNFs, Pd/NGO-MWCNTs, Pd/GO-MWCNTs, Pd/GO-N-MWCNTs and Pd/rGO-MWCNTs exhibited ECSA values of 2.92, 2.89, 3.99, 4.57, 2.66 and 2.03 m^2/g respectively while in Pd-Ru binary electrocatalysts, Pd-Ru/GO, Pd-Ru/NGO, Pd-Ru/MWCNTs, Pd-Ru/N-MWCNTs and Pd-Ru/CNFs showed ECSA values of 0.05, 0.28, 0.14, 0.04 and 0.03 m^2/g respectively. Therefore, Pd/N-MWCNTs, Pd/GO-MWCNTs and Pd-Ru/NGO electrocatalysts have exhibited the highest electroactive surface area of 5.53, 4.57 and 0.28 m^2/g among mono supported, hybrid supported and binary electrocatalysts respectively. Also, the methanol electrooxidation results of graphene based supported catalysts synthesized by modified polyol method and their modified counterparts shows that, Pd/NGO and Pd/NrGO were found to have the highest electroactivity towards methanol electrooxidation respectively. This better performance in electroactivity of Pd/NGO and Pd/NrGO which also agree with the stability results, can be ascribed to better dispersion of catalyst nanoparticles on their support materials (NGO and NrGO) and incorporation of dopant nitrogen into these support materials. This dopant nitrogen which exhibits significant chemical and structural changes serves as the defect sites to amplify the nucleation of the Pd nanoparticles thereby enhance the synergistic interaction between the Pd nanoparticles and these support materials. The nitrogen functional group on the surface of these support materials also intensifies the electron withdrawing effect against the Pd and the decrease in electron density of Pd facilitate the oxidation of methanol fuel (Maiyalagan *et al*., 2005). The stability test results also revealed that Pd/NGO proved better stability among graphene based supported Pd catalysts synthesized by

modified polyol method while Pd/NrGO showed better stability among modified graphene based supported Pd catalysts. In addition, during the methanol electrooxidation testing of MWCNTs, N-MWCNTs and CNFs supported catalysts synthesized by modified polyol method and their modified counterparts, Pd/N-MWCNTs shows a better electroactivity towards methanol electrooxidation in both cases. The stability test also revealed that Pd catalyst supported with N-MWCNTs shows the best stability among other supported electrocatalysts in both cases. These better performances in electroactivity of Pd/N-MWCNTs can be ascribed to the better ECSA value, better dispersion of catalyst nanoparticles on N-MWCNTs support material and incorporation of dopant nitrogen into the support material. Furthermore, Pd/GO-MWCNTs and Pd-Ru/NGO have proved to display better activity towards methanol electrooxidation among hybrid supported and binary electrocatalysts respectively. This performance was also maintained in their stability test as their chronoamperometry responses show that Pd/GO-MWCNTs and Pd-Ru/NGO exhibit better stability in hybrid supported and binary electrocatalysts respectively. This enhancement in the activity of Pd/GO-MWCNTs and Pd-Ru/NGO can also be ascribed to their higher electroactive surface area and better dispersion of catalyst nanoparticles on their support materials than their respective counterparts.

From the above results, the electroactivity of Pd electrocatalysts synthesized by modified polyol method were discovered to be better than the modified counterparts, hybrid supported Pd catalysts, and Pd-Ru binary electrocatalysts. This better performance in Pd electrocatalysts synthesized by modified polyol method than their modified counterparts can be attributed to the lower pH in Pd electrocatalysts synthesized by modified polyol method since the higher the pH, the more the OH group present at the surface of the electrocatalyst. This more OH group reduces the interaction of the Pd catalyst with the methanol fuel for effective oxidation reaction to take place by blocking the active surface of the Pd catalyst (Spendelow & Wieckowski, 2007) while the better performance than hybrid supported Pd catalysts and Pd-Ru binary electrocatalysts can be attributed to better dispersion of catalyst nanoparticles on their support materials. Hence, support materials have been proved in this study to play a vital role in influencing the activity and stability of the synthesized electrocatalysts. It can be inferred from this study that synthesized NGO, N-MWCNTs and GO-MWCNTs have proved to be the best support materials among graphene based supported Pd catalysts and Pd-Ru binary electrocatalysts; MWCNTs, N-MWCNTs, CNFs supported Pd catalysts and hybrid supported Pd catalysts respectively while N-MWCNTs has displayed the best activity among all the synthesized support materials in this research since the catalyst supported

by this support material and synthesized by modified polyol method has showed the best activity and stability in basic (KOH) electrolyte compared to all other synthesized carbon supported catalysts.

In conclusion, after all the results obtained from the physical and electrochemical characterisation of mono supported Pd catalysts, hybrid supported Pd catalysts and carbon supported Pd-Ru binary catalysts were compared, it can be inferred that modification of electrocatalysts synthesis method by increasing the pH from 12 to 13, hybridization of the support materials and alloying of Pd and Ru nanoparticles in ratio 1:2 to form the catalyst mass loading, which is the same as the mass loading used for Pd monocatalysts, did not improve the activity of the support materials generally since the mono supported Pd catalysts synthesized by modified polyol method exhibited better electroactivity than others.

8.2   Recommendations for future study

❖ This study has shown that support materials are very important in enhancing the catalytic activity of catalysts. It is however important for further research to be conducted on the support materials using heterocyclic with heteroatom polymers as stabilizers during their synthesis. This could increase the nucleated and binding site on the support materials, thereby increase the electroactive surface area of the electrocatalyst.

❖ The ratio of each support material for the synthesis of hybrid support materials can be further varied which could reduce or prevent the restacking of exfoliated graphene sheets thereby provide better surface for catalyst loading.

❖ Since support materials like graphene is susceptible to restacking, organic linkers which contain azido group can also be incorporated into it in order to reduce or prevent the restacking and increase the surface area of the support material, reduce the agglomeration of the catalyst nanoparticles, reduce the metal loading (which will invariably reduce the cost) and enhance the catalyst electroactivity.

127

REFERENCES

Abaza, A., El-Sehiemy, R. A., Mahmoud, K., Lehtonen, M., & Darwish, M. M. F. (2021). Optimal Estimation of Proton Exchange Membrane Fuel Cells Parameter Based on Coyote Optimization Algorithm. *Applied Sciences*, *11*(5), 2052. https://doi.org/10.3390/app11052052

Ajeel, M. A., Taeib Aroua, M. K., & Ashri Wan Daud, W. M. (2016). Reactivity of carbon black diamond electrode during the electro-oxidation of Remazol Brilliant Blue R. *RSC Advances*, *6*(5), 3690–3699. https://doi.org/10.1039/C5RA21487D

Akalework, N. G., Pan, C.-J., Su, W.-N., Rick, J., Tsai, M.-C., Lee, J.-F., Lin, J.-M., Tsai, L.-D., & Hwang, B.-J. (2012). Ultrathin TiO2-coated MWCNTs with excellent conductivity and SMSI nature as Pt catalyst support for oxygen reduction reaction in PEMFCs. *Journal of Materials Chemistry*, *22*(39), 20977. https://doi.org/10.1039/c2jm34361d

Al-Marri, A. H., Khan, M., Shaik, M. R., Mohri, N., Adil, S. F., Kuniyil, M., Alkhathlan, H. Z., Al-Warthan, A., Tremel, W., Tahir, M. N., Khan, M., & Siddiqui, M. R. H. (2016). Green synthesis of Pd@graphene nanocomposite: Catalyst for the selective oxidation of alcohols. *Arabian Journal of Chemistry*, *9*(6), 835–845. https://doi.org/10.1016/J.ARABJC.2015.12.007

Alexei L.N. Pinheiroa, Almir Oliveira-Netoa, E. C. de S., Joelma Perezb, Valdecir A. Paganina, E. A. T., & Gonzaleza, and E. R. (2003). Electrocatalysis on Noble Metal and Noble Metal Alloys Dispersed on High Surface Area Carbon. *Journal of New Materials for Electrochemical Systems*, *6*, 1–8.

Alexeyeva, N., Sarapuu, A., Tammeveski, K., Vidal-Iglesias, F. J., Solla-Gullón, J., & Feliu, J. M. (2011). Electroreduction of oxygen on Vulcan carbon supported Pd nanoparticles and Pd–M nanoalloys in acid and alkaline solutions. *Electrochimica Acta*, *56*(19), 6702–6708. https://doi.org/10.1016/j.electacta.2011.05.058

Antolini, E., Cardellini, F., Giacometti, E., & Squadrito, G. (2002). Study on the formation of Pt/C catalysts by non-oxidized active carbon support and a sulfur-based reducing agent. *Journal of Materials Science 2002 37:1*, *37*(1), 133–139. https://doi.org/10.1023/A:1013166429216

Antolini, E., Lopes, T., & Gonzalez, E. R. (2008). An overview of Platinum-based catalysts as methanol-resistant oxygen reduction materials for direct methanol fuel cells. *Journal of Alloys and Compounds*, *461*(1–2), 253–262. https://doi.org/10.1016/J.JALLCOM.2007.06.077

128

Antolini, Ermete. (2003). Formation of carbon-supported PtM alloys for low temperature fuel cells: a review. *Materials Chemistry and Physics*, *78*(3), 563–573. https://doi.org/10.1016/S0254-0584(02)00389-9

Antolini, Ermete. (2007). Catalysts for direct ethanol fuel cells. *Journal of Power Sources*, *170*(1), 1–12. https://doi.org/10.1016/J.JPOWSOUR.2007.04.009

Antolini, Ermete. (2009). Carbon supports for low-temperature fuel cell catalysts. *Applied Catalysis B: Environmental*, *88*(1–2), 1–24. https://doi.org/10.1016/j.apcatb.2008.09.030

Antolini, Ermete. (2010). Composite materials: An emerging class of fuel cell catalyst supports. *Applied Catalysis B: Environmental*, *100*(3–4), 413–426. https://doi.org/10.1016/j.apcatb.2010.08.025

Antolini, Ermete. (2018). Photo-assisted methanol oxidation on Pt-TiO2 catalysts for direct methanol fuel cells: A short review. *Applied Catalysis B: Environmental*, *237*, 491–503. https://doi.org/10.1016/J.APCATB.2018.06.029

Anwar, M. T., Yan, X., Asghar, M. R., Husnain, N., Shen, S., Luo, L., & Zhang, J. (2019). Recent advances in hybrid support material for Pt-based electrocatalysts of proton exchange membrane fuel cells. *International Journal of Energy Research*, *43*(7), 2694–2721. https://doi.org/10.1002/er.4322

Avouris, P., & Dimitrakopoulos, C. (2012). Graphene: synthesis and applications. *Materials Today*, *15*(3), 86–97. https://doi.org/10.1016/S1369-7021(12)70044-5

Bahrami, H., & Faghri, A. (2013). Review and advances of direct methanol fuel cells: Part II: Modeling and numerical simulation. *Journal of Power Sources*, *230*, 303–320. https://doi.org/10.1016/j.jpowsour.2012.12.009

Balasubramanian, K., & Burghard, M. (2005). Chemically Functionalized Carbon Nanotubes. *Small*, *1*(2), 180–192. https://doi.org/10.1002/SMLL.200400118

Banerjee, S., Dasgupta, K., Kumar, A., Ruz, P., Vishwanadh, B., Joshi, J. B., & Sudarsan, V. (2015). Comparative evaluation of hydrogen storage behavior of Pd doped carbon nanotubes prepared by wet impregnation and polyol methods. *International Journal of Hydrogen Energy*, *40*(8), 3268–3276. https://doi.org/10.1016/J.IJHYDENE.2015.01.048

Bang, J. H., Han, K., Skrabalak, S. E., Kim, H., & Suslick, K. S. (2007). Porous Carbon Supports Prepared by Ultrasonic Spray Pyrolysis for Direct Methanol Fuel Cell Electrodes. *The Journal of Physical Chemistry C*, *111*(29), 10959–10964. https://doi.org/10.1021/jp071624v

Basri, S., Kamarudin, S. K., Daud, W. R. W., & Yaakub, Z. (2010). Nanocatalyst for direct methanol fuel cell (DMFC). *International Journal of Hydrogen Energy*, *35*(15), 7957–7970. https://doi.org/10.1016/j.ijhydene.2010.05.111

Bessel, C. A., Laubernds, K., Rodriguez, N. M., & Baker, R. T. K. (2001). Graphite Nanofibers as an Electrode for Fuel Cell Applications. *The Journal of Physical Chemistry B*, *105*(6), 1115–1118. https://doi.org/10.1021/jp003280d

Bharti, A., & Cheruvally, G. (2017). Influence of various carbon nano-forms as supports for Pt catalyst on proton exchange membrane fuel cell performance. *Journal of Power Sources*, *360*, 196–205. https://doi.org/10.1016/j.jpowsour.2017.05.117

Bianchini, C., & Shen, P. K. (2009). Palladium-Based Electrocatalysts for Alcohol Oxidation in Half Cells and in Direct Alcohol Fuel Cells. *Chemical Reviews*, *109*(9), 4183–4206. https://doi.org/10.1021/cr9000995

Bock, C., Paquet, C., Couillard, M., Botton, G. A., & MacDougall, B. R. (2004). Size-Selected Synthesis of PtRu Nano-Catalysts: Reaction and Size Control Mechanism. *Journal of the American Chemical Society*, *126*(25), 8028–8037. https://doi.org/10.1021/ja0495819

Bojarska, Z., Mazurkiewicz-Pawlicka, M., & Makowski, Ł. (2019). Graphene oxide-based nanomaterials as catalysts for oxygen reduction reaction. *Chemical and Process Engineering - Inzynieria Chemiczna i Procesowa*. https://doi.org/10.24425/cpe.2019.130212

Bonnamy, S., & Oberlin, A. (2016). Transmission Electron Microscopy. *Materials Science and Engineering of Carbon*, 45–70. https://doi.org/10.1016/B978-0-12-805256-3.00004-0

Boskovic, B. O., Golovko, V. B., Cantoro, M., Kleinsorge, B., Chuang, A. T. H., Ducati, C., Hofmann, S., Robertson, J., & Johnson, B. F. G. (2005). Low temperature synthesis of carbon nanofibres on carbon fibre matrices. *Carbon*, *43*(13), 2643–2648. https://doi.org/10.1016/j.carbon.2005.04.034

Brame, J., & Griggs, C. (2016). Surface Area Analysis Using the Brunauer-Emmett-Teller (BET) Method Scient. *Engineer Research and Development Center*, *September*, 23. https://doi.org/39180-6199

Bulushev, D. A., Yuranov, I., Suvorova, E. I., Buffat, P. A., & Kiwi-Minsker, L. (2004). Highly dispersed gold on activated carbon fibers for low-temperature CO oxidation. *Journal of Catalysis*, *224*(1), 8–17. https://doi.org/10.1016/j.jcat.2004.02.014

Bunaciu, A. A., Udriştioiu, E. gabriela, & Aboul-Enein, H. Y. (2015). X-Ray Diffraction: Instrumentation and Applications. *Http://Dx.Doi.Org/10.1080/10408347.2014.949616*, *45*(4), 289–299. https://doi.org/10.1080/10408347.2014.949616

Calderón Gómez, J., Moliner, R., & Lázaro, M. (2016). Palladium-Based Catalysts as Electrodes for Direct Methanol Fuel Cells: A Last Ten Years Review. *Catalysts*, *6*(9), 130. https://doi.org/10.3390/catal6090130

Calderón, J. C., Mahata, N., Pereira, M. F. R., Figueiredo, J. L., Fernandes, V. R., Rangel, C. M., Calvillo, L., Lázaro, M. J., & Pastor, E. (2012). Pt–Ru catalysts supported on carbon xerogels for PEM fuel cells. *International Journal of Hydrogen Energy*, *37*(8), 7200–7211. https://doi.org/10.1016/j.ijhydene.2011.12.029

Calvillo, L., Lázaro, M. J., García-Bordejé, E., Moliner, R., Cabot, P. L., Esparbé, I., Pastor, E., & Quintana, J. J. (2007). Platinum supported on functionalized ordered mesoporous carbon as electrocatalyst for direct methanol fuel cells. *Journal of Power Sources*, *169*(1), 59–64. https://doi.org/10.1016/j.jpowsour.2007.01.042

Carrera-Cerritos, R., Baglio, V., Aricò, A. S., Ledesma-García, J., Sgroi, M. F., Pullini, D., Pruna, A. J., Mataix, D. B., Fuentes-Ramírez, R., & Arriaga, L. G. (2014). Improved Pd electro-catalysis for oxygen reduction reaction in direct methanol fuel cell by reduced graphene oxide. *Applied Catalysis B: Environmental*, *144*, 554–560. https://doi.org/10.1016/j.apcatb.2013.07.057

Chalgin, A., Song, C., Tao, P., Shang, W., Deng, T., & Wu, J. (2020). Effect of supporting materials on the electrocatalytic activity, stability and selectivity of noble metal-based catalysts for oxygen reduction and hydrogen evolution reactions. *Progress in Natural Science: Materials International*, *30*(3), 289–297. https://doi.org/10.1016/j.pnsc.2020.01.003

Chen, D., Feng, H., & Li, J. (2012). Graphene Oxide: Preparation, Functionalization, and Electrochemical Applications. *Chemical Reviews*, *112*(11), 6027–6053. https://doi.org/10.1021/cr300115g

Chen, L. H., Zang, J. B., Wang, Y. H., & Bian, L. Y. (2008). Electrochemical oxidation of nitrite on nanodiamond powder electrode. *Electrochimica Acta*, *53*(8), 3442–3445. https://doi.org/10.1016/j.electacta.2007.12.023

Chen, Y., Wang, J., Liu, H., Banis, M. N., Li, R., Sun, X., Sham, T.-K., Ye, S., & Knights, S. (2011). Nitrogen Doping Effects on Carbon Nanotubes and the Origin of the Enhanced Electrocatalytic Activity of Supported Pt for Proton-Exchange Membrane Fuel Cells. *The Journal of Physical Chemistry C*, *115*(9), 3769–3776. https://doi.org/10.1021/jp108864y

Cheng, K., He, D., Peng, T., Lv, H., Pan, M., & Mu, S. (2014). Porous graphene supported Pt catalysts for proton exchange membrane fuel cells. *Electrochimica Acta*, *132*, 356–363. https://doi.org/10.1016/j.electacta.2014.03.181

Chhowalla, M., Teo, K. B. K., Ducati, C., Rupesinghe, N. L., Amaratunga, G. A. J., Ferrari, A. C., Roy, D., Robertson, J., & Milne, W. I. (2001). Growth process conditions of vertically aligned carbon nanotubes using plasma enhanced chemical vapor deposition. *Journal of*

Applied Physics, *90*(10), 5308–5317. https://doi.org/10.1063/1.1410322

Choi, S. M., Seo, M. H., Kim, H. J., & Kim, W. B. (2011). Synthesis of surface-functionalized graphene nanosheets with high Pt-loadings and their applications to methanol electrooxidation. *Carbon*, *49*(3), 904–909. https://doi.org/10.1016/j.carbon.2010.10.055

Choucair, M., Thordarson, P., & Stride, J. A. (2009). Gram-scale production of graphene based on solvothermal synthesis and sonication. *Nature Nanotechnology*, *4*(1), 30–33. https://doi.org/10.1038/nnano.2008.365

Ciureanu, M., & Roberge, R. (2001). Electrochemical Impedance Study of PEM Fuel Cells. Experimental Diagnostics and Modeling of Air Cathodes. *Journal of Physical Chemistry B*, *105*(17), 3531–3539. https://doi.org/10.1021/JP003273P

Coloma, F., Sepulveda-Escribano, A., Fierro, J. L. G., & Rodriguez-Reinoso, F. (1994). Preparation of Platinum Supported on Pregraphitized Carbon Blacks. *Langmuir*, *10*(3), 750–755. https://doi.org/10.1021/la00015a025

Cookson, J. (2012). <I>The Preparation of Palladium Nanoparticles</I>. *Platinum Metals Review*, *56*(2), 83–98. https://doi.org/10.1595/147106712X632415

Daoush, W. M., & Imae, T. (2012). Syntheses and characterizations of multiwalled carbon nanotubes-supported Palladium nanocomposites. *Journal of Materials Research*, *27*(13), 1680–1687. https://doi.org/10.1557/jmr.2012.123

de la Fuente, J. L. G., Rojas, S., Martínez-Huerta, M. V., Terreros, P., Peña, M. A., & Fierro, J. L. G. (2006). Functionalization of carbon support and its influence on the electrocatalytic behaviour of Pt/C in H2 and CO electrooxidation. *Carbon*, *44*(10), 1919–1929. https://doi.org/10.1016/j.carbon.2006.02.009

De Miguel, S. R., Vilella, J. I., Jablonski, E. L., Scelza, O. A., Salinas-Martinez de Lecea, C., & Linares-Solano, A. (2002). Preparation of Pt catalysts supported on activated carbon felts (ACF). *Applied Catalysis A: General*, *232*(1–2), 237–246. https://doi.org/10.1016/S0926-860X(02)00112-6

Dector, A., Cuevas-Muñiz, F. M., Guerra-Balcázar, M., Godínez, L. A., Ledesma-García, J., & Arriaga, L. G. (2013). Glycerol oxidation in a microfluidic fuel cell using Pd/C and Pd/MWCNT anodes electrodes. *International Journal of Hydrogen Energy*, *38*(28), 12617–12622. https://doi.org/10.1016/j.ijhydene.2012.12.030

Derbyshire, F. J., de Beer, V. H. J., Abotsi, G. M. K., Scaroni, A. W., Solar, J. M., & Skrovanek, D. J. (1986). The influence of surface functionality on the activity of carbon-supported catalysts. *Applied Catalysis*, *27*(1), 117–131. https://doi.org/10.1016/S0166-9834(00)81051-9

Doña Rodríguez, J. M., Melián, J. A. H., & Peña, J. P. (2000). Determination of the Real Surface Area of Pt Electrodes by Hydrogen Adsorption Using Cyclic Voltammetry. *Journal of Chemical Education*, *77*(9), 1195–1197. https://doi.org/10.1021/ED077P1195

Dong Jin Suh, Tae-Jin, P., & Son-Ki, I. (1993). Effect of surface oxygen groups of carbon supports on the characteristics of Pd/C catalysts. *Carbon*, *31*(3), 427–435. https://doi.org/10.1016/0008-6223(93)90130-3

Down, W. B., & Baker, R. T. K. (1995). Modification of the surface properties of carbon fibers via the catalytic growth of carbon nanofibers. *Journal of Materials Research*, *10*(3), 625–633. https://doi.org/10.1557/JMR.1995.0625

Du, C., Chen, M., Cao, X., Yin, G., & Shi, P. (2009). A novel CNT@SnO2 core–sheath nanocomposite as a stabilizing support for catalysts of proton exchange membrane fuel cells. *Electrochemistry Communications*, *11*(2), 496–498. https://doi.org/10.1016/j.elecom.2008.12.034

Du, H.-Y., Wang, C.-H., Hsu, H.-C., Chang, S.-T., Chen, U.-S., Yen, S. C., Chen, L. C., Shih, H.-C., & Chen, K. H. (2008). Controlled Platinum nanoparticles uniformly dispersed on nitrogen-dopedcarbon nanotubes for methanol oxidation. *Diamond and Related Materials*, *17*(4–5), 535–541. https://doi.org/10.1016/j.diamond.2008.01.116

Du, L., Shao, Y., Sun, J., Yin, G., Liu, J., & Wang, Y. (2016). Advanced catalyst supports for PEM fuel cell cathodes. *Nano Energy*, *29*, 314–322. https://doi.org/10.1016/j.nanoen.2016.03.016

EHRBURGER, P., MAHAJAN, O., & WALKERJR, P. (1976). Carbon as a support for catalystsI. Effect of surface heterogeneity of carbon on dispersion of Platinum. *Journal of Catalysis*, *43*(1–3), 61–67. https://doi.org/10.1016/0021-9517(76)90293-1

Eigler, S., Enzelberger-Heim, M., Grimm, S., Hofmann, P., Kroener, W., Geworski, A., Dotzer, C., Röckert, M., Xiao, J., Papp, C., Lytken, O., Steinrück, H.-P., Müller, P., & Hirsch, A. (2013). Wet Chemical Synthesis of Graphene. *Advanced Materials*, *25*(26), 3583–3587. https://doi.org/10.1002/adma.201300155

Electrochemistry - P.H. Rieger - Google Books. (n.d.). Retrieved April 11, 2022, from https://books.google.es/books?hl=en&lr=&id=b_MacaF5yq8C&oi=fnd&pg=PR9&dq=P.+H.+Rieger,+Electrochemistry&ots=1oj_-Si9It&sig=lexwUpDbnI10YtRJBcyR9rNJj18&redir_esc=y#v=onepage&q=P. H. Rieger%2C Electrochemistry&f=false

Electron Microscopy: Principles and Techniques for Biologists - John J. Bozzola, Lonnie Dee Russell - Google Books. (n.d.). Retrieved March 10, 2022, from

https://books.google.co.za/books?hl=en&lr=&id=zMkBAPACbEkC&oi=fnd&pg=PR21&dq=John+J.+Bozzola,+L.+D.+R.+(2006)+Electron+Microscopy:+Principles+and+Techniques+for+Biologists+-+John+J.+Bozzola,+Lonnie+Dee+Russell+-+Google+Books.+Available+at:+https://books.google.co.za/books%3Fhl%3Den%26lr%3D%26id%3DzMkBAPACbEkC%26oi%3Dfnd%26pg%3DPR21%26dq%3DJ%2BBozzola%253B%2BL%2BD&ots=AdN-WlkIO5&sig=gC967YUVhHCTdbi7FKGNtq7lKj8&redir_esc=y#v=onepage&q&f=false

Elgrishi, N., Rountree, K. J., McCarthy, B. D., Rountree, E. S., Eisenhart, T. T., & Dempsey, J. L. (2018). A Practical Beginner's Guide to Cyclic Voltammetry. *Journal of Chemical Education*, *95*(2), 197–206. https://doi.org/10.1021/ACS.JCHEMED.7B00361/SUPPL_FILE/ED7B00361_SI_002.DOCX

Emiru, T. F., & Ayele, D. W. (2017). Controlled synthesis, characterization and reduction of graphene oxide: A convenient method for large scale production. *Egyptian Journal of Basic and Applied Sciences*, *4*(1), 74–79. https://doi.org/10.1016/j.ejbas.2016.11.002

Farooqui, U. R., Ahmad, A. L., & Hamid, N. A. (2018). Graphene oxide: A promising membrane material for fuel cells. *Renewable and Sustainable Energy Reviews*, *82*, 714–733. https://doi.org/10.1016/j.rser.2017.09.081

Farsadrooh, M., Yazdan-Abad, M. Z., Noroozifar, M., Javadian, H., Alfi, N., & Modarresi-Alam, A. R. (2020). Fast improved polyol method for synthesis of Pd/C catalyst with high performance toward ethanol electrooxidation. *International Journal of Hydrogen Energy*, *45*(51), 27312–27319. https://doi.org/10.1016/j.ijhydene.2020.07.149

Fischer, A. E., & Swain, G. M. (2005). Preparation and Characterization of Boron-dopedDiamond Powder. *Journal of The Electrochemical Society*, *152*(9), B369. https://doi.org/10.1149/1.1984367

Fraga, M. A., Jordão, E., Mendes, M. J., Freitas, M. M. A., Faria, J. L., & Figueiredo, J. L. (2002). Properties of Carbon-Supported Platinum Catalysts: Role of Carbon Surface Sites. *Journal of Catalysis*, *209*(2), 355–364. https://doi.org/10.1006/jcat.2002.3637

Gálvez, M., Calvillo, L., Alegre, C., Sebastián, D., Suelves, I., Pérez-Rodríguez, S., Celorrio, V., Pastor, E., Pardo, J., Moliner, R., & Lázaro, M. (2013). Nanostructured Carbon Materials as Supports in the Preparation of Direct Methanol Fuel Cell Electrocatalysts. *Catalysts*, *3*(3), 671–682. https://doi.org/10.3390/catal3030671

Gangeri, M., Centi, G., Malfa, A. La, Perathoner, S., Vieira, R., Pham-Huu, C., & Ledoux, M. J. (2005). Electrocatalytic performances of nanostructured Platinum–carbon materials.

Catalysis Today, *102–103*, 50–57. https://doi.org/10.1016/j.cattod.2005.02.035

Garsany, Y., Baturina, O. A., Swider-Lyons, K. E., & Kocha, S. S. (2010). Experimental Methods for Quantifying the Activity of Platinum Electrocatalysts for the Oxygen Reduction Reaction. *Analytical Chemistry*, *82*(15), 6321–6328. https://doi.org/10.1021/ac100306c

Gasteiger, H. A., Kocha, S. S., Sompalli, B., & Wagner, F. T. (2005). Activity benchmarks and requirements for Pt, Pt-alloy, and non-Pt oxygen reduction catalysts for PEMFCs. *Applied Catalysis B: Environmental*, *56*(1–2), 9–35. https://doi.org/10.1016/J.APCATB.2004.06.021

Gharibi, H., Mirzaie, R. A., Shams, E., Zhiani, M., & Khairmand, M. (2005). Preparation of Platinum electrocatalysts using carbon supports for oxygen reduction at a gas-diffusion electrode. *Journal of Power Sources*, *139*(1–2), 61–66. https://doi.org/10.1016/j.jpowsour.2004.06.075

Gottesfeld, S., & Zawodzinski, T. A. (2008). Polymer Electrolyte Fuel Cells. *Advances in Electrochemical Science and Engineering*, *5*, 195–301. https://doi.org/10.1002/9783527616794.CH4

Groves, M. N., Malardier-Jugroot, C., & Jugroot, M. (2012). Improving Platinum Catalyst Durability with a Doped Graphene Support. *The Journal of Physical Chemistry C*, *116*(19), 10548–10556. https://doi.org/10.1021/jp203734d

Guerrero-Ruiz, A., Badenes, P., & Rodríguez-Ramos, I. (1998). Study of some factors affecting the Ru and Pt dispersions over high surface area graphite-supported catalysts. *Applied Catalysis A: General*, *173*(2), 313–321. https://doi.org/10.1016/S0926-860X(98)00187-2

Gui, M. M., Yap, Y. X., Chai, S.-P., & Mohamed, A. R. (2013). Multi-walled carbon nanotubes modified with (3-aminopropyl)triethoxysilane for effective carbon dioxide adsorption. *International Journal of Greenhouse Gas Control*, *14*, 65–73. https://doi.org/10.1016/j.ijggc.2013.01.004

Guo, D.-J., & Jing, Z.-H. (2011). Electrocatalytic properties of Platinum nanoparticles supported on fluorine tin dioxide/multi-walled carbon nanotube composites for methanol electrooxidation in acidic medium. *Journal of Colloid and Interface Science*, *359*(1), 257–260. https://doi.org/10.1016/j.jcis.2011.03.019

Guo, D.-J., Zhao, L., Qiu, X.-P., Chen, L.-Q., & Zhu, W.-T. (2008). Novel hollow PtRu nanospheres supported on multi-walled carbon nanotube for methanol electrooxidation. *Journal of Power Sources*, *177*(2), 334–338. https://doi.org/10.1016/j.jpowsour.2007.11.087

Guo, S., & Sun, S. (2012). FePt Nanoparticles Assembled on Graphene as Enhanced Catalyst for Oxygen Reduction Reaction. *Journal of the American Chemical Society*, *134*(5), 2492–2495. https://doi.org/10.1021/ja2104334

Gupta, V., Sharma, N., Singh, U., Arif, M., & Singh, A. (2017). Higher oxidation level in graphene oxide. *Optik*, *143*, 115–124. https://doi.org/10.1016/j.ijleo.2017.05.100

Han, M., Zhang, W., Gao, C., Liang, Y., Xu, Z., Zhu, J., & He, J. (2006). Hollow nickel microspheres covered with oriented carbon nanotubes and its magnetic property. *Carbon*, *44*(2), 211–215. https://doi.org/10.1016/j.carbon.2005.07.039

Hasegawa, F., Yokoyama, S., & Imou, K. (2010). Methanol or ethanol produced from woody biomass: Which is more advantageous? *Bioresource Technology*, *101*(1), S109–S111. https://doi.org/10.1016/j.biortech.2009.05.008

He, D., Jiang, Y., Lv, H., Pan, M., & Mu, S. (2013). Nitrogen-dopedreduced graphene oxide supports for noble metal catalysts with greatly enhanced activity and stability. *Applied Catalysis B: Environmental*, *132–133*, 379–388. https://doi.org/10.1016/j.apcatb.2012.12.005

Higgins, D. C., Meza, D., & Chen, Z. (2010). Nitrogen-dopedCarbon Nanotubes as Platinum Catalyst Supports for Oxygen Reduction Reaction in Proton Exchange Membrane Fuel Cells. *The Journal of Physical Chemistry C*, *114*(50), 21982–21988. https://doi.org/10.1021/jp106814j

Hofmann, S., Ducati, C., Robertson, J., & Kleinsorge, B. (2003). Low-temperature growth of carbon nanotubes by plasma-enhanced chemical vapor deposition. *Applied Physics Letters*, *83*(1), 135–137. https://doi.org/10.1063/1.1589187

Huang, H. X., Chen, S. X., & Yuan, C. (2008). Platinum nanoparticles supported on activated carbon fiber as catalyst for methanol oxidation. *Journal of Power Sources*, *175*(1), 166–174. https://doi.org/10.1016/J.JPOWSOUR.2007.08.107

Huang, X.-J., Li, Y., Im, H.-S., Yarimaga, O., Kim, J.-H., Jang, D.-Y., Cho, S.-O., Cai, W.-P., & Choi, Y.-K. (2006). Morphology-controlled SWCNT/polymeric microsphere arrays by a wet chemical self-assembly technique and their application for sensors. *Nanotechnology*, *17*(12), 2988–2993. https://doi.org/10.1088/0957-4484/17/12/028

Hudson, J. L., Casavant, M. J., & Tour, J. M. (2004). Water-Soluble, Exfoliated, Nonroping Single-Wall Carbon Nanotubes. *Journal of the American Chemical Society*, *126*(36), 11158–11159. https://doi.org/10.1021/ja0467061

Hung, C.-T., Liou, Z.-H., Veerakumar, P., Wu, P.-H., Liu, T.-C., & Liu, S.-B. (2016). Ordered mesoporous carbon supported bifunctional PtM (M = Ru, Fe, Mo) electrocatalysts for a fuel

cell anode. *Chinese Journal of Catalysis*, *37*(1), 43–53. https://doi.org/10.1016/S1872-2067(15)60878-6

Jafri, R. I., Arockiados, T., Rajalakshmi, N., & Ramaprabhu, S. (2010). Nanostructured Pt Dispersed on Graphene-Multiwalled Carbon Nanotube Hybrid Nanomaterials as Electrocatalyst for PEMFC. *Journal of The Electrochemical Society*, *157*(6), B874. https://doi.org/10.1149/1.3374353

Jang, J., & Ryu, S. K. (2006). Physical property and electrical conductivity of electroless Ag-plated carbon fiber-reinforced paper. *Journal of Materials Processing Technology*, *180*(1–3), 66–73. https://doi.org/10.1016/J.JMATPROTEC.2006.05.003

Jha, N., Jafri, R. I., Rajalakshmi, N., & Ramaprabhu, S. (2011). Graphene-multi walled carbon nanotube hybrid electrocatalyst support material for direct methanol fuel cell. *International Journal of Hydrogen Energy*, *36*(12), 7284–7290. https://doi.org/10.1016/j.ijhydene.2011.03.008

Jiang, L., & Gao, L. (2003). Modified carbon nanotubes: an effective way to selective attachment of gold nanoparticles. *Carbon*, *41*(15), 2923–2929. https://doi.org/10.1016/S0008-6223(03)00339-7

Job, N., Panariello, F., Marien, J., Crine, M., Pirard, J. P., & Léonard, A. (2006). Synthesis optimization of organic xerogels produced from convective air-drying of resorcinol–formaldehyde gels. *Journal of Non-Crystalline Solids*, *352*(1), 24–34. https://doi.org/10.1016/J.JNONCRYSOL.2005.11.024

Ju, H., Lee, K.-S., & Um, S. (2008). Multi-dimensional modeling of CO poisoning effects on proton exchange membrane fuel cells (PEMFCs). *Journal of Mechanical Science and Technology*, *22*(5), 991–998. https://doi.org/10.1007/s12206-008-0207-1

Jyothirmayee Aravind, S. S., Imran Jafri, R., Rajalakshmi, N., & Ramaprabhu, S. (2011). Solar exfoliated graphene–carbon nanotube hybrid nano composites as efficient catalyst supports for proton exchange membrane fuel cells. *Journal of Materials Chemistry*, *21*(45), 18199. https://doi.org/10.1039/c1jm13908h

Kakaei, K. (2012). Electrochemical Characteristics and Performance of Platinum Nanoparticles Supported by Vulcan/Polyaniline for Oxygen Reduction in PEMFC. *Fuel Cells*, *12*(6), 939–945. https://doi.org/10.1002/fuce.201200053

Kamarudin, S. K., Achmad, F., & Daud, W. R. W. (2009). Overview on the application of direct methanol fuel cell (DMFC) for portable electronic devices. *International Journal of Hydrogen Energy*, *34*(16), 6902–6916. https://doi.org/10.1016/j.ijhydene.2009.06.013

Kamarudin, S. K., Daud, W. R. W., Ho, S. L., & Hasran, U. A. (2007). Overview on the

challenges and developments of micro-direct methanol fuel cells (DMFC). *Journal of Power Sources*, *163*(2), 743–754. https://doi.org/10.1016/j.jpowsour.2006.09.081

Karim, N. A., Kamarudin, S. K., Shyuan, L. K., Yaakob, Z., Daud, W. R. W., & Kadhum, A. A. H. (2015). Study on the electronic properties and molecule adsorption of W 18 O 49 nanowires as a catalyst support in the cathodes of direct methanol fuel cells. *Journal of Power Sources*, *288*, 461–472. https://doi.org/10.1016/j.jpowsour.2015.04.111

Karthikeyan, N., Vinayan, B. P., Rajesh, M., Balaji, K., Subramani, A. K., & Ramaprabhu, S. (2015). Highly Durable Platinum based Cathode Electrocatalysts for PEMFC Application using Oxygen and Nitrogen Functional Groups Attached Nanocarbon Supports. *Fuel Cells*, *15*(2), 278–287. https://doi.org/10.1002/fuce.201400134

Kasumov, A. Y., Bouchiat, H., Reulet, B., Stephan, O., Khodos, I. I., Gorbatov, Y. B., & Colliex, C. (1998). Conductivity and atomic structure of isolated multiwalled carbon nanotubes. *Europhysics Letters (EPL)*, *43*(1), 89–94. https://doi.org/10.1209/epl/i1998-00324-1

Kasuya, D., Yudasaka, M., Takahashi, K., Kokai, F., & Iijima, S. (2002). Selective Production of Single-Wall Carbon Nanohorn Aggregates and Their Formation Mechanism. *The Journal of Physical Chemistry B*, *106*(19), 4947–4951. https://doi.org/10.1021/jp020387n

Kepenienė, V., Stagniūnaitė, R., Tamašauskaitė-Tamašiūnaitė, L., Stalnionienė, I., & Norkus, E. (2015). Graphene and niobium(V) oxide/graphene supported Platinum–cobalt catalysts as cathode material for oxygen reduction. *Chemija*, *26*(3), 165–169.

Khotseng, L., Bangisa, A., Modibedi, R. M., & Linkov, V. (2016). Electrochemical Evaluation of Pt-Based Binary Catalysts on Various Supports for the Direct Methanol Fuel Cell. *Electrocatalysis*, *7*(1), 1–12. https://doi.org/10.1007/s12678-015-0282-x

Kim, B.-J., & Park, S.-J. (2006). Preparation of nanoporous carbons from graphite nanofibres. *Nanotechnology*, *17*(17), 4395–4398. https://doi.org/10.1088/0957-4484/17/17/018

Kim, C., Kim, Y. J., Kim, Y. A., Yanagisawa, T., Park, K. C., Endo, M., & Dresselhaus, M. S. (2004). High performance of cup-stacked-type carbon nanotubes as a Pt–Ru catalyst support for fuel cell applications. *Journal of Applied Physics*, *96*(10), 5903–5905. https://doi.org/10.1063/1.1804242

Kim, S.-I., Yamamoto, T., Endo, A., Ohmori, T., & Nakaiwa, M. (2006). Preparation of Platinum Nanoparticles Supported on Resorcinol-Formaldehyde Carbon Cryogel Microspheres. *Journal of Industrial and Engineering Chemistry*, *12*(5), 769–776. https://www.cheric.org/research/tech/periodicals/view.php?seq=541381

Kim, S., & Park, S.-J. (2006). Effects of chemical treatment of carbon supports on electrochemical behaviors for Platinum catalysts of fuel cells. *Journal of Power Sources*,

159(1), 42–45. https://doi.org/10.1016/j.jpowsour.2006.04.041

Kim, Y., Kim, H. W., Lee, S., Han, J., Lee, D., Kim, J., Kim, T., Kim, C., Jeong, S., Chae, H., Kim, B., Chang, H., Kim, W. B., Choi, S. M., & Kim, H. J. (2017). The Role of Ruthenium on Carbon-Supported PtRu Catalysts for Electrocatalytic Glycerol Oxidation under Acidic Conditions. *ChemCatChem*, *9*(9), 1683–1690. https://doi.org/10.1002/cctc.201601325

Kissinger, P. T., & Heineman, W. R. (1983). Cyclic voltammetry. *Journal of Chemical Education*, *60*(9), 702–706. https://doi.org/10.1021/ED060P702

Kiyani, R., Parnian, M. J., & Rowshanzamir, S. (2017). Investigation of the effect of carbonaceous supports on the activity and stability of supported Palladium catalysts for methanol electro-oxidation reaction. *International Journal of Hydrogen Energy*, *42*(36), 23070–23084. https://doi.org/10.1016/j.ijhydene.2017.07.113

Klaas, L., Modibedi, M., Mathe, M., Su, H., & Khotseng, L. (2020). Electrochemical Studies of Pd-Based Anode Catalysts in Alkaline Medium for Direct Glycerol Fuel Cells. *Catalysts*, *10*(9), 968. https://doi.org/10.3390/catal10090968

Knupp, S. L., Li, W., Paschos, O., Murray, T. M., Snyder, J., & Haldar, P. (2008). The effect of experimental parameters on the synthesis of carbon nanotube/nanofiber supported Platinum by polyol processing techniques. *Carbon*, *46*(10), 1276–1284. https://doi.org/10.1016/j.carbon.2008.05.007

Kou, R., Shao, Y., Mei, D., Nie, Z., Wang, D., Wang, C., Viswanathan, V. V, Park, S., Aksay, I. A., Lin, Y., Wang, Y., & Liu, J. (2011). Stabilization of Electrocatalytic Metal nanoparticles at Metal−Metal Oxide−Graphene Triple Junction Points. *Journal of the American Chemical Society*, *133*(8), 2541–2547. https://doi.org/10.1021/ja107719u

Kuniyil, M., Shanmukha Kumar, J. V., Adil, S. F., Shaik, M. R., Khan, M., Assal, M. E., Siddiqui, M. R. H., & Al-Warthan, A. (2019). One-Pot Synthesized Pd@N-doped Graphene: An Efficient Catalyst for Suzuki–Miyaura Couplings. *Catalysts 2019, Vol. 9, Page 469*, *9*(5), 469. https://doi.org/10.3390/CATAL9050469

Kuo, P.-L., Hsu, C.-H., Wu, H.-M., Hsu, W.-S., & Kuo, D. (2012). Controllable-Nitrogen Doped Carbon Layer Surrounding Carbon Nanotubes as Novel Carbon Support for Oxygen Reduction Reaction. *Fuel Cells*, *12*(4), 649–655. https://doi.org/10.1002/fuce.201100130

Latorrata, S., Pelosato, R., Stampino, P. G., Cristiani, C., & Dotelli, G. (2018). Use of electrochemical impedance spectroscopy for the evaluation of performance of PEM fuel cells based on carbon cloth gas diffusion electrodes. *Journal of Spectroscopy*, *2018*. https://doi.org/10.1155/2018/3254375

Lee, J., Kim, K., Park, W. I., Kim, B.-H., Park, J. H., Kim, T.-H., Bong, S., Kim, C.-H., Chae,

G., Jun, M., Hwang, Y., Jung, Y. S., & Jeon, S. (2012). Uniform Graphene Quantum Dots Patterned from Self-Assembled Silica Nanodots. *Nano Letters*, *12*(12), 6078–6083. https://doi.org/10.1021/nl302520m

Lee, K., Zhang, J., Wang, H., & Wilkinson, D. P. (2006). Progress in the synthesis of carbon nanotube- and nanofiber-supported Pt electrocatalysts for PEM fuel cell catalysis. *Journal of Applied Electrochemistry*, *36*(5), 507–522. https://doi.org/10.1007/s10800-006-9120-4

Li, J., Liu, J., Tan, G., Jiang, J., Peng, S., Deng, M., Qian, D., Feng, Y., & Liu, Y. (2014). High-sensitivity paracetamol sensor based on Pd/graphene oxide nanocomposite as an enhanced electrochemical sensing platform. *Biosensors and Bioelectronics*, *54*, 468–475. https://doi.org/10.1016/J.BIOS.2013.11.001

Li, L., Hu, L., Li, J., & Wei, Z. (2015). Enhanced stability of Pt nanoparticle electrocatalysts for fuel cells. *Nano Research*, *8*(2), 418–440. https://doi.org/10.1007/s12274-014-0695-5

Li, W., Liang, C., Zhou, W., Qiu, J., Zhou, Sun, G., & Xin, Q. (2003). Preparation and Characterization of Multiwalled Carbon Nanotube-Supported Platinum for Cathode Catalysts of Direct Methanol Fuel Cells. *The Journal of Physical Chemistry B*, *107*(26), 6292–6299. https://doi.org/10.1021/jp022505c

Li, Yueming, Tang, L., & Li, J. (2009). Preparation and electrochemical performance for methanol oxidation of pt/graphene nanocomposites. *Electrochemistry Communications*, *11*(4), 846–849. https://doi.org/10.1016/j.elecom.2009.02.009

Li, Yujing, Li, Y., Zhu, E., McLouth, T., Chiu, C.-Y., Huang, X., & Huang, Y. (2012). Stabilization of High-Performance Oxygen Reduction Reaction Pt Electrocatalyst Supported on Reduced Graphene Oxide/Carbon Black Composite. *Journal of the American Chemical Society*, *134*(30), 12326–12329. https://doi.org/10.1021/ja3031449

Li, Z.-F., Xin, L., Yang, F., Liu, Y., Liu, Y., Zhang, H., Stanciu, L., & Xie, J. (2015). Hierarchical polybenzimidazole-grafted graphene hybrids as supports for Pt nanoparticle catalysts with excellent PEMFC performance. *Nano Energy*, *16*, 281–292. https://doi.org/10.1016/j.nanoen.2015.06.031

Liu, J., Ye, J., Xu, C., Jiang, S. P., & Tong, Y. (2007). Kinetics of ethanol electrooxidation at Pd electrodeposited on Ti. *Electrochemistry Communications*, *9*(9), 2334–2339. https://doi.org/10.1016/j.elecom.2007.06.036

Liu, Z., Abdelhafiz, A. A., Jiang, Y., Qu, C., Chang, I., Zeng, J., Liao, S., & Alamgir, F. M. (2019). Pt/graphene with intercalated carbon nanotube spacers introduced by electrostatic self-assembly for fuel cells. *Materials Chemistry and Physics*, *225*, 371–378. https://doi.org/10.1016/j.matchemphys.2018.12.100

140

Long, D., Li, W., Ling, L., Miyawaki, J., Mochida, I., & Yoon, S.-H. (2010). Preparation of Nitrogen-dopedGraphene Sheets by a Combined Chemical and Hydrothermal Reduction of Graphene Oxide. *Langmuir*, *26*(20), 16096–16102. https://doi.org/10.1021/la102425a

Maiyalagan, T., & Scott, K. (2010). Performance of carbon nanofiber supported Pd–Ni catalysts for electro-oxidation of ethanol in alkaline medium. *Journal of Power Sources*, *195*(16), 5246–5251. https://doi.org/10.1016/j.jpowsour.2010.03.022

Maiyalagan, T., Viswanathan, B., & Varadaraju, U. V. (2005). Nitrogen containing carbon nanotubes as supports for Pt – Alternate anodes for fuel cell applications. *Electrochemistry Communications*, *7*(9), 905–912. https://doi.org/10.1016/j.elecom.2005.07.007

Malek Abbaslou, R. M., Tavasoli, A., & Dalai, A. K. (2009). Effect of pre-treatment on physico-chemical properties and stability of carbon nanotubes supported iron Fischer–Tropsch catalysts. *Applied Catalysis A: General*, *355*(1–2), 33–41. https://doi.org/10.1016/j.apcata.2008.11.023

Marken, F., Neudeck, A., & Bond, A. M. (2005). Cyclic Voltammetry. *Electroanalytical Methods*, 51–97. https://doi.org/10.1007/978-3-662-04757-6_4

Matshitse, R. (2010). Brunauer-Emmett-Teller (BET) surface area analysis. *Rhodes University, National Research Foundation*. https://www.ru.ac.za/media/rhodesuniversity/content/nanotechnology/documents/BET Refilwe Matshitse.pdf

Matsumoto, T., Komatsu, T., Arai, K., Yamazaki, T., Kijima, M., Shimizu, H., Takasawa, Y., & Nakamura, J. (2004). Reduction of Pt usage in fuel cell electrocatalysts with carbon nanotube electrodes. *Chemical Communications*, *4*(7), 840. https://doi.org/10.1039/b400607k

McBreen, J., Olender, H., Srinivasan, S., & Kordesch, K. V. (1981). Carbon supports for phosphoric acid fuel cell electrocatalysts: alternative materials and methods of evaluation. *Journal of Applied Electrochemistry*, *11*(6), 787–796. https://doi.org/10.1007/BF00615184

Mehta, V., & Cooper, J. S. (2003). Review and analysis of PEM fuel cell design and manufacturing. *Journal of Power Sources*, *114*(1), 32–53. https://doi.org/10.1016/S0378-7753(02)00542-6

Meza, D., Higgins, D. C., Wu, J., & Chen, Z. (2011). One-Step Synthesized Tungsten Oxide/Carbon Nanotube Composites as Pt Catalyst Supports for Oxygen Reduction Reaction in Proton Exchange Membrane Fuel Cells. *Journal of Nanoengineering and Nanomanufacturing*, *1*(3), 280–286. https://doi.org/10.1166/jnan.2011.1031

Minh, N. Q. (1993). Ceramic Fuel Cells. *Journal of the American Ceramic Society*, *76*(3), 563–

588. https://doi.org/10.1111/J.1151-2916.1993.TB03645.X

Mironenko, R. M., Belskaya, O. B., Gulyaeva, T. I., Nizovskii, A. I., Kalinkin, A. V., Bukhtiyarov, V. I., Lavrenov, A. V., & Likholobov, V. A. (2015). Effect of the nature of carbon support on the formation of active sites in Pd/C and Ru/C catalysts for hydrogenation of furfural. *Catalysis Today*, *249*, 145–152. https://doi.org/10.1016/J.CATTOD.2014.10.037

Moraes, F. C., Cabral, M. F., Mascaro, L. H., & Machado, S. A. S. (2011). The electrochemical effect of acid functionalisation of carbon nanotubes to be used in sensors development. *Surface Science*, *605*(3–4), 435–440. https://doi.org/10.1016/j.susc.2010.11.014

Muhich, C. L., Westcott, J. Y., Morris, T. C., Weimer, A. W., & Musgrave, C. B. (2013). The Effect of N and B Doping on Graphene and the Adsorption and Migration Behavior of Pt Atoms. *The Journal of Physical Chemistry C*, *117*(20), 10523–10535. https://doi.org/10.1021/jp401665r

Muneendra Prasad, A., Santhosh, C., & Nirmala Grace, A. (2012). Carbon nanotubes and polyaniline supported Pt nanoparticles for methanol oxidation towards DMFC applications. *Applied Nanoscience*, *2*(4), 457–466. https://doi.org/10.1007/s13204-012-0061-4

Munjewar, S. S., Thombre, S. B., & Mallick, R. K. (2017). A comprehensive review on recent material development of passive direct methanol fuel cell. *Ionics*, *23*(1), 1–18. https://doi.org/10.1007/s11581-016-1864-1

Narreddula, M., Balaji, R., Ramya, K., Rajalakshmi, N., & Ramachandraiah, A. (2019). Nitrogen doped graphene supported Pd as hydrogen evolution catalyst for electrochemical methanol reformation. *International Journal of Hydrogen Energy*, *44*(10), 4582–4591. https://doi.org/10.1016/j.ijhydene.2019.01.037

Nassr, A. B. A. A., Quetschke, A., Koslowski, E., & Bron, M. (2013). Electrocatalytic oxidation of formic acid on Pd/MWCNTs nanocatalysts prepared by the polyol method. *Electrochimica Acta*, *102*, 202–211. https://doi.org/10.1016/j.electacta.2013.03.173

Nirmala Grace, A., & Pandian, K. (2006). Pt, Pt–Pd and Pt–Pd/Ru nanoparticles entrapped polyaniline electrodes – A potent electrocatalyst towards the oxidation of glycerol. *Electrochemistry Communications*, *8*(8), 1340–1348. https://doi.org/10.1016/j.elecom.2006.06.007

Pandey, R. P., Shukla, G., Manohar, M., & Shahi, V. K. (2017). Graphene oxide based nanohybrid proton exchange membranes for fuel cell applications: An overview. *Advances in Colloid and Interface Science*, *240*, 15–30. https://doi.org/10.1016/j.cis.2016.12.003

Park, C., & Baker, R. T. K. (1998). Catalytic Behavior of Graphite Nanofiber Supported Nickel

Particles. 2. The Influence of the Nanofiber Structure. *The Journal of Physical Chemistry B*, *102*(26), 5168–5177. https://doi.org/10.1021/jp981210p

Park, C., & Baker, R. T. K. (1999). Catalytic Behavior of Graphite Nanofiber Supported Nickel Particles. 3. The Effect of Chemical Blocking on the Performance of the System. *The Journal of Physical Chemistry B*, *103*(13), 2453–2459. https://doi.org/10.1021/jp983802d

Park, I.-S., Park, K.-W., Choi, J.-H., Park, C. R., & Sung, Y.-E. (2007). Electrocatalytic enhancement of methanol oxidation by graphite nanofibers with a high loading of PtRu alloy nanoparticles. *Carbon*, *45*(1), 28–33. https://doi.org/10.1016/j.carbon.2006.08.011

Park, J. E., Lim, J., Kim, S., Choi, I., Ahn, C.-Y., Hwang, W., Lim, M. S., Cho, Y.-H., & Sung, Y.-E. (2018). Enhancement of mass transport in fuel cells using three-dimensional graphene foam as flow field. *Electrochimica Acta*, *265*, 488–496. https://doi.org/10.1016/j.electacta.2018.01.191

Park, K.-W., Sung, Y.-E., Han, S., Yun, Y., & Hyeon, T. (2004). Origin of the Enhanced Catalytic Activity of Carbon Nanocoil-Supported PtRu Alloy Electrocatalysts. *The Journal of Physical Chemistry B*, *108*(3), 939–944. https://doi.org/10.1021/jp0368031

Perkins, W. D. (1986). Fourier transform-infrared spectroscopy: Part l. Instrumentation. *Journal of Chemical Education*, *63*(1), A5. https://doi.org/10.1021/ed063pA5

Pham, K.-C., McPhail, D. S., Mattevi, C., Wee, A. T. S., & Chua, D. H. C. (2016). Graphene-Carbon Nanotube Hybrids as Robust Catalyst Supports in Proton Exchange Membrane Fuel Cells. *Journal of The Electrochemical Society*, *163*(3), F255–F263. https://doi.org/10.1149/2.0891603jes

Poh, C. K., Lim, S. H., Pan, H., Lin, J., & Lee, J. Y. (2008). Citric acid functionalized carbon materials for fuel cell applications. *Journal of Power Sources*, *176*(1), 70–75. https://doi.org/10.1016/j.jpowsour.2007.10.049

Pollet, B. G., Staffell, I., & Shang, J. L. (2012). Current status of hybrid, battery and fuel cell electric vehicles: From electrochemistry to market prospects. *Electrochimica Acta*, *84*, 235–249. https://doi.org/10.1016/J.ELECTACTA.2012.03.172

Prabhuram, J., Zhao, T. S., Tang, Z. K., Chen, R., & Liang, Z. X. (2006). Multiwalled Carbon Nanotube Supported PtRu for the Anode of Direct Methanol Fuel Cells. *The Journal of Physical Chemistry B*, *110*(11), 5245–5252. https://doi.org/10.1021/jp0567063

Priya, K., Rajasekar, N., Santhosh, C., & Nirmala Grace, A. (2014). Preparation and characterization of graphene supported Palladium nanoparticlesfor Direct Methanol Fuel Cells. *2014 International Conference on Advances in Electrical Engineering (ICAEE)*, *January*, 1–6. https://doi.org/10.1109/ICAEE.2014.6838553

Qu, L., Liu, Y., Baek, J.-B., & Dai, L. (2010). Nitrogen-dopedGraphene as Efficient Metal-Free Electrocatalyst for Oxygen Reduction in Fuel Cells. *ACS Nano*, *4*(3), 1321–1326. https://doi.org/10.1021/nn901850u

Raghuveer, V., & Manthiram, A. (2004). Mesoporous Carbon with Larger Pore Diameter as an Electrocatalyst Support for Methanol Oxidation. *Electrochemical and Solid-State Letters*, *7*(10), A336. https://doi.org/10.1149/1.1792264

RAJALAKSHMI, N., RYU, H., SHAIJUMON, M., & RAMAPRABHU, S. (2005). Performance of polymer electrolyte membrane fuel cells with carbon nanotubes as oxygen reduction catalyst support material. *Journal of Power Sources*, *140*(2), 250–257. https://doi.org/10.1016/j.jpowsour.2004.08.042

Ramesh, P., Itkis, M. E., Tang, J. M., & Haddon, R. C. (2008). SWNT−MWNT Hybrid Architecture for Proton Exchange Membrane Fuel Cell Cathodes. *The Journal of Physical Chemistry C*, *112*(24), 9089–9094. https://doi.org/10.1021/jp711280j

Ramli, Z. A. C., & Kamarudin, S. K. (2018). Platinum-Based Catalysts on Various Carbon Supports and Conducting Polymers for Direct Methanol Fuel Cell Applications: a Review. *Nanoscale Research Letters*, *13*(1), 410. https://doi.org/10.1186/s11671-018-2799-4

Ranganathan, S., Kuo, T.-C., & McCreery, R. L. (1999). Facile Preparation of Active Glassy Carbon Electrodes with Activated Carbon and Organic Solvents. *Analytical Chemistry*, *71*(16), 3574–3580. https://doi.org/10.1021/ac981386n

Rao, V., Simonov, P. A., Savinova, E. R., Plaksin, G. V., Cherepanova, S. V., Kryukova, G. N., & Stimming, U. (2005). The influence of carbon support porosity on the activity of PtRu/Sibunit anode catalysts for methanol oxidation. *Journal of Power Sources*, *145*(2), 178–187. https://doi.org/10.1016/j.jpowsour.2004.12.064

Reed, S. J. B. (1995). Electron probe microanalysis. *Microprobe Techniques in the Earth Sciences*, 49–89. https://doi.org/10.1007/978-1-4615-2053-5_2

Reimer, & Kohl. (2008). 9780387347585_Toc. *Springer Series in Optical Sciences*, *5*.

Ren, Z. F., Huang, Z. P., Xu, J. W., Wang, J. H., Bush, P., Siegal, M. P., & Provencio, P. N. (1998). Synthesis of Large Arrays of Well-Aligned Carbon Nanotubes on Glass. *Science*, *282*(5391), 1105–1107. https://doi.org/10.1126/science.282.5391.1105

Rivera Gavidia, L., Sebastián, D., Pastor, E., Aricò, A., & Baglio, V. (2017). Carbon-Supported Pd and PdFe Alloy Catalysts for Direct Methanol Fuel Cell Cathodes. *Materials*, *10*(6), 580. https://doi.org/10.3390/ma10060580

Rodríguez-reinoso, F. (1998). The role of carbon materials in heterogeneous catalysis. *Carbon*, *36*(3), 159–175. https://doi.org/10.1016/S0008-6223(97)00173-5

144

Román-Martínez, M. C., Cazorla-Amorós, D., Linares-Solano, A., De Lecea, C. S.-M., Yamashita, H., & Anpo, M. (1995). Metal-support interaction in Pt/C catalysts. Influence of the support surface chemistry and the metal precursor. *Carbon*, *33*(1), 3–13. https://doi.org/10.1016/0008-6223(94)00096-I

Ryoo, R., Joo, S. H., Kruk, M., & Jaroniec, M. (2001). Ordered Mesoporous Carbons. *Advanced Materials*, *13*(9), 677–681. https://doi.org/10.1002/1521-4095(200105)13:9<677::AID-ADMA677>3.0.CO;2-C

Sahoo, M., Scott, K., & Ramaprabhu, S. (2015). Platinum decorated on partially exfoliated multiwalled carbon nanotubes as high performance cathode catalyst for PEMFC. *International Journal of Hydrogen Energy*, *40*(30), 9435–9443. https://doi.org/10.1016/j.ijhydene.2015.05.113

Saito, R., Fujita, M., Dresselhaus, G., & Dresselhaus, M. S. (1992). Electronic structure of chiral graphene tubules. *Applied Physics Letters*, *60*(18), 2204–2206. https://doi.org/10.1063/1.107080

Samad, S., Loh, K. S., Wong, W. Y., Lee, T. K., Sunarso, J., Chong, S. T., & Wan Daud, W. R. (2018). Carbon and non-carbon support materials for Platinum-based catalysts in fuel cells. *International Journal of Hydrogen Energy*, *43*(16), 7823–7854. https://doi.org/10.1016/j.ijhydene.2018.02.154

Sano, N., & Ukita, S. ichiro. (2006). One-step synthesis of Pt-supported carbon nanohorns for fuel cell electrode by arc plasma in liquid nitrogen. *Materials Chemistry and Physics*, *99*(2–3), 447–450. https://doi.org/10.1016/J.MATCHEMPHYS.2005.11.019

SANTHOSH, P., GOPALAN, A., & LEE, K. (2006). Gold nanoparticles dispersed polyaniline grafted multiwall carbon nanotubes as newer electrocatalysts: Preparation and performances for methanol oxidation. *Journal of Catalysis*, *238*(1), 177–185. https://doi.org/10.1016/j.jcat.2005.12.014

Scimeca, M., Bischetti, S., Lamsira, H. K., Bonfiglio, R., & Bonanno, E. (2018). Energy Dispersive X-ray (EDX) microanalysis: A powerful tool in biomedical research and diagnosis. *European Journal of Histochemistry : EJH*, *62*(1), 89–99. https://doi.org/10.4081/EJH.2018.2841

Selvaraj, V., Grace, A. N., & Alagar, M. (2009). Electrocatalytic oxidation of formic acid and formaldehyde on nanoparticle decorated single walled carbon nanotubes. *Journal of Colloid and Interface Science*, *333*(1), 254–262. https://doi.org/10.1016/j.jcis.2009.01.020

Sepúlveda-Escribano, A., Coloma, F., & Rodríguez-Reinoso, F. (1998). Platinum catalysts supported on carbon blacks with different surface chemical properties. *Applied Catalysis A:*

General, *173*(2), 247–257. https://doi.org/10.1016/S0926-860X(98)00183-5

Serp, P. (2003). Carbon nanotubes and nanofibers in catalysis. *Applied Catalysis A: General*, *253*(2), 337–358. https://doi.org/10.1016/S0926-860X(03)00549-0

Seselj, N., Engelbrekt, C., & Zhang, J. (2015). Graphene-supported Platinum catalysts for fuel cells. *Science Bulletin*, *60*(9), 864–876. https://doi.org/10.1007/s11434-015-0745-8

Sevilla, M., Lota, G., & Fuertes, A. B. (2007). Saccharide-based graphitic carbon nanocoils as supports for PtRu nanoparticles for methanol electrooxidation. *Journal of Power Sources*, *171*(2), 546–551. https://doi.org/10.1016/j.jpowsour.2007.05.096

Shaari, N., & Kamarudin, S. K. (2017). Graphene in electrocatalyst and proton conductiong membrane in fuel cell applications: An overview. *Renewable and Sustainable Energy Reviews*, *69*, 862–870. https://doi.org/10.1016/j.rser.2016.07.044

Sharma, S., & Pollet, B. G. (2012). Support materials for PEMFC and DMFC electrocatalysts—A review. *Journal of Power Sources*, *208*, 96–119. https://doi.org/10.1016/j.jpowsour.2012.02.011

Shi, J., Wang, Z., & Li, H. (2007). Electrochemical fabrication of polyaniline/multi-walled carbon nanotube composite films for electrooxidation of methanol. *Journal of Materials Science*, *42*(2), 539–544. https://doi.org/10.1007/s10853-006-1043-2

Shioyama, H., Honjo, K., Kiuchi, M., Yamada, Y., Ueda, A., Kuriyama, N., & Kobayashi, T. (2006). C2F6 plasma treatment of a carbon support for a PEM fuel cell electrocatalyst. *Journal of Power Sources*, *161*(2), 836–838. https://doi.org/10.1016/j.jpowsour.2006.05.046

Shukla, A. K., Raman, R. K., Choudhury, N. A., Priolkar, K. R., Sarode, P. R., Emura, S., & Kumashiro, R. (2004). Carbon-supported Pt–Fe alloy as a methanol-resistant oxygen-reduction catalyst for direct methanol fuel cells. *Journal of Electroanalytical Chemistry*, *563*(2), 181–190. https://doi.org/10.1016/J.JELECHEM.2003.09.010

Skrabalak, S. E., & Suslick, K. S. (2006). Porous Carbon Powders Prepared by Ultrasonic Spray Pyrolysis. *Journal of the American Chemical Society*, *128*(39), 12642–12643. https://doi.org/10.1021/ja064899h

Sohail, M., Saleem, M., Ullah, S., Saeed, N., Afridi, A., Khan, M., & Arif, M. (2017). Modified and improved Hummer's synthesis of graphene oxide for capacitors applications. *Modern Electronic Materials*, *3*(3), 110–116. https://doi.org/10.1016/j.moem.2017.07.002

Song, H., Yang, L., Tang, Y., Yan, D., Liu, C., & Luo, S. (2015). Three-Dimensional Nitrogen-Doped Reduced Graphene Oxide–Carbon Nanotubes Architecture Supporting Ultrafine Palladium nanoparticlesfor Highly Efficient Methanol Electrooxidation. *Chemistry – A*

European Journal, *21*(46), 16631–16638. https://doi.org/10.1002/chem.201502804

Spendelow, J. S., & Wieckowski, A. (2007). Electrocatalysis of oxygen reduction and small alcohol oxidation in alkaline media. *Physical Chemistry Chemical Physics*, *9*(21), 2654. https://doi.org/10.1039/b703315j

Stankovich, S., Dikin, D. A., Piner, R. D., Kohlhaas, K. A., Kleinhammes, A., Jia, Y., Wu, Y., Nguyen, S. T., & Ruoff, R. S. (2007). Synthesis of graphene-based nanosheets via chemical reduction of exfoliated graphite oxide. *Carbon*, *45*(7), 1558–1565. https://doi.org/10.1016/j.carbon.2007.02.034

Stankovich, S., Piner, R. D., Chen, X., Wu, N., Nguyen, S. T., & Ruoff, R. S. (2006). Stable aqueous dispersions of graphitic nanoplatelets via the reduction of exfoliated graphite oxide in the presence of poly(sodium 4-styrenesulfonate). *J. Mater. Chem.*, *16*(2), 155–158. https://doi.org/10.1039/B512799H

Steigerwalt, E. S., Deluga, G. A., Cliffel, D. E., & Lukehart, C. M. (2001). A Pt−Ru/Graphitic Carbon Nanofiber Nanocomposite Exhibiting High Relative Performance as a Direct-Methanol Fuel Cell Anode Catalyst. *The Journal of Physical Chemistry B*, *105*(34), 8097–8101. https://doi.org/10.1021/jp011633i

Stein, A. (2003). Advances in Microporous and Mesoporous Solids—Highlights of Recent Progress. *Advanced Materials*, *15*(10), 763–775. https://doi.org/10.1002/adma.200300007

Stephenson, J. J., Hudson, J. L., Azad, S., & Tour, J. M. (2006). Individualized Single Walled Carbon Nanotubes from Bulk Material Using 96% Sulfuric Acid as Solvent. *Chemistry of Materials*, *18*(2), 374–377. https://doi.org/10.1021/cm052204q

Stonehart, P. (1984). Carbon substrates for phosphoric acid fuel cell cathodes. *Carbon*, *22*(4–5), 423–431. https://doi.org/10.1016/0008-6223(84)90015-0

Su, F., Li, X., Lv, L., & Zhao, X. S. (2006). Ordered mesoporous carbon particles covered with carbon nanotubes. *Carbon*, *44*(4), 801–803. https://doi.org/10.1016/j.carbon.2005.10.056

Subramanian, A., & Rodriguez-Saona, L. (2009). Fourier Transform Infrared (FTIR) Spectroscopy. In *Infrared Spectroscopy for Food Quality Analysis and Control* (pp. 145–178). Elsevier. https://doi.org/10.1016/B978-0-12-374136-3.00007-9

Sun, S., Zhang, G., Geng, D., Chen, Y., Banis, M. N., Li, R., Cai, M., & Sun, X. (2010). Direct Growth of Single-Crystal Pt Nanowires on Sn@CNT Nanocable: 3D Electrodes for Highly Active Electrocatalysts. *Chemistry - A European Journal*, *16*(3), 829–835. https://doi.org/10.1002/chem.200902320

TANG, S., SUN, G., QI, J., SUN, S., GUO, J., XIN, Q., & HAARBERG, G. M. (2010). Review of New Carbon Materials as Catalyst Supports in Direct Alcohol Fuel Cells. *Chinese*

147

Journal of Catalysis, *31*(1), 12–17. https://doi.org/10.1016/S1872-2067(09)60034-6

Tessonnier, J. (2017). Carbon materials in heterogeneous catalysis. *Modern Methods in Heterogeneous Catalysis Research*.

Torres, G. C., Jablonski, E. L., Baronetti, G. T., Castro, A. A., de Miguel, S. R., Scelza, O. A., Blanco, M. D., Pen˜a Jiménez, M. A., & Fierro, J. L. G. (1997). Effect of the carbon pre-treatment on the properties and performance for nitrobenzene hydrogenation of Pt/C catalysts. *Applied Catalysis A: General*, *161*(1–2), 213–226. https://doi.org/10.1016/S0926-860X(97)00071-9

Tripathi, P., Patel, C. R. P., Shaz, M. A., & Srivastava, O. N. (2013). *Synthesis of High-Quality Graphene through Electrochemical Exfoliation of Graphite in Alkaline Electrolyte*. https://arxiv.org/abs/1310.7371v1

Uchida, M., Aoyama, Y., Eda, N., & Ohta, A. (1995). Investigation of the Microstructure in the Catalyst Layer and Effects of Both Perfluorosulfonate Ionomer and PTFE-Loaded Carbon on the Catalyst Layer of Polymer Electrolyte Fuel Cells. *Journal of The Electrochemical Society*, *142*(12), 4143–4149. https://doi.org/10.1149/1.2048477

Uvarov, V., & Popov, I. (2007). Metrological characterization of X-ray diffraction methods for determination of crystallite size in nano-scale materials. *Materials Characterization*, *58*(10), 883–891. https://doi.org/10.1016/j.matchar.2006.09.002

Vanyorek, L., Halasi, G., Pekker, P., Kristály, F., & Kónya, Z. (2016). Characterization and Catalytic Activity of Different Carbon Supported Pd Nanocomposites. *Catalysis Letters*, *146*(11), 2268–2277. https://doi.org/10.1007/S10562-016-1857-8

Vinayan, B. P., Nagar, R., Rajalakshmi, N., & Ramaprabhu, S. (2012). Novel Platinum-Cobalt Alloy Nanoparticles Dispersed on Nitrogen-dopedGraphene as a Cathode Electrocatalyst for PEMFC Applications. *Advanced Functional Materials*, *22*(16), 3519–3526. https://doi.org/10.1002/adfm.201102544

Wang, C., Waje, M., Wang, X., Tang, J. M., Haddon, R. C., & Yan. (2004). Proton Exchange Membrane Fuel Cells with Carbon Nanotube Based Electrodes. *Nano Letters*, *4*(2), 345–348. https://doi.org/10.1021/nl034952p

Wang, F., Arai, S., & Endo, M. (2005). The preparation of multi-walled carbon nanotubes with a Ni–P coating by an electroless deposition process. *Carbon*, *43*(8), 1716–1721. https://doi.org/10.1016/j.carbon.2005.02.015

Wang, Haibo, Maiyalagan, T., & Wang, X. (2012). Review on Recent Progress in Nitrogen-dopedGraphene: Synthesis, Characterization, and Its Potential Applications. *ACS Catalysis*, *2*(5), 781–794. https://doi.org/10.1021/cs200652y

Wang, Hongjuan, Zheng, J., Peng, F., & Yu, H. (2013). Pt/IrO2/CNT anode catalyst with high performance for direct methanol fuel cells. *Catalysis Communications*, *33*, 34–37. https://doi.org/10.1016/j.catcom.2012.12.026

Wang, J., Yin, G., Shao, Y., Zhang, S., Wang, Z., & Gao, Y. (2007). Effect of carbon black support corrosion on the durability of Pt/C catalyst. *Journal of Power Sources*, *171*(2), 331–339. https://doi.org/10.1016/j.jpowsour.2007.06.084

Wang, X., Li, W., Chen, Z., Waje, M., & Yan, Y. (2006). Durability investigation of carbon nanotube as catalyst support for proton exchange membrane fuel cell. *Journal of Power Sources*, *158*(1), 154–159. https://doi.org/10.1016/j.jpowsour.2005.09.039

Wang, Y.-J., Fang, B., Li, H., Bi, X. T., & Wang, H. (2016). Progress in modified carbon support materials for Pt and Pt-alloy cathode catalysts in polymer electrolyte membrane fuel cells. *Progress in Materials Science*, *82*, 445–498. https://doi.org/10.1016/j.pmatsci.2016.06.002

Wang, Y.-J., Wilkinson, D. P., Neburchilov, V., Song, C., Guest, A., & Zhang, J. (2014). Ta and Nb co-doped TiO 2 and its carbon-hybrid materials for supporting Pt–Pd alloy electrocatalysts for PEM fuel cell oxygen reduction reaction. *J. Mater. Chem. A*, *2*(32), 12681–12685. https://doi.org/10.1039/C4TA02062F

Wang, Y., Zang, J., Dong, L., Pan, H., Yuan, Y., & Wang, Y. (2013). Graphitized nanodiamond supporting PtNi alloy as stable anodic and cathodic electrocatalysts for direct methanol fuel cell. *Electrochimica Acta*, *113*, 583–590. https://doi.org/10.1016/j.electacta.2013.09.091

Wang, Z.-B., Yin, G.-P., & Shi, P.-F. (2006). Effects of ozone treatment of carbon support on Pt–Ru/C catalysts performance for direct methanol fuel cell. *Carbon*, *44*(1), 133–140. https://doi.org/10.1016/j.carbon.2005.06.043

Wang, Z., Zhu, Z.-Z., Shi, J., & Li, H.-L. (2007). Electrocatalytic oxidation of formaldehyde on Platinum well-dispersed into single-wall carbon nanotube/polyaniline composite film. *Applied Surface Science*, *253*(22), 8811–8817. https://doi.org/10.1016/j.apsusc.2007.03.005

Watanabe, M., Saegusa, S., & Stonehart, P. (1988). Electro-catalytic Activity on Supported Platinum Crystallites for Oxygen Reduction in Sulphuric Acid. *Chemistry Letters*, *17*(9), 1487–1490. https://doi.org/10.1246/cl.1988.1487

Watanabe, M., Tsurumi, K., Mizukami, T., Nakamura, T., & Stonehart, P. (1994). Activity and Stability of Ordered and Disordered Co-Pt Alloys for Phosphoric Acid Fuel Cells. *Journal of The Electrochemical Society*, *141*(10), 2659–2668. https://doi.org/10.1149/1.2059162/XML

Wei, J., Lv, R., Guo, N., Wang, H., Bai, X., Mathkar, A., Kang, F., Zhu, H., Wang, K., Wu, D., Vajtai, R., & Ajayan, P. M. (2012). Preparation of highly oxidized nitrogen-dopedcarbon

nanotubes. *Nanotechnology*, *23*(15), 155601. https://doi.org/10.1088/0957-4484/23/15/155601

Wei, Z. D., Yan, C., Tan, Y., Li, L., Sun, C. X., Shao, Z. G., Shen, P. K., & Dong, H. W. (2008). Spontaneous Reduction of Pt(IV) onto the Sidewalls of Functionalized Multiwalled Carbon Nanotubes as Catalysts for Oxygen Reduction Reaction in PEMFCs. *The Journal of Physical Chemistry C*, *112*(7), 2671–2677. https://doi.org/10.1021/jp709936p

Wongyao, N., Therdthianwong, A., & Therdthianwong, S. (2011). Performance of direct alcohol fuel cells fed with mixed methanol/ethanol solutions. *Energy Conversion and Management*, *52*(7), 2676–2681. https://doi.org/10.1016/j.enconman.2011.01.005

Wu, G., Li, D., Dai, C., Wang, D., & Li, N. (2008). Well-Dispersed High-Loading Pt Nanoparticles Supported by Shell−Core Nanostructured Carbon for Methanol Electrooxidation. *Langmuir*, *24*(7), 3566–3575. https://doi.org/10.1021/la7029278

Wu, G., Li, L., Li, J.-H., & Xu, B.-Q. (2006). Methanol electrooxidation on Pt particles dispersed into PANI/SWNT composite films. *Journal of Power Sources*, *155*(2), 118–127. https://doi.org/10.1016/j.jpowsour.2005.04.035

Wu, J., Pisula, W., & Müllen, K. (2007). Graphenes as Potential Material for Electronics. *Chemical Reviews*, *107*(3), 718–747. https://doi.org/10.1021/cr068010r

Xia, B. Y., Ding, S., Wu, H. Bin, Wang, X., & Wen (David), X. (2012). Hierarchically structured Pt/CNT@TiO 2 nanocatalysts with ultrahigh stability for low-temperature fuel cells. *RSC Adv.*, *2*(3), 792–796. https://doi.org/10.1039/C1RA00587A

Xia, Y., & Mokaya, R. (2005). Generalized and Facile Synthesis Approach to N-doped Highly Graphitic Mesoporous Carbon Materials. *Chemistry of Materials*, *17*(6), 1553–1560. https://doi.org/10.1021/cm048057y

Xing, Y. (2004). Synthesis and Electrochemical Characterization of Uniformly-Dispersed High Loading Pt Nanoparticles on Sonochemically-Treated Carbon Nanotubes. *The Journal of Physical Chemistry B*, *108*(50), 19255–19259. https://doi.org/10.1021/jp046697i

Xiong, B., Zhou, Y., Zhao, Y., Wang, J., Chen, X., O'Hayre, R., & Shao, Z. (2013). The use of nitrogen-dopedgraphene supporting Pt nanoparticles as a catalyst for methanol electrocatalytic oxidation. *Carbon*, *52*, 181–192. https://doi.org/10.1016/j.carbon.2012.09.019

Xiong, L., & Manthiram, A. (2004). Synthesis and characterization of methanol tolerant Pt/TiOx/C nanocomposites for oxygen reduction in direct methanol fuel Cells. *Electrochimica Acta*, *49*(24), 4163–4170. https://doi.org/10.1016/J.ELECTACTA.2004.04.011

150

Xu, Changwei, Cheng, L., Shen, P., & Liu, Y. (2007). Methanol and ethanol electrooxidation on Pt and Pd supported on carbon microspheres in alkaline media. *Electrochemistry Communications*, *9*(5), 997–1001. https://doi.org/10.1016/j.elecom.2006.12.003

Xu, Chunchuan, Pietrasz, P., Yang, J., Soltis, R., Sun, K., Sulek, M., & Novak, R. (2013). Pt-Based ORR Catalyst on Carbon-Supported Amorphous Niobium Oxide Support. *ECS Transactions*, *58*(1), 1779–1788. https://doi.org/10.1149/05801.1779ecst

Xu, X., Zhou, Y., Yuan, T., & Li, Y. (2013). Methanol electrocatalytic oxidation on Pt nanoparticles on nitrogen doped graphene prepared by the hydrothermal reaction of graphene oxide with urea. *Electrochimica Acta*, *112*, 587–595. https://doi.org/10.1016/j.electacta.2013.09.038

Yang, S., Zhang, X., Mi, H., & Ye, X. (2008). Pd nanoparticles supported on functionalized multi-walled carbon nanotubes (MWCNTs) and electrooxidation for formic acid. *Journal of Power Sources*, *175*(1), 26–32. https://doi.org/10.1016/j.jpowsour.2007.09.080

Yao, T., Zhang, J., Zuo, Q., Wang, H., Wu, J., Zhang, X., & Cui, T. (2016). A simple way to prepare reduced graphene oxide nanosheets/Fe2O3-Pd/N-doped carbon nanosheets and their application in catalysis. *Journal of Colloid and Interface Science*, *468*, 62–69. https://doi.org/10.1016/J.JCIS.2016.01.027

Yi, Q., Chu, H., Chen, Q., Yang, Z., & Liu, X. (2015). High Performance Pd, PdNi, PdSn and PdSnNi Nanocatalysts Supported on Carbon Nanotubes for Electrooxidation of C2☐C4 Alcohols. *Electroanalysis*, *27*(2), 388–397. https://doi.org/10.1002/elan.201400423

Yi, Q., Niu, F., & Sun, L. (2011). Fabrication of novel porous Pd particles and their electroactivity towards ethanol oxidation in alkaline media. *Fuel*, *90*(8), 2617–2623. https://doi.org/10.1016/j.fuel.2011.03.038

Yin, J., Wang, L., Tian, C., Tan, T., Mu, G., Zhao, L., & Fu, H. (2013). Low-Pt Loaded on a Vanadium Nitride/Graphitic Carbon Composite as an Efficient Electrocatalyst for the Oxygen Reduction Reaction. *Chemistry - A European Journal*, *19*(41), 13979–13986. https://doi.org/10.1002/chem.201300933

Yoo, Eunjoo, Okada, T., Kizuka, T., & Nakamura, J. (2008). Effect of carbon substrate materials as a Pt–Ru catalyst support on the performance of direct methanol fuel cells. *Journal of Power Sources*, *180*(1), 221–226. https://doi.org/10.1016/j.jpowsour.2008.01.065

Yoo, EunJoo, Okata, T., Akita, T., Kohyama, M., Nakamura, J., & Honma, I. (2009). Enhanced Electrocatalytic Activity of Pt Subnanoclusters on Graphene Nanosheet Surface. *Nano Letters*, *9*(6), 2255–2259. https://doi.org/10.1021/nl900397t

You, P. Y., & Kamarudin, S. K. (2017). Recent progress of carbonaceous materials in fuel cell

applications: An overview. *Chemical Engineering Journal*, *309*, 489–502.

https://doi.org/10.1016/j.cej.2016.10.051

Yu, S., Liu, R., Yang, W., Han, K., Wang, Z., & Zhu, H. (2014). Synthesis and electrocatalytic performance of MnO 2 -promoted Ag@Pt/MWCNT electrocatalysts for oxygen reduction reaction. *J. Mater. Chem. A*, *2*(15), 5371–5378. https://doi.org/10.1039/C3TA14564F

Yu, X., & Pickup, P. G. (2008). Recent advances in direct formic acid fuel cells (DFAFC). *Journal of Power Sources*, *182*(1), 124–132. https://doi.org/10.1016/J.JPOWSOUR.2008.03.075

Yuan, F., & Ryu, H. (2004). The synthesis, characterization, and performance of carbon nanotubes and carbon nanofibres with controlled size and morphology as a catalyst support material for a polymer electrolyte membrane fuel cell. *Nanotechnology*, *15*(10), S596–S602. https://doi.org/10.1088/0957-4484/15/10/017

Zakil, F. A., Kamarudin, S. K., & Basri, S. (2016). Modified Nafion membranes for direct alcohol fuel cells: An overview. *Renewable and Sustainable Energy Reviews*, *65*, 841–852. https://doi.org/10.1016/j.rser.2016.07.040

Zarrin, H., Higgins, D., Jun, Y., Chen, Z., & Fowler, M. (2011). Functionalized Graphene Oxide Nanocomposite Membrane for Low Humidity and High Temperature Proton Exchange Membrane Fuel Cells. *The Journal of Physical Chemistry C*, *115*(42), 20774–20781. https://doi.org/10.1021/jp204610j

Zhang, G., Yan, J., Wang, J., Jia, D., Zheng, H., & Li, Z. (2018). Effect of carbon support on the catalytic performance of Cu-based nanoparticles for oxidative carbonylation of methanol. *Applied Surface Science*, *455*, 696–704. https://doi.org/10.1016/j.apsusc.2018.05.114

Zhang, X., Zhu, J., Tiwary, C. S., Ma, Z., Huang, H., Zhang, J., Lu, Z., Huang, W., & Wu, Y. (2016). Palladium nanoparticlesSupported on Nitrogen and Sulfur Dual-Doped Graphene as Highly Active Electrocatalysts for Formic Acid and Methanol Oxidation. *ACS Applied Materials & Interfaces*, *8*(17), 10858–10865. https://doi.org/10.1021/acsami.6b01580

Zhao, D.-Y., Wang, H.-L., Qi, H.-P., & Jiang, W.-F. (2020). N-doped graphene aerogels as efficient heterogeneous catalytic activators for peroxymonosulfate to remove 2-sec-butyl-4,6-dinitrphenol (DNBP) in aqueous solution. *Materials Research Express*, *7*(1), 015511. https://doi.org/10.1088/2053-1591/ab664f

Zhao, H., & Zhao, T. S. (2013). Highly active carbon nanotube-supported Pd catalyst for oxidation of formic acid prepared by etching copper template method. *International Journal of Hydrogen Energy*, *38*(3), 1391–1396. https://doi.org/10.1016/j.ijhydene.2012.11.009

Zhao, L., Wang, Z.-B., Li, J.-L., Zhang, J.-J., Sui, X.-L., & Zhang, L.-M. (2016). Hybrid of

carbon-supported Pt nanoparticles and three dimensional graphene aerogel as high stable electrocatalyst for methanol electrooxidation. *Electrochimica Acta*, *189*, 175–183. https://doi.org/10.1016/j.electacta.2015.12.072

Zhao, Y., Zhou, Y., O'Hayre, R., & Shao, Z. (2013). Electrocatalytic oxidation of methanol on Pt catalyst supported on nitrogen-dopedgraphene induced by hydrazine reduction. *Journal of Physics and Chemistry of Solids*, *74*(11), 1608–1614. https://doi.org/10.1016/j.jpcs.2013.06.004

Zhou, X., Qiao, J., Yang, L., & Zhang, J. (2014). A Review of Graphene-Based Nanostructural Materials for Both Catalyst Supports and Metal-Free Catalysts in PEM Fuel Cell Oxygen Reduction Reactions. *Advanced Energy Materials*, *4*(8), 1301523. https://doi.org/10.1002/aenm.201301523

Zhu, Z.-Z., Wang, Z., & Li, H.-L. (2008). Functional multi-walled carbon nanotube/polyaniline composite films as supports of Platinum for formic acid electrooxidation. *Applied Surface Science*, *254*(10), 2934–2940. https://doi.org/10.1016/j.apsusc.2007.10.033

Zielinski, J., Intertek, L. K.-L., & 2013, undefined. (2013). Physical characterization: surface area and porosity. *Researchgate.Net*. https://www.researchgate.net/profile/Rafik-Karaman/post/How-to-measure-surface-area-of-volatile-compounds-with-BET-Specifically-pharmaceuticals-like-ibuprofen/attachment/59d62e0879197b807798c456/AS%3A352697057333248%401461100939237/download/BET.pdf

APPENDICES

APPENDIX 1: Electrochemical evaluations of pH 12 electrocatalysts.
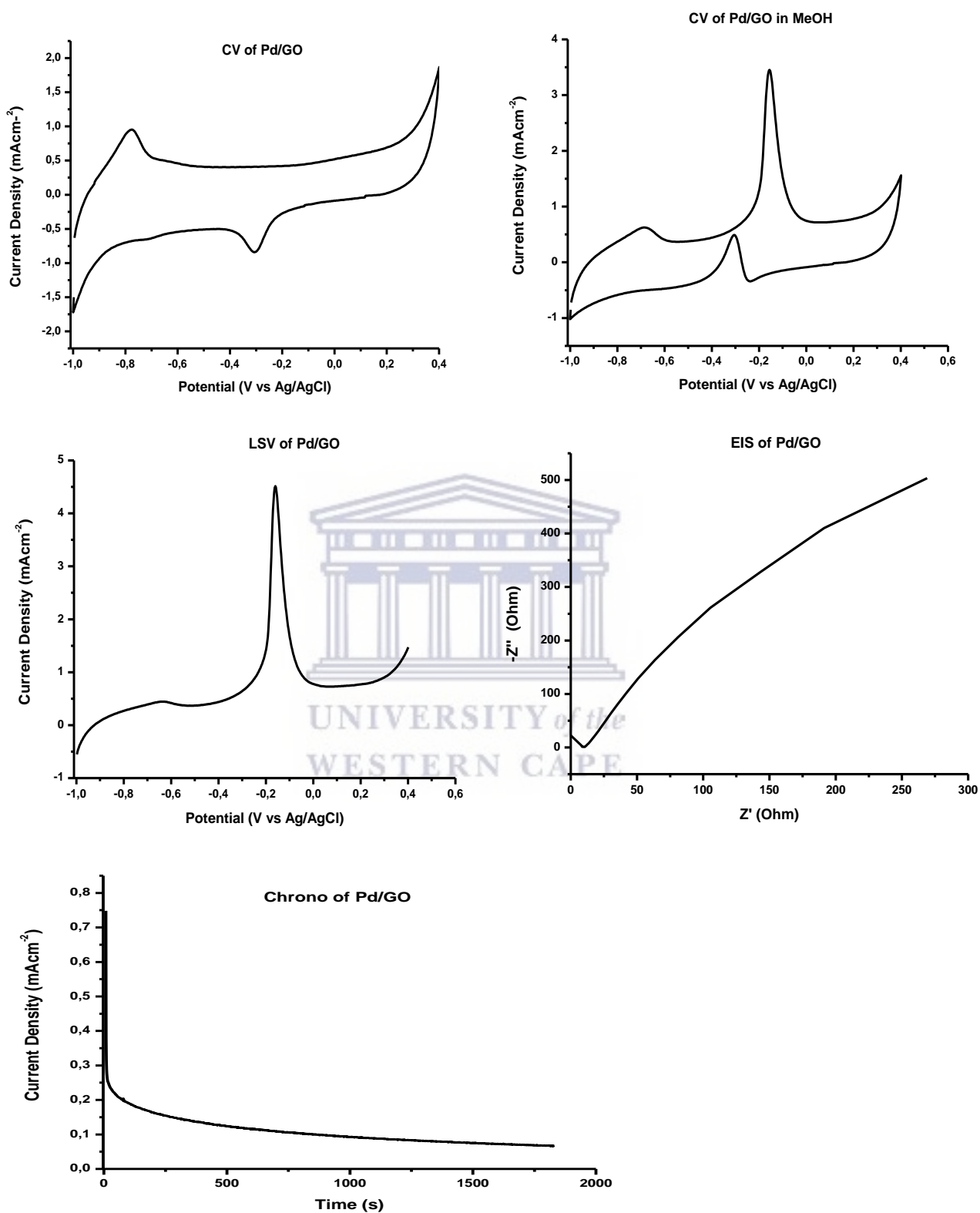
Electrochemical evaluations of pH 12 Pd/GO
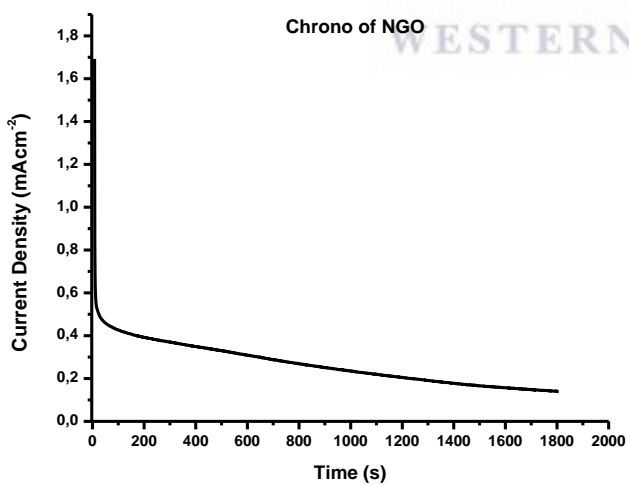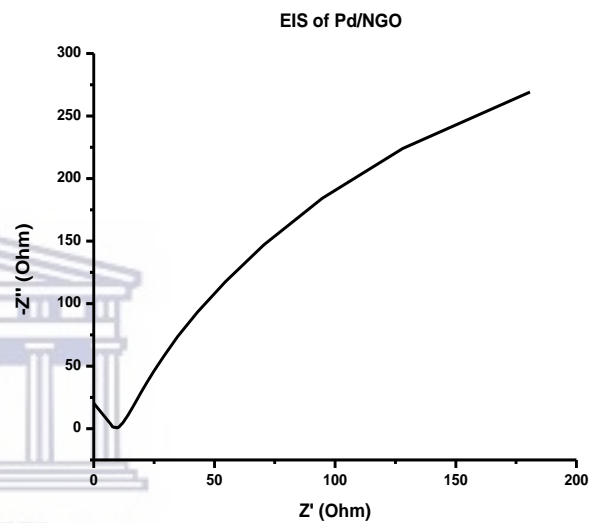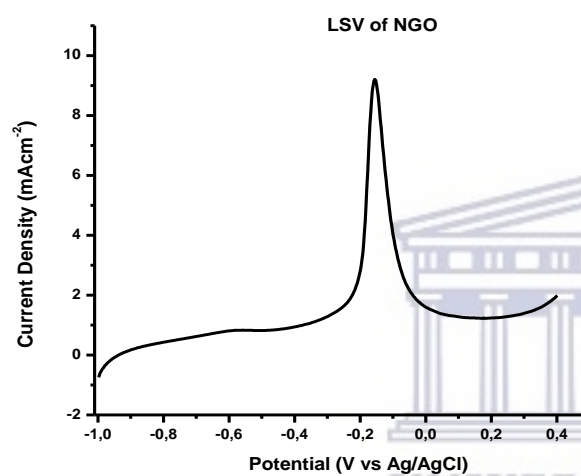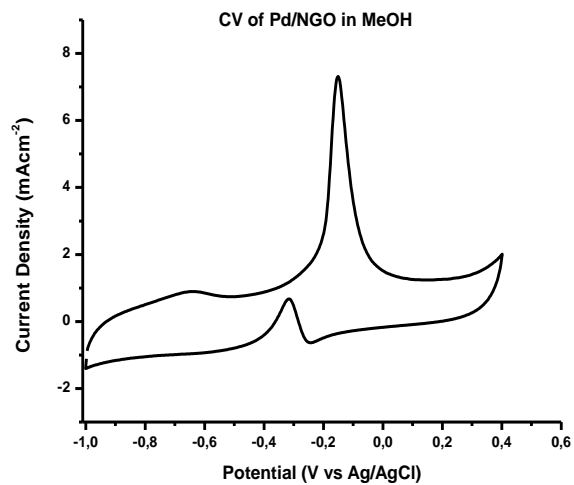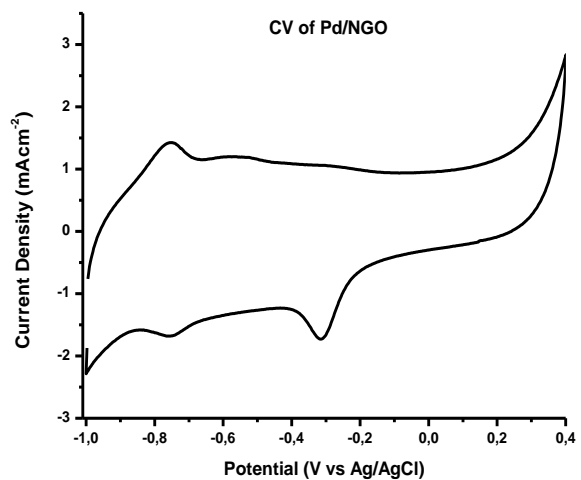
Electrochemical evaluations of pH 12 Pd/NGO
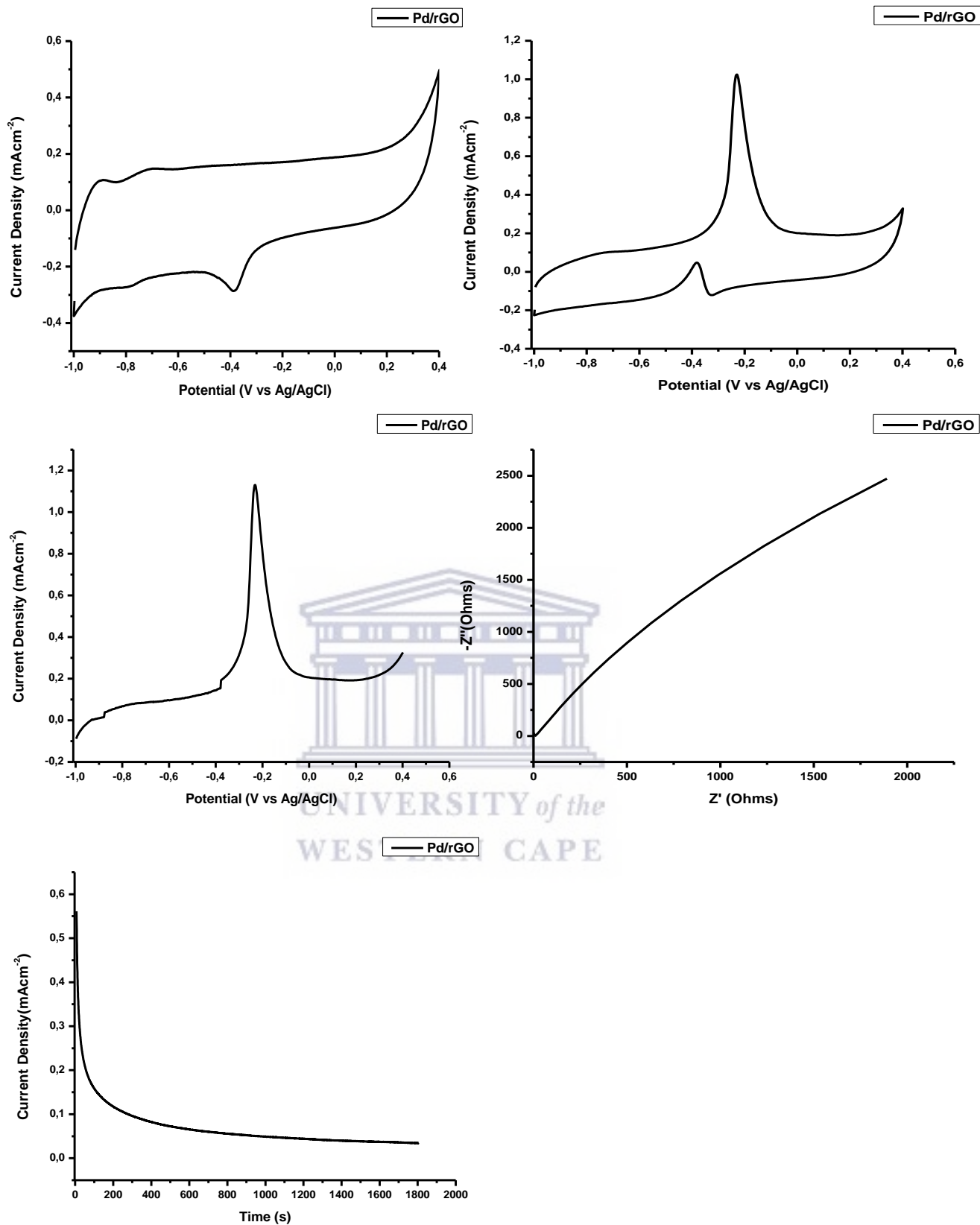
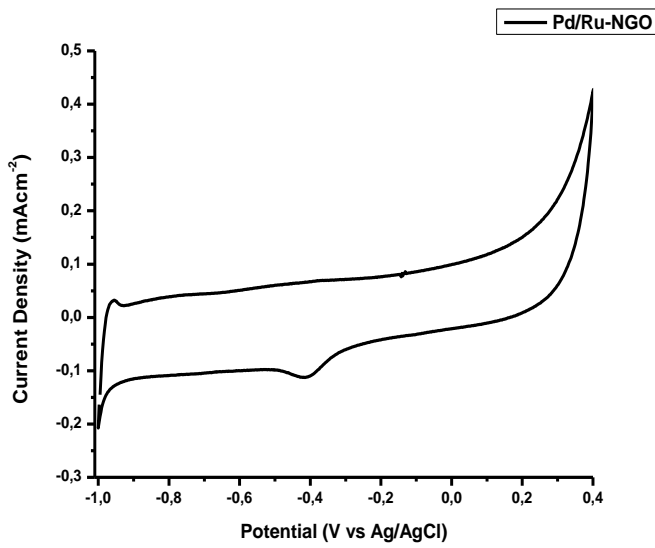Electrochemical evaluations of pH 12 Pd/rGO.
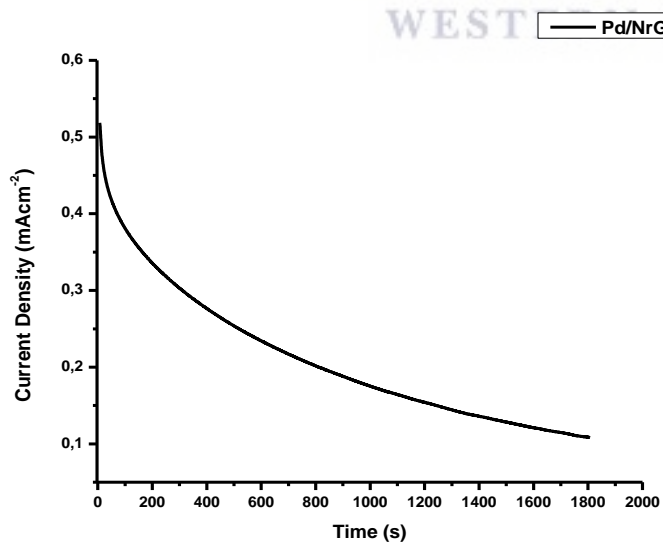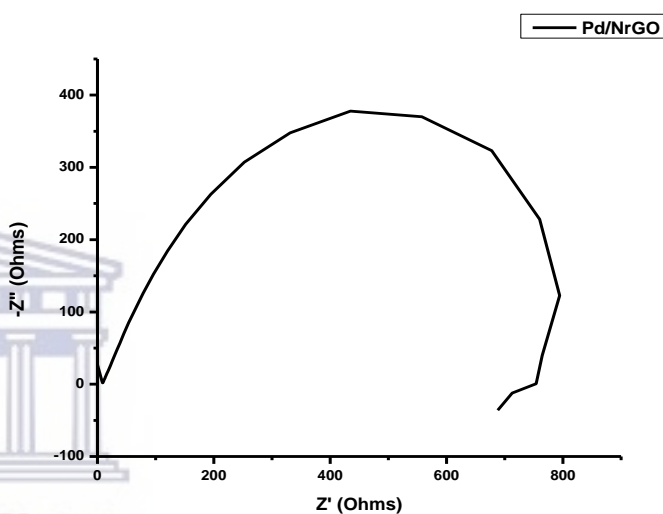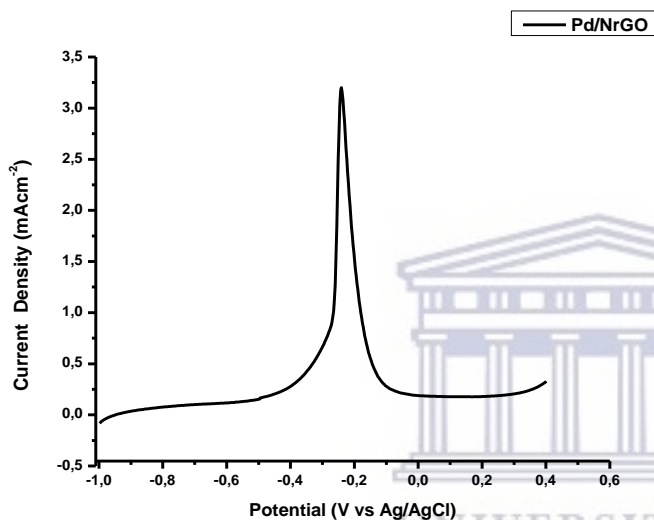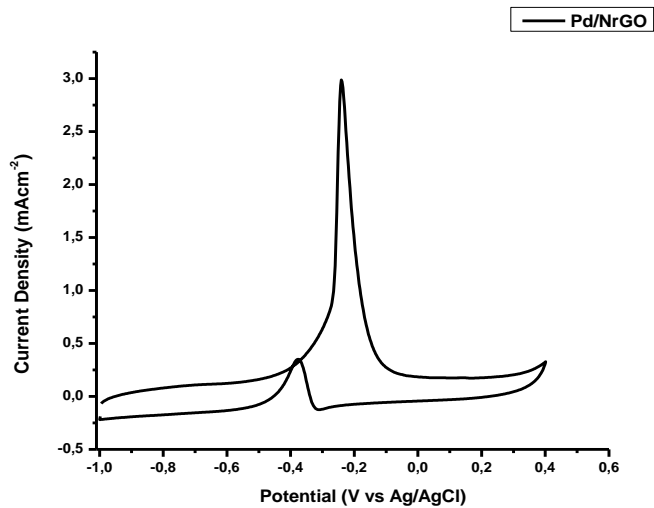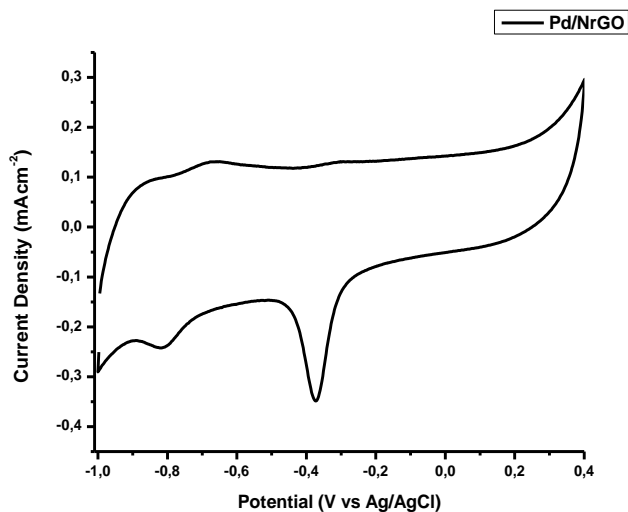
Electrochemical evaluations of pH 12 Pd/NrGO
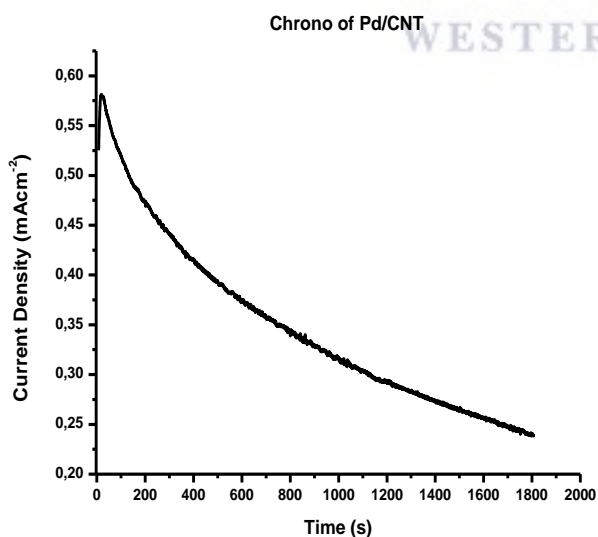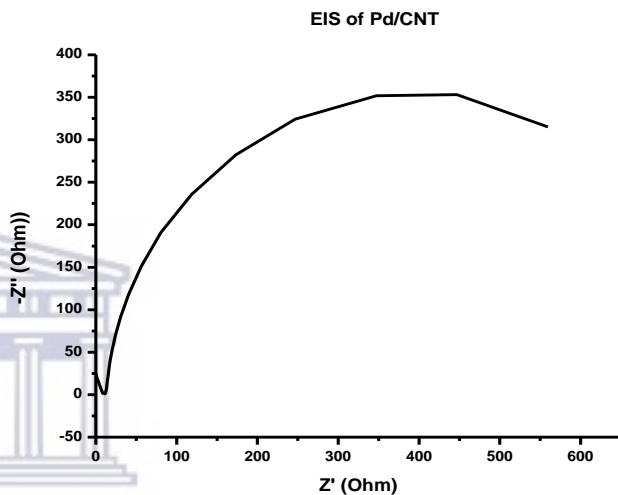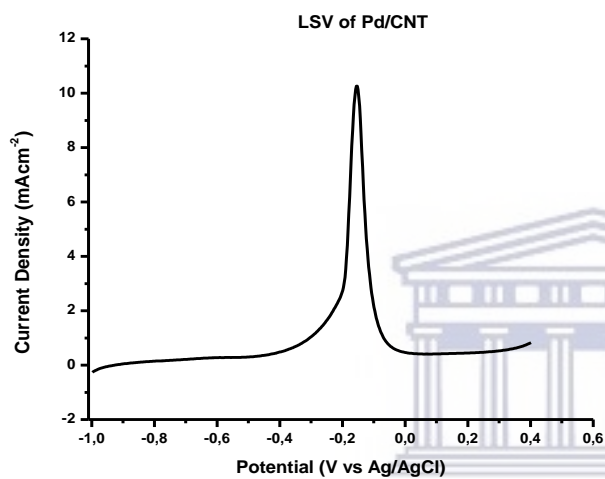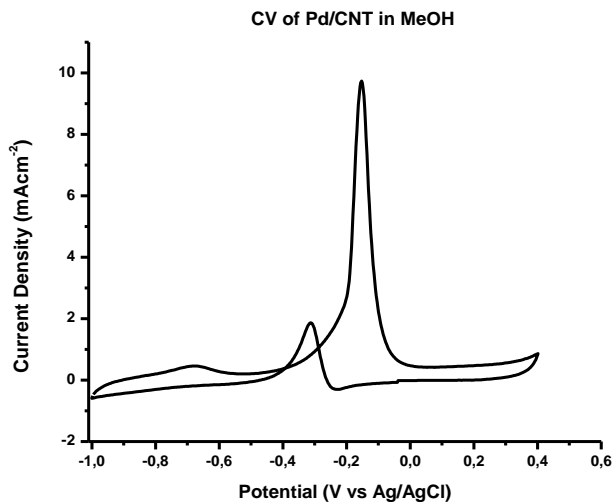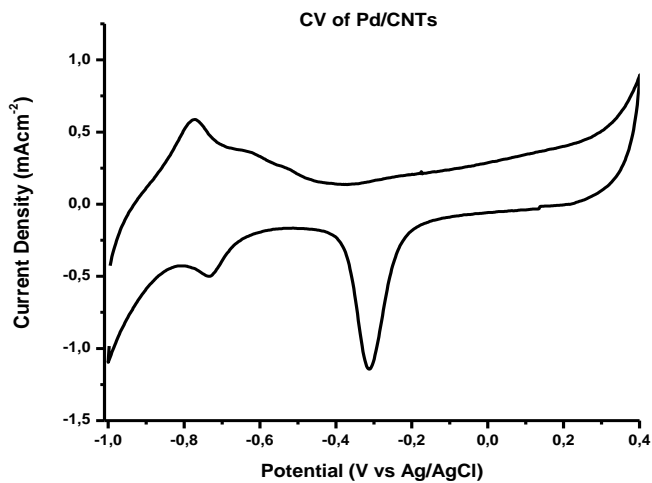
Electrochemical evaluations of pH 12 Pd/MWCNTs.

158
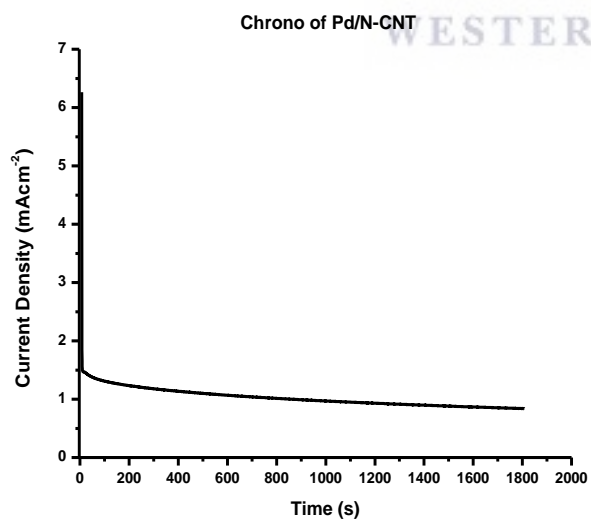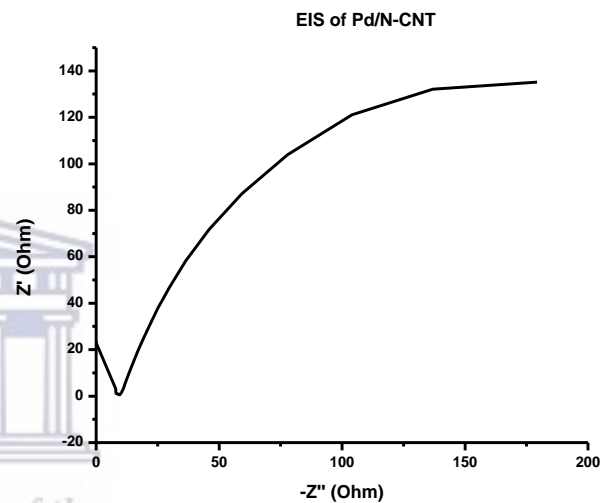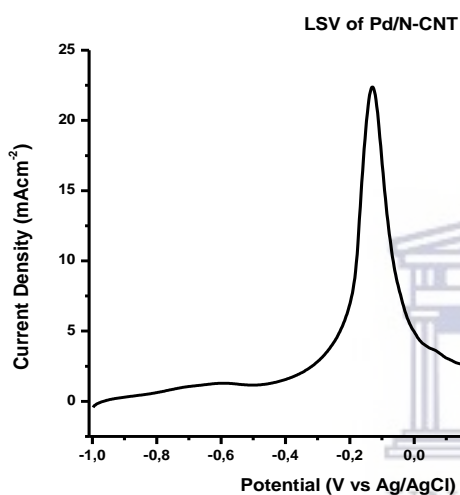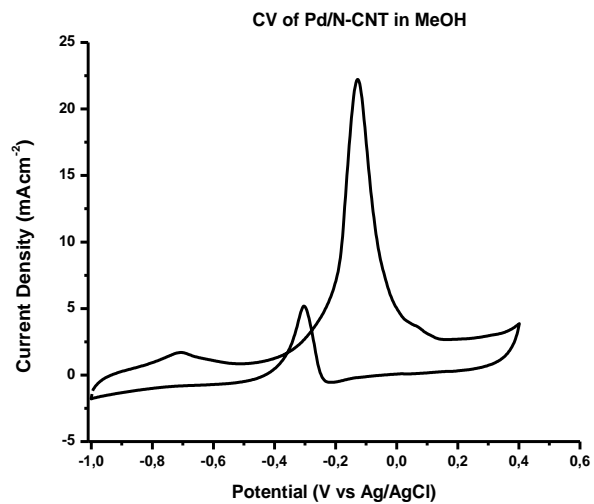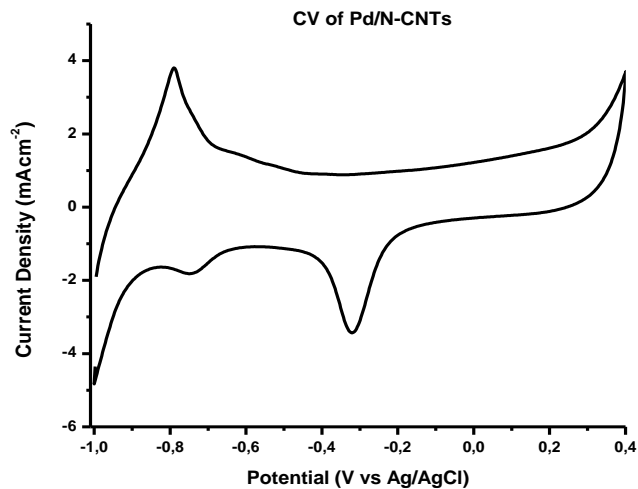
Electrochemical evaluations of pH 12 Pd/N-MWCNTs

159

CV of Pd/CNF

CV of Pd/CNF in MeOH

LSV of Pd/CNF

EIS of Pd/CNF

Chrono of Pd/CNF
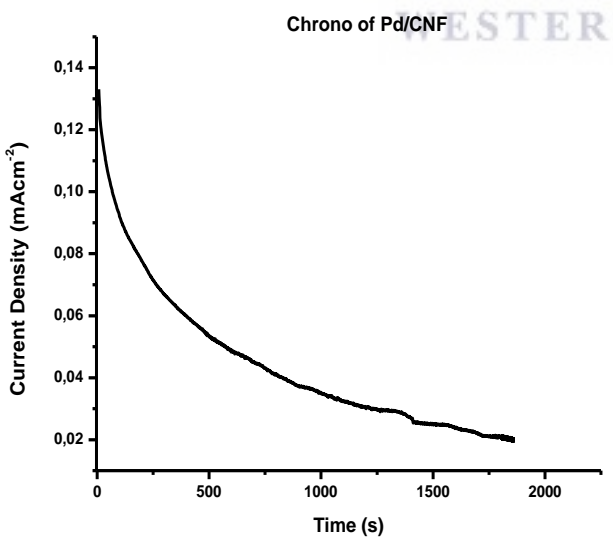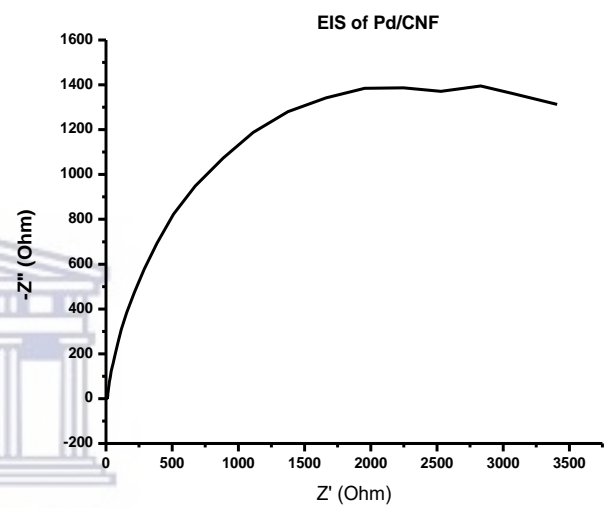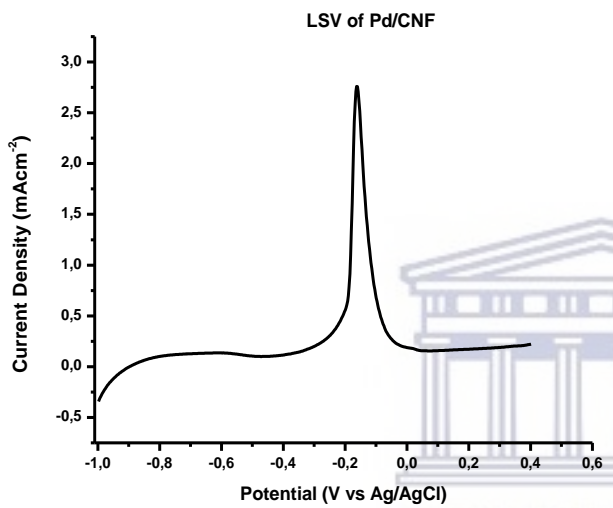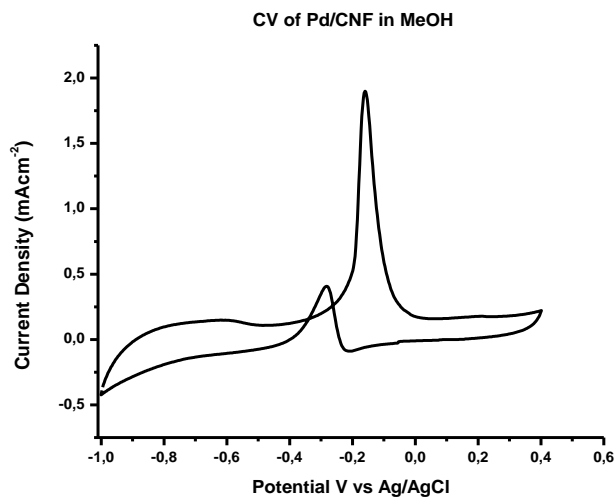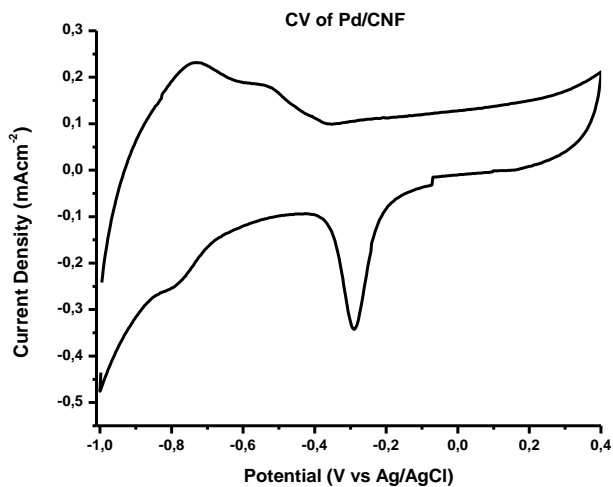
Electrochemical evaluations of pH 12 Pd/CNFs

160

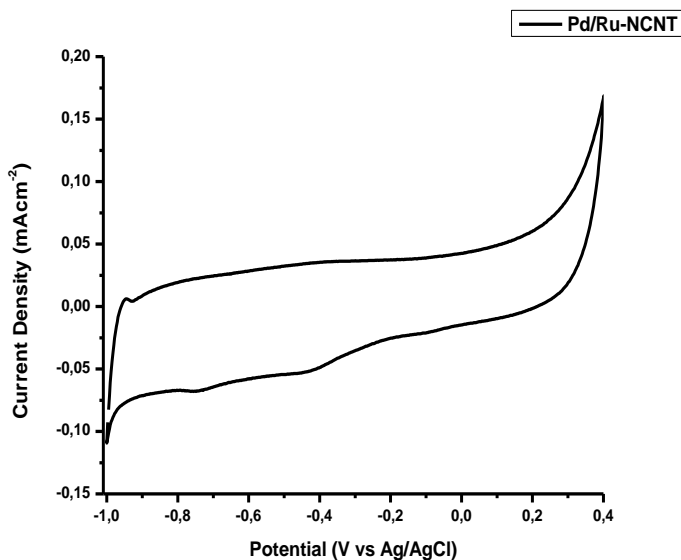**APPENDIX 2: Electrochemical evaluations of pH 13 electrocatalysts.**
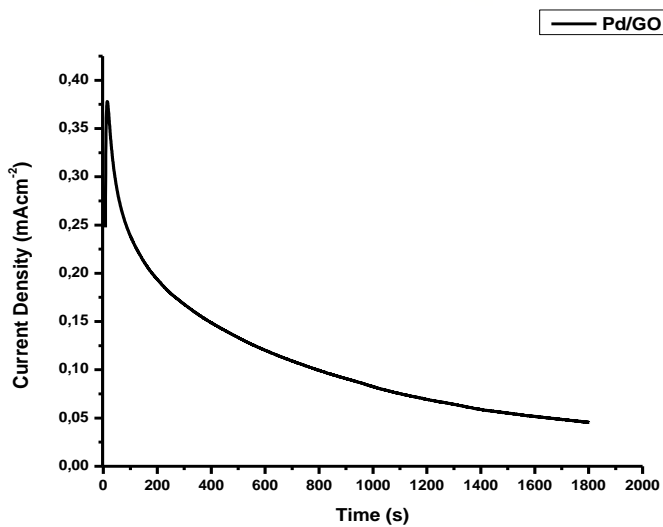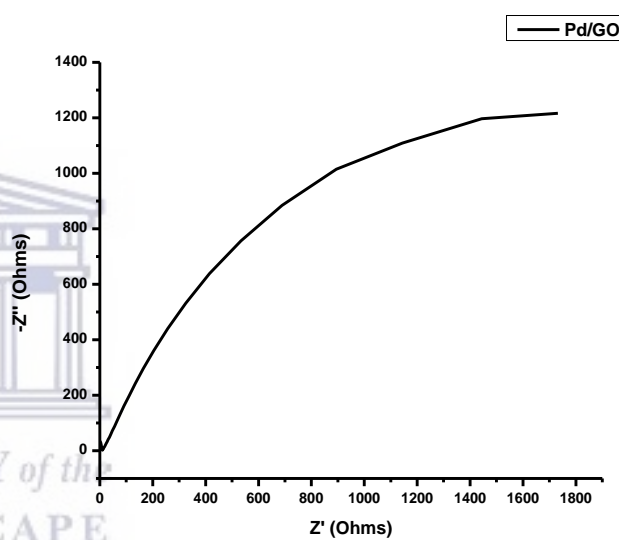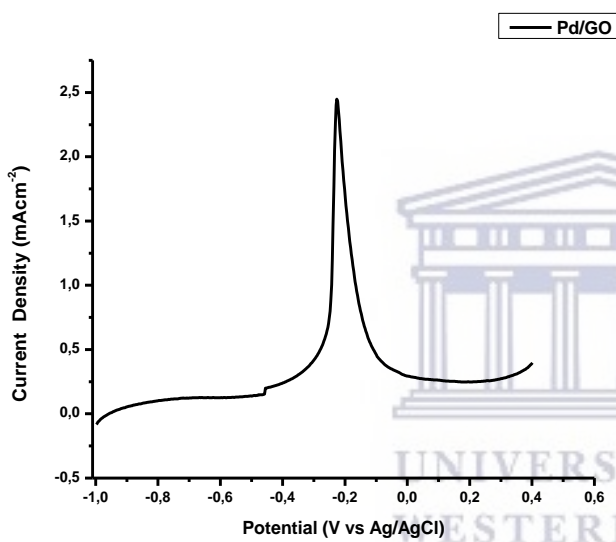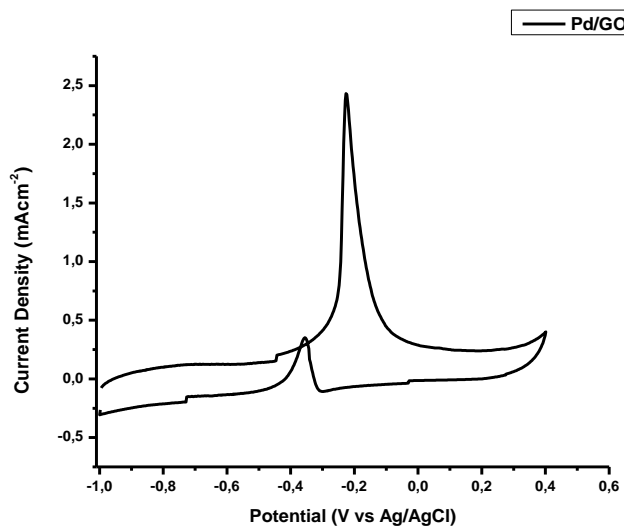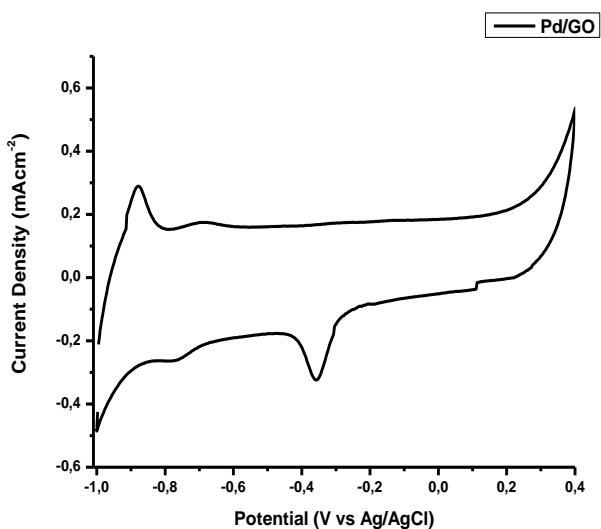
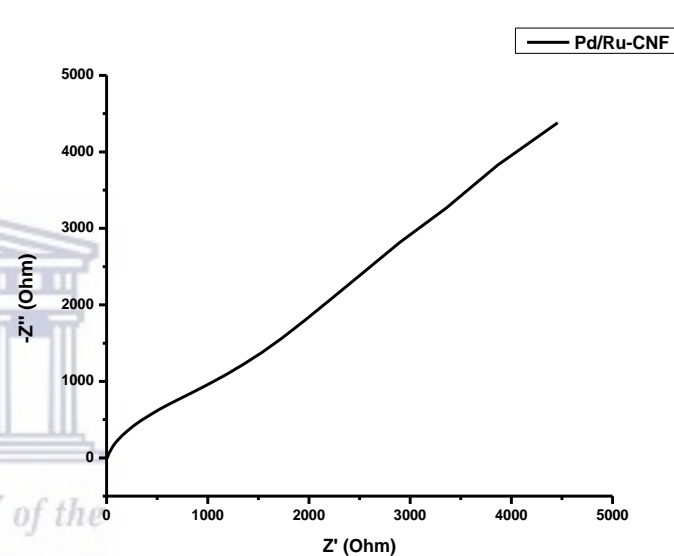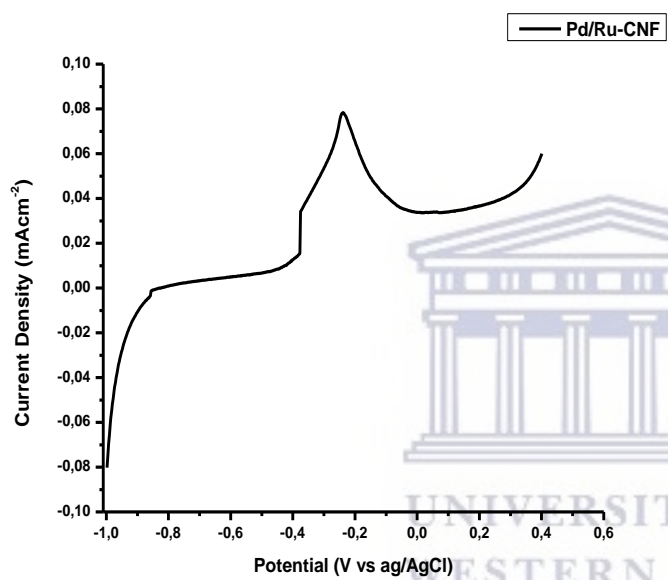Electrochemical evaluations of pH 13 Pd/GO

161
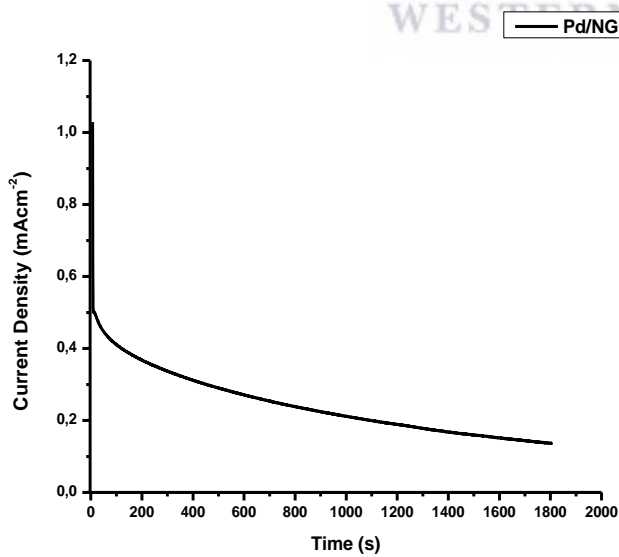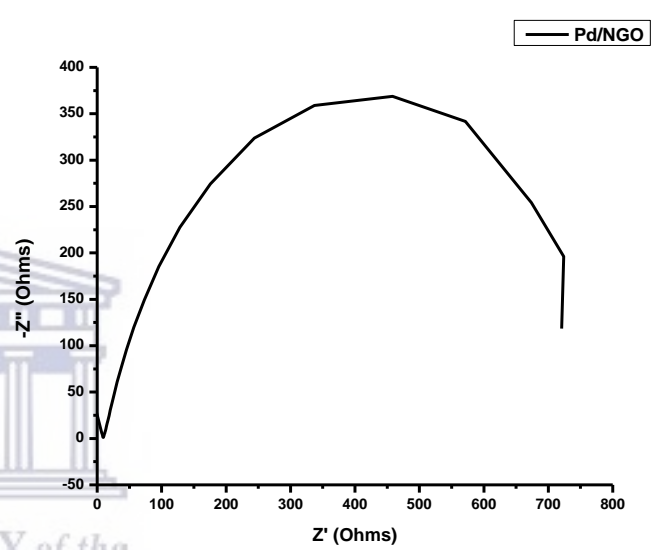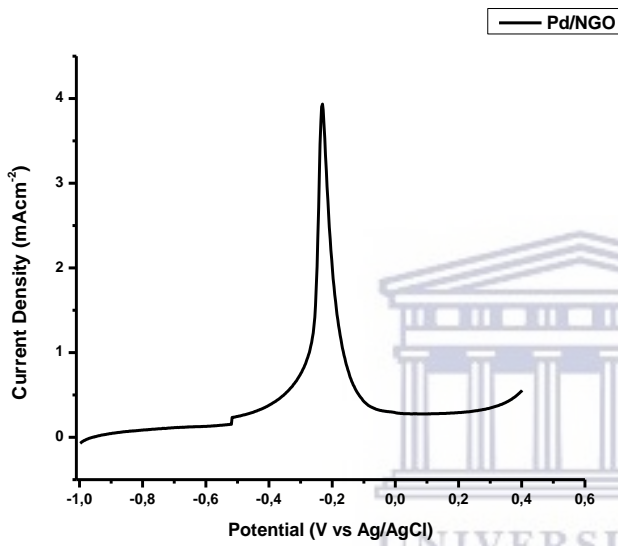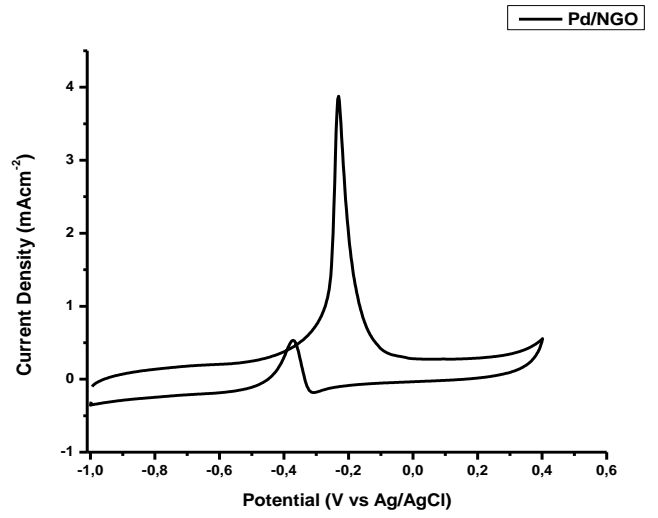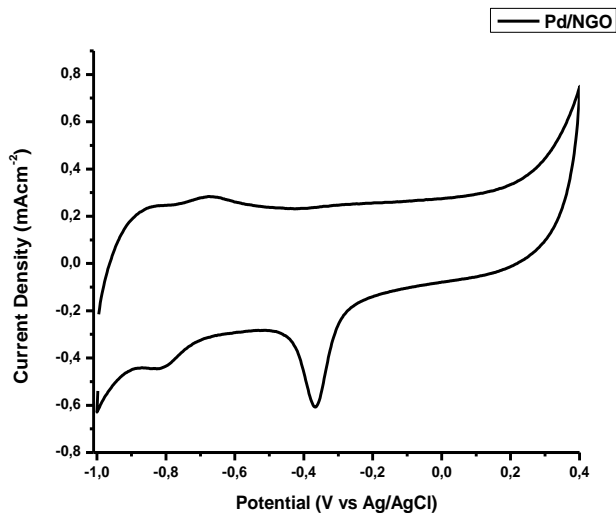
Electrochemical evaluations of pH 13 Pd/NGO
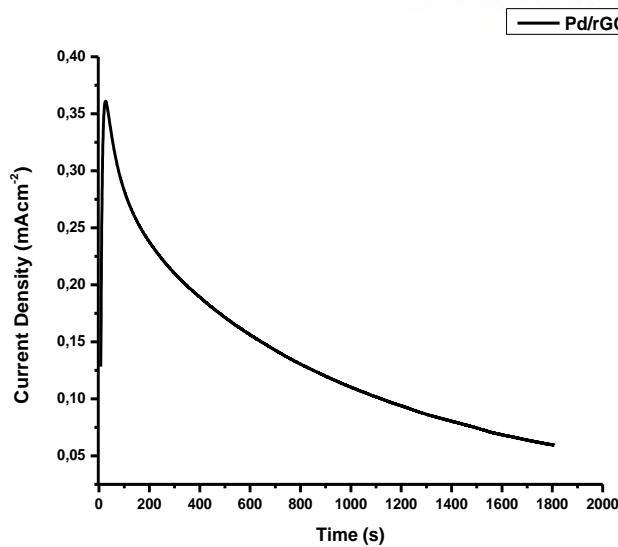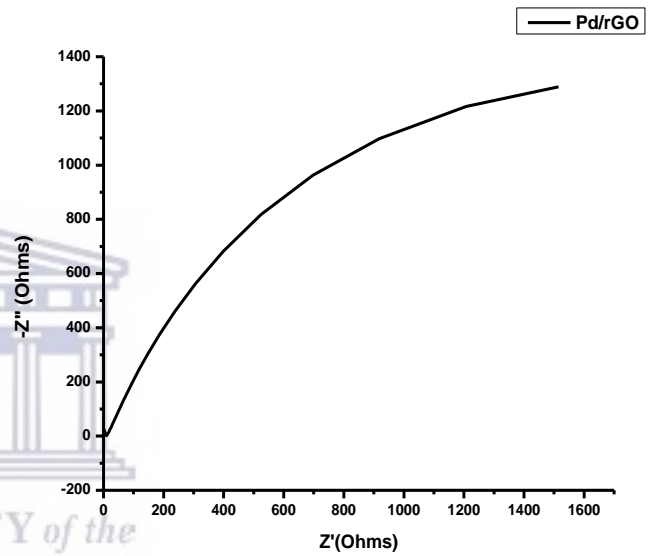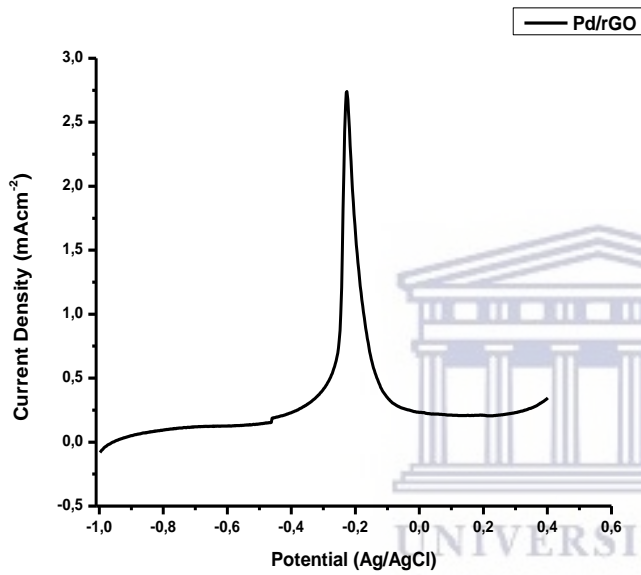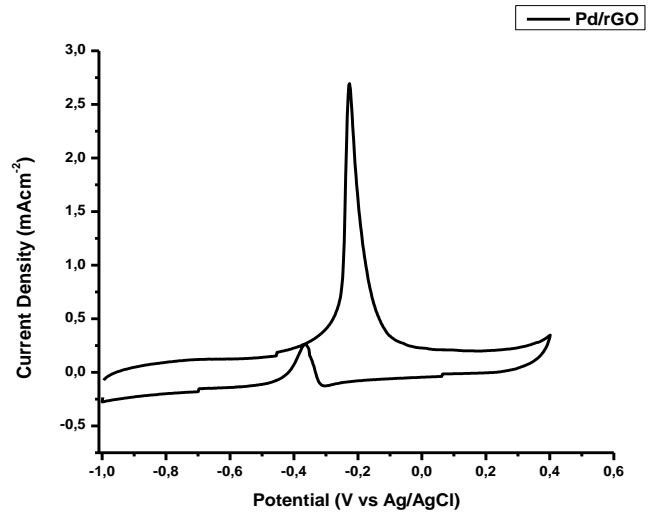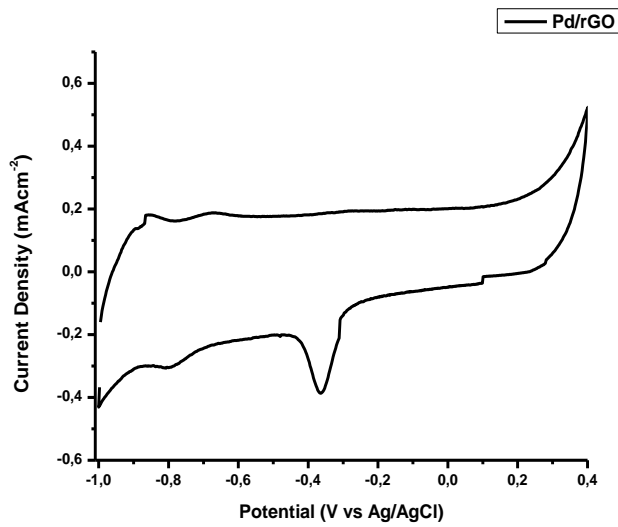
Electrochemical evaluations of pH 13 Pd/rGO

163
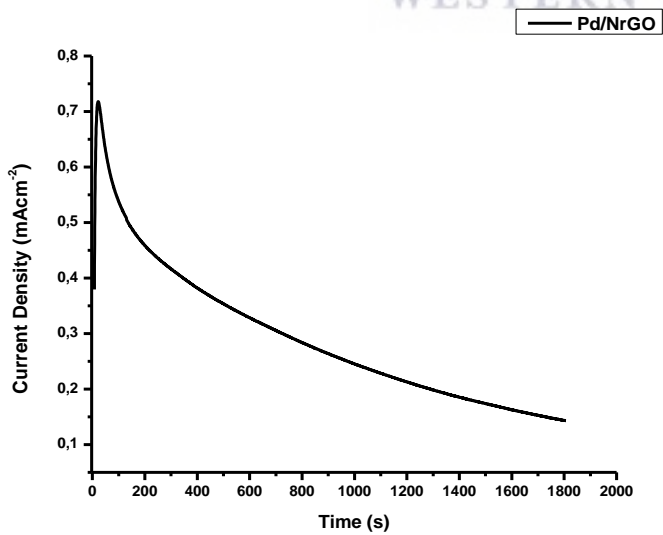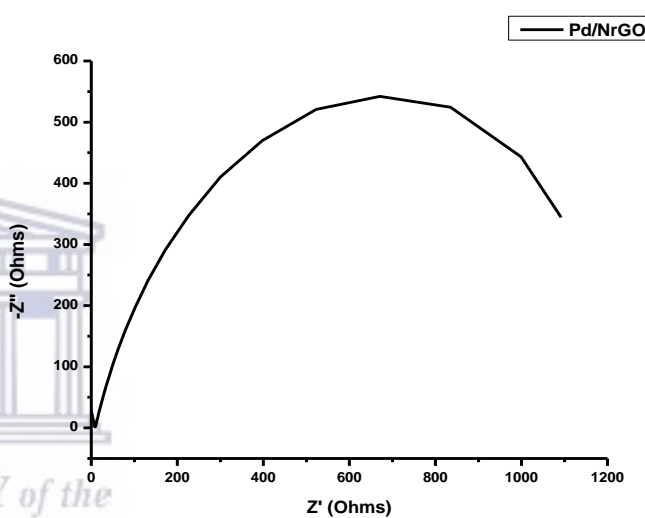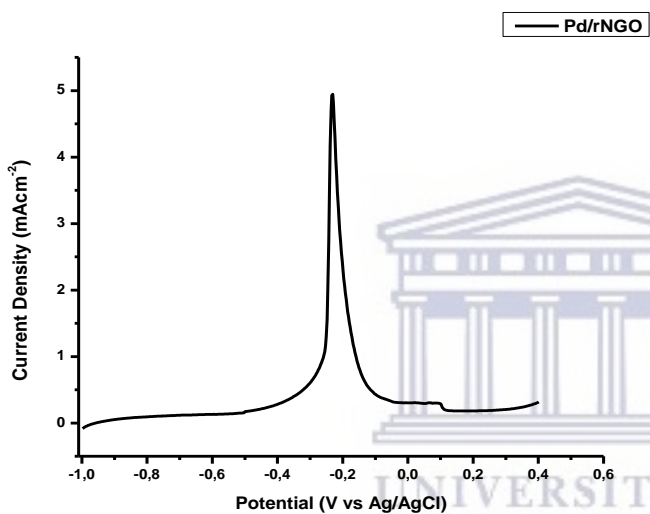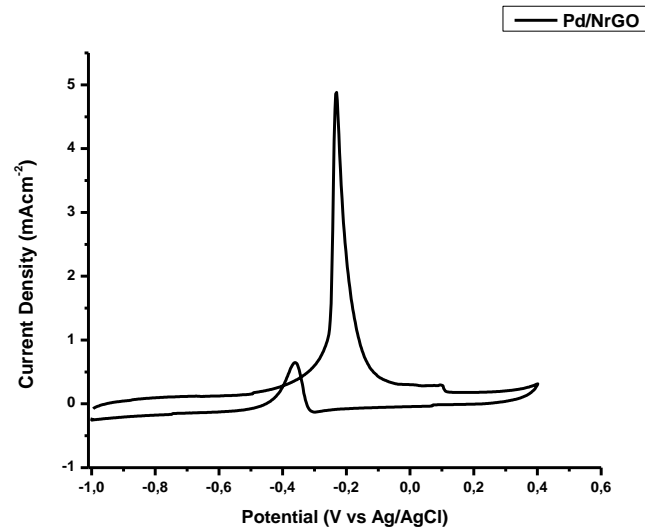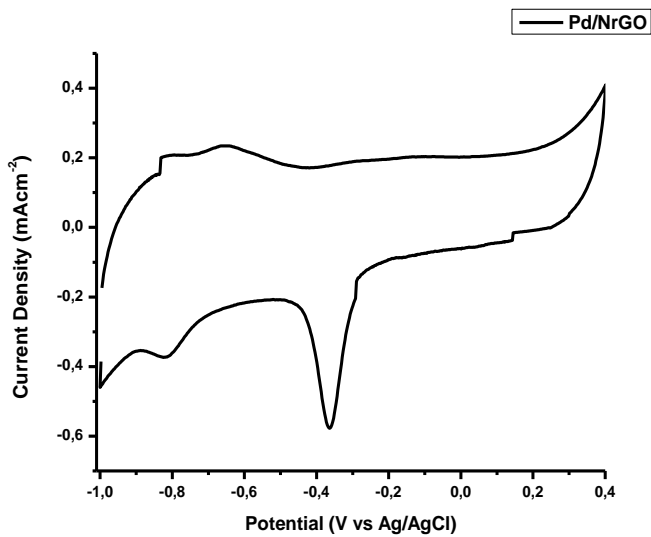
Electrochemical evaluations of pH 13 Pd/NrGO

164
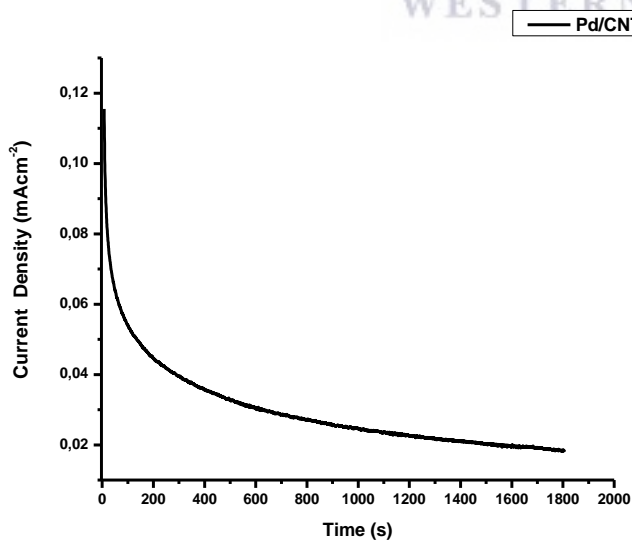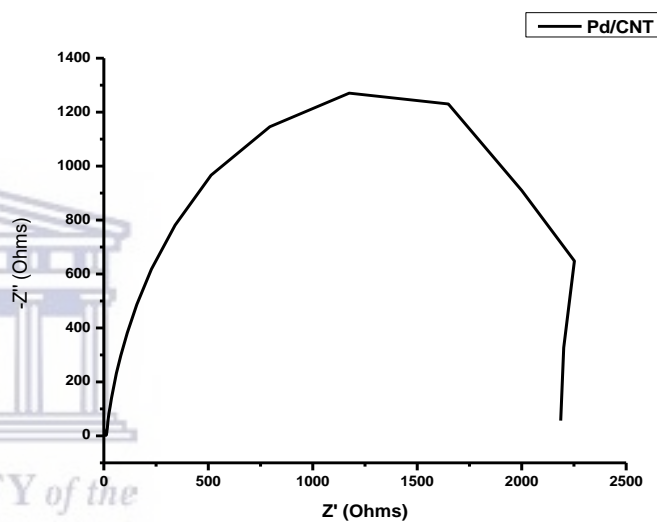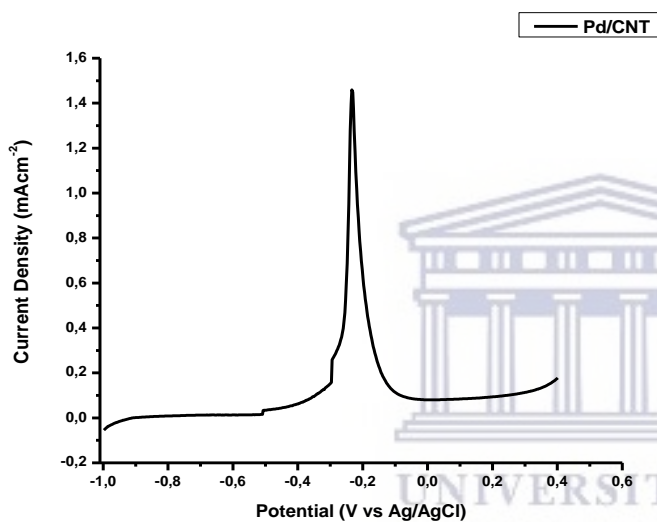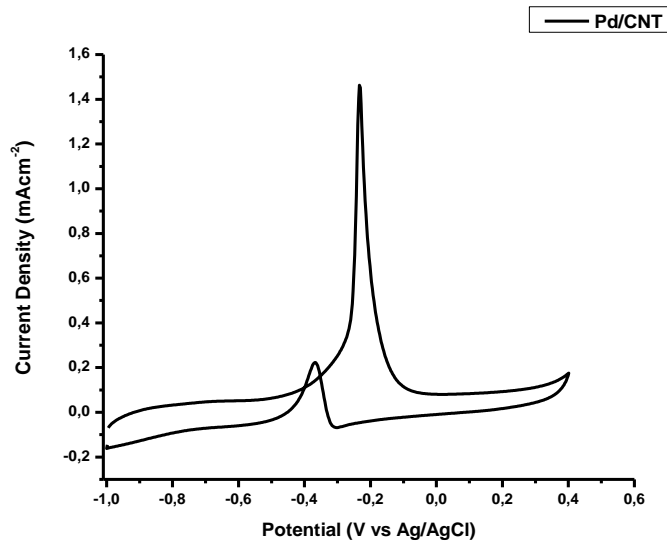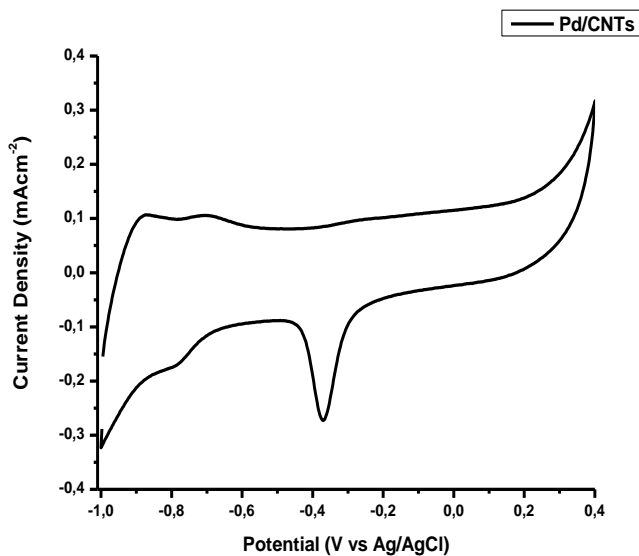
Electrochemical evaluations of pH 13 Pd/MWCNTs

165
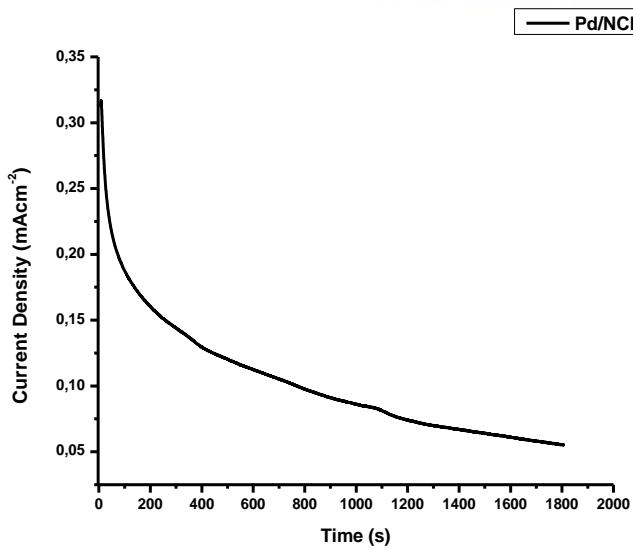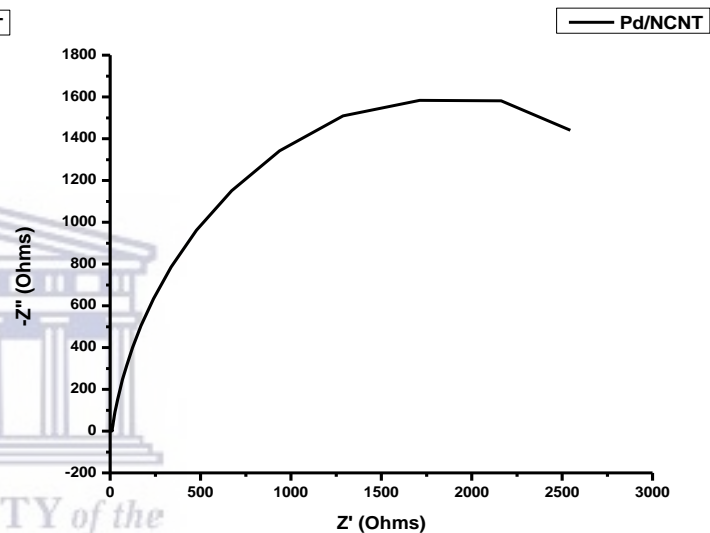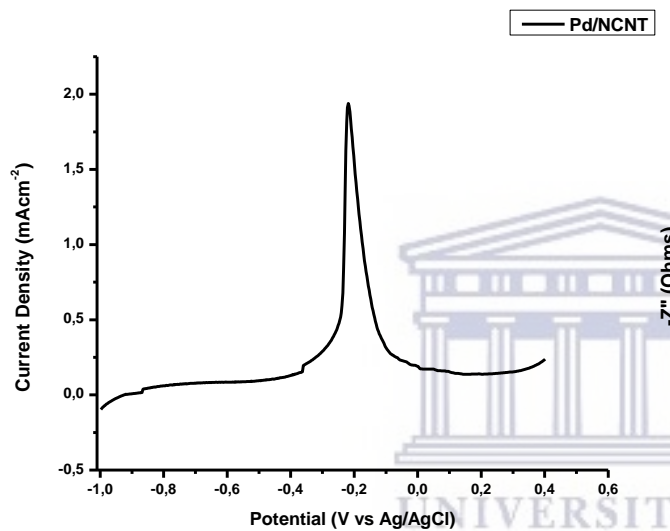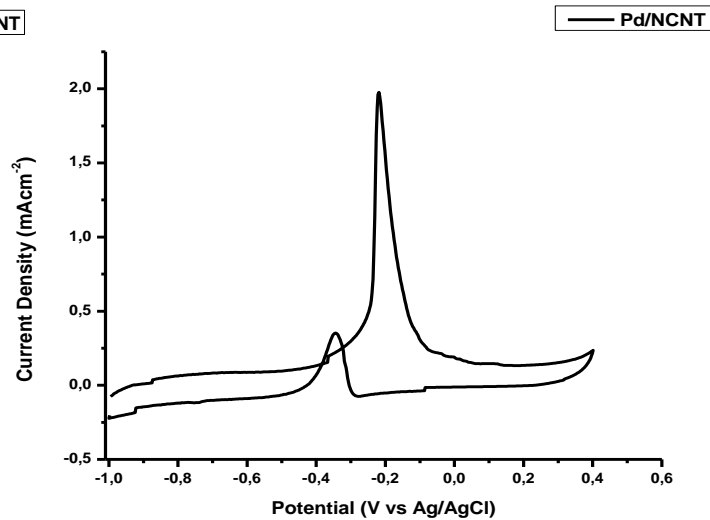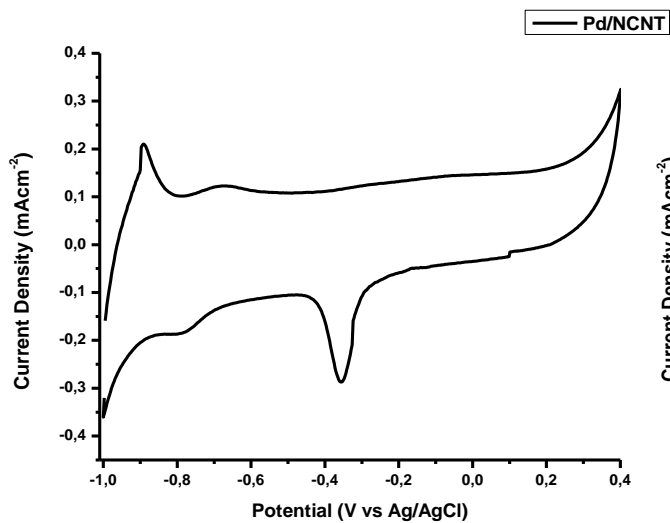
Electrochemical evaluations of pH 13 Pd/N-MWCNTs
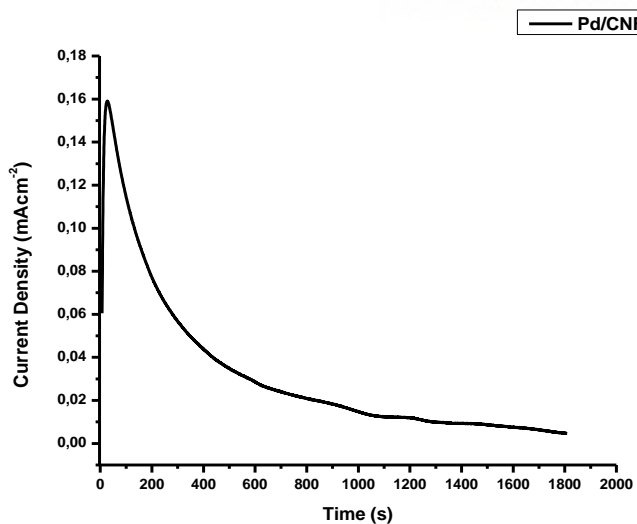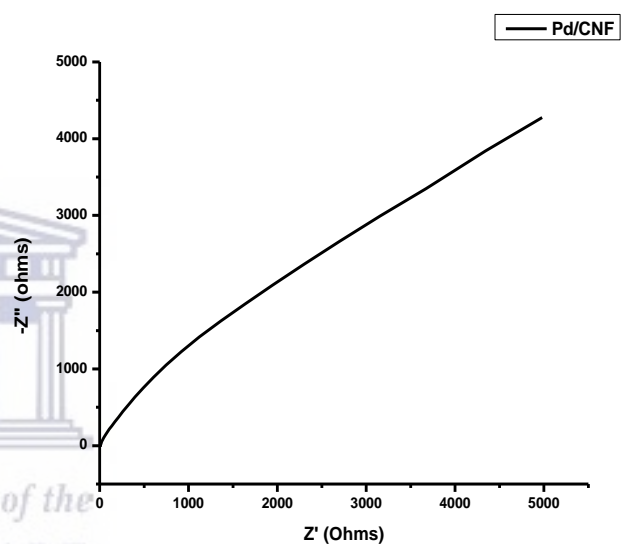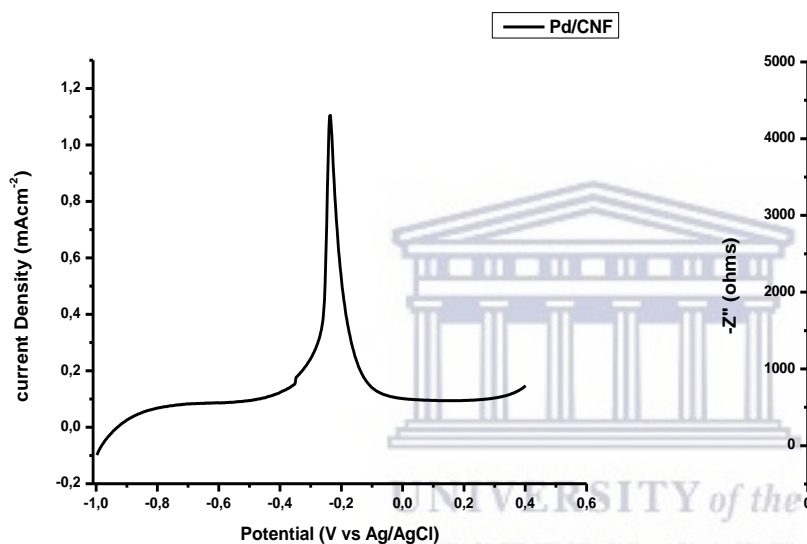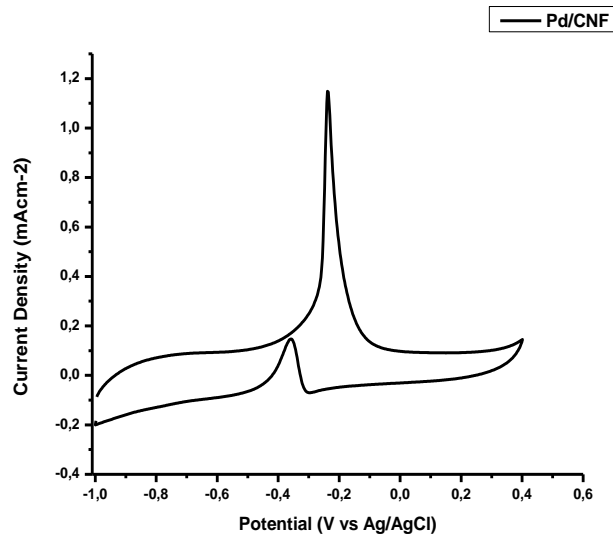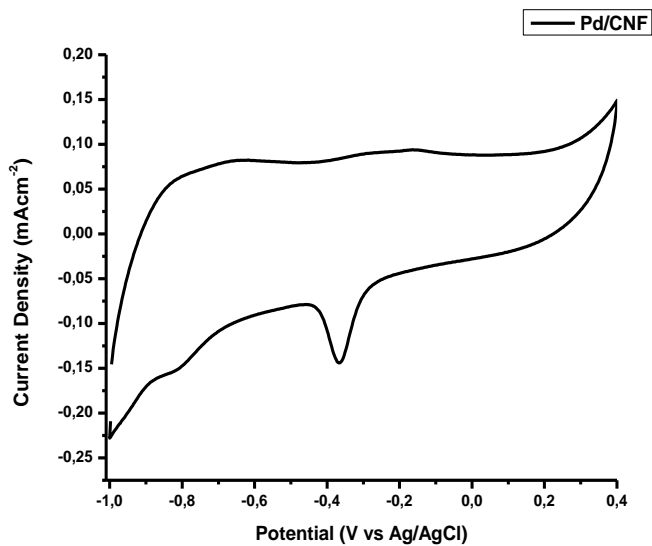
166

Electrochemical evaluations of pH 13 Pd/CNFs
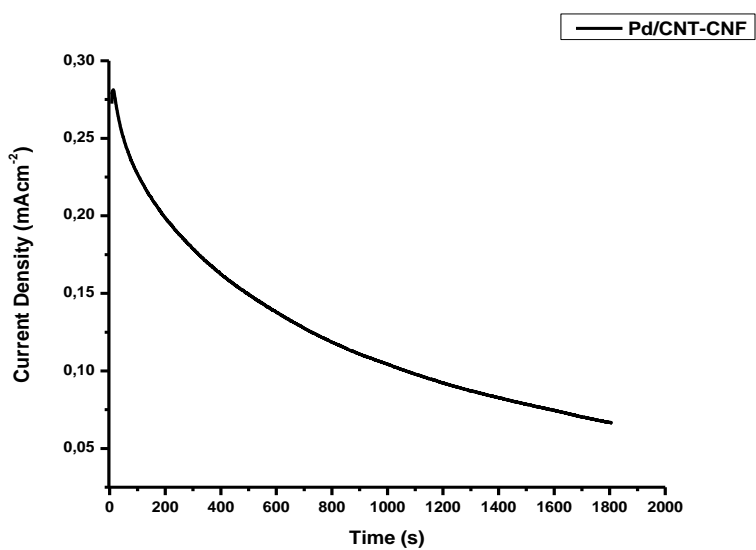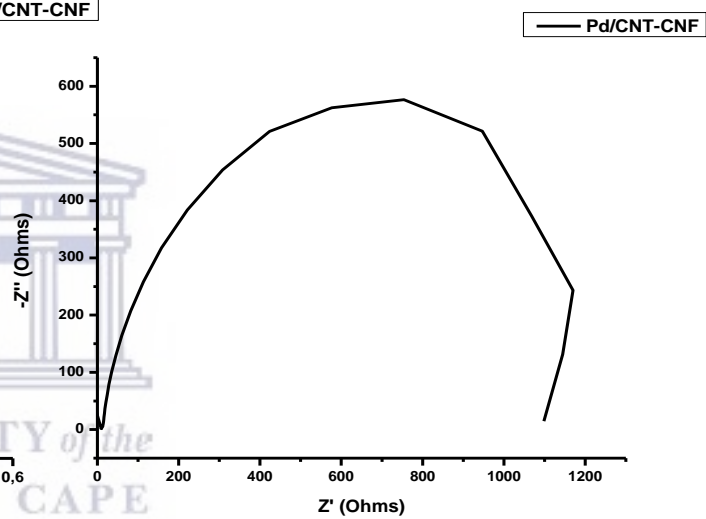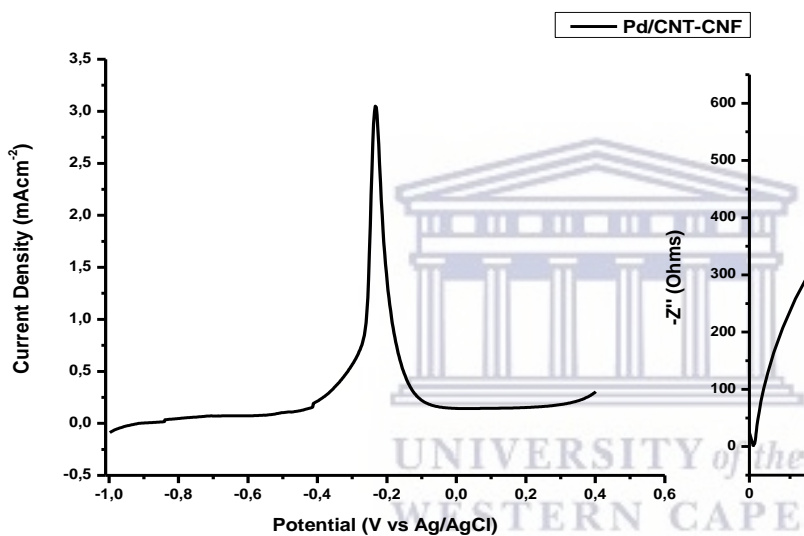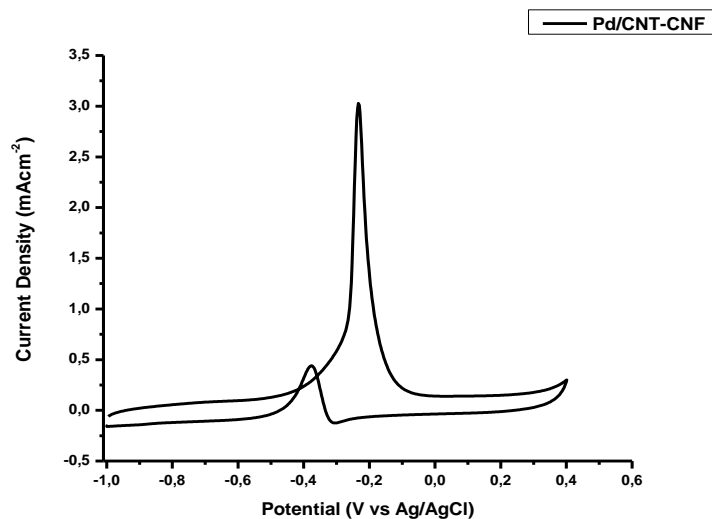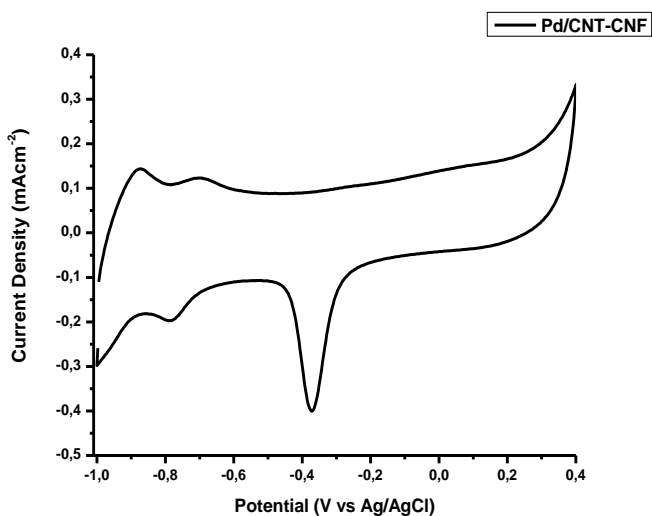
Electrochemical evaluations of Pd/MWCNTs-CNFs

168
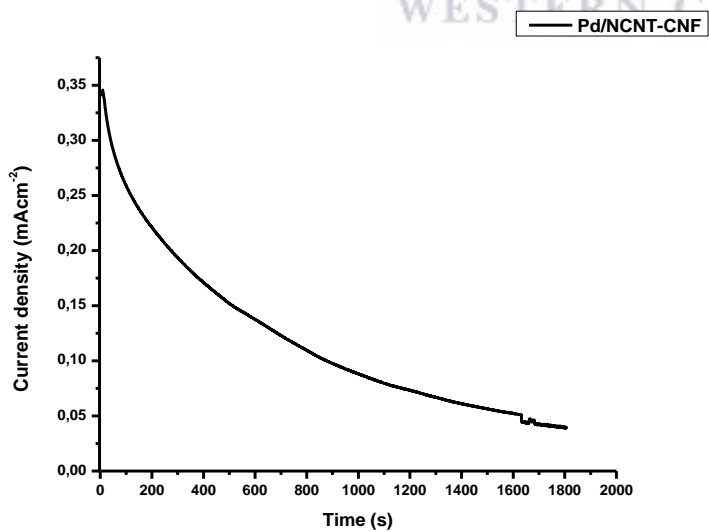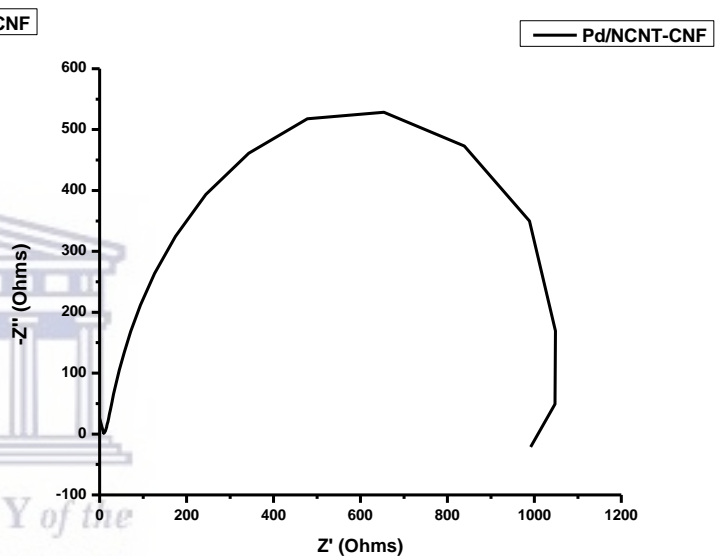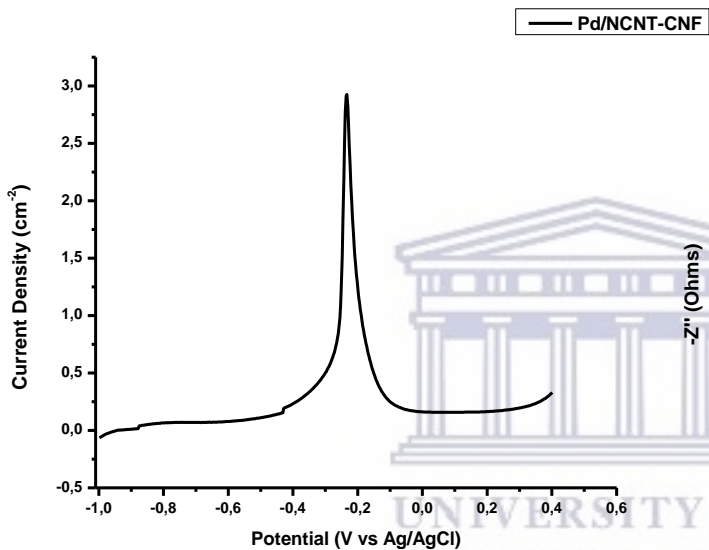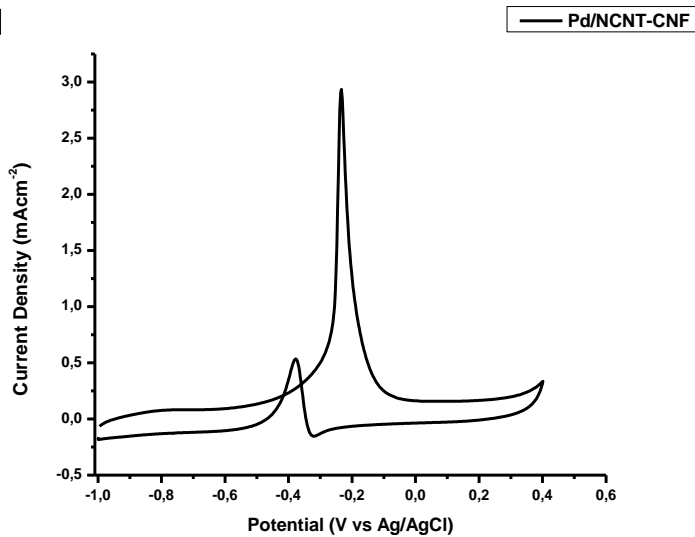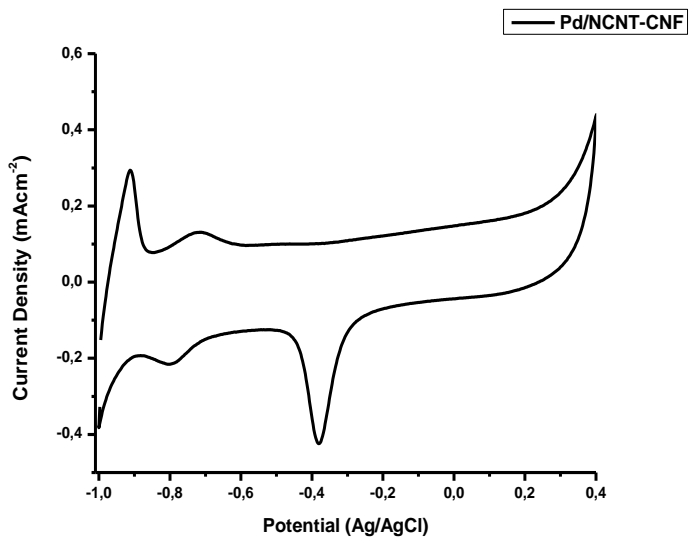
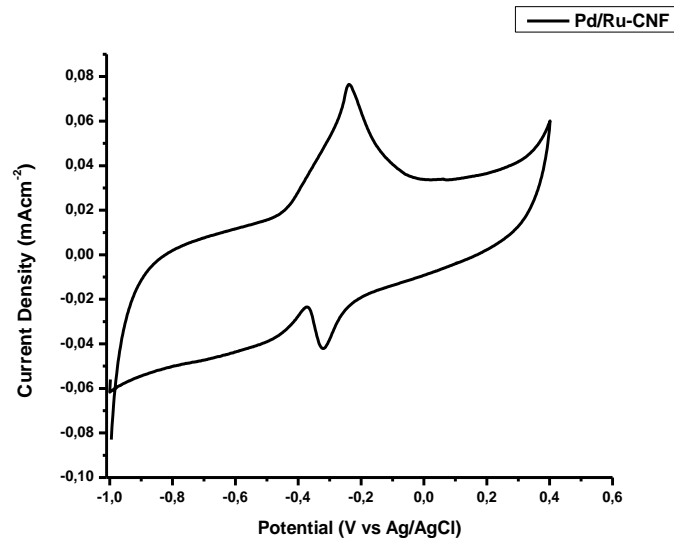Electrochemical evaluations of Pd/N-MWCNTs-CNFs

169
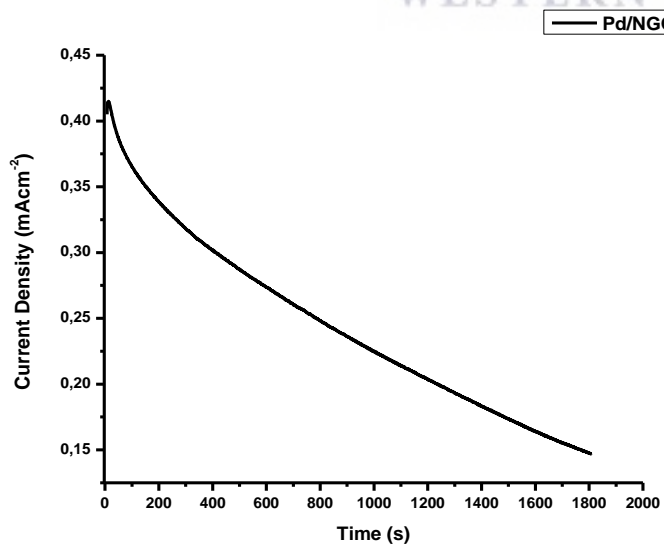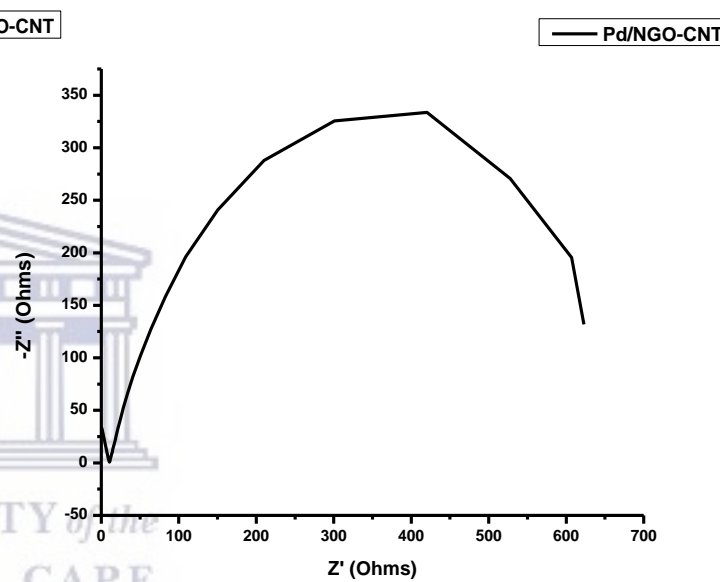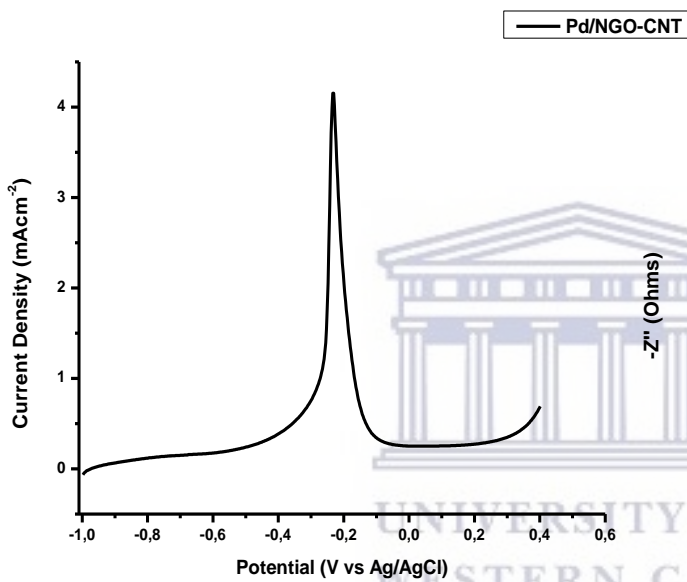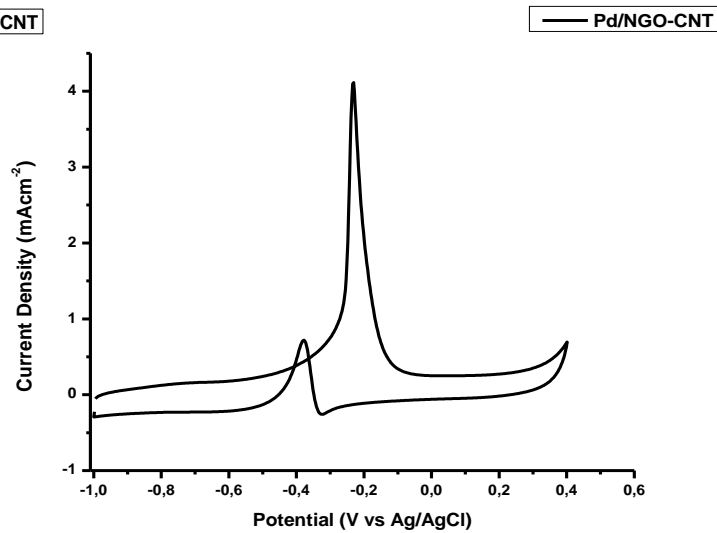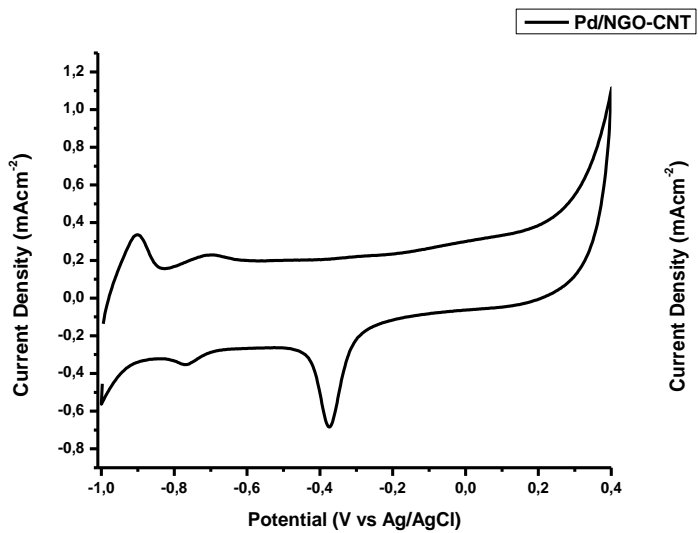
Electrochemical evaluations of Pd/NGO-MWCNTs
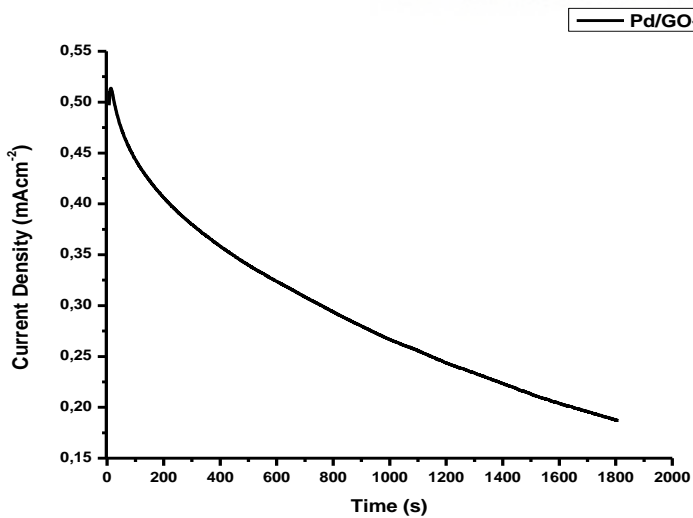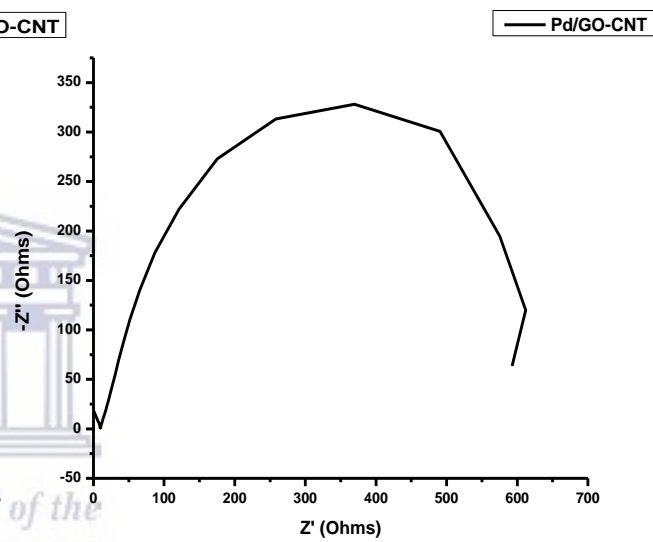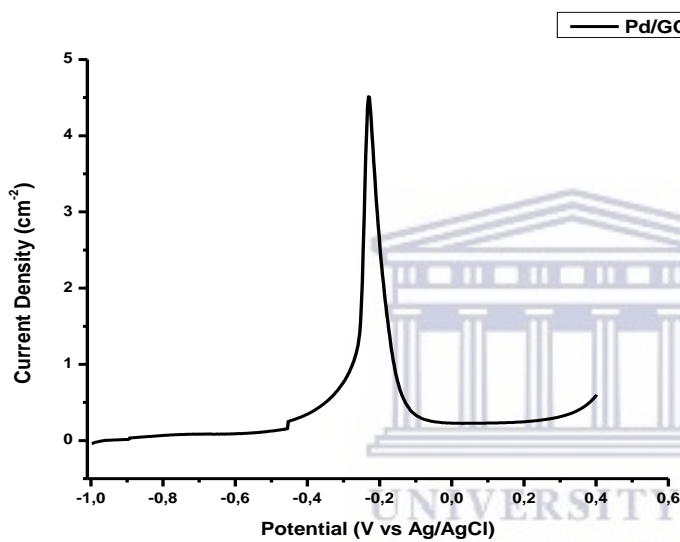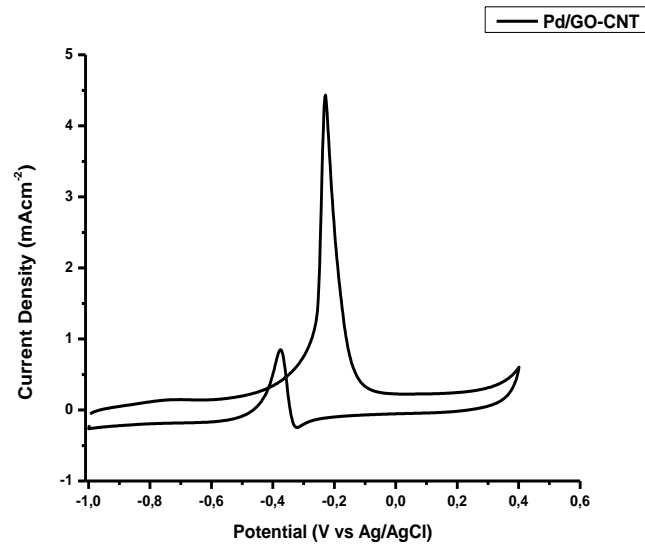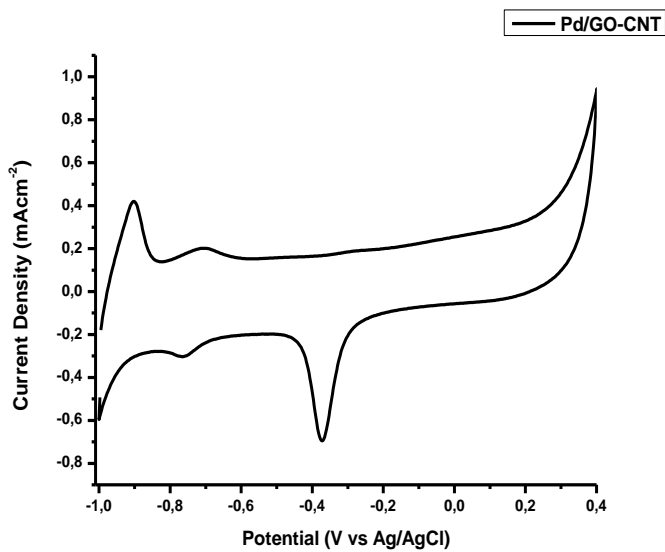
Electrochemical evaluations of Pd/GO-MWCNTs
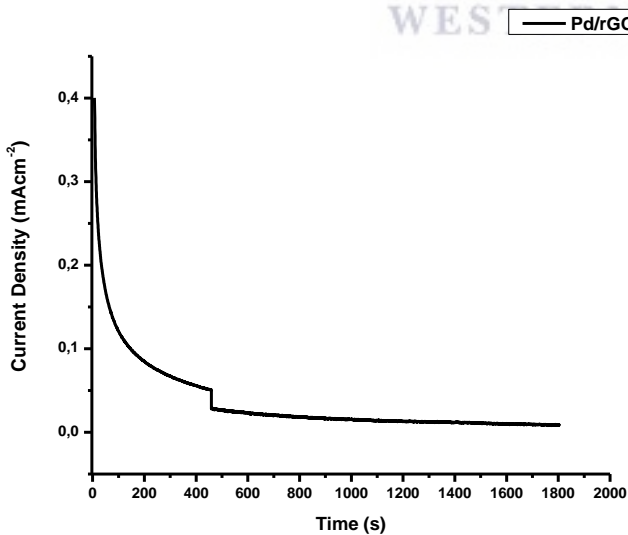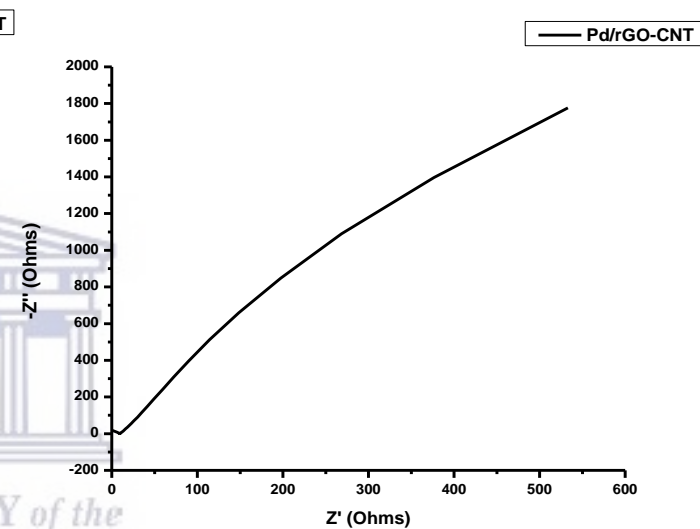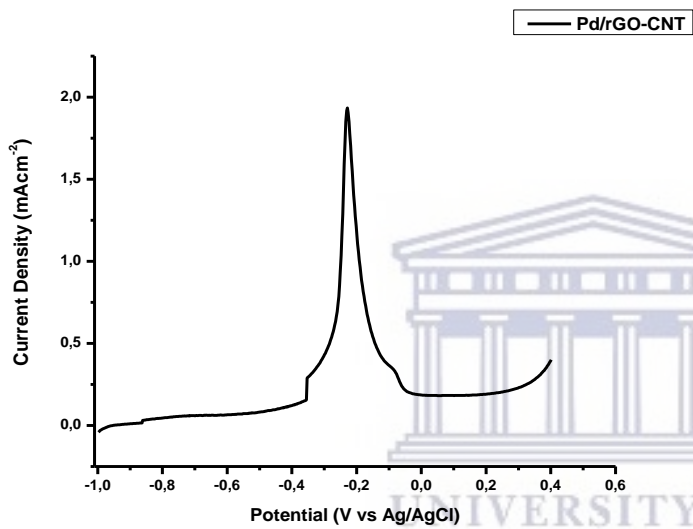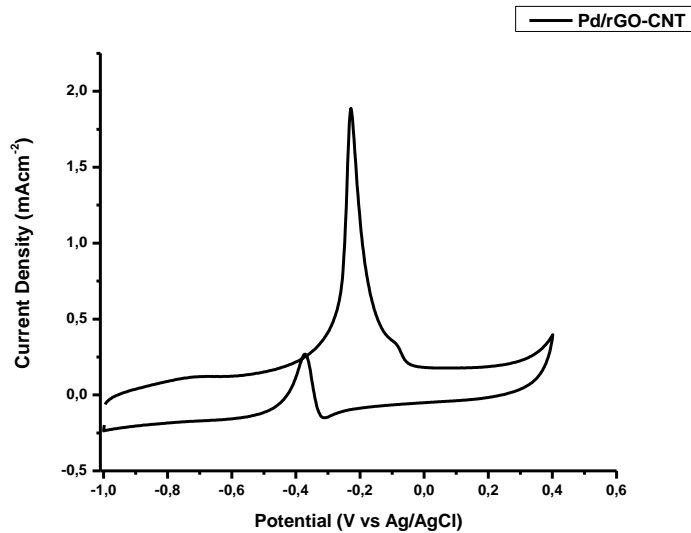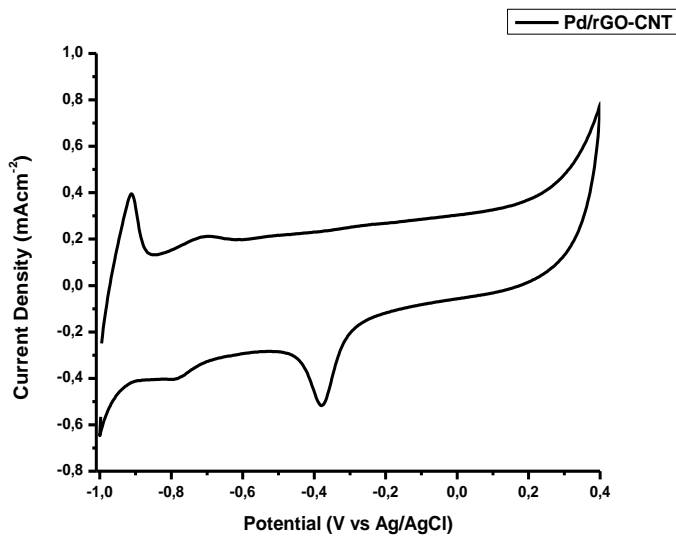
Electrochemical evaluations of Pd/rGO-MWCNTs

172
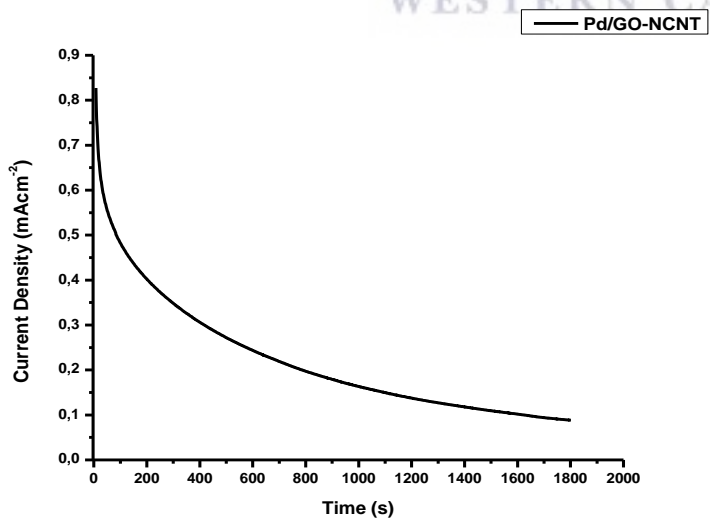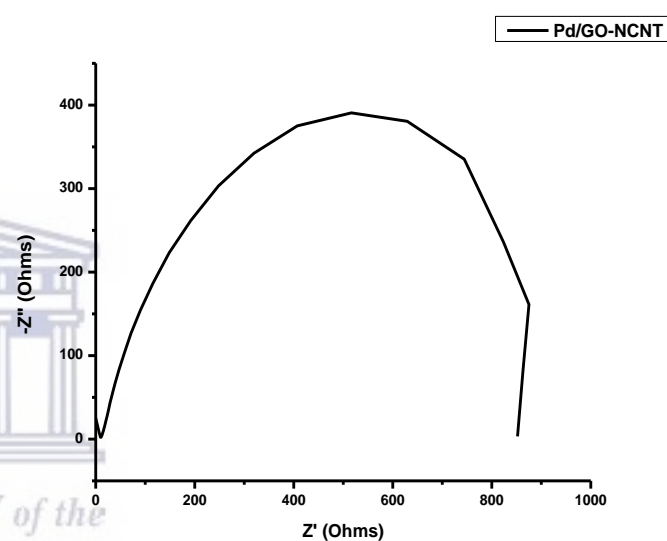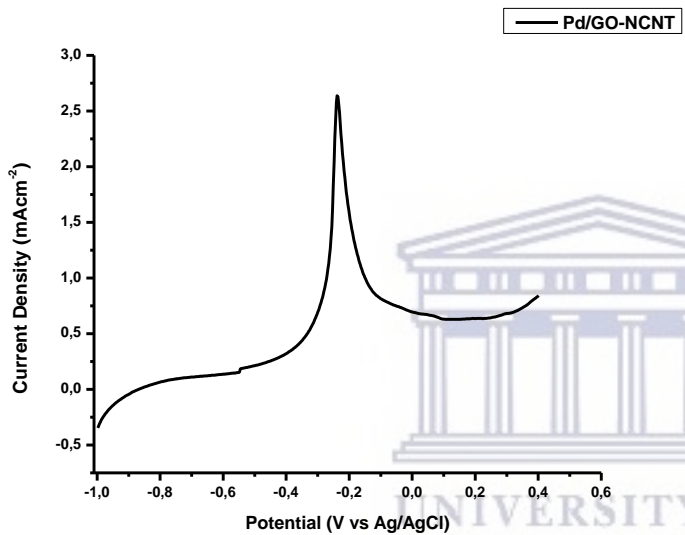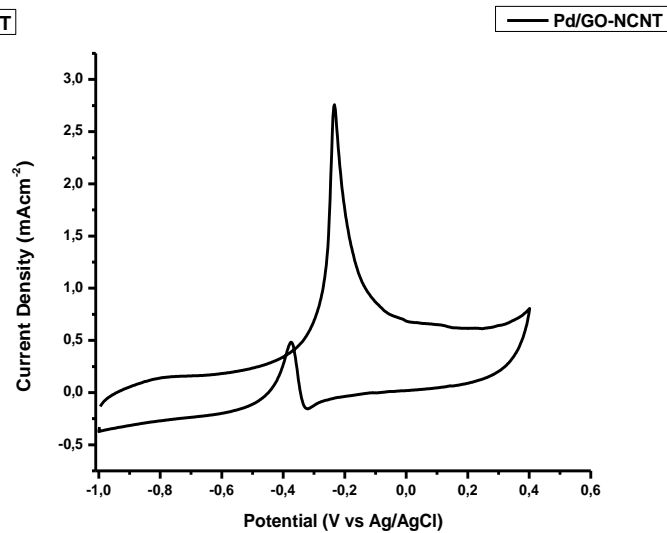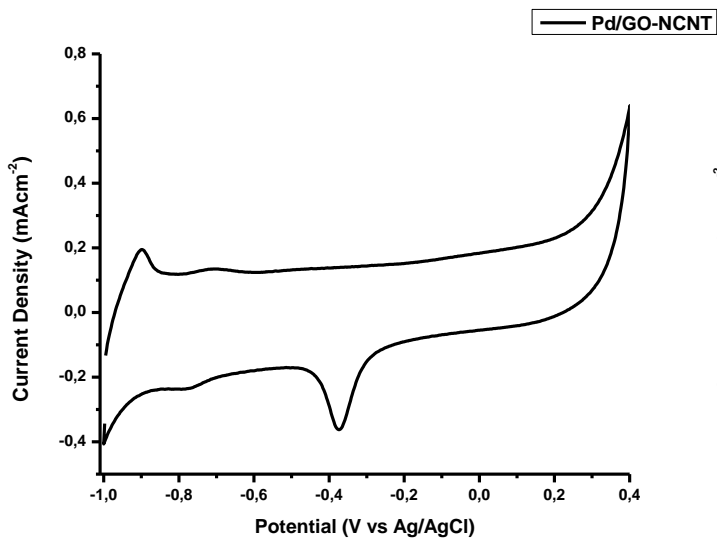
Electrochemical evaluations of Pd/GO-N-MWCNTs

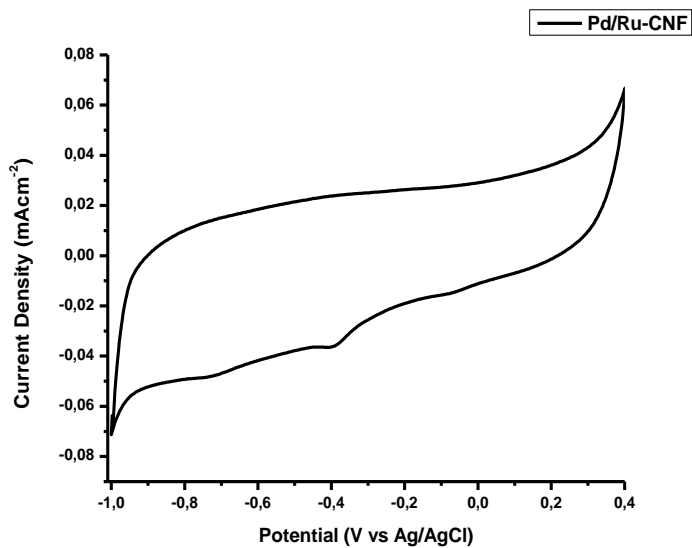# APPENDIX 4: Electrochemical evaluations of binary electrocatalysts
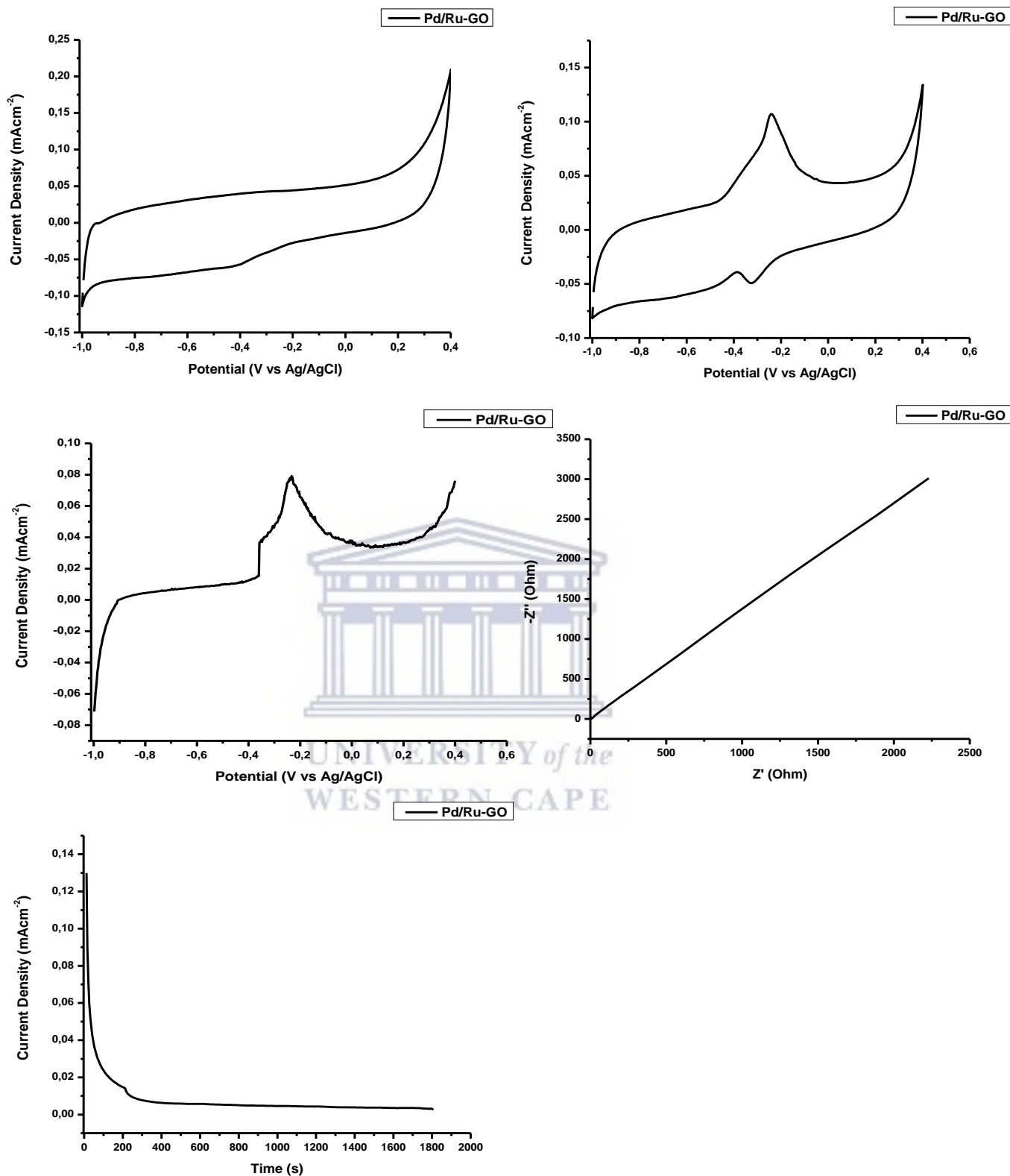
Electrochemical evaluations of Pd-Ru/GO
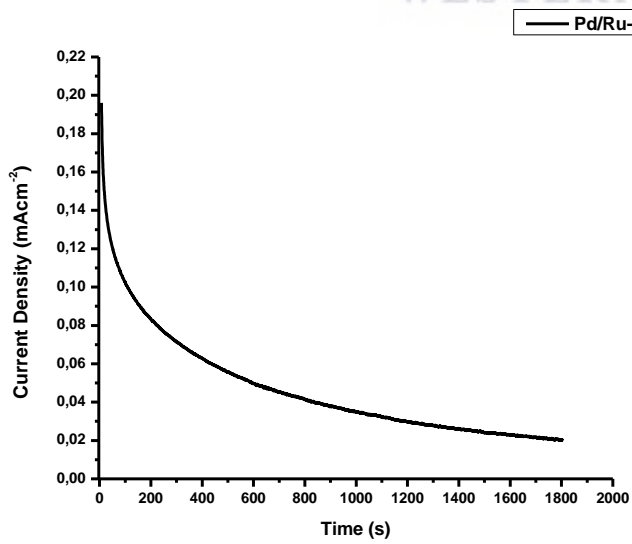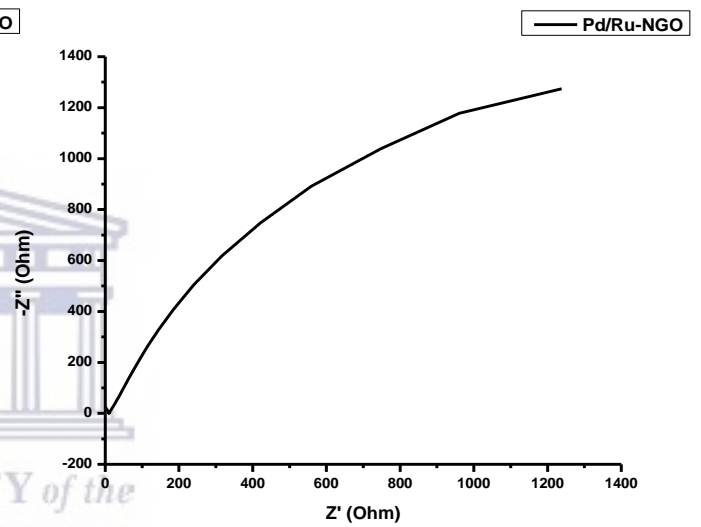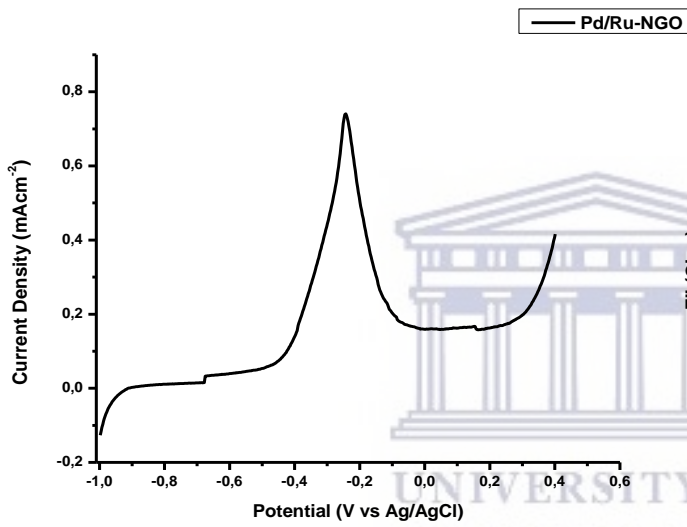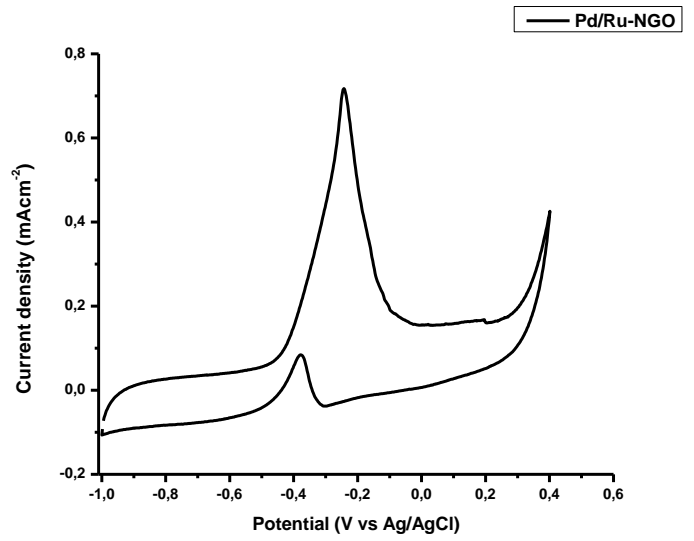
Electrochemical evaluations of Pd-Ru/NGO

175
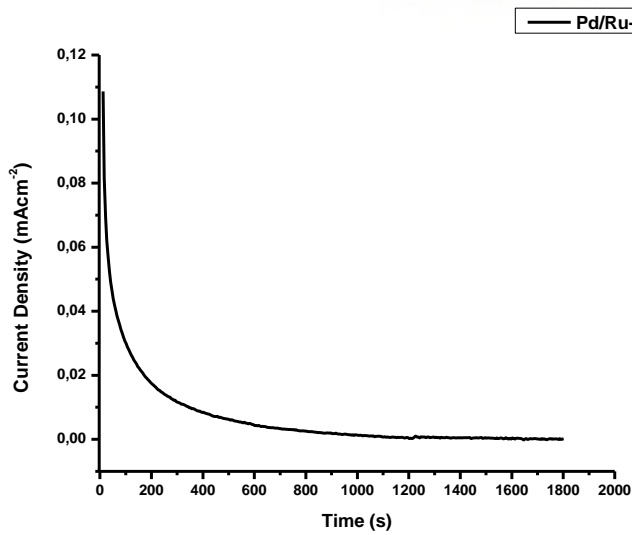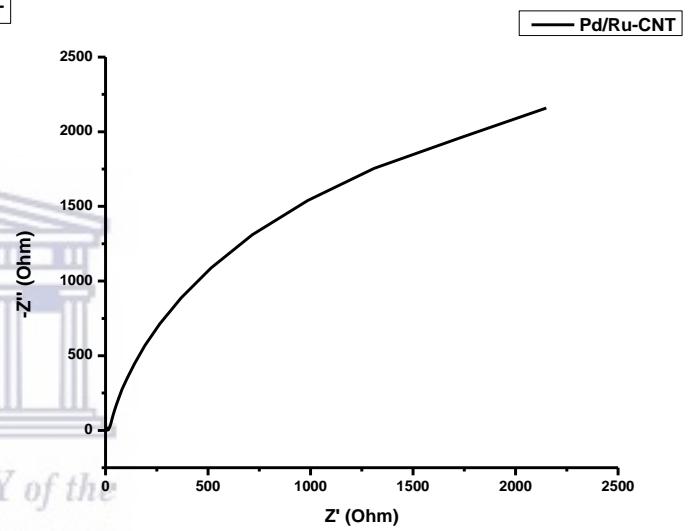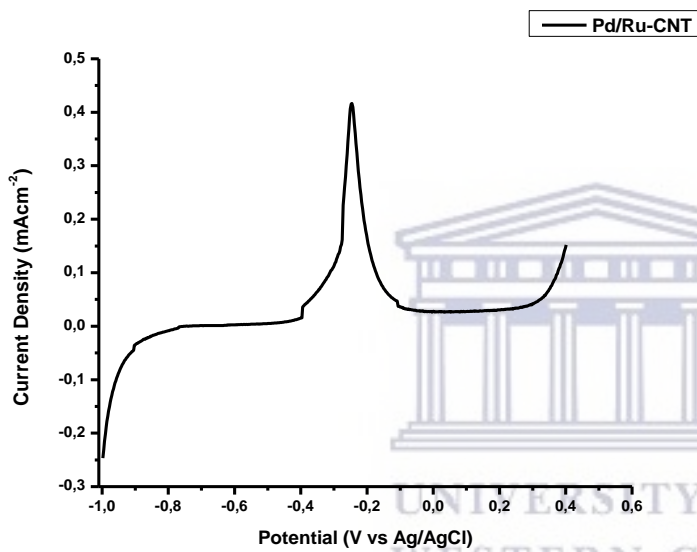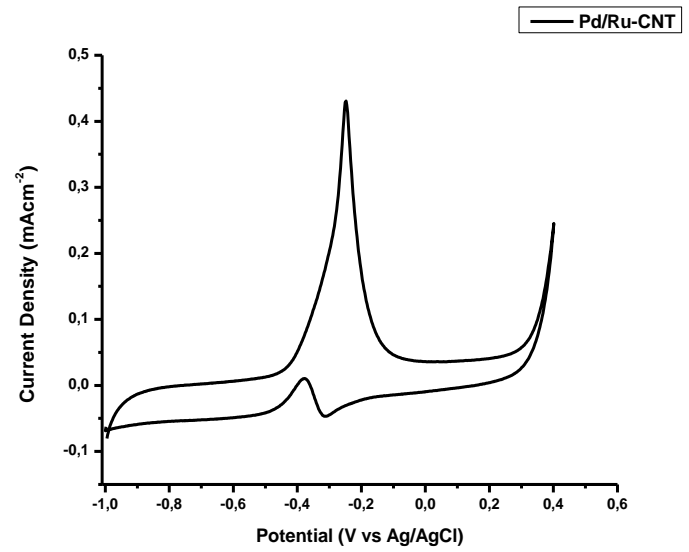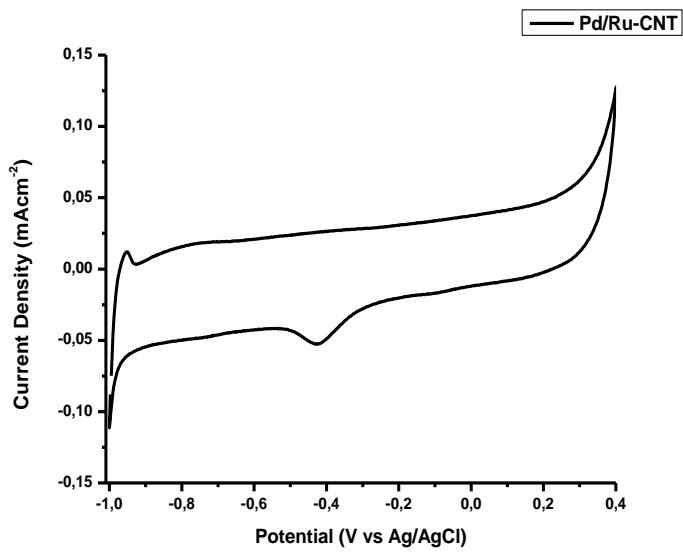
Electrochemical evaluations of Pd-Ru/MWCNTs

176
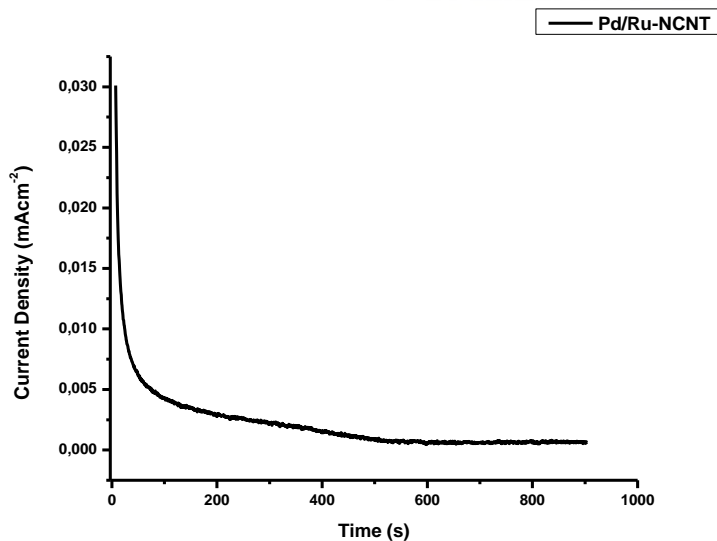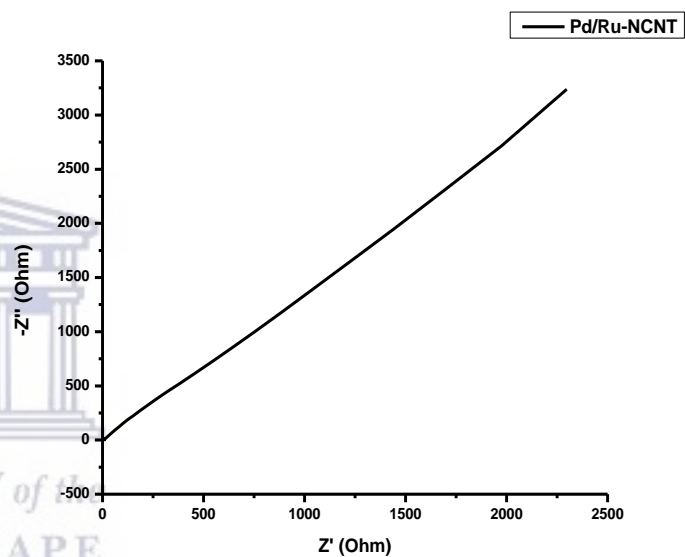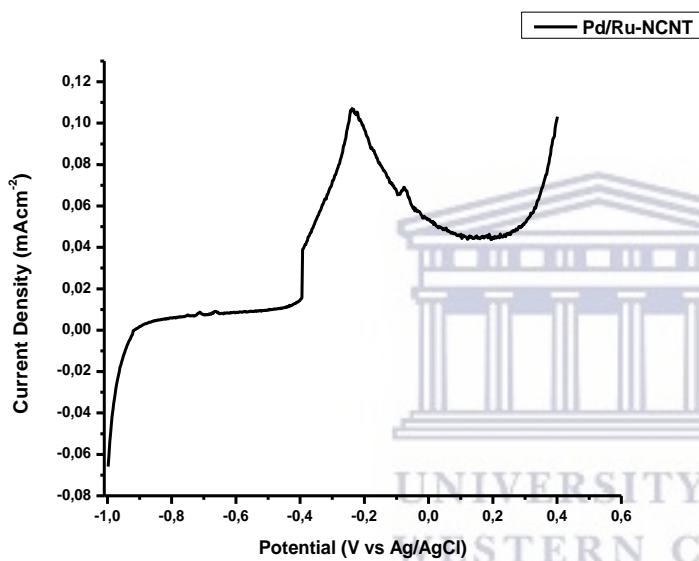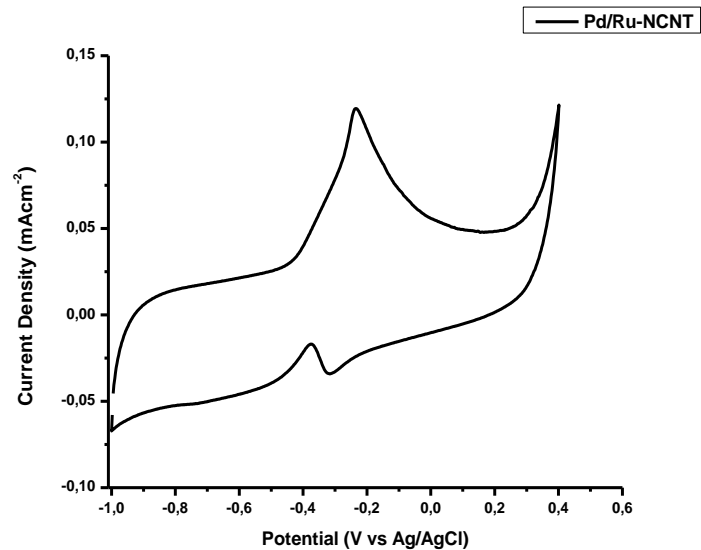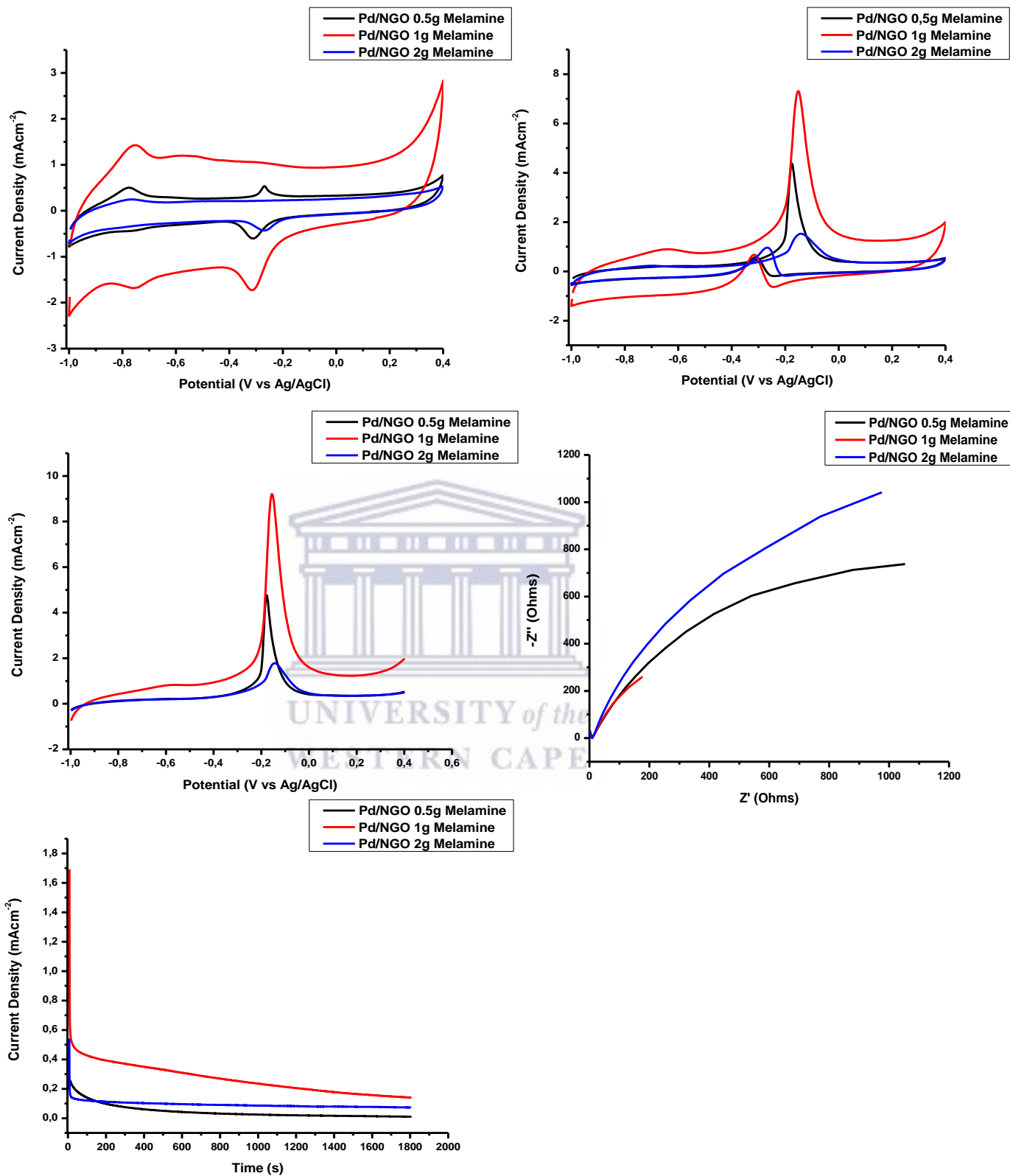
Electrochemical evaluations of Pd-Ru/N-MWCNTS
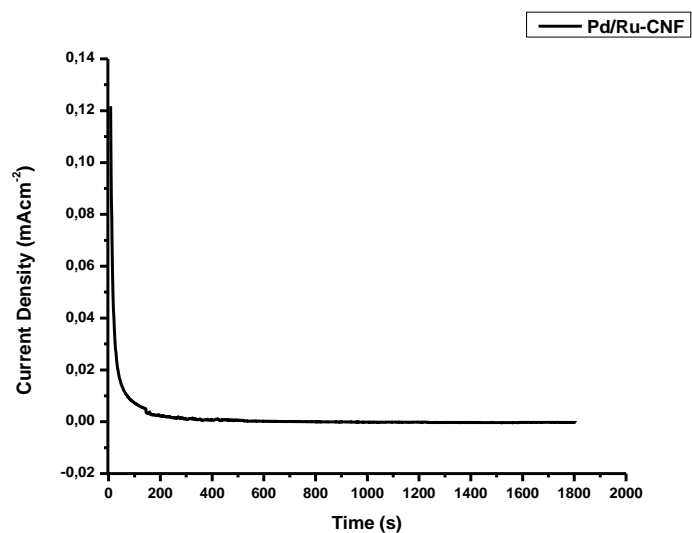
Electrochemical evaluations of Pd-Ru/CNFs.

178

Comparison of electrochemical evaluations of Pd/NGO with 0.5g, 1g and 2g of melamine.